An investigation into the effect of hydrocarbon stapling on a series of polyproline peptides and its subsequent implementation into the development of an array of α-helix mimetics.

Elliott Fenn

This thesis is submitted for the degree of *Master of Science.*

Supervisor: **Dr Aniello Palma**

School of Physical Sciences

Date: 13/09/2021

Contents

Declaration

I hereby declare that except where specific reference is made to the work of others, the contents of this dissertation are original and have not been submitted in whole or in part for consideration for any other degree or qualification in this, or any other university. This dissertation is the result of my own work and includes nothing which is the outcome of work done in collaboration except where specifically indicated in the text and acknowledgements.

Abstract

The structural scope and attractive properties presented by polyproline peptides has resulted in a heightening of research surrounding the development and application of these compounds. Examples of such applications include use as peptide-based self-assembled mono-layers (SAMs), tri-helical peptide scaffolds as well as supramolecular peptide-metal frameworks. During the work of this thesis, the effect of hydrocarbon stapling on an array of polyproline-7 ($(Pro)_7$) peptides is firstly investigated whereby the positioning of a fixed spanning-length linker was altered and the resulting conformational structure probed. This presented an opportunity to discover a novel secondary structure with possible biological applications as a supramolecular scaffold. The results of this study then provided a foundation of knowledge surrounding the application of hydrocarbon stapling in the development of an α-helix mimetic peptide. After selecting a substrate protein named talin, a set of functionalized polyproline peptides, each comprised of varying non-natural amino acid building blocks, were constructed and their binding properties vs the talin protein analysed.

5.0 Abbreviations

PPI – Polyproline 1 conformation
PPII – Polyproline 2 conformation
DNA – De-oxy ribonucleic acid
RCM – Ring-closing metathesis
Lk-PPI/2 – Conformationally locked polyproline structure
CD – Circular dichroism
NMR – Nuclear magnetic resonance (spectroscopy)
HPLC – High performance liquid chromatography
LCMS – Liquid chromatography mass spectrometry
MS – Mass spectrometry
FT-IR – Fourier transform infra-red spectroscopy
IM-MS – Ion mobility – mass spectrometry
THF - Tetrahydrofuran
DMSO - Dimethyl sulfoxide
DCM - Dichloromethane
DMF – Dimethyl formamide
TFA – Trifluoroacetic acid
Boc – tertiary-butoxycarbonyl group
Fmoc – Fluorenylmethyloxycarbonyl group
Cbz – Carboxybenzyl group
SPPS – Solid phase peptide synthesis
DIPEA – Di-isopropyl ethylamine
HOBt - Hydroxybenzotriazol
PyBOP - benzotriazol-1-yl-oxytripyrrolidinophosphonium hexafluorophosphate
Et_2O – Diethyl ether
EtOAc – Ethyl acetate
Pd/C – Palladium/carbon
DOSY (NMR) – Diffusion-ordered spectroscopy
IMes - 1,3-Dimesitylimidazol-2-ylidene
FCC – Flash column chromatography
TLC – Thin layer chromatography
TBAI – Tertiary butyl ammonium iodide
MsCl – Methanesulfonyl chloride

Chapter 1 - Polyproline, hydrocarbon stapling and the effects on conformational structure

1.0 Background Information

Polyproline is known to exist in two structural conformations: polyproline II (PPII) and polyproline I (PPI), with the two conformers varying structurally and their formation/presence mediated by a number of factors (e.g, solvent media, temperature, de-naturing agent presence etc).[1]

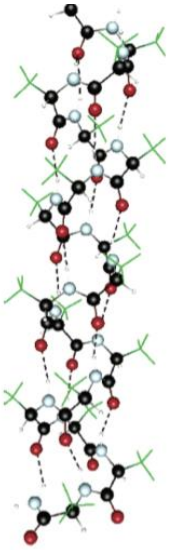

Figure 1 *– An α-helical peptide with intramolecular hydrogen bonding indicated by dotted lines.*[9]

The PPII left-handed helix is defined by its backbone dihedral angles (ϕ, ψ) of roughly (-75^0, 145^0) and with its peptide bonds occupying the *trans* conformation.[2] This PPII helix has subsequently been identified as a major, recognizable protein structure which can even be adopted by non-proline-containing peptides[3] with additional evidence showing the structure's presence in natural polypeptides and globular proteins.[4,5,6] Three residues per turn and a rise of 3.1 Å per residue results in the PPII helix adopting an extended and somewhat open and low density structure.[2] Furthermore, unlike other secondary protein structures such as the α-helix, with an '$i \rightarrow i + 4$' residue H-bonding pattern (Fig. 1), polyproline helices do not support internal H-bonding and their structural organization is a lot more localized. The main interaction responsible for their structural stability occurs as a result of the $n \rightarrow \pi^*$ interaction between adjacent carbonyl bonds along the peptide chain.[7,8]

The result of this lack of intramolecular hydrogen bonding is that polyproline peptides are increasingly labile with respect to forming both *cis* and *trans* amide bonds along the peptide chain. Although the PPII structure is the most common and energetically favourable structure adopted by polyproline strands, under certain conditions, a more compact, higher density and higher energy conformational structure can be formed – polyproline I (PPI). In comparison to the PPII conformation, PPI consists of a right-handed helix with all amide bonds along the peptide chain in the cis conformation and dihedral angles (ϕ, ψ) of roughly (-75^0, 160^0). With the exception of similar backbone dihedral angles, the structural properties of PPI are significantly different to those of PPII with PPI being a lot more tightly wound and having a greater density than the PPII conformation (Fig. 2). Leading on from this, the tightly

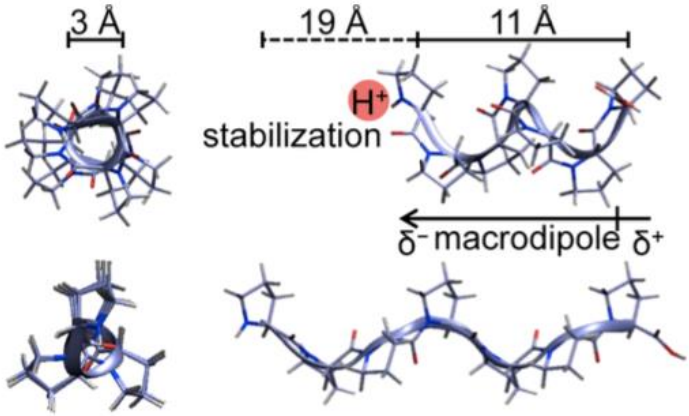

Figure 2 *– Structural comparison of the right-handed, all-cis PPI (top) and left handed, all-trans PPII (bottom) polyproline-7 structure. Dimensions of the macrodipole as well as charge stabilisation are also included.*[10]

folded PPI structure excludes solvent from the peptide backbone and is favoured in low-polarity solvents such as propanol.[10] However, when placed in more polar solvents such as water, methanol or organic acids, all amide bonds flip to a *trans* configuration where the interaction of the backbone carbonyl bonds with the polar solvent stabilises the PPII conformation. This conformational change with *cis* amide bonds switching to *trans* has been shown to occur through two mechanisms: a primary exothermic proton transfer process, proceeding through a PPI-like transition state and a much slower, entropically driven, endothermic conformational change.[10,11] The reverse process moving from *trans* to *cis* amide bonds is however significantly slower and far less energetically favourable with 96% conversion to the PPI configuration requiring 6 days in propanol for longer residue polyprolines.[12]

The structural scope and attractive properties presented by polyproline peptides have allowed such compounds to be utilized in the development of extended framework constructs. Recent work by Renner *et al*. has utilized polyproline peptides as anchors in the development of peptide-based self-assembled monolayers (SAMs)[13] whereby PPII helical peptides are assembled on gold atoms and the kinetics of SAM formation investigated. Further work has employed prolyl peptides as tri-helical macrocyclic scaffolds[14(a)]. This work is particularly interesting and displays the promising supramolecular and biological scope presented by polyproline peptides. The presentation of ligand patterns on the nanoscale at the cell surface is essential in modulating receptor signalling. Employing polyproline scaffolds allows for the precise control and presentation of ligands at the cell surface which is key in the maintenance and manipulation of receptor signalling. Furthermore, extensive recent research has been executed by Wennemers' group[14(b)] whereby the supramolecular applications of prolyl peptides have been highlighted further. The modularity and biocompatibility of peptidic ligands has been exploited in the development of peptide-metal frameworks which are comprised of various metals, connected by helical oligoproline ligands.

Over the years, there have been a variety of approaches attempting to alter and stabilise the confirmational structure of a given peptide, namely: the use of hydrogen bonding and electrostatic forces between side chains at select positions,[15] the use of α,α-disubstituted amino acids,[16] or with the installation of di-sulfide[17] and lactam[18,19] bridges. Following on from this, Grubb's and Blackwell showed that a hydrocarbon cross-link between O-allylserine residues could be "clipped together" with the use of the Grubb's catalyst in a ring-closing metathesis (RCM) reaction (Fig. 4) to induce an α-helical structure.[20] As well as increased helical stability, the chief benefits of employing a hydrocarbon staple are firstly that the aliphatic alkene side-chain increases lipophilicity of the chosen peptide,[21] making the peptide more cell-penetrating. This is a result of the peptide being able to more easily pass through lipid bi layers and transverse the cell membrane. Secondly, utilizing a hydrocarbon staple increases a peptide's protease resistance as

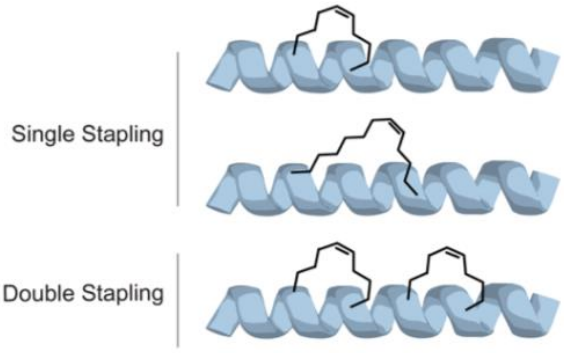

Figure 3 *– (Top + middle) Singly-stapled peptides utilising varying alkene linker lengths. (Bottom) 'Double-stapled' peptide utilising two alkene linker residues.[23]*

a result of the back-bone amide bonds being shielded in the tightly-wound core of the peptide chain and therefore presenting themselves as poor substrates for enzymatic hydrolysis.[22(a)] Interestingly, the versatility of the RCM reaction using the Hoveyda-Grubbs catalysts has been highlighted by recent success of RCM reactions in aqueous conditions.[22(b)] This has been attributed to the marked stability of ruthenium-carbene complexes, where previously dry reaction conditions were pivotal to success. Attachment position, stereochemistry and alkene linker length all affect the induced strain by the linker as well as RCM reaction efficiency. For example, linkers positioned too distantly or in unfavourable positions have shown poor efficiency and minimal cross-linking during RCM reactions.[22(a)] Literature examples also include 'double-stapled peptides' (Fig. 3) in an attempt to further influence conformational structure in longer residue peptides.[23] In light of this, the use of stapled peptides whereby hydrocarbon linkers are attached to amino-acid units at specific positions along the peptide chain, is a promising and attractive method for forming conformationally constrained peptides.

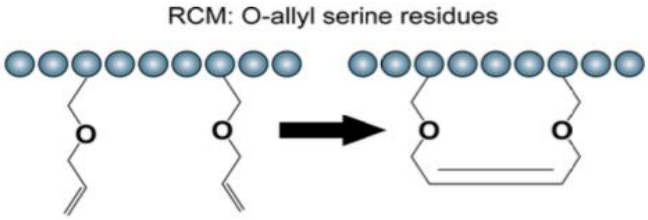

Figure 4 *– Work of Grubbs and Blackwell in the utilization of ruthenium-based olefin metathesis in the installation of macrocyclic all-hydrocarbon cross-linkers onto synthetic peptide chains.[23]*

Monitoring the level of induced structural stability, RCM reaction efficiency and conformational response to aqueous conditions with the staple attached at different points along the peptide chain will allow for the optimum positioning of the staple to be identified. It has been elegantly shown that un-metathesised alkene linker length as well as linker spanning distance play a key role in the efficiency of the RCM reaction as well as the level of induced conformational strain (Fig. 5), with small structural differences yielding drastically different results.[25] The *i and i + 3* residues were initially selected for the linker spanning length as polyproline peptides feature 3 residues per turn. Attaching the linker at these positions therefore results in the linker occupying the same face of the peptide structure, allowing ring-closing metathesis reactions to be carried out with maximum efficiency. An *i, i + 4* linker relationship was also trialled to probe its effectiveness and structural impact, with the results of this study discussed in later sections of this report. One important factor to mention here is that after completing PM6 computational simulations for the stapled basis peptides, it was found that in order for metathesis to be completed successfully, the distance between the C_4 atom on the two linker-functionalized proline units would have to be constrained together to a distance of 6.46 Å. Expected C_4 spatial distances: PPI ~ 6.5 Å, PPII ~ 9 Å.

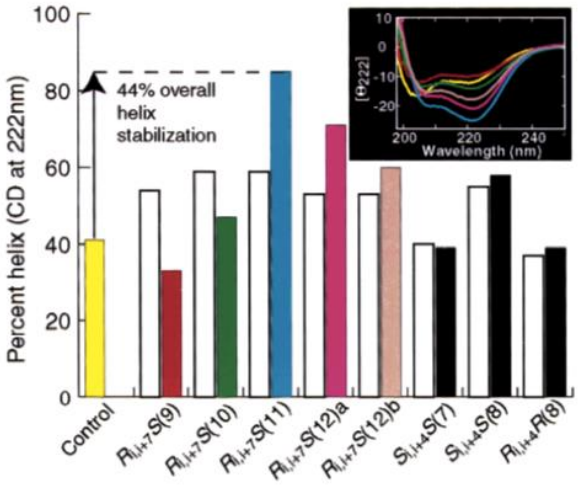

Figure 5 *– Here the importance of hydrocarbon linker length on induced peptide helicity is shown - (from left to right) For alkene linkers positioned at the i, i + 7 positions, RCM reaction efficiency increases up to a carbon unit length of 11, whereby longer unit linkers then constrain the peptide to a lesser extent and a reduction of induced helicity is observed.[25]*

With this knowledge in hand, we set out to investigate the effects of so-called 'hydrocarbon stapling' on the conformational structure of a set of $(Pro)_7$ peptides. It was hoped that a novel secondary structure, differing from both the well-defined PPI and PPII structures, could be developed. This structure would then have the potential to be used as a supramolecular building block in the design of new biomaterials as well as a novel mimetic scaffold, with the latter application being the focus of the second part of this thesis. Non-natural amino acids were synthesised in order to yield a series of stapled polyproline structures. The aim was to characterise these constructs in order to better understand their potential as supramolecular building blocks and mimetics. Furthermore, stapling may lead to locking of a PPI or PPII conformation in aqueous media (Lk-PPI/II) or alternatively the formation of a new conformational structure.

With all of this information in mind, it was set out to implement hydrocarbon stapling into a series of short polyproline peptides, firstly to evaluate the propensity of hydrocarbon stapling and its effects on conformational structure within a group of prolyl peptides. This would be carried out using a set of preliminary non-functionalised $(Pro)_7$ peptides as a basis, with a single hydrocarbon staple spanning the *i, i + 3* positions (Fig. 6) at varying locations along the peptide chain. Initially, the alkene linker fragment was tethered at the 4-position of the proline ring (Fig. 6) whilst analysing the structural effects of stapling. The 4-position was selected based on success experienced in previous work by the group as well as the 4-position presenting itself as a remarkably facile route of attachment in comparison to functionalization at the 3 or 5 positions.

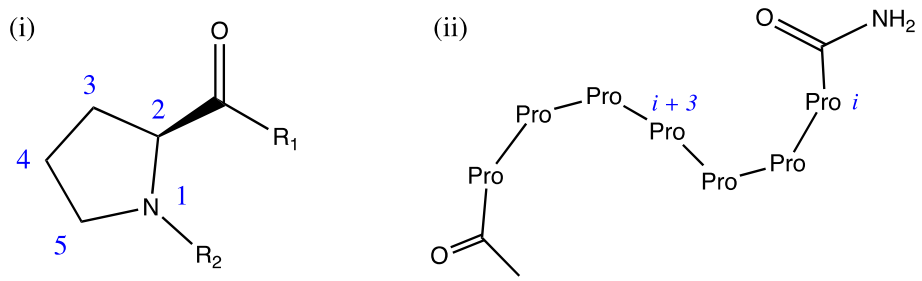

Figure 6 *– (i) The proline ring numbering convention used when referring to hydrocarbon linker attachment position. (ii) Simplified polyproline-7 peptide with the i, i + 3 residue linker spanning length indicated in blue. (Peptide shown post-cleavage from resin and capped with acetyl group at the N-terminus).*

Additionally, functionalization at the 4 position offers only small influence on the steric energy of the peptide, and therefore any conformational change observed can be solely attributed to the constraint imposed by the staple and not any steric stabilisation/destabilisation presented by the linker.

1.0.1 Conformational Probing Techniques

There are various analytical techniques that present themselves as suitable methods for the analysis of polyproline conformational structure. Firstly, NMR spectroscopy is a useful technique for monitoring the progress of RCM and hydrogenation reactions. The appearance and disappearance of specific peaks provides an indication of the progress of metathesis and hydrogenation respectively. In addition

to this, NMR methods have proven useful in the conformational analysis of a range of different residue length prolyl peptides.[30]

HPLC/LCMS methods are not only key in the purification and characterization of the polyproline peptides but can also be utilized to monitor the progress of RCM and hydrogenation reactions, providing a rough idea of the conformational structure present in a given sample. Again, the appearance of new peaks and disappearance of starting material peaks on the UV chromatogram will provide an indication of the number as well as type of conformational structures present in a given sample.

One method able to provide conformation-specific data regarding a polyproline sample is circular dichroism (CD) analysis, with clear differences in spectra being produced by PPI and PPII structures (Fig. 7(a)). PPII structures present a minima ≈204 nm and a maxima ≈225 nm in comparison to PPI structures which present a shallower minima ≈198 nm and a notably sharper maxima ≈212 nm, accompanied by a small negative band ≈230 nm. This shift in data has been well documented for polyproline peptides, 10 residues and longer.[26,27,28]

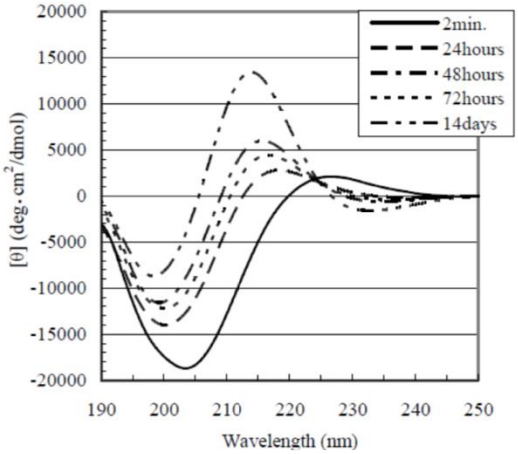

Figure 7(a) *– Circular dichroism (CD) spectra of a polyproline-13 peptide in propan-1-ol at 5 ^{0}C illustrating the change from PPII to PPI with time, accompanied by a shift in data with maxima and minima of each data set shifting to lower wavelengths.[29]*

A second method that has previously been utilized to monitor the shift from PPII to PPI conformational structure is Fourier-transform-infra-red (FT-IR) spectroscopy.[30] This technique probes the wavenumber exhibited by the amide carbonyl bond of the polyproline backbone with PPII structures exhibiting an amide C=O stretching band at 1623 cm^{-1} and PPI structures exhibiting this band at 1635 cm^{-1}. A transitional band ≈1651 cm^{-1} may also be observed which suggests the presence of an intermediate form of structure with both PPI and PPII structures being present.

Finally, recent years have seen an increased use of ion-mobility mass-spectrometry (IM-MS) in the analysis of biomolecular structures[31] with the technique's ability to probe the conformational structure of a polyproline peptide.[11] Clemmer *et al*. have made use of this technique to identify the mechanism of conversion between the PPI and PPII structures as well as identify various intermediates which form during this transition. More specifically, the PPII to PPI conversion occurs *via* a drastically different mechanism to that of its reverse process and that early on, the PPII population splits into various

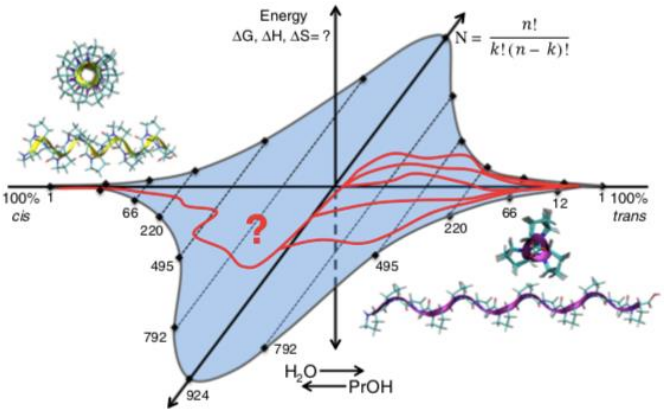

Figure 7(b) *– Energy landscape showing the solvent response of a polyproline-13 peptide and the corresponding energetic pathways for interconversion between PPI and PPII conformational structures.[11(b)]*

different pathways which go on to converge through a later intermediate to form the PPI helix (Fig. 7(b)). Access to this knowledge helps us better understand the transitions between PPI and PPII structures as well as allow us to fine tune the synthesis of peptides in an attempt to avoid a specific transition.

Collectively, the effectiveness of hydrocarbon stapling in the locking and stabilisation of polyproline secondary structures would be investigated, whereby linker positioning and spanning distance would be altered in an attempt to probe a range of structural conditions. Should stapling prove effective in the locking of a specific conformational structure, the opportunity to develop a novel polyproline scaffold with biological and supramolecular applications would arise. Along-side this study and in accordance with the results obtained, a range of cyclic mimetic peptides would be developed.

1.1 Results and discussion

1.1.0 Construction of the stapled polyproline-7 basis peptides

Work began synthesising the functionalized basis polyproline-7 peptides with the hydrocarbon linker fragment tethered to different positions along the peptide chain. Prior to construction of the prolyl peptide, the non-natural functionalized proline linker residue (**1.1**) was first synthesised as shown in **Fig. 8**. As discussed in detail in section **1.0**, the alkene linker to be stapled during later RCM reactions was attached at the 4-position of the proline ring (Fig. 6).

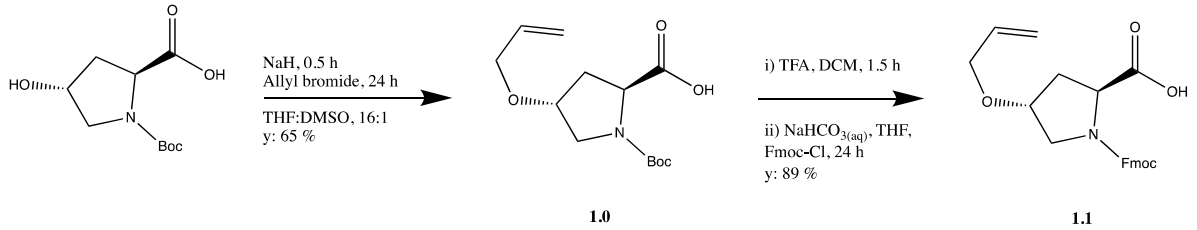

1.0 **1.1**

Figure 8 *- Synthesis of the 4-positioned, functionalized proline monomer*

The first step towards the synthesis of compound **1.1** involved a basic alkylation of the hydroxyl group to yield compound **1.0**. This step was carried out successfully with DMSO successfully solvating the carboxy-anion group to protect it from electrophilic attack and subsequent alkylation.[32] Alkylation at this carboxy-anion would have resulted in additional reaction steps being required (ester hydrolysis) as well as a reduced yield of the desired product (**1.0**). Work by Mihali *et al*. highlight the importance of a 16:1 THF:DMSO solvent ratio in the success of such reactions and so this solvent ratio was utilized in our reaction. After work-up and extraction, ^{1}H and ^{13}C NMR spectra (appendix 1.0) produced by the crude yellow oil evidenced a successful alkylation with the appearance of a doublet of triplets centred at 5.9 ppm and a double doublet, centred at 5.2 ppm, representative of the three alkene proton environments present on the staple side-chain. Further purification was therefore not required and the crude product carried forward to the next synthetic step.

The second and final step required to construct compound **1.1** involved removal of the boc-protecting group followed by re-protection of the secondary amine with an Fmoc protecting group. The Fmoc-

protected proline monomer is required for solid phase peptide synthesis (SPPS). After an acidic work-up, compound **1.1** was isolated in 89 % yield with the final off-white oil offering the desired peaks in ^{1}H and ^{13}C NMR analysis (appendix 1.1). A full disappearance of peaks around the 1.4 ppm region suggests complete removal of the Boc protecting group as well as the emergence of a series of multiplets with the correct integrations in the 7-8 ppm region, evidencing the presence of the Fmoc protecting group. Further purification was therefore not carried out, with the final product being carried forward for use in SPPS.

Once the 4-position staple proline monomer (**1.1)** had been successfully synthesised, it was implemented into the construction of three basis functionalized polyproline-7 peptides. These three peptides were probed to study the effectiveness of hydrocarbon stapling on the level of induced conformational helicity in a polyproline-7 peptide. The three functionalized polyproline-7 peptides differed by their positioning of hydrocarbon staple monomers with each of the structures being shown in **Fig. 9.** A cartoon-like diagram is also included beneath each peptide, which shows the periodicity and how the hydrocarbon staple will be attached to proline residues occupying the same face of the helical structure. This is to enable the most efficient RCM reactions to occur as well as to provide the linker fragment with the greatest chance of constraining the proline chain.

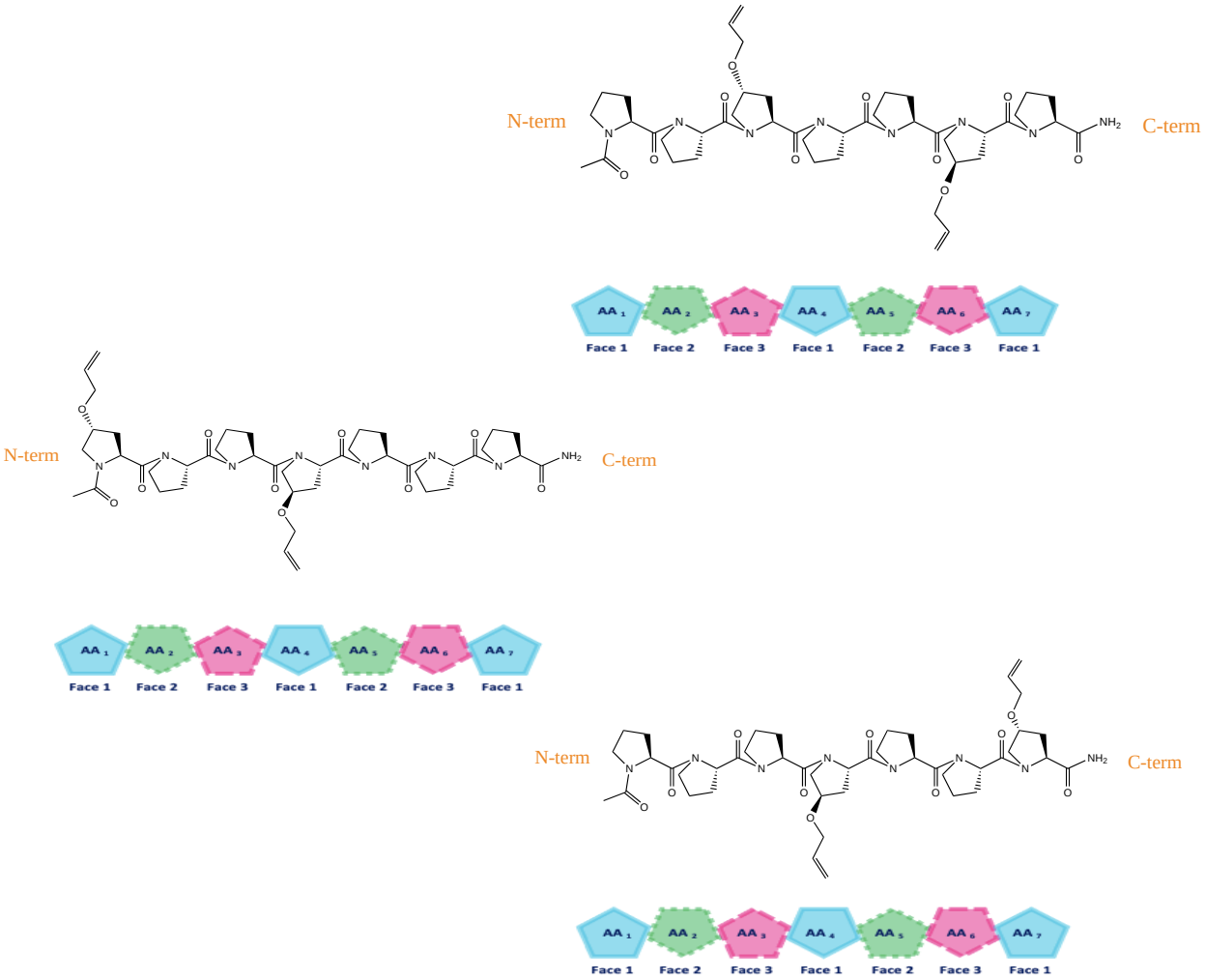

Figure 9 *- Molecular structures of each of the three basis peptides – with the hydrocarbon staple attached in the middle of the proline chain (top), to residues at the N-terminus (middle) and finally to residues at the C-terminus (bottom). Cartoon diagrams are also displayed below each structure to indicate the periodicity of each peptide.*

Following the *i, i + 3* linker spanning distance protocol discussed in section **1.0** of this report, the three peptides constructed had their respective hydrocarbon linkers tethered to residues at the C-terminus of the peptide, N-terminus residues and middle of the peptide chain. Analysing the effectiveness of stapling and the level of induced helicity with the staple fragment spanning different sections of the peptide chain allowed for the identification of an optimum position of linker attachment. Obtaining this information would be of great value when implementing stapling into the final mimetic peptide, whereby the position and length of linker attachment can be considered of great importance. The process involved with synthesising the functionalized polyproline-7 peptides is summarised in **Fig. 10**.

A CEM Liberty-Lite peptide synthesiser was used to synthesise each of the peptides, with all being synthesised using rink amide MBHA resin (100-200 mesh, loading = 0.336 mmol/g) on a 0.1 mmol scale. Prior to being placed on the peptide synthesis apparatus, the resin was left to swell in DCM for 0.5 h with the rest of the reagents placed on the apparatus and consumed by the machine as needed. **Fig. 11** below shows the quantities of reagents used, as well as reaction times for each step.

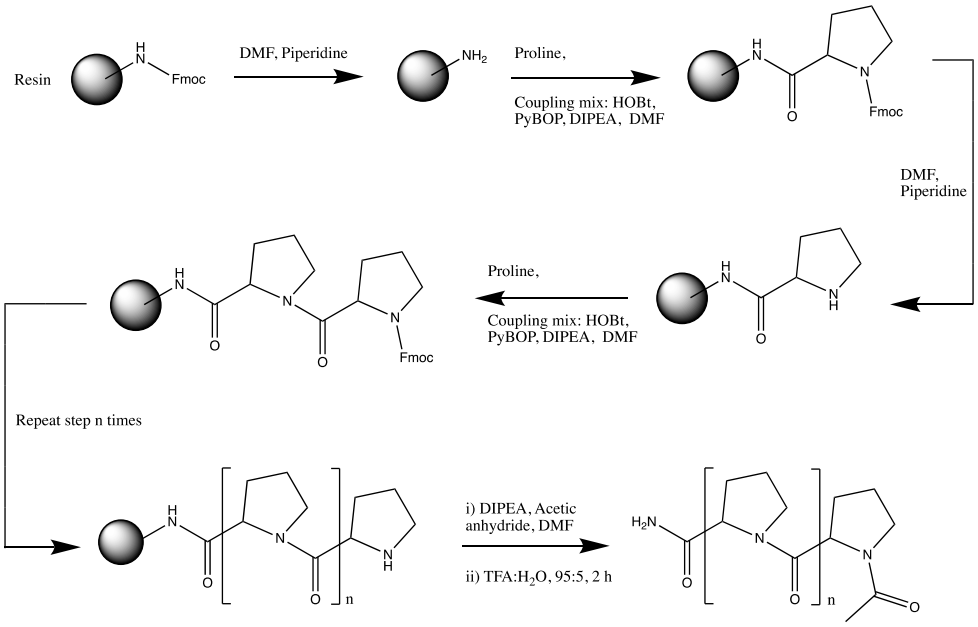

Figure 10 *- SPPS procedure used for the construction of the staple-functionalized polyproline-7 basis peptides.*

Procedure	Compound	Quantity	Reaction time
Resin swelling	DCM	Cover resin	0.5 h
Deprotection	DMF:Piperidine, 8:2	3 ml	0.5 h
Coupling	DIC	2.5 eq	20 mins
	Oxyma	2.5 eq	
	Amino acid	2 eq	
	DMF	2 ml	
Capping	DIPEA	2.5 eq	20 mins
	Acetic anhydride	10 eq	
	DMF	100 eq	
Resin cleavage	TFA:DCM, 95:5	5 ml	1.5 h

Figure 11 – *A summary of the reagents used and their quantities during SPPS on the CEM peptide synthesiser.*

A preliminary run using 2 equivalents of the amino acid per coupling proved successful with the desired peptide being isolated in high yields. Two equivalents of amino acid were therefore used throughout the SPPS procedure for all three basis peptides. The method used to construct the peptides also included a capping step after the first amino acid coupling to ensure any un-reacted, free amines exposed on the surface of the resin were acetylated and did not take part in future couplings. These couplings would have resulted in the generation of unwanted shorter-chain peptides during following coupling steps, reducing reaction yield and requiring additional purification steps. In addition to this, as we did not intend to carry the constructed polyproline-7 peptides forward for any additional coupling procedures, a final de-protection and capping step was added to acetylate the free secondary amine of the 7th residue (N-terminus). Once removed from the apparatus, the crude peptide was washed multiple times with DCM to remove any residual DMF before being cleaved from the resin using a TFA:H_2O (95:5) cleavage cocktail for 2 h. After removing the TFA under reduced pressure, the peptide was precipitated, centrifuged and washed three times with di-ethyl ether before being characterised.

HPLC and LCMS analysis was carried out on each of the obtained peptides and showed that synthesis of all three basis peptides had been successful. Clean HPLC spectra were observed accompanied by the correct molecular weight (m/z = 851.02) dominating all of the LCMS spectra. In light of these results, all three peptides were carried forward for RCM reactions without further purification.

1.1.1 RCM reactions of the open chain, basis peptides (See figure 4 for schematic)

The three basis peptides were next subjected to a RCM transformation whereby the two alkene linker chains would be ‘stapled together’ and an 18-atom macrocyclic structure would be formed connecting two parts of the helical structure. RCM reactions were carried out in anhydrous DCM, under an inert atmosphere and using the Hoveyda-Grubbs 2nd generation catalyst after previous work by the group had identified these to be the optimum reaction conditions.[31] The choice of catalyst for RCM reactions is also of great importance. Previous work conducted by the group has compared the effectiveness of the Hoveyda-Grubbs 2nd generation and the Grubbs 3rd generation catalyst.[33] The 2nd generation Hoveyda-Grubbs catalyst proved significantly more successful in the catalysis of this type of RCM reaction compared with the 3rd generation Grubbs catalyst. In light of this, the Hoveyda-Grubbs 2nd generation catalyst was used to avoid wastage of starting materials and expensive catalyst. Finally, it is desirable to perform RCM reactions on resin-bound peptides where possible to reduce cross-metathesis, however, this commonly requires the employment of large quantities of catalyst (up to 50 mol%)[22(b),34] and makes the reaction only economically viable on a very small scale. In light of this, RCM reactions were carried out on isolated peptides after they had been cleaved from the resin.
DCM is however a highly volatile solvent, so very small reaction vessels (5 ml r.b flasks) were used for the reactions and sealed with septums/laboratory film in an attempt to limit solvent evaporation.

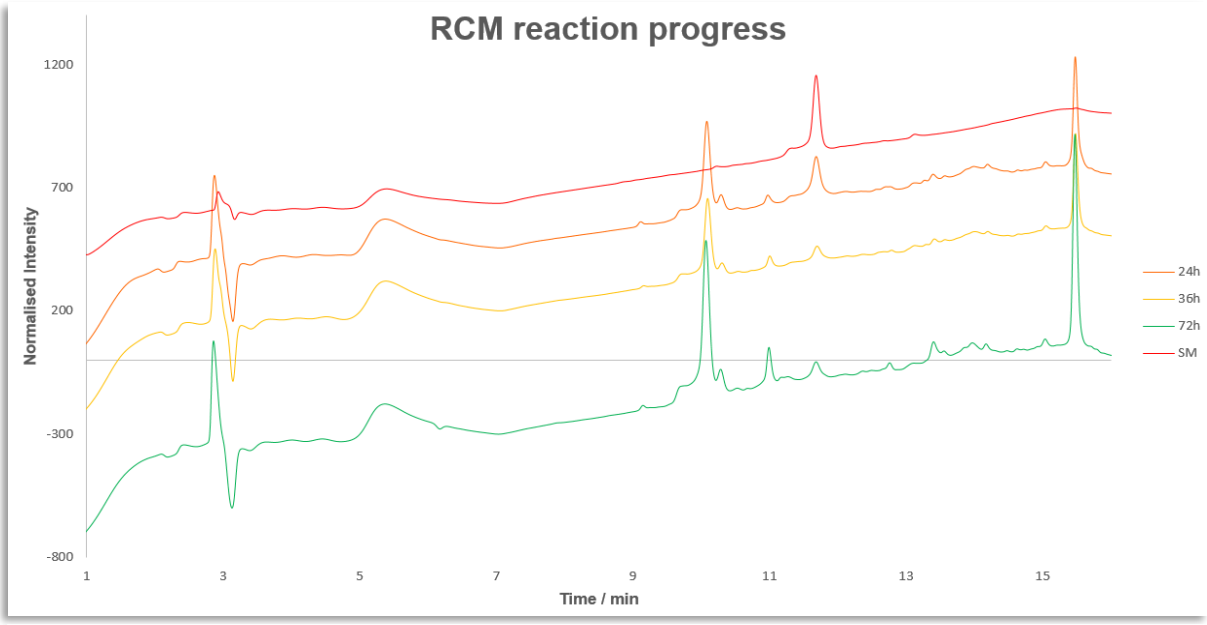

Figure 12(a) *– Reverse phase analytical HPLC UV chromatogram (225 nm) showing the progress of a generic RCM reaction (C-terminus functionalized peptide used as an example) after 24 h (orange), 48 h (yellow), and 72 h (green) with the emergence of a number of new peaks.*

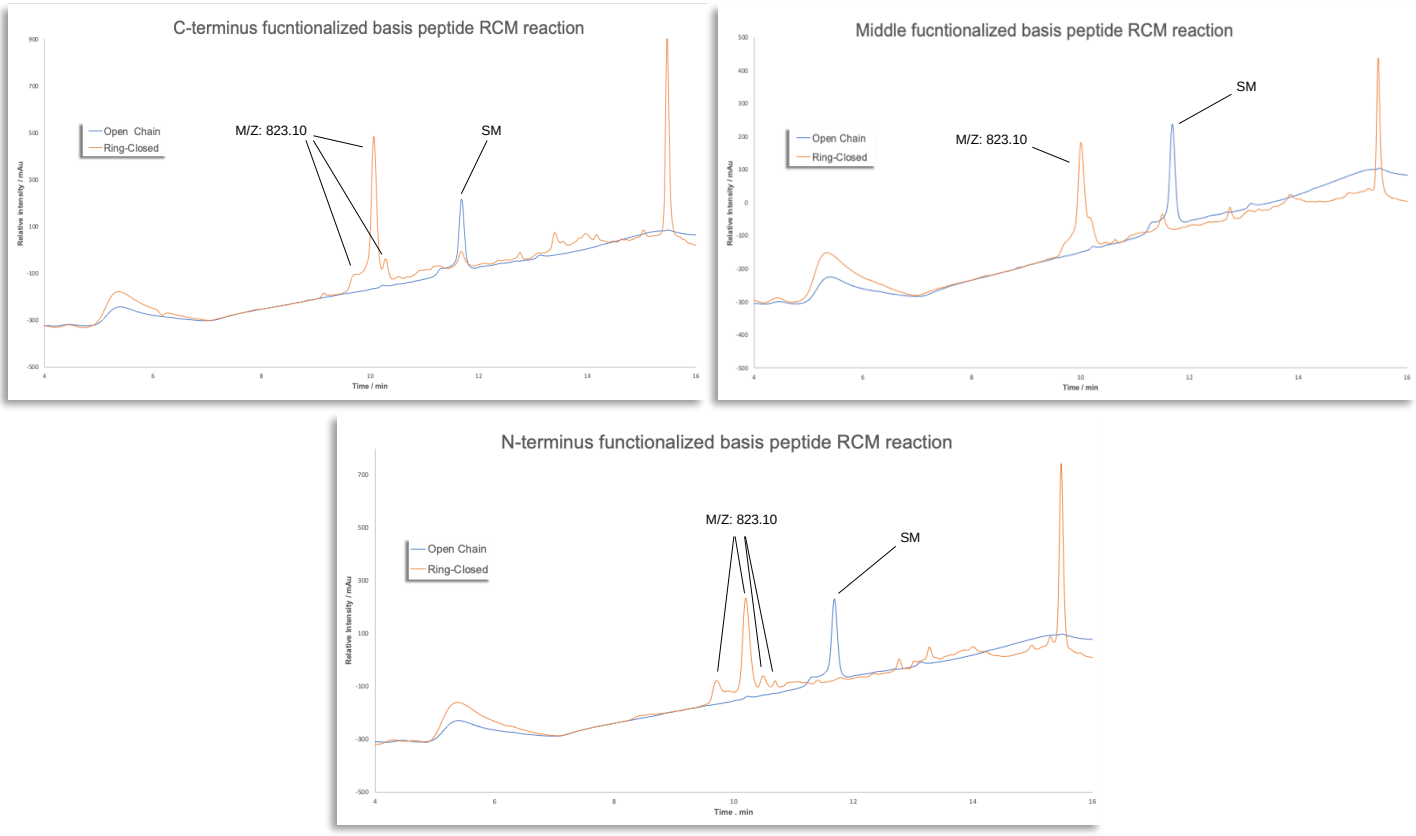

Figure 12(b) *– Reverse phase analytical HPLC UV chromatograms (225 nm) exhibited by the RCM reactions of the C-terminus (top left), middle (top right) and N-terminus (bottom) functionalized basis peptides. Reaction progress after 48 h is shown in orange with starting material indicated in blue for reference.*

Fig. 12(a) displays the 225 nm UV trace for a generic RCM reaction and provides a model of overall progression of an RCM reaction with time. The disappearance of the starting material peak is

accompanied by the formation of a range of new peaks, constituting both the ring-closed peptide and reaction side products. This is clearly shown moving from the red trace through to the green trace exhibited by **Fig. 12(a)**. Moreover, **Fig. 12(b)** shows the reversed-phase HPLC 225 nm UV chromatograms exhibited by each of the three basis peptides upon 48 h of subjection to RCM. The 225 nm trace exhibited by the open chain starting material is also displayed on each graph for reference. From **Fig. 12(b)**, a number of observations can be made. With disappearance of the starting material peaks, all three reactions were complete after 48 h of reaction time and exploiting a 10% w:w catalyst loading. The spectra produced by the middle functionalized peptide shows one major product peak with retention time of 10.0 mins. This peak is then accompanied by what appears to be two shoulder peaks either side of the main peak. The C-terminus functionalized peptide exhibits a somewhat similar trace to that of the middle-functionalized peptide, however with these shouldering peaks either side of the dominant product peak intensified slightly. These shoulder peaks suggest possible presence of conformational isomers of the stapled peptide due to their very similar retention times. With regards to the N-terminus functionalized peptide, a different distribution of product peaks is observed. 4 main peaks are observed between the 9.50 – 10.75 mins region. As was touched upon when discussing the C-terminus functionalized peptide, these 4 peaks were thought to constitute a range of conformational isomers of the stapled peptide. 4 peaks makes sense when one considers that two isomers should be formed as a result of cis/trans isomerism of the linker alkene bond and a further two conformational isomers are expected to be produced by PPI/PPII conformational variation. Each of the three basis peptides would next be subjected to hydrogenation in an attempt to remove any E/Z isomerism present and reduce the number of peaks produced by each peptide to two or even 1. One notable observation made when analysing all of the UV chromatograms obtained, was the emergence of a sharp peak with a retention time of around 10.9 mins. From LCMS data, this peak constituted an M/Z = 307.1 which after careful consideration was attributed to a compound known as 1,3-dimesitylimidazol-2-ylidene, or the IMes ligand as it is more commonly known. This compound is a heterocyclic ligand, thought to be a degradation product of the Hoveyda Grubbs 2nd generation catalyst. More specifically, the 10.9 min retention time peak seemed to grow significantly when reactions dried overnight and subsequently a brown ‘cake’ was left in the reaction flask. Upon obtaining poor yields of the desired peptide product peak, it was thought that the high concentration of RCM reactions being carried out was leading to intermolecular metathesis reactions, and subsequent formation of dimers/trimers/extended structures etc. In an attempt to obtain a greater product yield and avoid material loss via intermolecular side-reactions, the original reaction concentration of 166 mM was diluted to 33 mM. With the exception of an increased reaction time, this change proved highly successful with a significantly smaller peak at 10.9 min relative to the product peak being observed, as well as a far greater yield being retained after preparative HPLC.

LCMS analysis of each of the RCM reactions confirmed successful conversion to the desired products. Both the major peak and shoulders produced by the C-terminus and middle functionalized peptides as well as all four suspected product peaks from the N-terminal peptide constituted the desired mass (M/Z = 823.10). This was a promising result as it signified that the hydrocarbon staple fragments could be

placed at multiple positions along a prolyl peptide chain and that furthering this, RCM reactions could be carried out on these peptides to form hydrocarbon linkers within each of the peptides.

In addition to the use of HPLC in the monitoring of the RCM reaction, ^{1}H NMR was also utilised. The disappearance and emergence of characteristic peaks on ^{1}H NMR spectra is a useful tool for monitoring the progress of the RCM reaction and is shown in **Fig. 13** below.

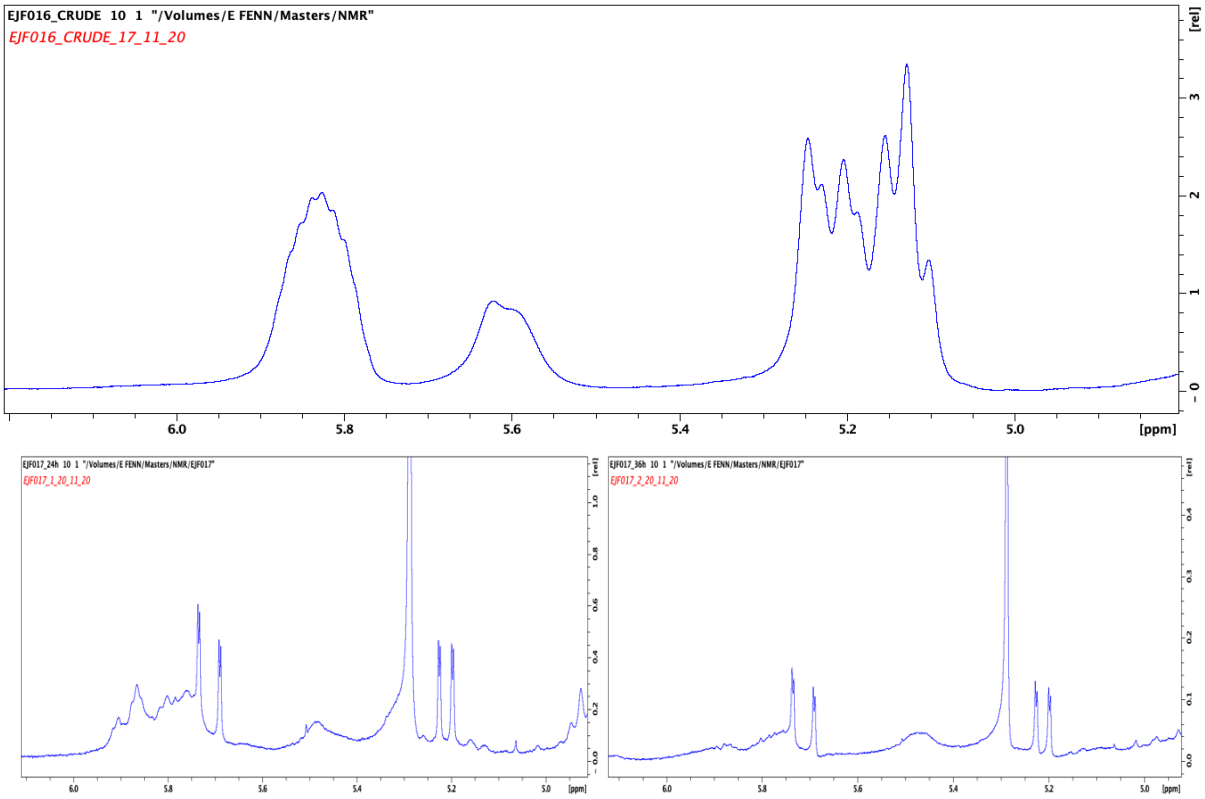

Figure 13 *– ^{1}H NMR 5 – 6 ppm region showing the N-terminus functionalized open chain peptide (top) and the progress of the RCM reaction after 24 h (bottom left) and 36 h (bottom right). Notice the gradual disappearance of the peaks at ≈5.2 ppm and ≈5.85 ppm and the formation of the two double-doublets in their place. (Sharp singlet at 5.3 ppm produced by DCM – reaction solvent).*

From the ^{1}H NMR spectra of the N-terminus functionalized RCM reaction shown in **Fig. 13**, the two peaks situated at ≈5.2 ppm and ≈5.85 ppm slowly reduce in size to almost disappearance over the course of 36 h, with these two peaks being known to represent the three protons situated on the free alkene linker chain. The emergence of a set of sharp double-doublets is characteristic of the RCM mechanism whereby the two alkene side chains are ‘clicked together’ to form the macro-cyclic stapled peptide and is clearly evident in the lower two spectra of **Fig. 13**.

1.1.2 Hydrogenation of the staple alkene bond

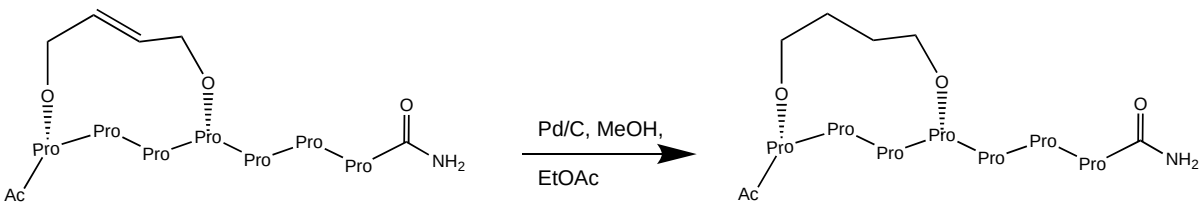

Figure 14 *– The use of palladium/carbon in the hydrogenation of the linker alkene double bond. N-terminus functionalized peptide shown as a generic example.*

The alkene bond located on the hydrocarbon linker chain introduces the minor complication of E/Z isomerism into analysis of the ring-closed peptides. Previous work by the group has identified that four HPLC peaks can be produced as a result of alkene bond *cis/trans* isomerism. This information is however only known for the N-terminus functionalized peptide with the work of this report being the first investigation into a C-terminus and middle-positioned hydrocarbon linker. With this in mind, the hydrocarbon linker fragments were hydrogenated following RCM reactions in an attempt to remove any E/Z isomerism and make characterisation of the final structures simpler. This was carried out using palladium carbon (Pd/C) and hydrogen gas overnight, with the reduced double bond structure later being filtered to remove residual Pd/C and concentrated under reduced pressure.

The linker alkene bond contained within all three of the basis peptides was successfully hydrogenated with LCMS analysis showing the desired mass (m/z = 825.10) for each of the peptides. As indicated in **Fig. 15** below, both the C-terminus and middle functionalized peptides offered similar UV chromatograms to that produced after RCM transformation. The N-terminus functionalized peptide however now featured two product peaks pertaining to the correct molecular mass. As previously discussed, this was an expected result with E/Z isomerism likely being removed during hydrogenation. The two product peaks were therefore suggested to represent two conformational isomers present within the sample. With confirmation of the desired stapled, reduced peptides, purification was begun whereby residual catalyst would be removed from the crude reaction mixture. After dissolving each of the crude peptides in MeOH:H_2O, 4:6, v:v, the solutions were centrifuged and filtered whereby a small mass of dark brown solid was retained from each of the solutions. **Fig. 15** below shows the UV chromatogram (225 nm) produced by each of the three basis peptides after hydrogenation.

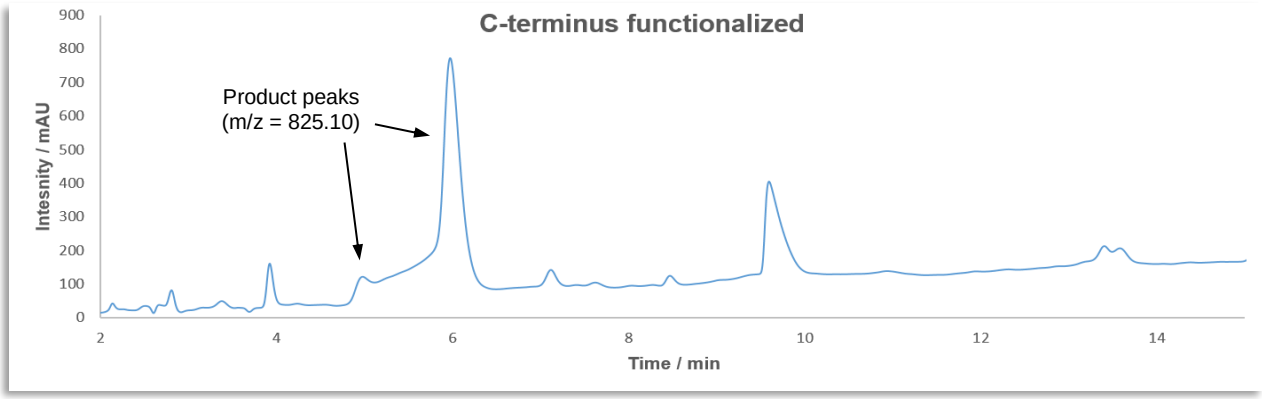

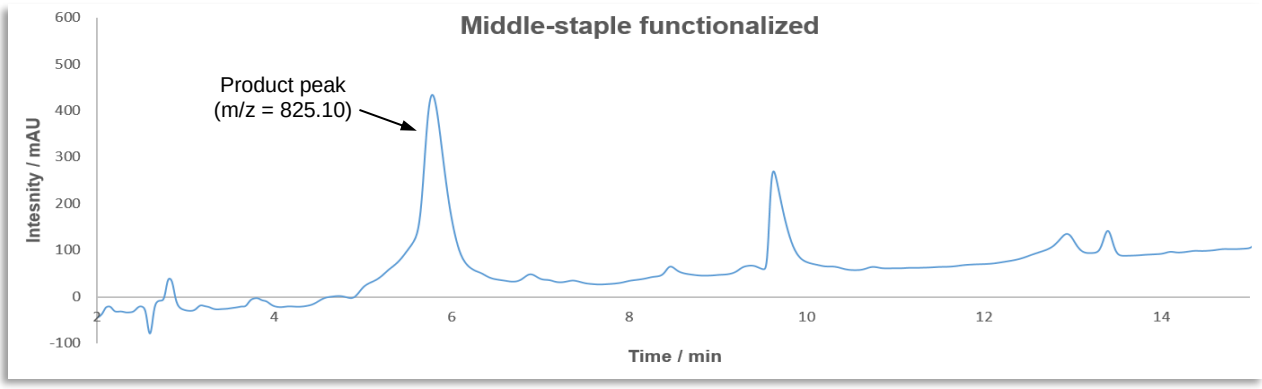

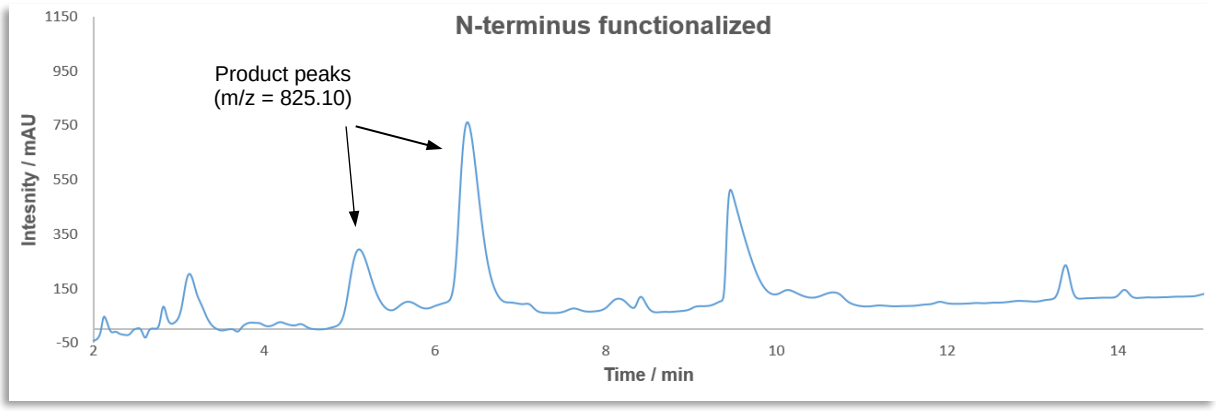

Figure 15 *– Reverse-phase HPLC UV chromatogram (225 nm) of the hydrogenated basis peptides with staple attached at the C-terminus (top), middle (middle) and N-terminus (bottom).*

Looking deeper into each of the UV chromatograms produced, in addition to the IMes impurity peak with a retention time of 9.8 min, both the C-terminus and N-terminus stapled peptides appear to show one dominant product peak with a retention time of around 6.0 mins, accompanied by a smaller peak eluting the column around one minute before this major peak. Although this shoulder can be considered more significant for the C-terminus stapled peptide as a pose to its middle stapled counterpart, when compared to the N-terminus stapled peptide, this peak becomes a more defined and all-together more significant peak. From the total ion chromatogram, both the major and minor peaks produced by the C and N-terminus stapled peptides constituted the correct molecular weight and so both peaks would be purified during product isolation. With this knowledge in hand, it is thought that a mixture of conformational isomers were present within the N and C-terminus functionalized peptide samples. Both peaks were isolated and analysed, however the somewhat tidier single peak offered by the middle-staple peptide was thought to be 'mono-conformational' and preliminarily attracted interest as a possible stapling location for the mimetic peptide.

Following hydrogenation of the three peptides' staple alkene bonds, purification was required so that the conformational structure of the three peptides synthesised could be determined. In order to do this, preparatory HPLC was utilized, whereby the major product peaks from each of the three chromatograms shown in **Fig. 15** were isolated. The purification method involved the use of an Agilent C18 25x10mm, 5 μm column and consisted of a 12 minute gradient elution, rising from 40% to 65% MeOH at a flow rate of 4.3 ml/min. Prep-HPLC purification proved successful in isolating the desired peaks for all three of the basis peptides, with all being obtained in generous yields. One major peak was retained during purification of the middle-stapled peptide whilst the major and minor peaks were isolated for the C and N-terminus functionalized peptides. All retained peaks were analysed and found to be pure and contain the desired molecular weight (m/z = 825.10) after LCMS.

1.2 Structural analysis and characterization of the isolated basis peptides

1.2.1 CD analysis

A number of analytical techniques were used to probe the structural characteristics of each sample. As explained in greater detail in section **1.0** of this report, FT-IR and CD are two techniques which present themselves as useful tools for the probing of polyproline conformational structures. Diffusion-ordered spectroscopy (DOSY) NMR was also utilized as an additional conformational probe.

With regards to CD studies, measurements of the open chain, un-metathesised peptides were taken in both EtOH and H_2O to provide a foundation of data to which the final stapled peptide products could be compared to. For reference, all water and ethanol samples were left to equilibrate for 7 days before measurements were taken. Comparing the CD spectra of the open chain and ring-closed peptides would therefore provide a strong indication of the level of helicity induced by placing the linker at each position of the proline chain. **Fig. 16** below displays a comparison between the CD spectra of the three open-chain peptides in both ethanol and water, with the CD spectra produced by the respective ring-closed derivatives overlaid for each peptide.

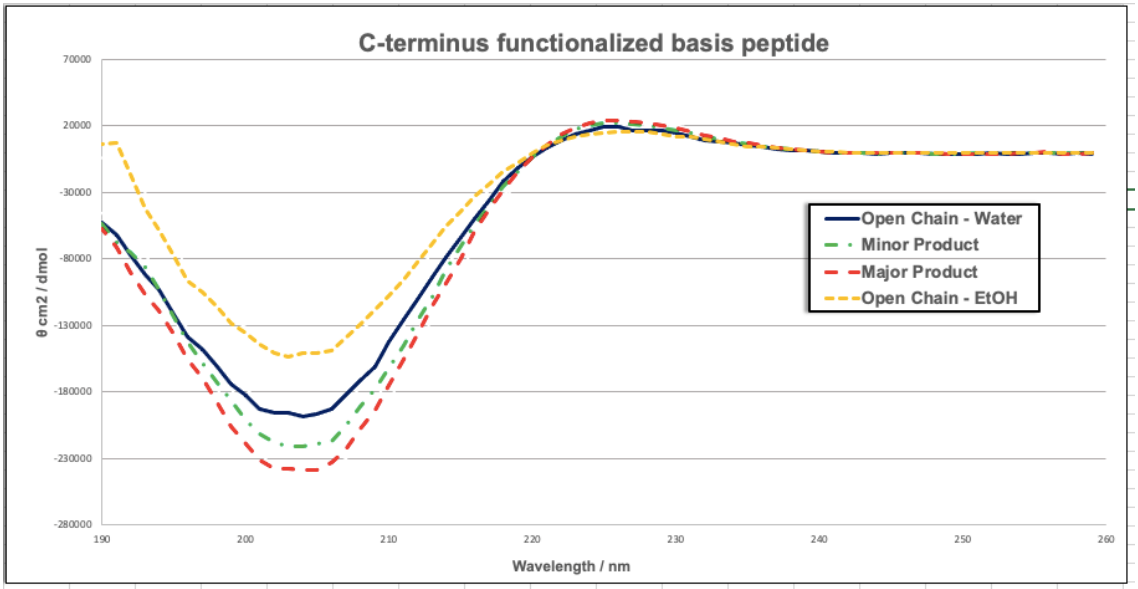

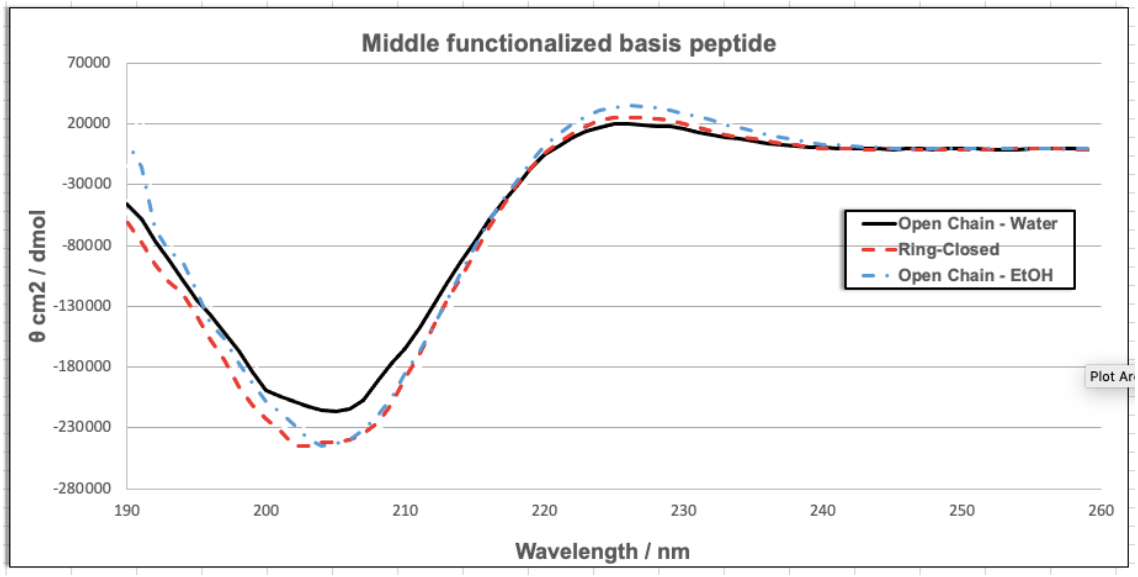

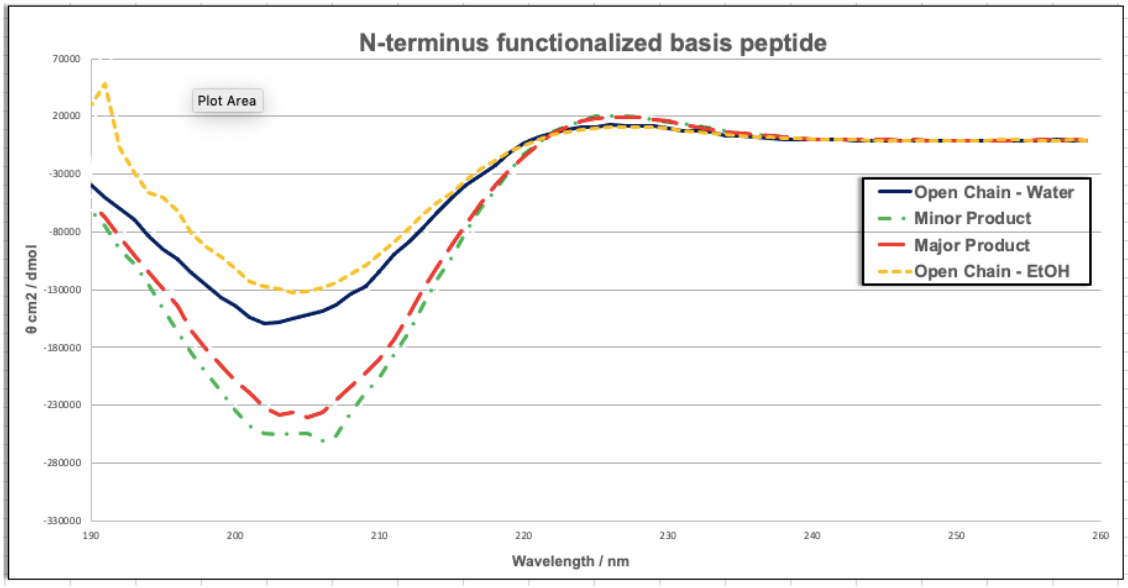

Figure 16 *– CD spectra produced by the open chain basis peptides in both H_2O and EtOH. The respective ring-closed derivatives are then overlaid on top of each basis peptide for comparison: (top) – C-terminus functionalised, (middle) – middle functionalised, (bottom) – N-terminus functionalised.*

From **Fig. 16**, with the exception of an intensity shift for the C-terminus peptide, it can be seen that all peptides seemingly adopt a similar conformational structure in both ethanol and water in their open chain form. A stronger intensity minima centred at 205 nm and a weaker intensity maxima centred at 226 nm can be seen for all three open-chain peptides both in water and ethanol, which is characteristic of a PPII-like structure. Following **Fig. 15,** both the major and minor peaks for the C- and N-terminal functionalized peptides displaying the desired molecular weight were isolated during prep-HPLC and subjected to CD analysis. All ring-closed peptides analysed presented a deepening of the minima at 205 nm in comparison to their open-chain form with the minor products retained after purification of the C and N-terminus functionalized derivatives offering very similar peak profiles and intensities as the major product peak profiles. This deepening of intensity of the 205 nm minima was an unexpected result, and when considering the predicted induced strain and inter-atomic distances discussed previously in this report, the peak profiles produced suggest the formation of a novel conformational structure. This also alludes to the idea that some form of distorted/bent hybrid intermediate structure is present within the peptides which is yet to be characterized. This idea is also re-enforced by the 226 nm maxima which remains un-altered moving from open to ring-closed structure. Furthermore, an additional possibility is that the strain introduced by the linker may be simply locking the peptides in a novel conformation as a pose to a PPII to PPI switch which was initially predicted. This will therefore lead to an increase in conformational stability and unlock the potential to develop a new class of peptide scaffolds with possible biological applications.

Another possible explanation for the results observed could be attributed to the presence of an R-stereo centre at the proline C_4 position. It has been well documented that installing an electron withdrawing group at the 4R position of the proline ring leads to a puckering of the pyrrolidine ring, which subsequently favours a *trans* configuration of the backbone amide bond[35]. This is the result of a favourable $n \rightarrow \pi^*$interaction within the C_4 – O bond. With the alkenyloxy linker fragment occupying the

4R position, it is possible that the electron withdrawing nature of the group is leading to puckering of the proline ring, subsequent *trans* amide bond formation and a PPII conformation. Furthering this, upon completing RCM, this PPII conformation may become locked and stabilised further by joining the two linker fragments.

1.2.2 FT-IR analysis

With the possibility of a novel secondary structure being present within the stapled peptides, Further analysis was carried out, whereby other analytical techniques were used as tools in the probing of conformational structure. One such technique used was FT-IR analysis. The FT-IR spectra obtained for the three open chain peptides as well as their ring-closed counterparts is displayed in **Fig. 17** below.

As was the case with the previously discussed CD analysis, open chain samples were left to equilibrate in EtOH or H_2O for 7 days prior to being analysed.

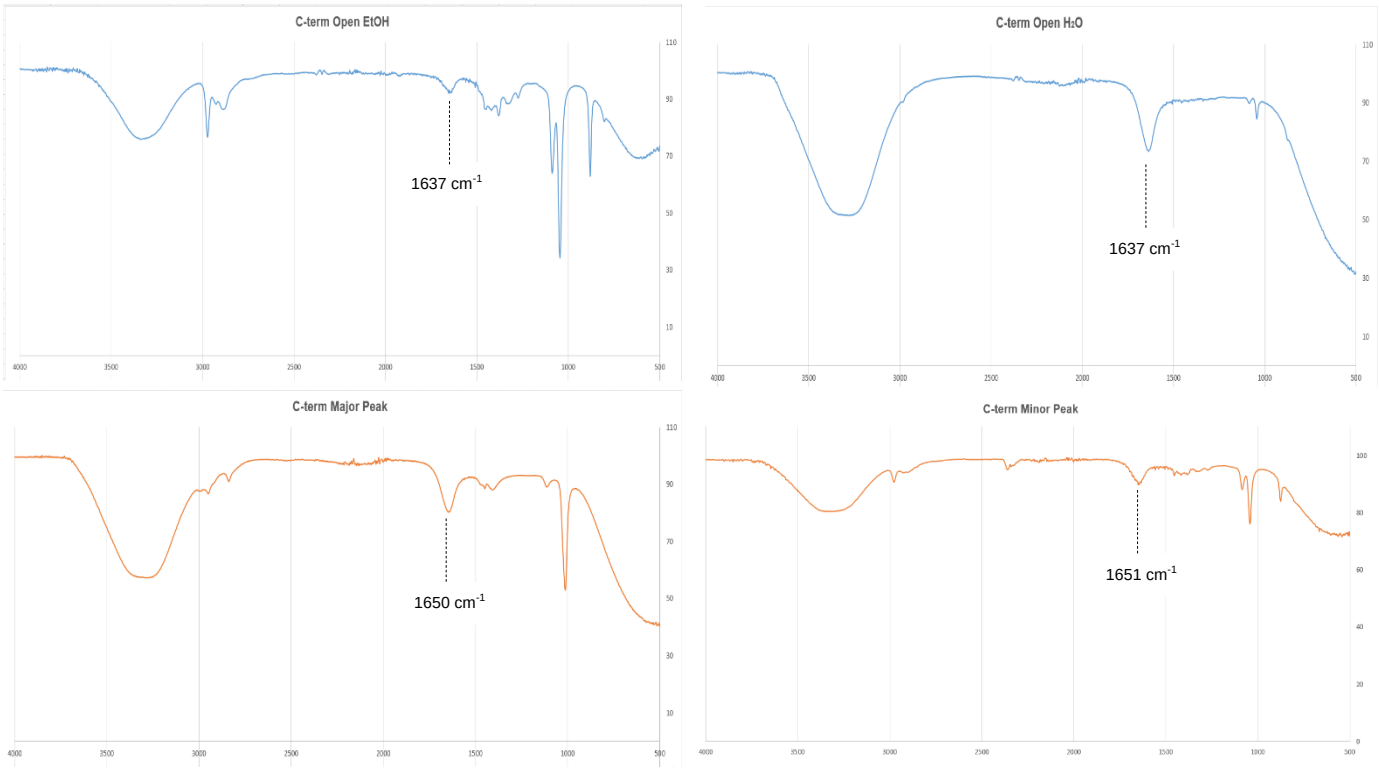

Figure 17(a) *– FT-IR spectra obtained for the C-terminus functionalised basis peptide. Top left – open chain in EtOH, top right – Open chain in H_2O, bottom left – ring-closed major isolated peak in H_2O, bottom right – ring-closed minor isolated peak in H_2O. Wavenumbers for carbonyl peaks are also included for each sample.*

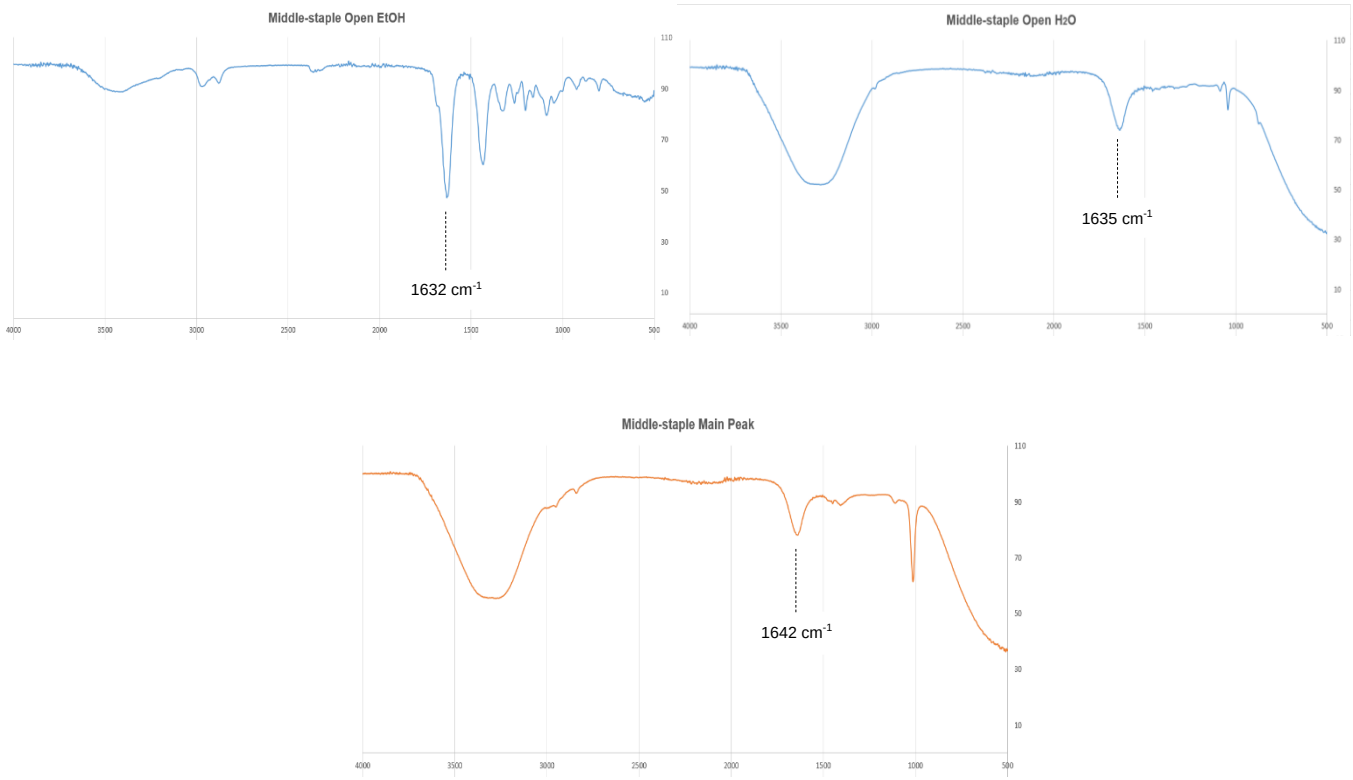

Figure 17(b) *– FT-IR spectra obtained for the middle functionalised basis peptide. Top left – open chain in EtOH, top right – Open chain in H_2O, bottom – ring-closed isolated peak in H_2O. Wavenumbers for carbonyl peaks are also included for each sample.*

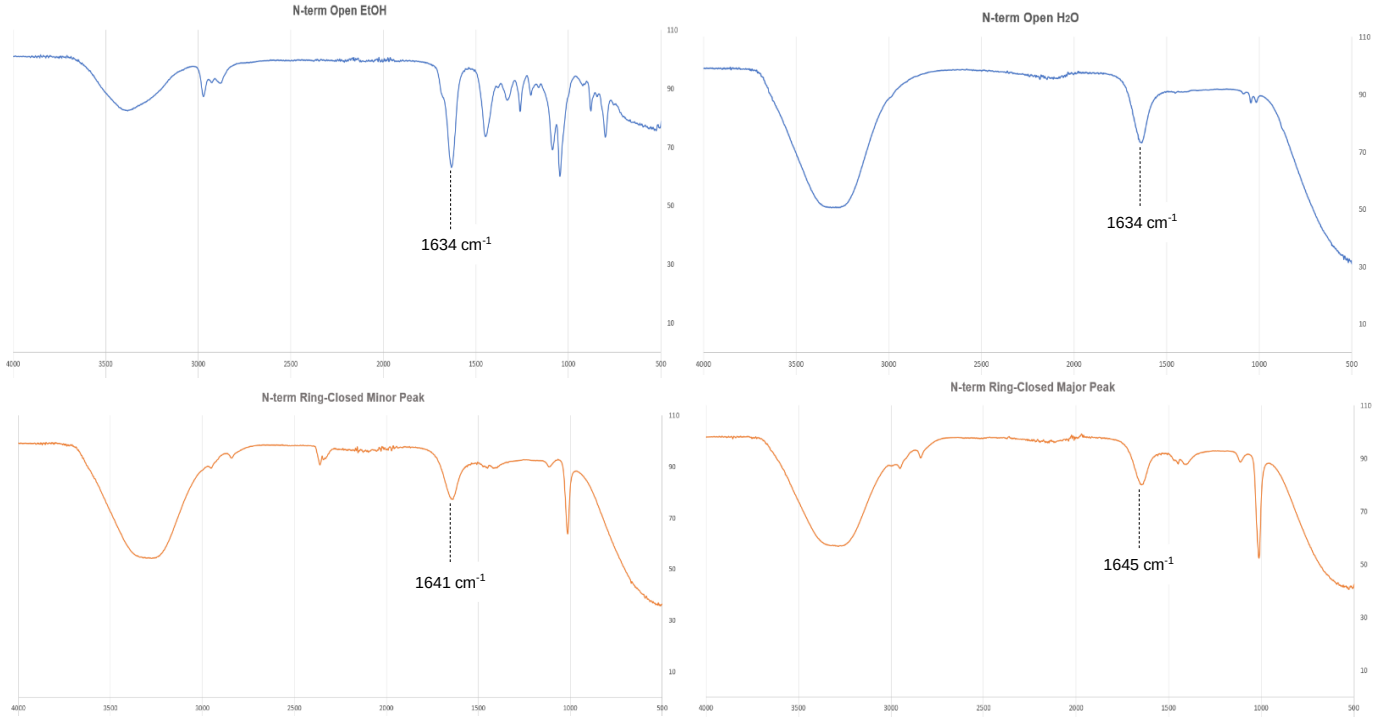

Figure 17(c) *– FT-IR spectra obtained for the N-terminus functionalised basis peptide. Top left – open chain in EtOH, top right – Open chain in H_2O, bottom left – ring-closed minor isolated peak in H_2O, bottom right – ring-closed major isolated peak in H_2O. Wavenumbers for carbonyl peaks are also included for each sample.*

From **Fig. 17**, a number of trends and observations can be noted. Firstly, both the H_2O and EtOH equilibrated open chain samples for each peptide seem to exhibit similar carbonyl peak wavenumbers, especially between individual peptides. Wavenumbers of 1637 and 1634 cm^{-1} being observed for the C and N-terminus open chain peptides respectively is an interesting result. As discussed in section **1.0**, a carbonyl peak wavenumber of around 1635 cm^{-1} can be associated with a PPI conformational structure. This somewhat contradicts the CD results obtained which suggested that the two samples were occupying a similar but more PPII-like conformation. With regards to the middle-stapled peptide, a slight variation in wavenumber is observed between the two open chain samples, however again, both with values characteristic of a PPI conformational structure. A trend exhibited throughout the three peptide structures is a shift of the ring-closed peptides' carbonyl minima to a higher wavenumber. A transition from a PPII to a PPI conformation is usually accompanied by a shift to a higher wavenumber, however in a much lower range than is observed for these peptide samples (see section **1.0**). With all three peptides offering an increase of at least 7 cm^{-1} once ring-closed, it is predicted that a different conformational structure is being formed by each peptide. FT-IR is a technique used somewhat more scarcely than CD in the probing of peptide conformational structure and the exact structure being formed cannot however be defined with the shift in wavenumbers observed being in an uncharacteristic range for a polyproline peptide. The employment of additional analytical methods was therefore required to deduce a clearer picture of the structures that had formed.

1.2.3 DOSY NMR analysis

Following the results obtained from FT-IR analysis, DOSY NMR was finally used as an additional technique in the hope that it would provide a clearer picture regarding the structure of the three peptides. DOSY NMR is a technique that separates the NMR signals within a sample according to their diffusion co-efficients. The Stokes-Einstein equation denotes the relationship between diffusion and hydrodynamic radius, so when used accordingly, the hydrodynamic radius and hence the volume occupied by a species may be calculated from a DOSY NMR experiment. It is however important to mention that the Stokes-Einstein equation is only obeyed by spherical particles and seeing as the peptides being analysed here are significantly more rod-like in shape, the results will be used only relatively in the interpretation of particle size. The Stokes-Einstein equation is shown below (i), as well as the relation of a radius to its spherical volume (ii):

$$D = \frac{K_B T}{6\pi\eta R} \qquad R = \frac{K_B T}{6\pi\eta D} \tag{i}$$

$$v = \frac{4}{3}\pi r^3 \tag{ii}$$

Both the open chain and ring-closed peptides were subjected to DOSY NMR analysis with a mixed sample also run as a standard and to monitor differences in diffusion co-efficient. The spectra obtained for each of the three peptides is displayed in **Fig. 18** below. All samples were dissolved in deuterated water as a solvent.

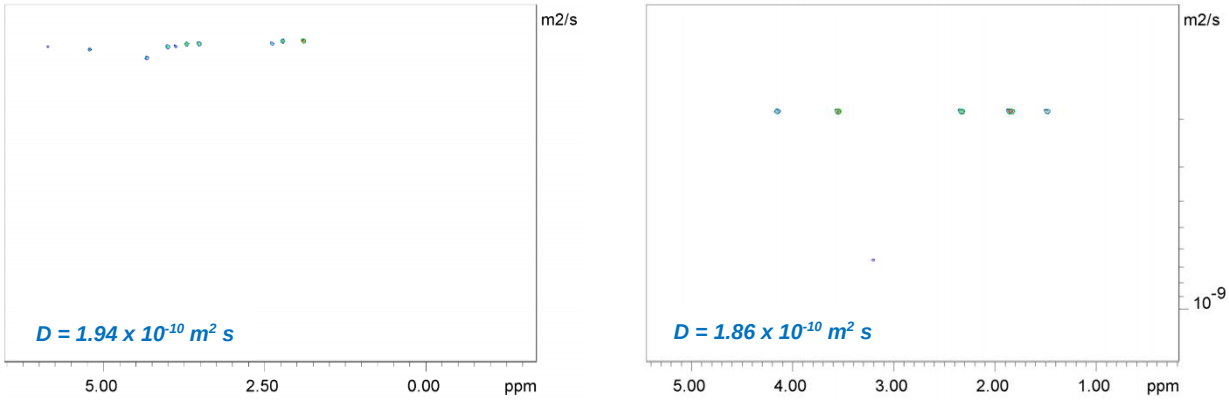

Figure 18(a) *– DOSY NMR spectra for the C-terminus stapled peptide. (Left) – open-chain form, (right) – ring-closed form. Diffusion co-efficient (D) values are also displayed.*

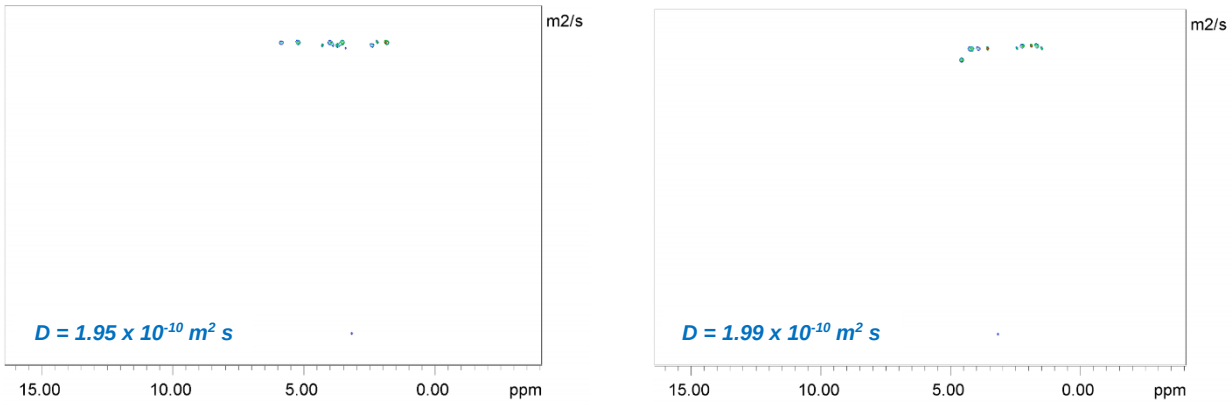

Figure 18(b) *– DOSY NMR spectra for the middle stapled peptide. (Left) – open-chain form, (right) – ring-closed form. Diffusion co-efficient (D) values are also displayed.*

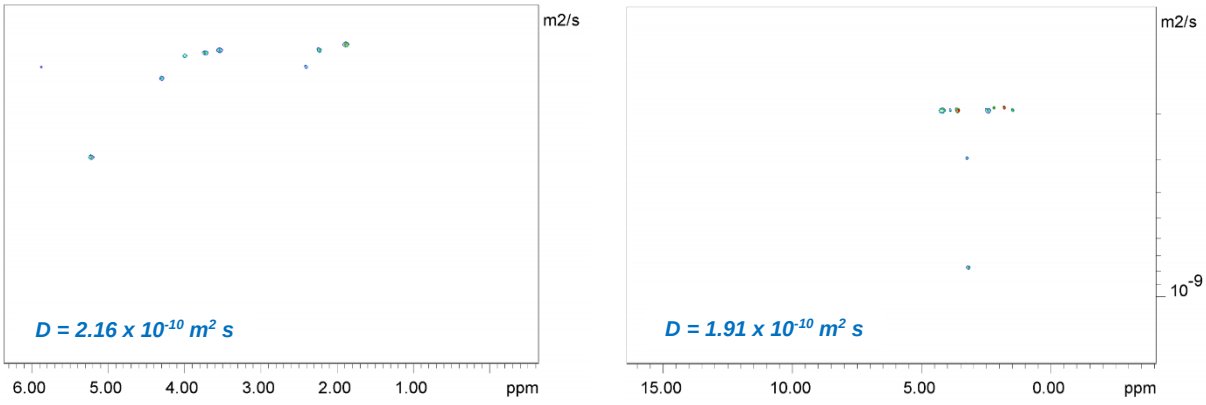

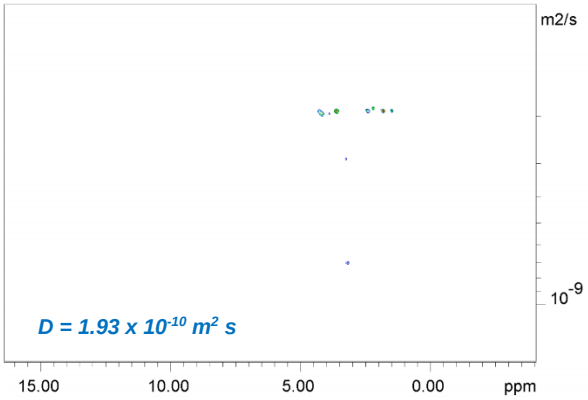

Figure 18(c) *– DOSY NMR spectra for the N-terminus stapled peptide. (Top left) – open-chain form, (top right) – ring-closed form major product, (bottom) – ring-closed form minor product. Diffusion co-efficient (D) values are also displayed.*

From the diffusion spectra presented in **Fig. 18**, there can be considered little variation in diffusion coefficient and hence relative volume between open chain and ring-closed peptide structures. Looking closer at the C-terminus and middle-stapled spectra, a 0.08 x 10^{-10} m^2/s decrease and a 0.04 x 10^{-10} m^2/s increase in D value is observed for the two peptides respectively. Following the Stokes-Einstein equation, hydrodynamic radius is inversely proportional to the diffusion coefficient. For the C-terminus stapled peptide, a slight decrease in diffusion coefficient therefore suggests an increase in hydrodynamic radius. This is an interesting yet strange result when considering the theoretical computational predictions discussed in section **1.0** whereby the strain imposed by the linker was expected to reduce molecular volume. The middle-stapled peptide on the other hand exhibits a slight increase in diffusion coefficient and hence a decrease in molecular volume. Although this is more of an expected result, the decrease in volume is marginal with volume values expected to half for a PPII-PPI transition. For the N-terminus functionalized peptide, a greater difference in diffusion coefficient was observed with decreases of 0.25 x 10^{-10} m^2/s and 0.23 x 10^{-10} m^2/s exhibited by the major and minor ring-closed structures respectively. Although the corresponding change in molecular volume is greater than that of the two other peptides, it is still not of the magnitude expected by a PPII-PPI transition. In addition to this, the decreases in diffusion coefficient again imply an increase in molecular volume.

The DOSY data obtained is therefore in agreement with the previously made hypothesis that a distorted PPII conformational structure is being locked and further stabilised upon RCM of the linker chains. The minuscule differences in diffusion co-efficient and subsequent hydrodynamic radius suggest a very similar molecular size between open-chain and ring-closed samples, a difference certainly nor great enough to evident a PPII → PPI conformational shift. As previously mentioned, the Stokes-Einstein equation applies specifically to spherical molecules and therefore one possible source of error here could be the rod-like shape of the peptides. As observed by the C and N-terminus functionalized peptides, an increase in molecular volume upon installing a hydrocarbon staple into the three peptides cannot be explained using computational calculations and therefore to fully understand these structures, further analysis was required utilising different analytical techniques.

Firstly, an attempt to grow crystals suitable for single crystal X-ray diffraction (XRD) was made. This would allow for XRD studies to be carried out, thus providing a detailed picture of the conformational structure occupied by the peptide. Previous work by other members of the research group had experienced success crystallising peptides of a similar length, whereby the secondary amine located at the N-terminus was protected with an Fmoc group. A middle-stapled polyproline-7 peptide with an Fmoc-protected N-terminus was therefore synthesised (**Fig. 19**), and after purification a mosquito crystallisation apparatus was used to trial 96 varying 'conditions' in an attempt to crystallise the peptide. Finally, the standard middle-stapled basis peptide with an acetyl-capped N-terminus was also attempted to be crystallised utilising the same condition set. A JCSG-Plus MD1-37 assay was used in an attempt to crystallise the peptides of interest.

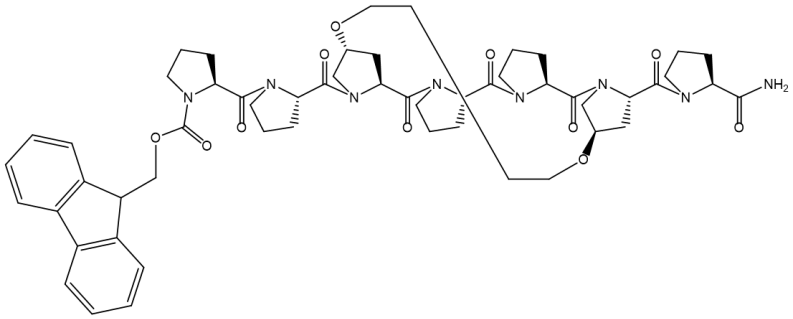

Figure 19 *– Molecular structure of the middle-stapled N-terminus Fmoc-protected polyproline-7 peptide, attempted to be crystalized for the probing of conformational structure.*

The acetyl-capped, middle-stapled basis peptide gave a crystal in the well plate containing 0.1 BICINE buffer at pH 9.0 with 10% v/v MPD as precipitant. However after repeated attempts to obtained crystal-XRD data for this sample, crystal size proved insufficient. The concentration of precipitant and pH are now under investigation to yield a larger crystal suitable for single crystal XRD in-house analysis.

In addition to the efforts made to grow a crystal structure, there was concern that the hydrocarbon staple may not be inducing sufficient strain into each of the peptides. The spanning length of the hydrocarbon linker was therefore increased to an *i, i + 4* relationship (**Fig. 20**), in the hope that increasing the spanning distance of the same length staple would lead to an increased amount of steric strain induced within the peptide.

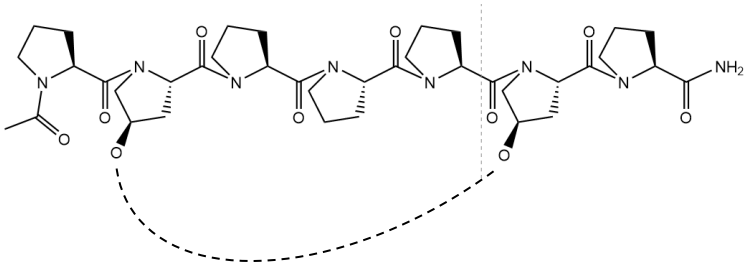

Figure 20 *– Molecular structure of the i, i + 4 functionalised staple peptide. The alkene linker is represented by a dotted line and constituted the same length as all other alkene linkers discussed in this report.*

In addition to this, employing an *i, i + 4* linker relationship would result in the two linker chains occupying differing faces of the secondary structure. In light of this, not only was it anticipated that the staple would induce more strain as a result of it spanning a greater distance, but also due to it needing to twist and connect different faces when undergoing metathesis. The same reaction conditions were employed during this RCM reaction as for the three basis peptides and after 48 h, the reaction was subjected to analytical HPLC analysis (**Fig. 21**).

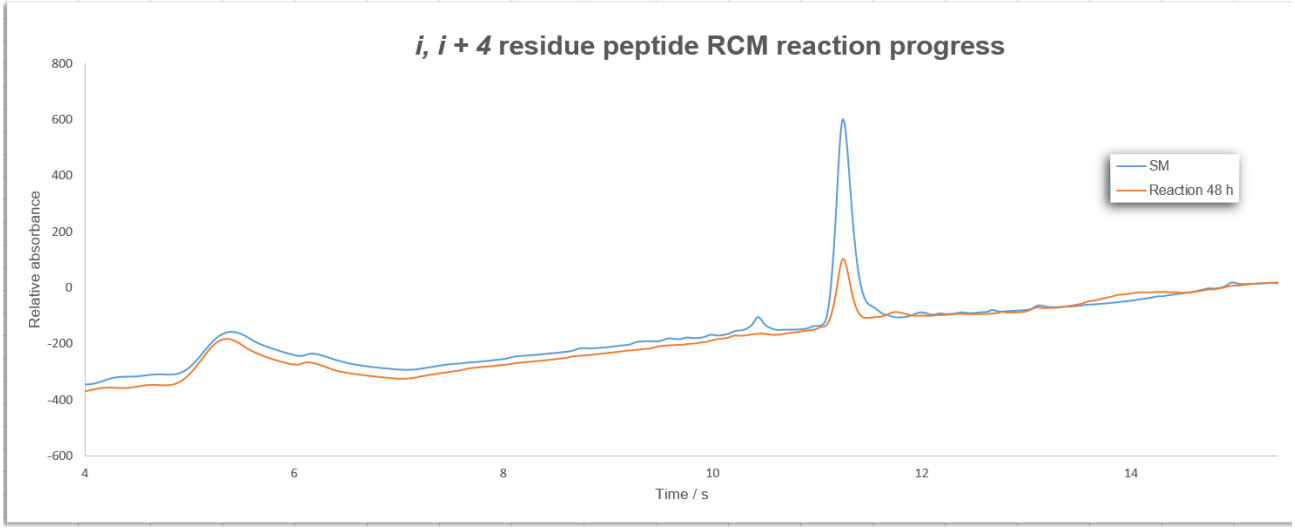

Figure 21 *– Reversed-phase HPLC 225 nm UV chromatogram for the RCM reaction of the i, i + 4 residue stapled polyproline-7 peptide. Starting material and reaction progress after 48 h is shown for comparison.*

Upon analysis of the HPLC chromatogram, it is clear that after 48 h, no product evolution had occurred. This was a somewhat disappointing result which showed the importance of the hydrocarbon linker being tethered to proline residues occupying the same face of the helical structure. In addition to the positioning of the linker, it is possible that a higher RCM reaction concentration is required to enable stapling to occur, however as discussed in greater detail earlier in this section, a higher reaction concentration poses the risk of intermolecular metathesis as well as catalyst degradation. Trialling altered reaction conditions and other positions for linker attachment is an area which presents potential, however time constraints meant that this would have to be a future investigation.

In summary of the findings discovered thus far, as well as each of the basis peptides suspected to be forming some form of locked or distorted PPII conformation, a crystal structure had been pursued as well as the effects of linker spanning distance analysed. With an increased linker spanning distance proving to be inefficient during RCM, it was decided that moving forward, an *i, i + 3* linker relationship would be implemented into future mimetic peptides. Furthering this, based on the single peak exhibited by the middle-stapled basis peptide, mimetic structures would be constructed with a middle-positioned staple. Not only was this decided as a result of one conformational isomer being produced but also for the ease of purification whereby only one peak would need to be isolated.

Chapter 2 - Implementation of hydrocarbon stapling in the development of α-helix mimetic peptides

2.0 Background Information

The α-helix is a fundamental component of many biological fields, including transmembrane protein structures, DNA binding and protein-protein interactions, with the latter topic being of greatest interest in the work of this report. Protein-protein interactions mediated by α-helices make up around 60% of all protein-protein interactions currently known.[36] The surface interaction between partnering proteins plays a key role in many biological processes, with the mis-regulation of these interactions often leading to states of disease.[37] However, despite their importance and fundamental role, protein-protein interactions between partner proteins are usually not considered attractive target areas for novel drug design due to their contact surfaces often being large and flat.[38,39] Research and analysis of these protein interfaces has however shown that although their areas of contact are large, there is commonly a small subset of amino acid residues which contribute substantially to the free energy of binding between the partnering proteins. Furthermore, it has been identified that secondary protein structures are effective scaffolds for facilitating these interactions,[40,41,42] as well as the fact that 60% of all protein-protein interactions occurring between short peptide motifs and a globular protein domain, contain short peptides adopting an α-helical (or closely related) structure.[24] Identifying and hence targeting these so-called 'hot-spots' will therefore allow novel therapeutics to be developed using helical, synthetic peptides that mimic the key structural and energetic elements of the significant protein, with high affinity and specificity.[43,44] These synthetic species are known as α-helix mimetics and an increasing amount of research is being conducted in an attempt to increase the conformational stability, binding affinity and cell permeability of such compounds.[45]

Peptide stapling methodologies have already been implemented in the construction of α-helix mimetics in literature, with Verdine, Walensky *et al*. providing the first example of a stapled peptide that kills cancer cells *via* the targeting of a transcriptional pathway in 2007.[46] The transcription factor, p53 induces cell apoptosis in response to DNA damage[47] and cellular stress.[48] It therefore plays a vital role in preventing malignant transformation of cells. A reduction in p53 activity *via* deletion, mutation or overexpression of the E3 ubiquitin ligase, hDM2, is the most commonly-encountered defect in human cancer. hDM2 targeting has therefore been identified as an effective approach for restoring p53 activity to re-sensitize cancerous cells to apoptosis.[49] The p53-hDM2 protein interaction is mediated by a 15-residue α-helical transactivation domain of the p53 protein which slots itself into a hydrophobic cavity on the surface of the hDM2 protein.[50] There are three amino acid residues within this domain which are essential for hDM2 binding.[51] When alkene stapling is utilized to stabilize the α-helicity of p53 (Fig 22),

increased affinity for hDM2 was experienced together with increased levels of cell penetration *via* an active uptake mechanism in comparison to the unmodified p53 peptide. The stapled p53 peptide residue then showed reactivation of the p53 tumour suppressor cascade by inducing the transcription of p53-responsive genes.

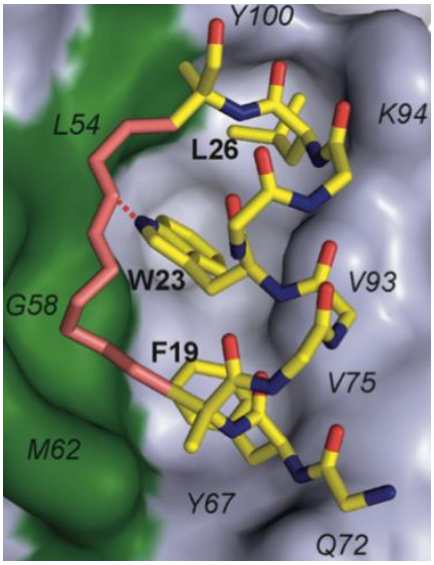

Figure 22 – *Structure of the complex formed between the stapled p53 peptide (SAH-p53-8) (yellow) and E3 ubiquitin ligase Mdm2 (purple/green) – Italics indicate the boundary of the binding pocket on the surface of the Mdm2 protein with the hydrocarbon staple attached to p53 shown in pink.*[52]

With the data from the basis peptide study in hand, a greater understanding of the effects of hydrocarbon stapling on short prolyl peptides was now possessed. The study had discovered that stapling led to the formation of a distorted PPII structure which had possible supramolecular applications as a novel secondary structure. It was therefore hypothesised that this technique could be used to structurally constrain a given peptide and enable it to function as a mimetic. Moving forward, it was set out to incorporate all-hydrocarbon stapling into the design of a set of novel mimetic peptides, with the ambition of mimicking the key active regions ("hot spots") of a designated protein. It was hoped that stapling these peptides at specific positions would structurally constrain and lock their conformations, allowing them to bind to a target protein with a stable conformational structure and induce the desired biological response.

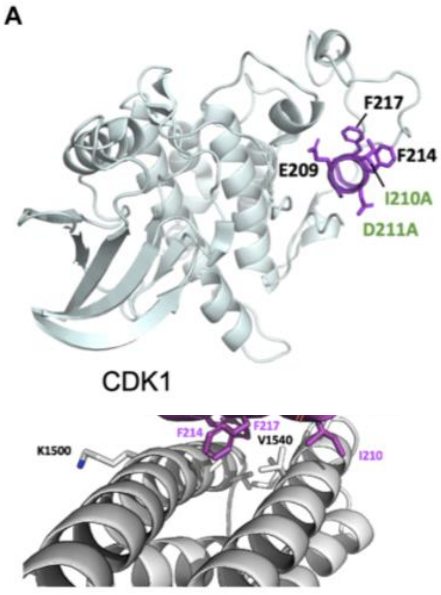

Figure 23 *– (A): Structure of CDK1 with the talin-binding LD motif highlighted in magenta – LD motif consensus residues also indicated. (B): Side-on view of the animated representation X-ray structure for the R7R8 talin-CDK1 binding complex*[53]*.*

The target protein selected was talin. As a ubiquitous cytosolic protein, talin is a key component of adhesion complexes which couple integrin to the cytoskeleton. An essential process involved with talin's integrin-mediated adhesion is the binding to cyclin-dependant kinase-1 (CDK1), a master cell cycle regulator, at specific binding sites located on the talin structure. Mutagenesis studies conducted by Ben Goult *et al*. have shown the significance of an LD motif present within the CDK1 structure,[53] which is key to successful substrate binding. The mechanosensitivity of talin is also thought to play a pivotal role in its binding to other significant substrates, one of which being the cytoskeletal adaptor, KANK. With this knowledge in hand, it was set out to develop a set of mimetic peptides which have the ability to mimic the key active binding regions of the CDK1 and KANK peptides. Talin was chosen as a target protein not only because of its biological importance and potential, but because it has been studied extensively here at the University of Kent. Moreover, an optimized binding assay has been developed whereby the binding

integrity of talin to substate peptides can be measured using simple and fast NMR techniques. The peptides to be constructed also have potential to bind to multiple talin binding sites (**Fig 23**).

In addition to the importance of the LD motif in talin binding, other hot-spots such as a tyrosine (tyr) and phenylalanine (phe) residue were identified. **Fig. 24** below shows the 3D diagrams of two planned mimetic structures (beige for (i), turquoise for (ii)) with the constituent binding region groups ('hot spots') to be replicated, overlayed on top of each. **Fig. 24(i)** features a mimetic structure containing functional groups to replicate the phe and tyr hot spots (blue) only, while **Fig 24(ii)** shows a mimetic utilized to probe the importance of the LD motif in substrate binding. This mimetic features the phe and tyr residues to be replicated (turquoise) except this time with the 3D model containing an acetyl-capped amine at the N-terminus for simplicity. Various functionalities situated at the N-terminus, including a free amine, succinimide cap and LDLD motif would then be trialled, as a means of probing the binding properties of this region of the peptide. Studying the binding affinities of all of these mimetics would allow us to identify the importance of specific hot-spots for binding to the target protein. In order to replicate these key hot spots, proline units would have to be functionalized with the appropriate functional groups, and so non-natural amino acids were therefore synthesised and implemented into the mimetic peptide structure. In order to construct the target mimetic peptides, a number of 'non-natural' amino acids were synthesised. Synthetic routes to each of these functionalized proline residues are discussed in detail in section **2.1**.

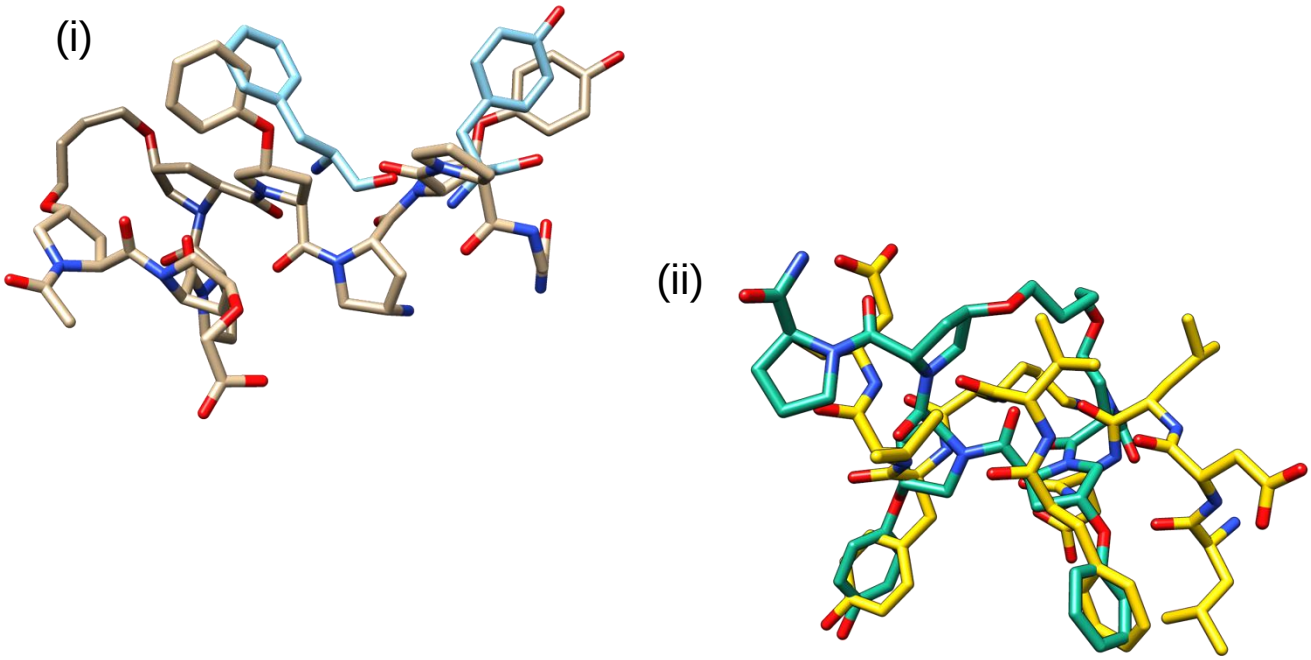

Figure 24 *– (i) – 3D molecular representation of the N-terminus stapled mimetic (beige), containing functional groups to mimic the phe and tyr hot spots (blue). (ii) – 3D molecular representation of the middle stapled mimetic (turquoise) containing functional groups to mimic the phe and tyr hot spots as well as to be used as a probe to ascertain the importance of the LD motif. The target structure to be replicated is indicated in yellow.*

As previously mentioned, the position of alkene linker attachment on the proline ring also bears great importance and has a known effect on stapling efficiency as well as bioactivity of the stapled peptide.[23] In light of this, the positioning of linker attachment must be carefully considered to make sure that it is not blocking or interfering with the highly specific binding regions of the mimetic peptide. Such interferences may reduce the binding affinity of the mimetic peptide, hence disabling it from performing its therapeutic role. Data gathered from the basis peptides investigation in chapter 1 of this thesis showed that attachment of the hydrocarbon linker in the middle position of the peptide chain not only produced a mono-conformational product but also presented the simplest, single peak purification process. Hydrocarbon staples were therefore placed in the middle of the mimetic chain and such that they did not interfere with any key binding regions. The work of chapter 2 was also carried out in tandem with that of chapter 1 and this resulted in the first mimetic constructed featuring a staple positioned at the N-terminus of the peptide chain. This idea is discussed in greater detail later in section 2.1. As previously discussed, the *i and i +3* linker spanning distance was selected to accommodate one turn of the helical structure and aid in efficiency of RCM reactions. This would also ensure that the stapled linker occupied only one face of the secondary structure and did not interfere with the active region or binding sites of the mimetic peptide.

2.1 Mimetic peptide synthesis

Alongside the work focused on the basis peptides and hydrocarbon stapling, a number of mimetic peptides were constructed, in the hope that they would present themselves as therapeutic molecules and bind to the target binding regions of the talin protein. It is important to note that the knowledge gathered thus far regarding staple positioning and spanning distance was only directly applied in the construction of mimetics **B(i)** and **C(i)**. Peptide **A(i)** was constructed in tandem with the basis peptide

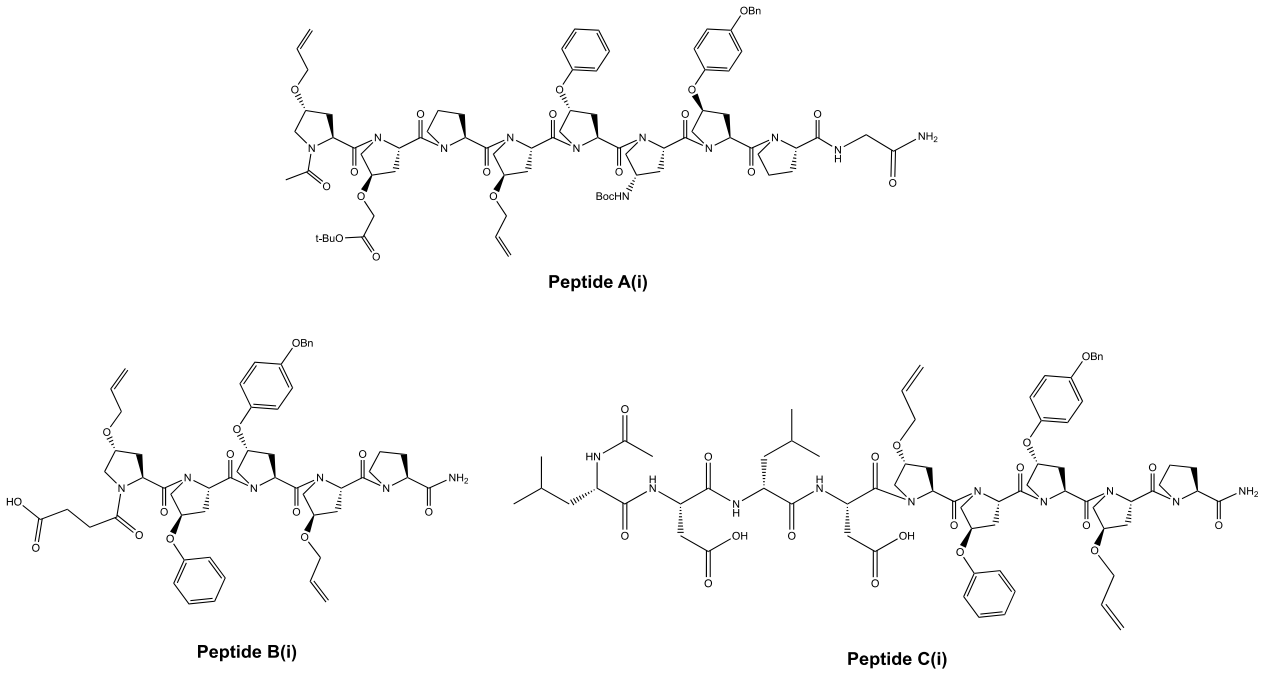

Figure 25 *– Molecular structures of the three mimetic peptides constructed using a range of functionalised, non-natural proline monomers. All peptides are shown in their open chain post-resin cleavage form with all relevant protecting groups still attached.*

work and therefore the staple was placed preliminarily at the N-terminus while further investigation was completed. The open chain structures of the three mimetic peptides constructed are shown above in **Fig. 25.** It was discussed in conjunction with **Fig. 24(ii)** that the importance and binding nature of the LD functionality would also be probed for the mimetic structure. Peptides **B** and **C** would be used to probe this idea, with the free amine and succinimide functionalities being probed *via* peptide **B** and attachment of an LDLD sequence monitored *via* peptide **C**.

2.1.1 Mimetic-specific monomer synthesis

It is clear from **Fig. 25** that a number of non-natural, functionalized proline derivatives would be required to synthesise each of the mimetic peptides. The structure of each of these non-natural amino acids in their protected forms (as they were placed on the peptide synthesiser apparatus) are described below (**Fig. 26**). The preparation of the stapling monomer **1.1** has already been discussed in detail in the results and discussion section.

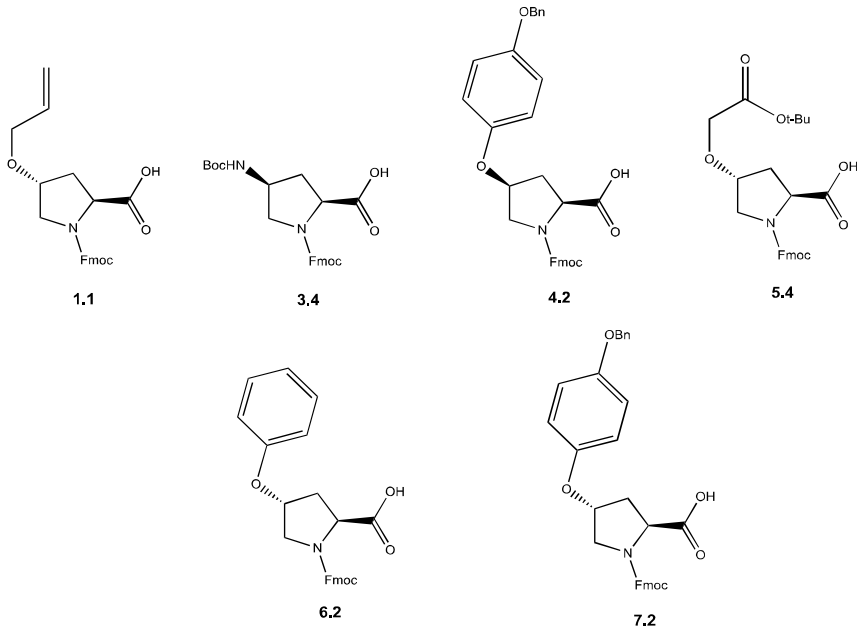

Figure 26 *– Molecular structures of the six non-natural functionalized proline compounds required for construction of the three mimetic peptides shown in* ***Fig. 25****.*

2.1.2 Synthesis of monomer 3.4 for use in mimetic peptide construction:

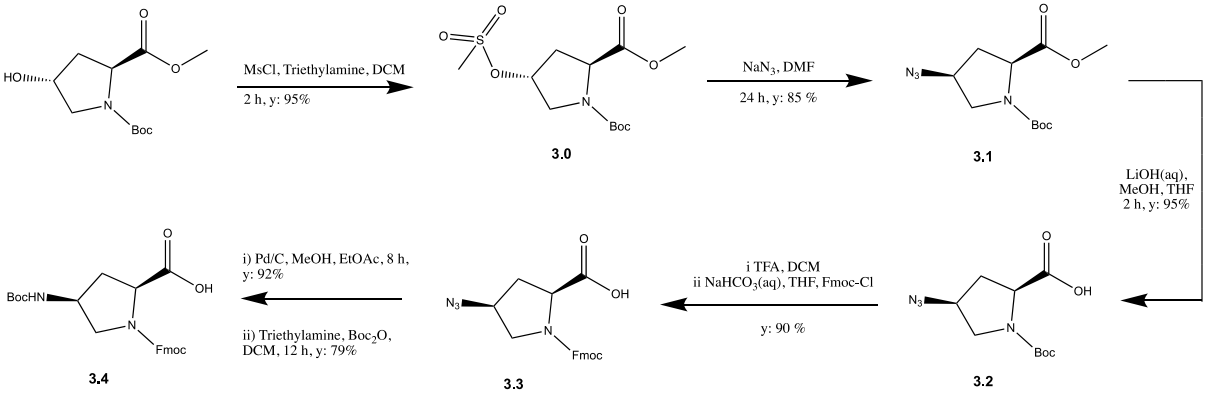

The first step featured in scheme **2.1.2** shows a simple de-protonation and mesylate formation at the 4-position of the hydroxy proline ring. The mesylate group is a potent leaving group and this step was required in order for the following step to be carried out, whereby the chiral centre would be inverted and the mesylate group replaced by an azide group. A high yield (95 %) of compound **3.0** was obtained after work up, with TLC being utilised to confirm product presence and purity. Compound **3.0** was then carried forward to step 2 where the mesylate group was to be converted to an azide functionality with the use of sodium azide. TLC analysis provided an initial indication of reaction progress, however the presence of the azide group was confirmed by FT-IR analysis, with the clear emergence of the N=N stretching mode at ≈2100 cm^{-1}. Following this, saponification was carried out to convert the methyl ester functionality to a carboxylic acid – a requirement for the monomer to be used in SPPS of the final mimetic peptide. This was unsurprisingly a fast reaction with TLC and ^{1}H NMR analysis proving sufficient to confirm success of the reaction with a new spot formed on the TLC plate as well as the disappearance of the methyl singlet peak at 3.7 ppm. The penultimate step in the synthesis of the final compound **3.4** involved a Boc de-protection of the proline ring nitrogen and a subsequent re-protection with the Fmoc group. An Fmoc-protected amino acid is required for SPPS procedure to produce the final mimetic peptide. The disappearance of the peak at 1.45 ppm corresponding to 9 methyl protons in ^{1}H NMR analysis (appendix A, 3.3) after the Boc de-protection step gave a clear indication that the boc protecting group had been successfully removed. The emergence of a range of aromatic peaks in the 7 - 8 ppm region after Fmoc protection gave further indication that Fmoc re-protection had also been carried out successfully, yielding product **3.3**. The final synthetic steps required to reach the target amino acid firstly involved a hydrogenation reaction with the use of a Pd/C catalyst and H_2 gas. The progress of this reaction was monitored *via* FT-IR analysis whereby the disappearance of the broad azide band at 2100 cm^{-1} provided an indication that the azide functionality had been reduced the primary amine. Following this, basic conditions were employed with the use of boc-anhydride to protect the primary amine during SPPS. Protection with a boc protecting group will prevent cross-coupling during SPPS and the formation of un-desired side products.

Where ever possible, azide compounds were also covered and stored away from UV light and at -20^{0}C in an attempt to minimise photo and thermal degradation. It is important to note that the pH of the reaction shown in step 2 of scheme **2.1.2** as well as any waste collected was constantly monitored and ensured that the pH was basic. Ensuring basic conditions in the presence of NaN_3 is vital as in acidic conditions, the compound has a tendency to form hydrazoic acid (HN_3), a highly explosive, volatile and toxic liquid. In addition to this, all azide compounds were kept away from any heat sources, e.g. rotary evaporators, with solvents being removed under compressed air to avoid possible initiation and subsequent explosion.

Synthesis of the alkene linker functionalised proline residue has already been described in section **1.1**, with the target compound being isolated in generous yields.

2.1.3 Synthesis of monomer 4.2 for use in mimetic peptide construction

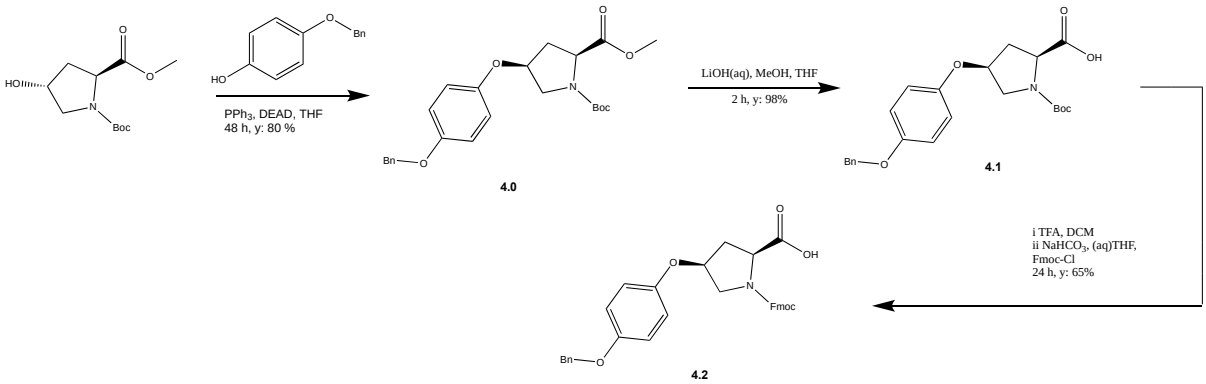

The second non-natural amino acid building block required for construction of the mimetic peptide was the functionalised proline compound **4.2**. Synthesis of this monomer again proved successful for the most part with generous yields obtained in all steps.

The first step towards furnishing compound **4.2** involved a Mitsunobu reaction, whereby the 4-benzyloxy-phenol nucleophile attacked in at the 4-position carbon, leading to a switch from an R to an S-stereocentre. The reaction was initially attempted using 1.1 eq of the 4-benzyloxy-phenol and triphenylphosphine (PPh_3) and 1.5 eq of diethylazodicarboxylate (DEAD) however after 72 h, the reaction appeared to have not progressed very far with only a faint new spot being observed in TLC analysis. This negative result could have been a consequence of a number of factors; firstly the large steric contribution presented by the bulky nucleophile may have reduced the rate of reaction, making it difficult for the nucleophile to attack in at the hydroxyl carbon atom. Secondly, the nucleophile used for the reaction is a weaker acid than most other typical nucleophiles used for this reaction. Mitsunobu reactions involving such compounds usually require the use of *1,1'-azodicarbonyl-dipiperidine* (ADDP)[54] of which the betaine intermediate is a stronger base. In an attempt to drive the reaction forward, the reaction concentration was increased drastically, whereby the absolute minimum quantity of THF was used to dissolve all reagents. This proved to have a marked effect on the progress of the reaction with the new spot significantly growing in intensity and the starting material spot disappearing. Following work-up and FCC purification, compound **4.0** was successfully isolated with NMR data (appendix A, 4.0) in agreement with the desired structure. A doublet of triplets at 6.70 and 6.80 ppm with a cumulative integration of 4 along with a multiplet centred at 7.4 ppm with integration of 5, confirmed attachment of the electrophile side chain to the proline hydroxyl group. The final two steps shown on scheme **2.1.3** involved the reduction of the methyl-ester functionality to a carboxylic acid at the 2-position of the proline ring, followed by removal of the Boc protecting group and re-protection with the Fmoc protecting group. The carboxylic acid and Fmoc protecting groups are a requirement for the amino acid to be used in SPPS to construct the final mimetic peptide. The saponification reaction proceeded smoothly, with TLC revealing full consumption of starting material and conversion to product with a high yield (98%) being obtained. The Boc-deprotection and Fmoc re-protection however proved somewhat more laborious. After ^1H NMR analysis was used to confirm complete removal of the Boc

group (disappearance of the large doublet peak around 1.4 ppm), isolation of the product compound involved the reaction being quenched with cold water and then washed with cold di-ethyl ether during a base-acid extraction, in an attempt to remove excess Fmoc-Cl as well as any other bi-products generated during the reaction. The amino acid this time round, features a bulky, aliphatic/greasy substituent at the 4-position however which made product isolation somewhat troublesome with some of the desired product being extracted into the cold di-ethyl ether wash. The desired product was therefore present (shown *via* TLC analysis) in both the di-ethyl ether wash as well as the final DCM extraction of the acidified aqueous layer meaning that FCC would have to be carried out on both isolated samples in order to obtain the maximum quantity of the desired product. FCC proved successful in isolating the target compound **4.2** in a 65% yield, with ^{1}H and ^{13}C NMR spectra (appendix A, 4.2) and LCMS data in agreement with the expected values.

2.1.4 Synthesis of monomer 5.4 for use in mimetic peptide construction

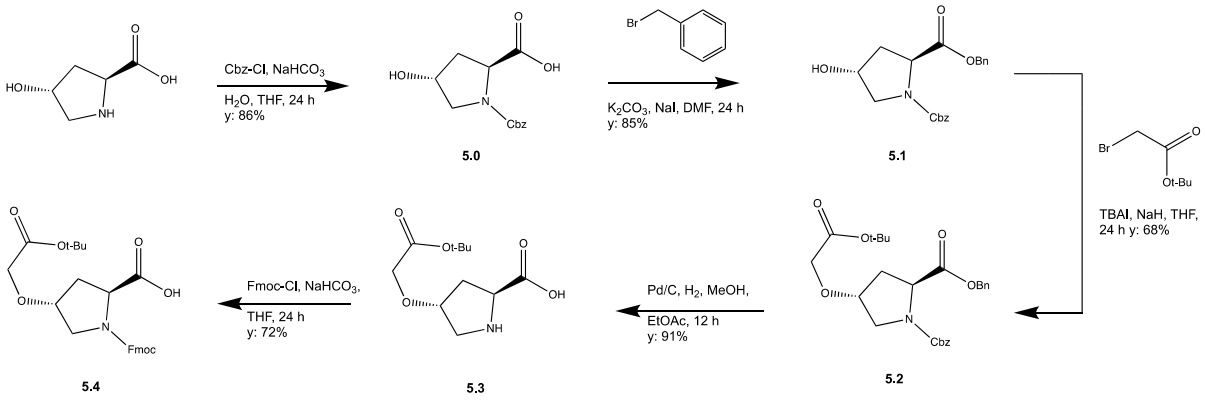

The first step required for the construction of monomer **5.4** involved protecting the free amine of the proline ring with the Cbz protecting group. This was carried out using Cbz-chloride in basic conditions with compound **5.0** isolated in generous yields and a high level of purity shown by NMR analysis (appendix A. 5.0). Following this, the free acid functionality was next protected with a benzyl group via the use of benzyl bromide and catalytic quantities of NaI. After FCC purification, compound **5.1** was isolated in high yields with high purity confirmed by a range of characterization methods. With both the amine and carboxylic acid groups now protected, the next step involved alkylation of the 4-position hydroxyl group under basic conditions with the use of NaH and catalytic quantities of t-butyl ammonium iodide (TBAI). Tertiary-butyl bromo-acetate was used as the electrophile in this reaction, and after FCC purification a high yield and purity of compound **5.2** was again achieved (appendix A, 5.2). Following this, a straight-forward hydrogenation reaction utilising Pd/C was utilised to remove the Cbz and benzyl protecting groups before the resulting secondary amine centre was protected with an Fmoc group. Both of these reactions proceeded smoothly, offering generous yields and with compound **5.4** containing a free carboxylic acid and Fmoc-protected amine group, requirements for the monomer to be used in mimetic SPPS.

2.1.5 Synthesis of monomer 6.2 for use in mimetic peptide construction

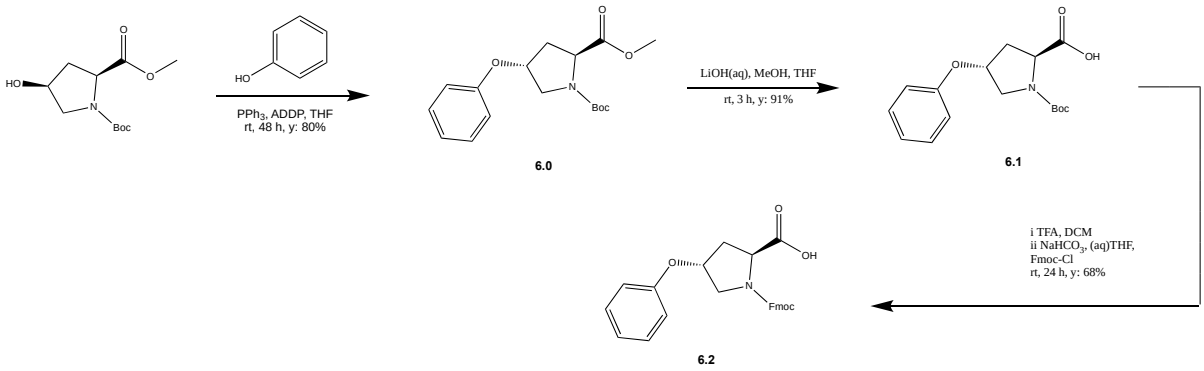

Monomer **6.0** was synthesised in a very similar fashion to that of monomer **4.2**, whereby the first step involved a Mitsunobu reaction resulting in an inversion in the stereochemistry of the 4-positioned proline carbon. This time however, phenol was used as the nucleophilic alcohol and with the difficulties experienced when using the bulkier 4-benzyloxy-phenol not being experienced. The desired product was purified via FCC in generous yield (80%) with ^{1}H and ^{13}C NMR data (appendix A, 6.0) in agreement with literature values. Following this step, simple basic-hydrolysis was carried out with the use of LiOH to convert the methyl ester group to a free carboxylic acid with the reaction monitored using TLC and the target compound being isolated in 91% yield. Finally, the boc-protecting group was removed with the use of a TFA:DCM mixture before re-protecting the free amine with an Fmoc protecting group so that the non-natural amino acid could be used effectively in SPPS coupling reactions. The Fmoc protection step again required FCC purification to remove residual Fmoc bi products, leading to the final target compound being isolated in a 68% yield with ^{1}H and ^{13}C NMR data (appendix A, 6.2) confirming isolation of the desired structure.

2.1.6 Synthesis of monomer 7.2 for use in mimetic peptide construction

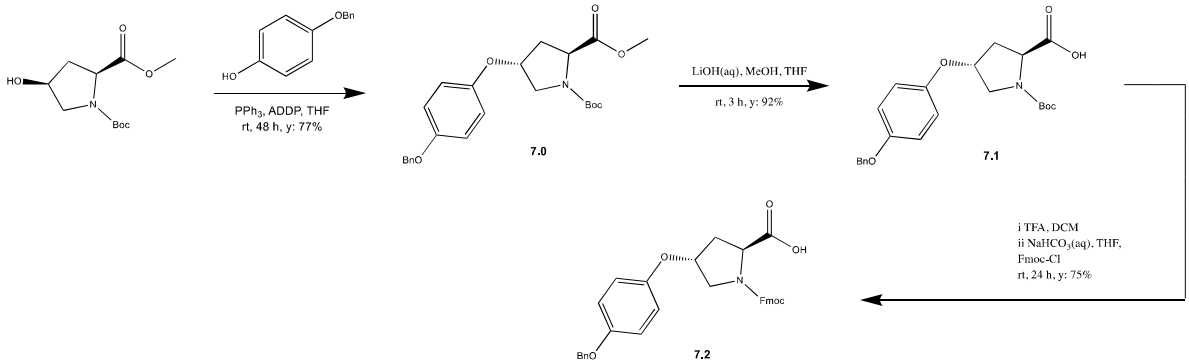

The target compound **7.2** was also synthesised in a very similar fashion to that of monomer **4.2**, with the two compounds being diastereoisomers. The first step involved an inversion of stereochemistry at the 4-position of the proline ring via a Mitsunobu addition of the 4-benzyloxy-phenol fragment. A high reaction concentration was again key for successful product development and upon FCC purification, the target compound was isolated in 77% yield. H^{1} and ^{13}C NMR data (appendix A, 7.0) as well as

LCMS analysis proved successful in characterising the desired product **7.0**. Basic hydrolysis was then utilised to construct compound **7.1**, which contained the free acid component required for SPPS. After acidification of the reaction, the target compound was extracted using EtOAc, with further purification not required. A disappearance of the singlet peak at 3.7 ppm as well as the correct molecular mass identified on LCMS spectra provided sufficient evidence to confirm isolation of the desired product. The Boc protecting group was then removed with the use of a TFA/DCM 1:1 solution over the course of 2 h. After monitoring starting material disappearance with TLC, the resultant solution was dried and residual TFA removed using compressed air overnight. The resulting colourless oil was then dissolved in 1:1 volume of THF and saturated $NaHCO_3$ solution. After cooling to 0^0 C, Fmoc-Cl was then added, before the resulting suspension was raised to room temperature and stirred for 12 h. After 12 h, and monitoring of reaction progress with TLC, the reaction mixture was worked-up before purification of the crude mixture via FCC was completed. The target compound **7.2** was then isolated in a 75% yield with LCMS and ^1H and ^{13}C NMR (appendix A, 7.2) analysis confirming presence of the desired compound.

At this stage it is important to discuss the removal of the various protecting groups attached to the side chains of some of the non-natural amino acids used. Without removing these protecting groups, the hot-spots and active regions located within side chain structures cannot be accessed and the mimetic would not perform its role in binding to substrates. Peptide **A** contains monomers **3.4** and **5.0** which contain a Boc and *tert*-Bu protecting groups respectively. These groups would be removed during cleavage of the peptide from the resin. This process makes use of stirring in TFA for 2 h, which is also an effective method in the removal of any Boc and *tert*-Bu protecting groups present. Monomers **4.2** and **7.2** on the other hand feature a benzyl protected hydroxyl group. This benzyl group requires hydrogenation to be removed fully and therefore was anticipated to be cleaved during the hydrogenation of the staple double bond. **Fig. 27** provides a schematic showing how each protecting group would be removed progressing to the final mimetic structure.

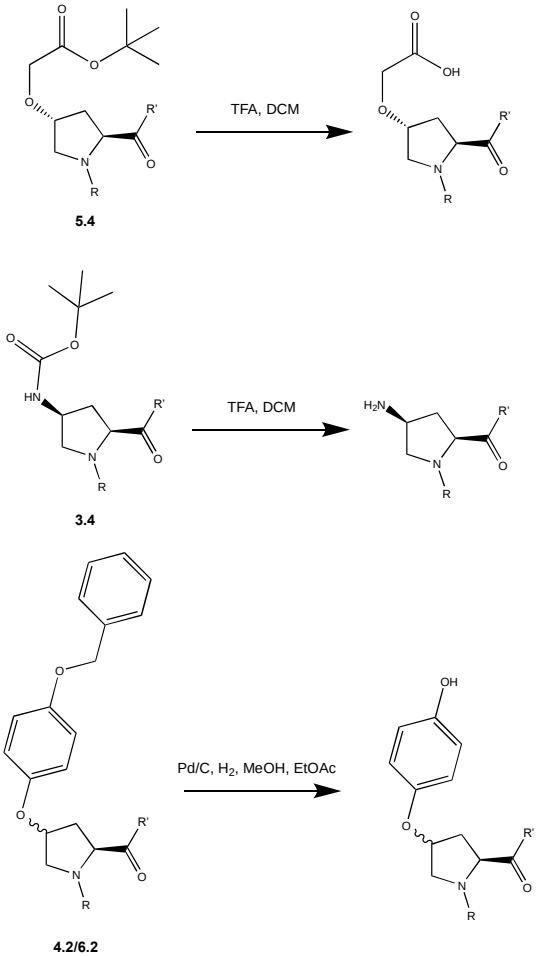

Figure 27 *– Reaction schemes showing the removal of relevant protecting groups from functionalised proline units comprising the three mimetic structures. R groups are used to represent the omitted peptide chains either side of each amino acid.*

2.2 Construction and isolation of the mimetic peptides

2.2.1 Mimetic peptides synthesis

Once the six non-natural proline compounds had been synthesised, construction of the three mimetic peptides could begin. As previously explained, peptide **A** was synthesised whilst research into the basis peptides and staple positioning/spanning distance was being carried out. An initial method was formulated on the CEM peptide synthesiser which used double deprotection cycles as well as coupling reactions at 90 ^{0}C. These relatively harsh reaction conditions were used as some of the coupling steps were expected to be difficult as a result of the bulky side-chains attached to the non-natural amino acids being coupled. The formulated method proved to be successful and was thus used to synthesise all three of the mimetic peptides.

2.2.2 Synthesis of mimetic peptide A(i)

The peptide itself was removed from the apparatus and cleaved from the Rink amide resin for 2 h using a TFA:H_2O, 95:5, v:v mixture – much the same procedure used for cleaving the basis peptides from their respective resins. After this first cleavage, a 30% yield was obtained and so the resin was exposed to more of the cleavage cocktail for a further 4 h. After this second cleavage, more solid white product was obtained, raising the crude yield to 50%. Although this may seem somewhat low, a yield value of 50% was a welcomed result when considering that each coupling involved non-natural amino acids with some containing sterically imposing side chains. Shown in **Fig. 28** below are the LCMS UV chromatograms obtained for the first and second cleavage products. Interestingly, multiple peaks are observed in both chromatograms, with separate peaks evidencing the same molecular mass.

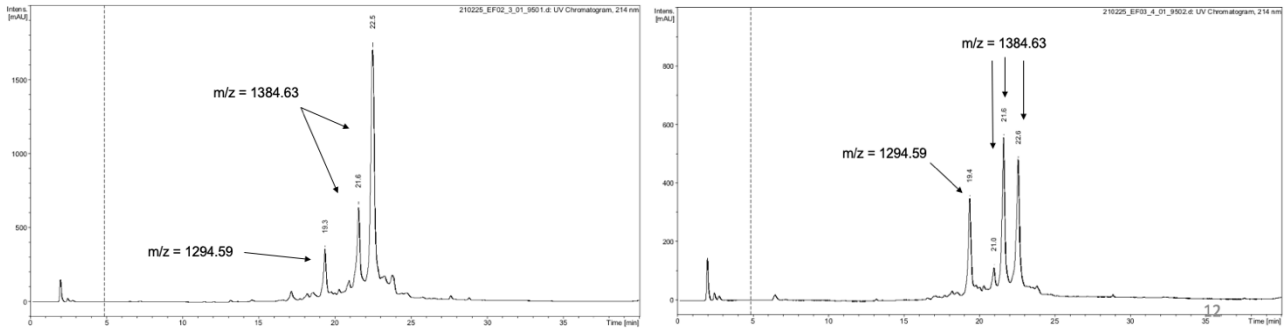

Figure 28 *– Reversed-phase LCMS UV chromatograms (225 nm) of the products obtained from the 1st cleavage (left) and second extended cleavage (right) of the mimetic peptide A(i) from the resin.*

Firstly, both of the spectra display three main peaks, with retention times of 19.4, 21.6 and 22.6 mins. From the accompanying MS data, the later of the two peaks correspond to the target mimetic structure (m/z = 1384.63) whereby only the desired protecting groups have been cleaved from the structure – the boc group from the free amine and the t-Bu group from the carboxylic acid. The origin of the two different peaks was suggested to be a possible result of a number of factors. Firstly, it was thought that two conformational isomers of the mimetic may be present in the sample, for example a PPI and PPII variation. To probe this concept, the sample was left to reflux in EtOH for 72 h in an attempt to convert any PPII-like structures to a PPI helix and hence lead to single peak formation. In addition to this, the

sample was run through LCMS apparatus again but this time raising the temperature of the run to 60^{0}C in an attempt to equilibrate any varying conformers present in the sample into a single peak. Both of these investigations however did not prove successful and the same peak distribution was observed in both cases. The purity of the component monomers was also checked using analytical-HPLC to ensure that this was not the origin of the multiple peak pattern, however all monomers proved to be of sufficient purity. Investigations into the origins of the two separate peaks is therefore ongoing.

Moving on, the third peak displayed by both samples' LCMS chromatogram with a retention time of 19.3/4 mins displayed a m/z = 1294.59. This mass corresponded to the correct mimetic structure however with the benzyl protecting group cleaved from the 3rd coupling residue. This hypothesis was confirmed when comparing the ratio of this peak to the other two peaks across the first and second cleavage samples whereby the m/z = 1294.59 peak grows in intensity moving from first to second cleavages. This makes sense seeing as the second cleavage sample was subject to the acidic cleavage cocktail for significantly more time than the first cleavage sample. It was later discovered that the heated evaporation of the cleavage cocktail via the use of a rotary evaporator was likely the cause of the benzyl group cleavage. This was suggested after the cleavage solution of future mimetic structures was instead evaporated with compressed air and loss of the benzyl protecting group was not experienced. This idea will be revisited and discussed further in future sections of this report.

2.2.3 RCM and hydrogenation reactions of mimetic peptide A(i)

The peptide retained from the first resin cleavage was next subjected to RCM and subsequent hydrogenation. This was to see if the mimetic could firstly be stapled in the presence of a number of functional groups such as amines and carboxylic acids, as a pose to the three basis peptides and secondly to see if the remaining benzyl protecting group could be removed easily, allowing the tyrosine hot-spot to be imitated. The RCM reaction was set up in much the same way as the basis peptides whereby the peptide was dissolved in anhydrous DCM to a concentration of 33 mM, before the Hoveyda-Grubbs 2nd generation catalyst was added under inert conditions. After again utilizing a 15 mol% catalyst loading and leaving the reaction to stir for 24 h, LCMS analysis revealed the reaction to have gone to completion and so hydrogenation, with the use of Pd/C was carried out. **Fig. 29** shows the LCMS spectrum exhibited after 36 h of hydrogenation.

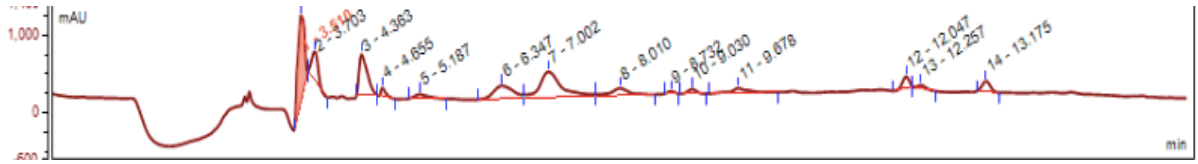

Figure 29 *– Reversed phase LCMS, 225 nm UV chromatogram for the ring closed and hydrogenated mimetic peptide A after 48 h of hydrogenation reaction progression.*

The results of this run showed two main peaks of interest on the UV chromatogram with a range of accompanying peaks. The doublet peak with a retention time of 3.5 and 3.7 mins respectively, constituted a mass of 1268.10, with the 7.0 min retention time peak constituting a mass of 1358.70. A mass of 1358.70 corresponds to the target peptide with the benzyl group (as previously discussed) still

attached. With a 20% Pd/C loading, w:w, and a 72 h reaction time, the benzyl group presented itself as a stubborn hurdle. In addition to this, the considerable size of this peak meant that significant product loss was likely during purification of the peptide. Nonetheless, it had been shown that a large and sterically imposing mimetic structure could be metathesised and reduced to yield the desired structure.

After preparatory-HPLC purification however, the target peptide structure was not isolated in high enough yield for analysis and characterisation. A combination of a 20 mg starting material quantity and incompletable hydrogenation reactions meant that a sufficient quantity of target peptide could not be isolated. The knowledge gained during the synthesis of this peptide would however be carried forward and utilized during the synthesis of the two remaining mimetic peptides.

2.2.4 Synthesis of mimetic peptide B(i)

As described earlier in section **2.1**, mimetic peptide B featured functional groups aiming to mimic phenylalanine and tyrosine residues, with a succinimide capping moiety also used to cap the N-terminus secondary amine in an attempt to mimic an aspartic acid functionality. After constructing the peptide using the CEM peptide synthesiser, it was cleaved from its respective resin using the same cleavage cocktail as that used for mimetic peptide A(i), except this time evaporating the cleavage cocktail with compressed air to avoid unwanted benzyl group cleavage. The N-terminal secondary amine was left exposed as a TFA salt with the succinimide cap to be attached in a reaction separate from the peptide synthesiser. With the open-chain TFA salt isolated and characterized via LCMS, succinimide capping was carried out, with **Fig. 30** below showing reaction progress.

The capping reaction concerned with **Fig. 30** involved the use of triethylamine and succinic anhydride,

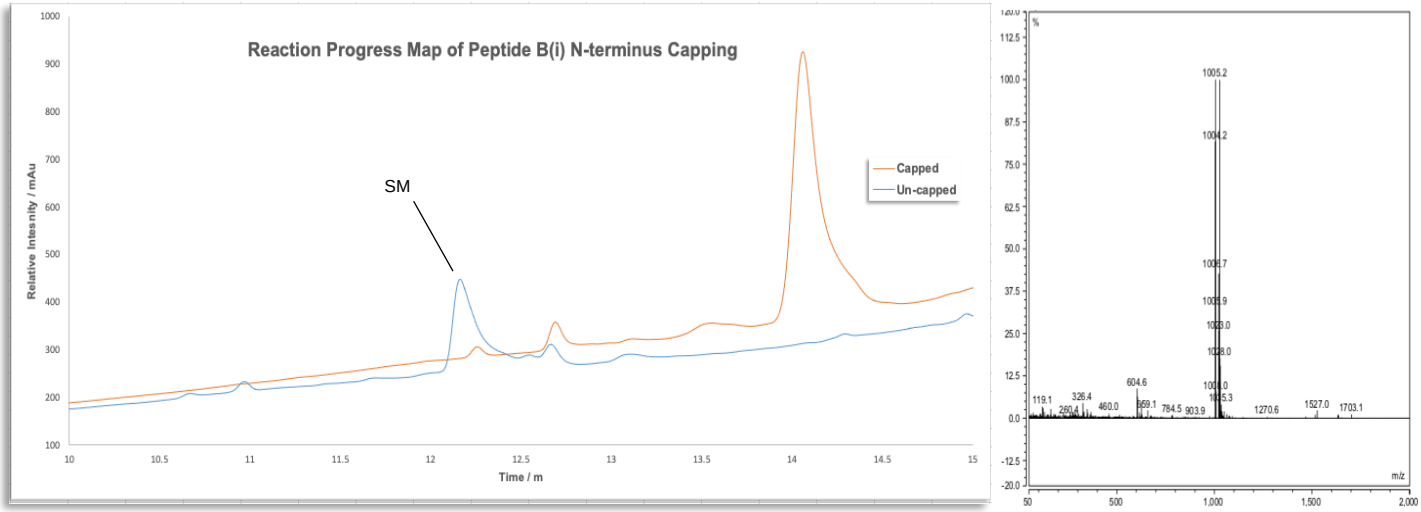

Figure 30 *– Reversed phase LCMS, 225 nm UV chromatogram, 10-15 min region (left) and TIC trace for peak at 14.10 mins (right) showing the reaction progress of the succinimide capping of peptide B(i). A clear starting material consumption can be observed when comparing reaction progress after 48 h (orange trace) with starting material (blue trace).*

with THF used as the reaction solvent. The appearance of a new peak with a retention time of 14.10 mins and disappearance of the starting material peak provided sufficient evidence that the reaction was complete. The product retained was then subjected to LCMS analysis whereby the target peptide mass

was identified from the major spectrum peak (m/z = 1004.2). Purification of the capped peptide would be carried out after RCM and hydrogenation reactions had been completed.

2.2.5 RCM and hydrogenation reactions of the mimetic peptide B(i)

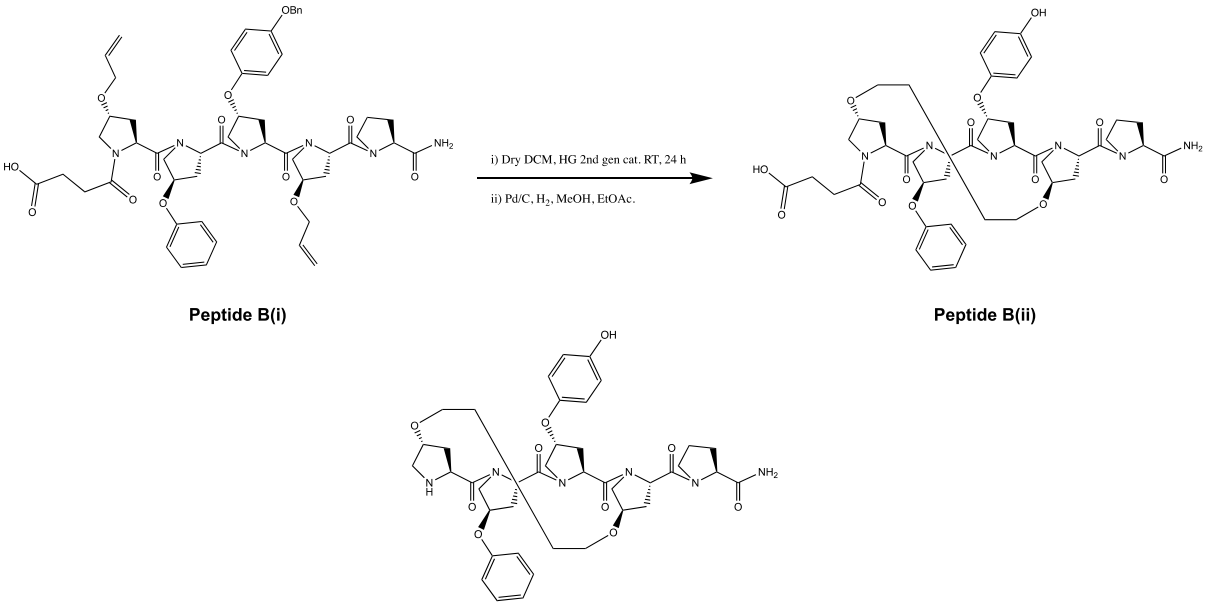

Peptide B(i) **Peptide B(ii)**

Peptide B(iii)

With the capped peptide in hand, RCM and hydrogenation reactions were next carried out. After utilising the optimized RCM reaction concentration and method devised for the basis peptides, the ring-closed derivative of mimetic B(i) was obtained (peptide B(ii), with a combination of analytical HPLC and LCMS analysis evidenting reaction completion.

Following this, hydrogenation of the crude peptide was completed, this time making use of a 20% Pd/C w:w loading as well as 100 μL of TFA, in the hope that this would drive full cleavage of the stubborn benzyl protecting group from the mimetic structure. After 48 h of reaction time, the target mimetic structure was identified during LCMS investigation and so the crude reaction mixture was subjected to

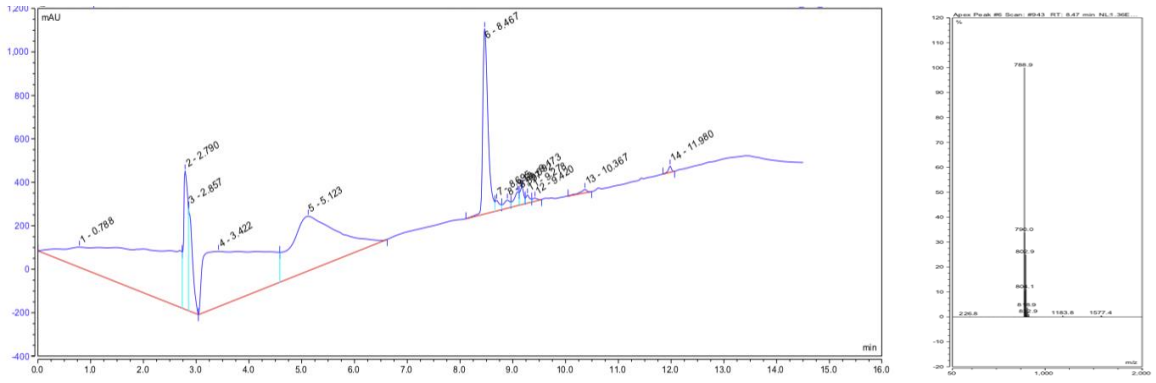

Figure 31(a) *– (Left): reversed phase LCMS, 225 nm UV chromatogram, for the first peak retained from prep-HPLC purification of mimetic peptide B(ii). (Right): TIC trace exhibited for the peak with retention time of 8.47 min; matching the expected mass to be produced by the target peptide with the succinimide cap cleaved.*

preparative HPLC, whereby the succinimide-capped peptide B(ii) was isolated successfully. After isolating all peaks exhibited by the preparatory HPLC apparatus, it was discovered that the reaction conditions employed during hydrogenation had resulted in cleavage of the succinimide cap from the N-terminus, leaving a free secondary amine at the N-terminus (peptide B(iii)). **Fig. 31** shows the LCMS and HRMS spectra obtained for both the capped and cap-cleaved mimetic structures retained.

As well as the succinimide-capped mimetic peptide mass being exhibited in **Fig. 31(b)**, the mass produced by the single peak from **Fig. 31(a)** (m/z = 788.90) matches that expected for the cap-cleaved derivative. Although a significant portion of the mimetic sample had suffered from succinimide group cleavage, this was a positive result, whereby construction of the open chain structure, RCM and hydrogenation had all been completed successful to yield the succinimide-capped structure.

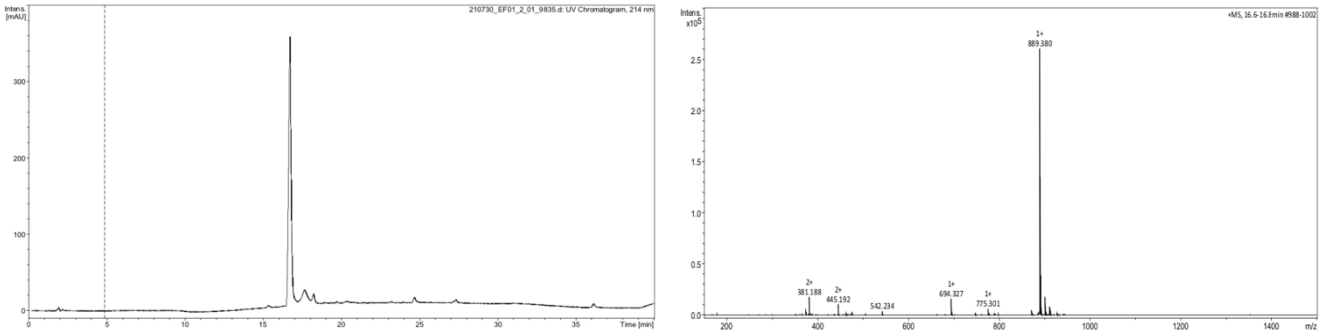

Figure 31(b) *– (Left): reversed phase HRMS, 214 nm UV chromatogram, for the second peak retained from prep-HPLC purification of mimetic peptide B(ii). (Right): HR-TIC trace exhibited for the peak with retention time of 16.7 min; matching the expected mass to be produced by the succinimide-capped mimetic peptide.*

Having isolated and characterized both the free amine and succinimide-capped peptide structures *via* LCMS, the samples were next passed on to a collaborator, Dr Ben Goult, here at the University of Kent School of Biosciences to probe their binding properties vs talin.

2.2.6 Synthesis of mimetic peptide C(i)

As was the case with mimetic peptides A and B, a method was constructed and the relevant amino acids were placed on the CEM apparatus to synthesise peptide C. **Fig. 32** below shows the LCMS UV chromatogram exhibited by the isolated compound, which was isolated in 85% yield.

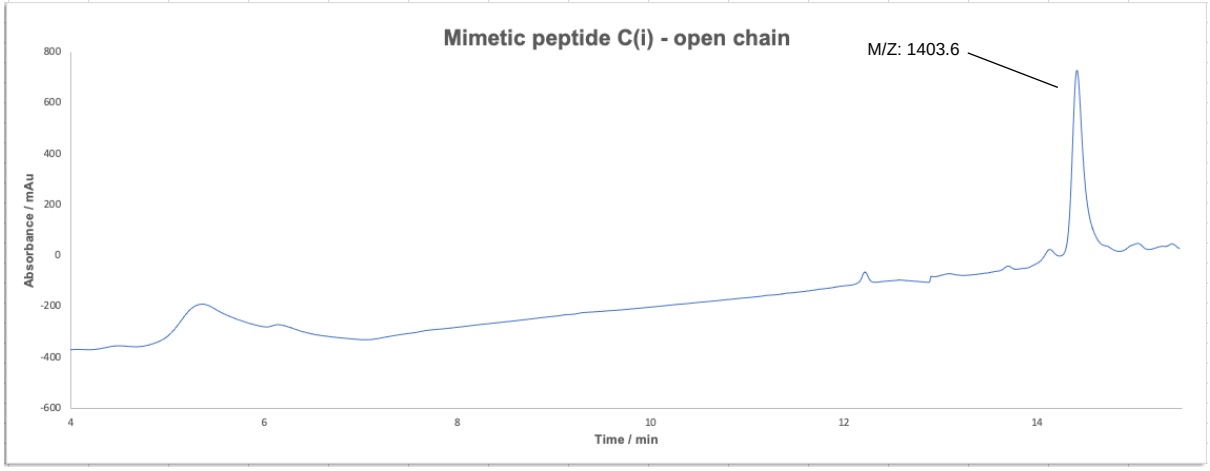

Figure 32 *– Reversed phase 225 nm UV chromatogram for the isolated, open-chain mimetic peptide C(i). The major peak with retention time of 14.41 mins constituted an m/z = 1403.60 when subjected to mass spectrometry.*

With the major peak shown on **Fig. 32** above constituting a mass of 1403.60 (appendix B), the target open chain peptide had been constructed, with a high level of purity. With the target structure in hand, RCM and hydrogenation reactions were therefore carried out.

2.2.7 RCM and hydrogenation reactions of mimetic peptide C(i)

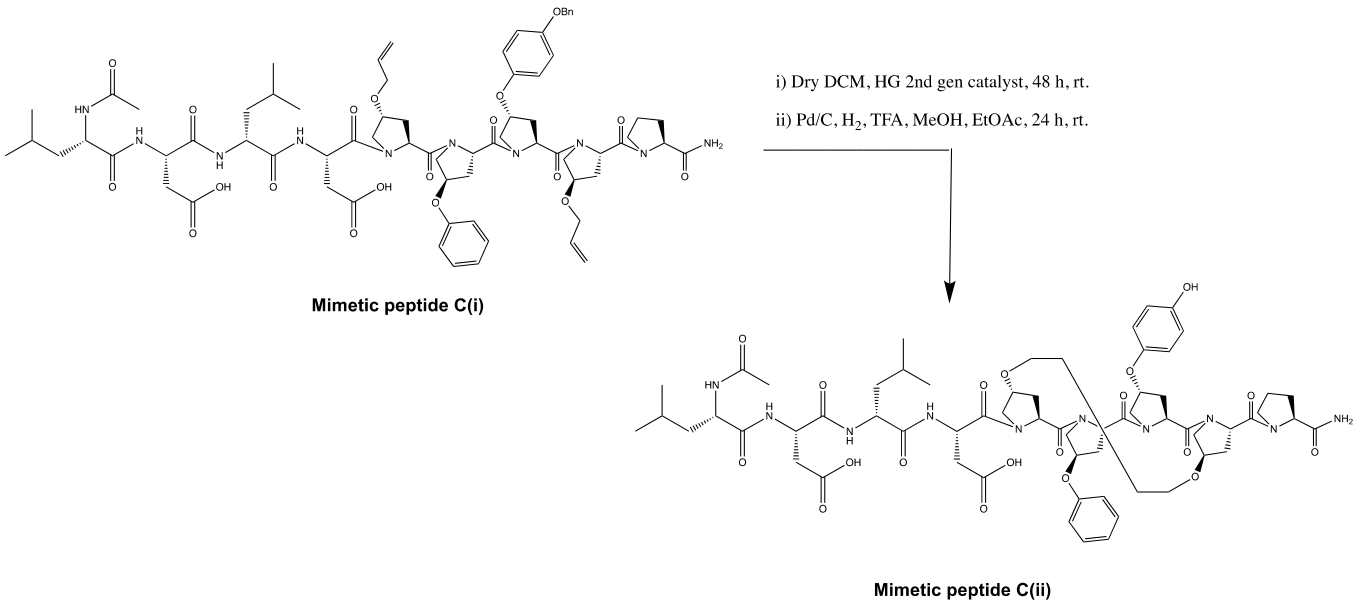

With the open-chain peptide in hand, RCM was next carried out, employing the same reaction conditions and method described for mimetic peptides A(i) and B(i). After 48 h, the RCM reaction of peptide C(i) was subjected to LCMS analysis and the resultant spectra showed the ring closed structure to have been successfully formed (**Fig. 33**).

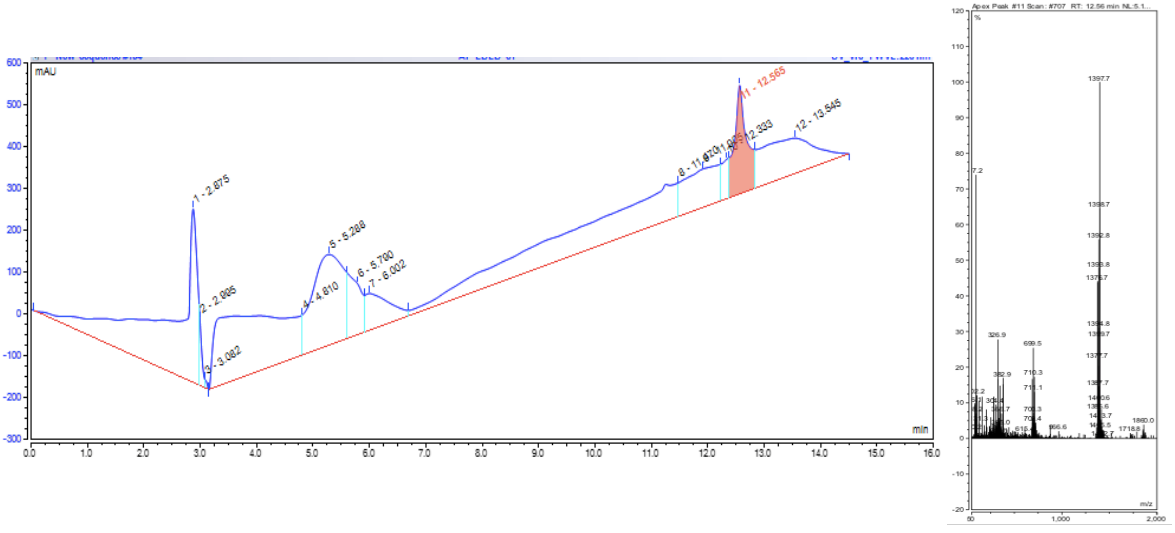

Figure 33 *– Reversed phase 225 nm UV chromatogram (left) and ion distribution for the peak with retention time of 12.565 min (right) for the RCM reaction of peptide C(i). A mass of 1397.7 signifies the presence of the desired [M + Na]⁺ ion and completion of reaction.*

An important point to make at this stage is the purification method employed for peptide C(ii). Initially, preparatory-HPLC purification was employed after the hydrogenation step, in the same way as for

mimetic peptide B(ii). The target mimetic structure was however isolated in very low yields. This was thought to be a result of Hoveyda-Grubbs catalyst degradation products preventing complete starting material consumption during hydrogenation as well as producing a complex HPLC chromatogram during purification. Purifying the peptide prior to hydrogenation proved to be a far more efficient methodology, whereby the HPLC spectra appeared noticeably cleaner and the target mimetic peptide was isolated in significantly higher yields.

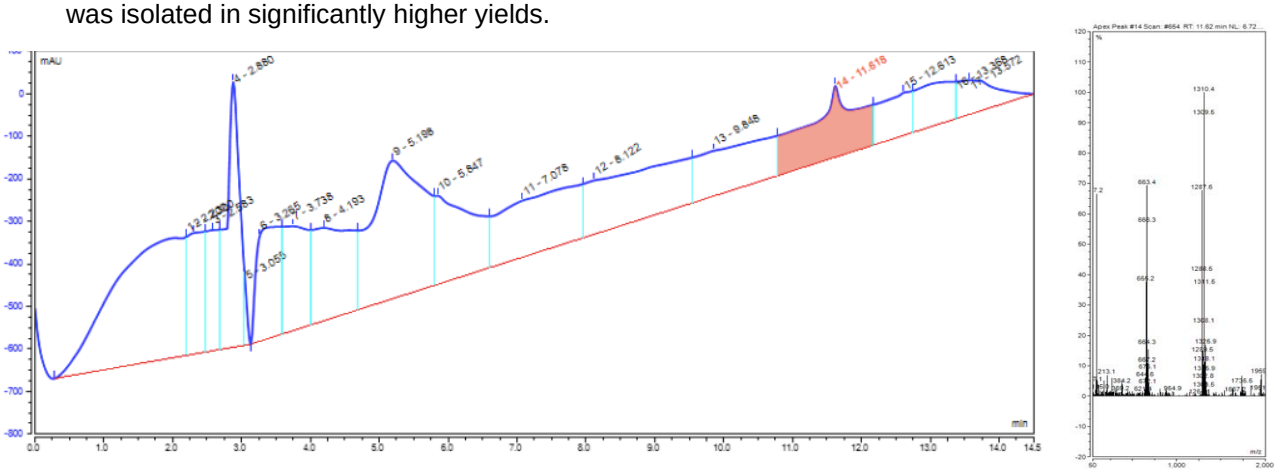

Figure 34 *– Reversed phase 225 nm UV chromatogram (left) and ion distribution for the peak with retention time of 11.618 mins (right) for the RCM reaction of the isolated peptide C(ii). A mass of 1310.40 signifies the presence of the desired [M + Na]$^+$ ion.*

After a smoother hydrogenation reaction, utilising a 15% Pd/C loading and without the use of TFA, the target mimetic peptide **C(ii)** was successfully isolated and characterised using LCMS as shown in **Fig. 34** below. A single peak constituting an m/z value of 1310.40 signifies the presence of the target mimetic peptide after preparatory-HPLC purification.

2.3 Structural analysis of the mimetic peptide structures

Dr. Ben Goult in the school of Biosciences here at the University of Kent has developed a highly specific assay to probe the possible interaction of the constructed mimetic with the talin substrate protein. This study will determine if the mimetic is binding to the talin substrate and more importantly, if binding is observed, the mimetic conformational structure may play a key role. Although samples of peptides B(ii), B(iii) and C(ii) have been passed on for binding analysis, project time restraints have resulted in data from this study not yet being received. As previously stated, the results of this study will allow us to determine the influence of varying functionalities attached to the N-terminus of the peptide, as well as the overall binding effectiveness of the constructed mimetic.

Chapter 3 - Conclusions and future work

To conclude the work of this thesis; the influence of hydrocarbon stapling on the conformational structure of a series of short-chain, unfunctionalized polyproline peptides has been investigated. After altering the positioning of a fixed-length hydrocarbon staple, a range of analytical techniques including CD, FT-IR and DOSY NMR analysis were employed in the probing of each peptide's structure. It was hypothesised after receiving results from these studies that within each peptide, a twisted or distorted PPII-like structure had been induced by the presence of the hydrocarbon staple. This structure has potential to be used as a novel extended framework with biological and supramolecular applications, however a crystal structure needs to firstly be obtained to fully understand the conformational structure present before carrying forward for any potential applications. In an attempt to gain a clearer picture of the conformational structure contained within each of the peptides, a single crystal was attempted to be grown, however with analysis of the produced crystal on going at the time of submission of this report. As a follow on from the aforementioned work, hydrocarbon stapling was next implemented into the development of a series of mimetic peptides. It was hoped that the use of hydrocarbon stapling would induce sufficient strain as to stabilise or even lock the conformational structure of these mimetic peptides, hereby enabling them to bind to a substrate protein more efficiently. The constructed mimetics, contained non-natural amino acid building blocks and differed by the structure of their N-terminal groups. With each structure being isolated and characterized, they were then passed on to a collaborator to determine their binding effectiveness vs a selected protein named talin. The results of this study are however yet to be received at the time of submission of this thesis.

With regards to future work and planning; one possible avenue to explore is the effect of an altered length and spanning distance hydrocarbon linker. Literature sources have employed double stapling as well as both longer and shorter hydrocarbon linkers in an attempt to induce conformational strain into a given peptide. In addition to these concepts, other forms of linkers (e.g, alkyne-azide, carbonate bridges) have been trialled. An investigation into the effectiveness of other linkage methods would be insightful and may lead to the discovery of other novel secondary structures with possible applications. Following on from this, the results from the crystallisation attempt of the basis peptides need to be reviewed when received in order to gain a fuller picture of conformational structures present. Tying-in with this, other crystallisation conditions and analyte concentrations could be trialled in attempt to grow a larger crystal of the desired peptide, which is sufficient to diffract and be analysed via crystal-XRD studies. Finally, the results of the mimetic peptide binding affinity studies need to be reviewed when received. The results of this study will help to identify the optimum functional group nature required at the N-terminus for effective binding to the target protein. Additional alterations of this group may be required as well as the experimentation of other functional groups attached to different proline units within the mimetic, to identify an effective mimetic structure which is able to interact and perform it's therapeutic role successfully.

Chapter 4 – Supporting material

4.0 Experimental

General aspects: Starting materials and reagents were used as purchased with no additional purification unless indicated otherwise. TLC was employed to monitor reactions. FluoroChem silica gel 60 aluminium plates were subjected to UV light and vanillin staining. Flash column chromatography (FCC) was carried out Acros Organics ultrapure 60 silica gel with a particle size 60-200 μm. Both ^{1}H and ^{13}C NMR measurements were carried out using a Bruker Avance II 400 MHz spectrometer, with TMS used as a reference. Liquid Chromatography Mass Spectrometry (LCMS) measurements were carried out using an Agilent Zorbax XDB C8 4.6 x 150 mm column, mobile phase = MeOH/H_2O, with both ESI+ and APCI+ ionisation methods used depending on the sample. Analytical and preparative HPLC measurements were carried out using an Agilent C18 25 x 10 mm column. For circular dichroism (CD) measurements, a Jasco J-715 spectropolarimeter was used to analyse 0.15 mg ml^{-1} samples in a 1 mm path length quartz cuvette. A spectral bandwidth of 190-260 nm was selected with results plotted as a function of molar elipticity (deg cm^2 $dmol^{-1}$). Fourier-Transform Infra-Red (FT-IR) measurements were carried out using a Shimadzu IR Affinity-1S spectrophotometer with peaks being reported in wavenumbers (cm^{-1}).

Synthesis of (2S,4R)-4-(allyloxy)-1-(tert-butoxycarbonyl)pyrrolidine-2-carboxylic acid (1.0):

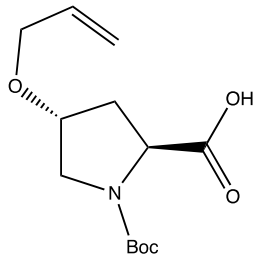

1.0

Sodium hydride (60% in mineral oil, 2.16 g, 54.05 mmol, 2.5 eq) was placed in a flame-dried, two neck flask, cooled under nitrogen. A solution of (2*S*,4*R*)-1-(*tert*-butoxycarbonyl)-4-hydroxypyrrolidine-2-carboxylic acid (4.95 g, 21.62 mmol, 1 eq) in anhydrous THF (21 ml) and DMSO (2.1 ml) was then added slowly at -20°C. The solution was then raised to 0°C for 30 min before allyl bromide (4.63 ml, 54.05 mmol, 2.5 eq) in anhydrous THF (12.6 ml) was added at -20°C. The solution was then left to stir at 24°C for 22 h. TLC was used to monitor the reaction (9:1, DCM:MeOH, v:v), with the product identified at R_f 0.4. The reaction was then diluted with water to pH 10 and washed with DCM (3 x 60 ml), before the collected aqueous layers were acidified to pH 3 with HCl (3 M) and quickly extracted into DCM (3 x 60 ml). The organic layers from the latter extraction were then washed with brine, dried with anhydrous magnesium sulphate and concentrated under reduced pressure, yielding a yellow oil **1.0 (3.70 g, 13.6 mmol, 63%).** ^{1}H NMR (400 MHz, $CDCl_3$) δ 9.68 (s, 1H), 6.00 – 5.74 (m, 1H), 5.25 – 5.13 (m, 2H), 4.38 (dt, *J* = 15.6, 7.6 Hz, 1H), 4.18 – 4.07 (m, 1H), 4.05 – 3.87 (m, 2H), 3.69 – 3.40 (m, 2H), 2.50 – 2.01

(m, 2H), 1.43 (d, *J* = 22.1 Hz, 9H). ^{13}C NMR (101 MHz, $CDCl_3$) δ 178.33 (s), 175.83 (s), 155.91 (s), 153.99 (s), 134.31 (s), 117.59 (s), 117.41 (s), 81.41 (s), 80.78 (s), 76.35 (s), 76.03 (s), 70.41 (s), 70.25 (s), 57.97 (s), 57.88 (s), 52.04 (s), 51.44 (s), 40.09 (s), 36.70 (s), 34.83 (s), 28.44 (s), 28. 30 (s). FT-IR = V_{max}/cm^{-1} 3010 (O-H), 1675 (C=O).

Synthesis of (2S,4R)-1-(((9H-fluoren-9-yl)methoxy)carbonyl)-4-(allyloxy)pyrrolidine-2-carboxylic acid (1.1):

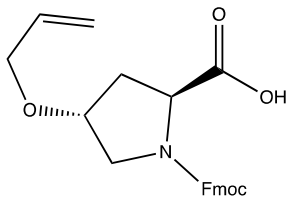

1.1

To a solution of compound **1.0** (3.6 g, 13.27 mmol, 1 eq) in DCM (19.8 ml), trifluoroacetic acid was added (19.8 ml, 265.4 mmol, 20 eq) and the solution allowed to stir for 90 min at 25°C, after which the solution was concentrated under reduced pressure to yield an orange oil. The oil was then dissolved in THF (20 ml) AT 0°C before saturated sodium bicarbonate (20 ml) was added slowly. Fmoc chloride (5.14 g, 19.87 mmol, 1.5 eq) was then added at 0°C before the solution was left to stir at 25°C for 24 h. TLC was used to monitor the reaction's progress (9:1, DCM:MeOH, v:v). After 24 h, the solution was acidified to pH 3 with HCl (3 M) before being quickly extracted into DCM (3 x 60 ml). The combined DCM layers were then dried with anhydrous magnesium sulphate and concentrated under reduced pressure to form **2.0 (4.63 g, 11.77 mmol, 89%).** ^{1}H NMR (400 MHz, $CDCl_3$) δ 10.49 (s, 1H), 7.83 – 7.66 (m, 2H), 7.64 – 7.50 (m, 2H), 7.47 – 7.21 (m, 4H), 5.98 – 5.78 (m, *J* = 15.1, 10.0, 5.6 Hz, 1H), 5.36 – 5.14 (m, 2H), 4.59 – 4.47 (m, 1H), 4.45 – 4.39 (m, 1H), 4.30 – 4.08 (m, 2H), 4.03 – 3.91 (m, 2H), 3.76 – 3.59 (m, 2H), 2.52 – 2.30 (m, 1H), 2.29 – 2.10 (m, 1H). ^{13}C NMR (101 MHz, $CDCl_3$) δ 177.04 (s), 176.11 (s), 155.81 (s), 154.98 (s), 143.93 – 143.43 (m), 141.40 (s), 141.30 (s), 134.22 (s), 134.13 (s), 127.96 – 127.69 (m), 127.18 (s), 125.10 (s), 124.98 (s), 120.08 (s), 120. 00 (s), 117.64 (s), 70.30 (s), 68.14 (s), 67. 99 (s), 58.13 (s), 57.62 (s), 52.12 (s), 51.84 (s), 47.20 (s), 47. 08 (s), 36.91 (s), 35.27 (s), 25.57 (s). FT-IR = V_{max}/cm^{-1} 3001 (O-H), 1681 (C=O), 1165, 1118 (C-O). LCMS (APCI-MS) *m/z*: $[M + H]^+$ calcd for $C_{23}H_{23}NO_5$ = 494.44, found = 494.10.

SPPS procedure for synthesis of the three basis peptides:

A CEM Liberty Lite peptide synthesiser was used in the construction of the three basis, functionalised prolyl peptides. Each amino acid addition cycle contained a double DMF/piperidine (20%) de-protection step, with acetyl capping steps inserted after the first and final amino acid couplings. The resin was swollen in DCM for 30 min prior to being placed on the peptide synthesis apparatus, all steps of the cycle were carried out at 75°C and once constructed, the final peptide was removed from the apparatus

and cleaved from the resin on the bench. **Table 1** shows the quantities of reagents used and the reaction times involved with each step of peptide synthesis.

Procedure	Compound	Quantity	Reaction time
Resin swelling	DCM	Cover resin	0.5 h
Deprotection	DMF:Piperidine, 8:2	3 ml	0.5 h
Coupling	DIC	2.5 eq	20 mins
	Oxyma	2.5 eq	
	Amino acid	2 eq	
	DMF	2 ml	
Capping	DIPEA	2.5 eq	20 mins
	Acetic anhydride	10 eq	
	DMF	100 eq	
Resin cleavage	TFA:DCM, 95:5	5 ml	1.5 h

Ring-closing metathesis reactions of functionalized, open chain peptides:

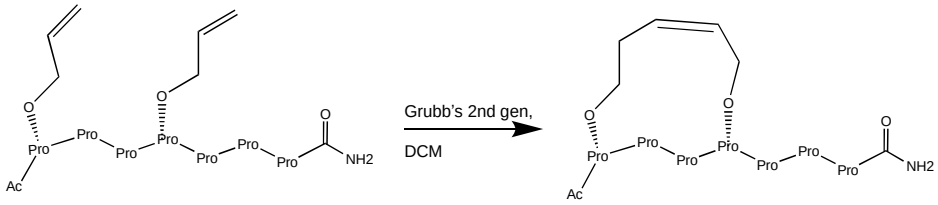

In accordance with results discussed earlier in this report, the optimized method for ring-closing metathesis is described here; with this being the method that resulted in greatest product conversion and minimal side-product generation.

A 10 ml r.b flask containing the open chain peptide (65 – 85 mg) was first purged with nitrogen and placed under an inert atmosphere. The peptide was then dissolved in anhydrous DCM (3.0 ml) with stirring at room temperature. Following this, the Hoveyda-Grubbs 2nd generation catalyst (6-8 mg, 10 mol%) in DCM (0.5 ml) was added dropwise over a period of 5 mins. The reaction vessel was sealed with a septum and laboratory film to prevent solvent evaporation and the reaction stirred for 24 h. After 24 h almost all reactions required an additional 5 mol% catalyst addition, with the high solvent volume/reaction dilution maintained throughout the course of the reaction. Reversed-phase analytical HPLC was used to monitor the progress of the reaction.

Hydrogenation reactions of ring-closed peptides (N-terminus staple position displayed):

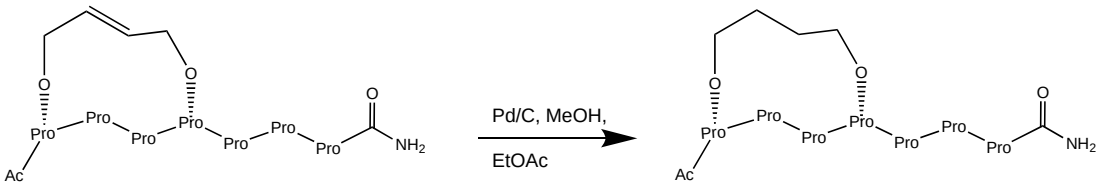

Pd/C (20%, w:w) was placed in a three-necked r.b flask which was sealed with two septa and attached to a Schlenk line apparatus. After carefully evacuating the flask and re-filling with nitrogen three times, EtOAc was dripped onto the Pd/C (enough to cover the solid) followed by the same volume of methanol. The peptide starting material was then dissolved in the minimum volume of methanol and injected into the reaction vessel with the vessel then being evacuated and re-filled with nitrogen 3 more times. A hydrogen-filled balloon was then inserted into the reaction vessel with the needle submerged in the solution and the reaction left to progress for 12 h. After 12 h, the H_2 balloon was removed, the flask filled with nitrogen and the reaction solution filtered through a 0.45 μm filter to remove any residual Pd/C. After solvent removal under reduced pressure, the stapled and hydrogenated peptide was isolated and carried forward for analysis.

Synthesis of 1-(tert-butyl) 2-methyl (2S,4S)-4-azidopyrrolidine-1,2-dicarboxylate (3.1):

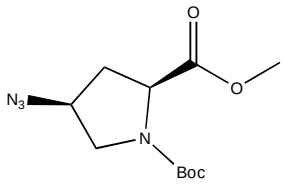

3.1

A solution of 1-(*tert*-butyl) 2-methyl (2*S*,4*R*)-4-hydroxypyrrolidine-1,2-dicarboxylate (2.00 g, 8.15 mmol, 1 eq) in DCM (18 ml) was cooled to 0°C under inert conditions and triethylamine (1.70 ml, 12.23 mmol, 1.5 eq) was added slowly. Methane sulfonyl chloride (0.95 ml, 12.23 mmol, 1.5 eq) was then added dropwise over the period of 30 mins after which, the reaction was raised to 25°C and left to stir for 2 h. After 2 h, TLC analysis (1:1, pet ether:EtOAc, v:v) revealed complete conversion of starting material to product so the reaction was diluted with DCM (20 ml) and the organic layer washed with brine (2 x 20 ml). The collected organic layer was then dried over anhydrous magnesium sulphate and the solvent removed under reduced pressure to yield compound **3.0** as a yellowish oil. **(2.50 g, 7.73 mmol, 94 %).** TLC analysis evidenced a high enough level of purity for the product to be carried forward for the next synthetic step and so further purification and characterization were not needed.

In a nitrogen-purged r.b flask, compound **3.0** (2.50 g, 7.73 mmol, 1 eq) was dissolved in anhydrous DMF (18 ml) and sodium azide (2.51 g, 38.65 mmol, 5 eq) added in one portion. The mixture was then stirred under nitrogen at 60°C for 12 h, behind a glass blast shield as a precaution for the explosive nature of the azide group. After 12 h, TLC analysis (1:1, pet ether:EtOAc, v:v) revealed completion of the reaction so the vessel was allowed to cool to room temperature and as much DMF as possible was removed under compressed air (2-3 hours). Once removed, the mixture was diluted with EtOAc (500 ml) and washed with water (2 x 250 ml) and brine (2 x 250 ml). The collected organic layer was then dried over anhydrous magnesium sulphate and the solvent removed with compressed air, to yield **3.1** as a yellowish oil **(1.77 g, 6.55 mmol, 85%).** ^{1}H NMR (400 MHz, $CDCl_3$) δ 4.36 (dm, *J* = 42.5, 8.9, 4.1 Hz, 1H), 4.23 – 4.07 (m, 1H), 3.75 (s, 3H), 3.73 – 3.64 (m, 1H), 3.46 (ddd, *J* = 15.8, 11.6, 3.9 Hz, 1H), 2.54 – 2.36 (m, *J* = 19.5, 8.8, 6.0 Hz, 1H), 2.23 – 2.10 (m, *J* = 13.0, 3.9 Hz, 1H), 1.43 (d, *J* = 22.0 Hz,

9H). ^{13}C NMR (101 MHz, $CDCl_3$) δ 172.25 (s), 171.17 (s), 153.79 (s), 153.73 (s), 80.69 (s), 80.61 (s), 59.33 (s), 58.34 (s), 57.81 (s), 57.42 (s), 52.47 (d, *J* = 16.3 Hz), 51.37 (s), 50.90 (s), 36.12 (s), 35.19 (s), 28.40 (s), 28.36 (s). FT-IR = V_{max}/cm^{-1} 3359 (O-H), 2108 (N=N=N), 1691, 1620 (C=Os), 1201, 1156 (C-O). LCMS (APCI-MS) *m/z*: $[M + H]^+$ calcd for $C_{11}H_{18}N_4O_4$ = 271.29, found = 271.10.

Synthesis of (2S,4S)-4-azido-1-(tert-butoxycarbonyl)pyrrolidine-2-carboxylic acid (3.2):

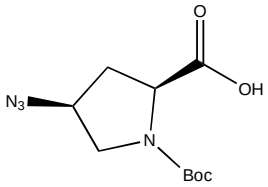

3.2

Compound **3.1** (1.70 g, 6.29 mmol, 1 eq) was first dissolved in THF (10 ml) MeOH (10 ml). LiOH (400 mg, 9.44 mmol, 1.5 eq) in water (5 ml) was then added and the solution left to stir for 2 h at 25°C. After 2 h, TLC analysis (6:4, pet ether:EtOAc, v:v) revealed complete conversion of starting material to product so the reaction was stopped and the solvent removed with compressed air. Crude compound **3.2** obtained as a yellow oil **(1.60 g, 6.25 mmol, 99%).** The crude product was then carried forward for use in further reactions without further purification. ^{1}H NMR (400 MHz, $CDCl_3$) δ 4.54 – 4.35 (m, 1H), 4.22 (s, 1H), 3.64 – 3.49 (m, 1H), 3.46 – 3.33 (m, *J* = 10.9 Hz, 1H), 2.81 – 2.63 (m, *J* = 12.7 Hz, 1H), 2.41 – 2.21 (m, 1H), 1.46 (d, *J* = 32.2 Hz, 9H).

Synthesis of (2S,4S)-1-(((9H-fluoren-9-yl)methoxy)carbonyl)-4-azidopyrrolidine-2-carboxylic acid (3.3):

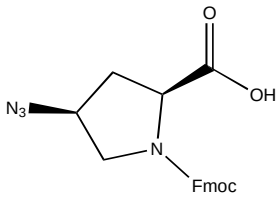

3.3

To compound **3.2** (1.60 g, 6.25 mmol, 1 eq) was added trifluoroacetic acid (9.30 ml, 124.88 mmol, 20 eq) and DCM (9.30 ml). The solution was then left to stir for 1.5 h at 25°C before removal of the TFA and DCM overnight with compressed air. The yellow oil remaining was next dissolved in THF (15 ml) and aqueous saturated sodium bicarbonate was added until the solution was basic (~ 20 ml). After being chilled to 0°C, Fmoc chloride (2.42 g, 9.35 mmol, 1.5 eq) was added in one portion and the solution left to stir for 30 mins before being warmed to room temperature and left to stir for 24 h. The resultant milky solution was monitored with TLC analysis (6:4, pet ether, EtOAc, v:v) after 24 h, with evolution of product being evidenced. The emulsion was then quenched with cold water (50 ml) and washed with cold di-ethyl ether. The aqueous layer was retained and acidified to pH 2 with 3 M HCl before being quickly extracted into EtOAc. The collected EtOAc layers were combined, washed with water (2 x 30 ml) and brine (2 x 30 ml) before being dried over anhydrous magnesium sulphate and the solvent being

removed by compressed air. Compound **3.3** was yielded as a yellow oil **(2.13 g, 5.62 mmol, 90 %).** ^{1}H NMR (400 MHz, $CDCl_3$) δ 7.83 – 7.68 (m, 2H), 7.65 – 7.52 (m, *J* = 12.3, 7.5 Hz, 2H), 7.45 – 7.27 (m, 4H), 4.66 – 4.11 (m, 5H), 3.73 – 3.60 (m, 1H), 3.53 (d, *J* = 11.1 Hz, 1H), 2.56 – 2.16 (m, 2H). ^{13}C NMR (101 MHz, $CDCl_3$) δ 141.49 (s), 128.01 (s), 127.30 (s), 125.20 (s), 125.12 (s), 120.19 (s), 120.15 (s), 68.81 (s), 58.97 (s), 53.56 (s), 47.20 (s), 34.02 (s), 28.51 (s).

Synthesis of (2S,4S)-1-(((9H-fluoren-9-yl)methoxy)carbonyl)-4-((tert-butoxycarbonyl)amino)pyrrolidine-2-carboxylic acid (3.4):

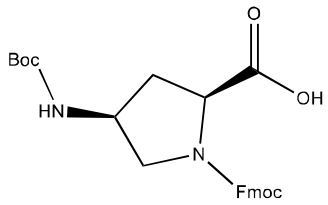

3.4

5% palladium on carbon (0.20 g, 10 wt %) was first placed in a three-necked, round-bottomed flask and evacuated/filled with N_2 three times. EtOAc was then dripped onto the Pd/C (enough to cover the solid), before the vessel was evacuated and re-filled with N_2 three times again. Compound **3.3 (2.12 g, 5.62 mmol, 1 eq)**, was dissolved in MeOH (10 ml) and dripped into the three-necked flask. After evacuating the vessel, a H_2 filled balloon was inserted so that its needle was suspended above the reaction mixture for 3 seconds. This was repeated twice before the third occasion whereby the H_2 balloon was submerged beneath the surface of the mixture and the reaction left to stir vigorously for 12 h with the H_2 balloon replaced when necessary. After 12 h, the reaction mixture was diluted with MeOH and filtered to remove residual Pd/C and to isolate the reduced amine **(1.82 g, 5.17 mmol, 92 %).** The crude compound obtained was then dissolved in THF (16 ml) before aqueous $NaHCO_3$ (2 ml) was added dropwise. Boc anhydride (1.35 g, 6.20 mmol, 1.2 eq) was then added and then solution left to stir at room temperature for 24 h. After 24 h, THF was removed using reduced pressure. After diluting with cold water, di-ethyl ether was then used to wash away any residual boc anhydride. The retained aqueous layer was then acidified and extracted into DCM, dried with Mg_2SO_4 and concentrated under reduced pressure to yield the final compound - **4.4 (4.08 mmol, 79 %).** ^{1}H NMR (400 MHz, $CDCl_3$) δ 7.83 – 7.68 (m, 2H), 7.65 – 7.52 (m, *J* = 12.3, 7.5 Hz, 2H), 7.45 – 7.27 (m, 4H), 4.66 – 4.11 (m, 5H), 3.73 – 3.60 (m, 1H), 3.53 (d, *J* = 11.1 Hz, 1H), 2.56 – 2.16 (m, 2H), 1.44 (d, *J* = 32.8 Hz, 9H). ^{13}C NMR (101 MHz, $CDCl_3$) δ 141.53 (s), 141.43(s), 128.01 (s), 127.30 (s), 125.18 (s), 125.06 (s), 120.19 (s), 68.81 (s), 58.97 (s), 53.56 (s), 47.31 (s), 47.19 (s), 34.02 (s), 28.51 (s). LCMS (APCI-MS) *m/z*: $[M + H]^+$ calcd for $C_{25}H_{28}N_2O_6$ = 453.51, found = 453.10.

Synthesis of 1-(tert-butyl) 2-methyl (2S,4S)-4-(4-(benzyloxy)phenoxy)pyrrolidine-1,2-dicarboxylate (4.0):

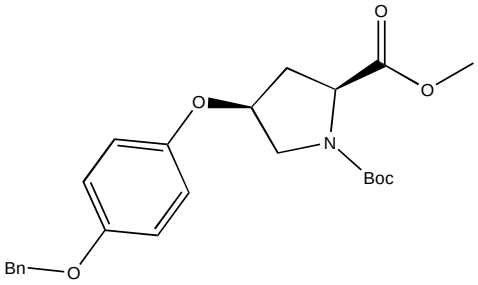

4.0

A solution of 1-(*tert*-butyl) 2-methyl (2*S*,4*R*)-4-hydroxypyrrolidine-1,2-dicarboxylate (0.50 g, 2.04 mmol, 1 eq) in THF (8 ml) was placed under nitrogen and 4-(benzyloxy)phenol (0.45 g, 2.24 mmol, 1.1 eq), diethyl azodicarboxylate (0.48 ml, 3.06 mmol, 1.5 eq) and triphenylphosphine (0.59 g, 2.24 mmol, 1.1 eq) were added. The solution was left to stir under nitrogen at 25°C and monitored *via* TLC analysis (8:2, pet ether:EtOAc, v:v), however with little to no evolution of product over the course of 24 h. Additional diethyl azodicarboxylate (0.48 ml, 1.5 eq), triphenylphosphine (1.02 g, 1.9 eq) and 4-(benzyloxy)phenol (0.78 g,1.9 eq) was therefore added and the reaction left to stir for a further 24 h. TLC after 48 h then revealed evolution of product spot and full consumption of starting material spot so column chromatography on silica (gradient elution, 0-30% EtOAc in pet ether) was carried out, isolating the pure compound **4.0** as a white solid **(700 mg, 1.64 mmol, 80 %)**. ^{1}H NMR (400 MHz, $CDCl_3$) δ 7.45 – 7.29 (m, 5H), 6.94 – 6.83 (m, *J* = 6.1, 3.0 Hz, 2H), 6.80 – 6.68 (m, 2H), 5.01 (s, 2H), 4.87 – 4.74 (m, *J* = 6.0, 3.1 Hz, 1H), 4.58 – 4.36 (m, 1H), 3.80 – 3.60 (m, 5H), 2.50 – 2.41 (m, 1H), 2.41 – 2.32 (m, *J* = 13.8, 9.1, 4.8 Hz, 1H), 1.45 (d, *J* = 17.7 Hz, 9H). ^{13}C NMR (101 MHz, $CDCl_3$) δ 173.35 (s), 173.31 (s), 154.36 (s), 153.63 (s), 151.03 (s), 137.09 (s), 128.52 (s), 127.88 (s), 127.41 (s), 117.03 (s), 116.96 (s), 115.93 (s), 80.32 (s), 75.55 (s), 70.58 (s), 57.98 (s), 57.57 (s), 52.25 (s), 52.04 (d), 51.82 (s), 36.54 (s), 35.58 (s), 28.32 (s), 28.22 (s). FT-IR = V_{max}/cm^{-1} 1753, 1697 (C=O), 1207, 1161 (C-O). LCMS (APCI-MS) *m/z*: $[M + H]^+$ calcd for $C_{24}H_{29}NO_6$ = 428.49, found = 428.10.

Synthesis of (2S,4S)-4-(4-(benzyloxy)phenoxy)-1-(tert-butoxycarbonyl)pyrrolidine-2-carboxylic acid (4.1):

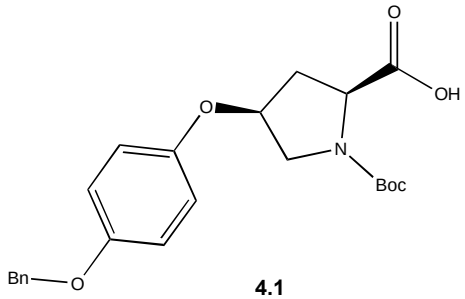

4.1

Compound **4.0** (650 mg, 1.52 mmol, 1 eq) was first dissolved in THF (5 ml) and MeOH (5 ml) with stirring before LiOH (64 mg, 2.66 mmol, 1.75 eq) in water (2.5 ml) was added to the solution and left to stir for 2 h. TLC was used to monitor the reaction (1:1, hexane:EtOAc, v:v) and once complete, THF

and MeOH were removed under reduced pressure. The crude product **4.1** was isolated as a white solid **(615 mg, 1.49 mmol, 98 %)**. ^{1}H NMR (400 MHz, $CDCl_3$) δ 7.44 – 7.26 (m, 5H), 6.93 – 6.85 (m, *J* = 13.6, 10.0 Hz, 2H), 6.83 – 6.75 (m, 2H), 5.00 (s, 2H), 4.78 (d, *J* = 2.9 Hz, 2H), 4.49 (dt, *J* = 45.2, 7.8 Hz, 1H), 3.84 – 3.51 (m, 2H), 2.65 – 2.17 (m, *J* = 21.2, 16.5, 10.4 Hz, 2H), 1.44 (d, *J* = 16.2 Hz, 9H). LCMS (ESI-MS) *m/z*: $[M + Na]^+$ calcd for $C_{23}H_{27}NO_6$ = 437.46, found = 437.10.

Synthesis of (2S,4S)-1-(((9H-fluoren-9-yl)methoxy)carbonyl)-4-(4-(benzyloxy)phenoxy)pyrrolidine-2-carboxylic acid (4.2):

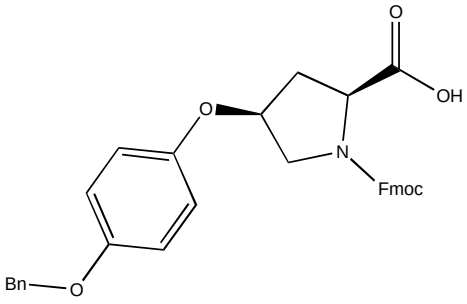

4.2

The crude compound **4.1** (615 mg, 1.49 mmol, 1 eq) was dissolved in TFA (2.21 ml, 29.74 mmol, 20 eq) and DCM (2.21 ml) before being left to stir at 25°C for 1.5 h. After 1.5 h, DCM and TFA were removed under reduced pressure and the resultant oil was dissolved in THF (4 ml) before saturated sodium bicarbonate (4 ml) was slowly added to the solution at 0°C. Following this, Fmoc-Cl (0.58 g, 2.23 mmol, 1.5 eq) was added and the solution left to stir for 30 min at 0°C before being warmed to room temperature and left to stir for 24 h. TLC analysis was used to monitor progress of the reaction (1:1, hexane:EtOAc, v:v) and when complete, the reaction was quenched with cold water (10 ml) and washed with cold diethyl ether (8 ml). The collected aqueous layers were then acidified with 3 M HCl to pH 3 before being quickly extracted into diethyl ether. The diethyl ether wash was also retained for fear of product presence in the wash. Both of the crude compounds obtained from the two separate ether fractions were then subjected to column chromatography on silica (gradient elution, 0 – 70% EtOAc in pet ether) where the pure product **4.2** was isolated (**518 mg, 0.97 mmol, 65%**). ^{1}H NMR (400 MHz, $CDCl_3$) δ 7.72 (d, *J* = 7.6 Hz, 2H), 7.56 (d, *J* = 7.3 Hz, 2H), 7.45 – 7.27 (m, 9H), 6.95 – 6.67 (m, 4H), 4.98 (d, 2H), 4.84 (s, 1H), 4.59 (s, 2H), 4.41 (s, 1H), 4.27 (s, 1H), 3.84 – 3.64 (m, 2H), 2.72 (d, *J* = 14.4 Hz, 1H), 2.37 (s, 1H). ^{13}C NMR (101 MHz, $CDCl_3$) δ 153.83 (s), 150.48 (s), 143.73 (s), 141.31 (s), 137.10 (s), 128.55 (s), 127.87 (s), 127.82 (s), 127.47 (s), 127.11 (s), 124.93 (s), 119.99 (s), 117.37 (s), 115.92 (s), 70.54 (s), 52.11 (s), 47.16 (s). FT-IR = V_{max}/cm^{-1} 1707 (C=O), 1203 (C-O). LCMS (ESI-MS) *m/z*: $[M + Na]^+$ calcd for $C_{33}H_{29}NO_6$ = 558.19, found = 558.10.

Synthesis of (2S,4R)-1-((benzyloxy)carbonyl)-4-hydroxypyrrolidine-2-carboxylic acid (5.0):

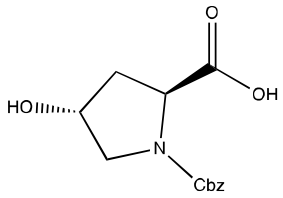

5.0

(2*S*,4*R*)-4-hydroxypyrrolidine-2-carboxylic acid(2*S*,4*R*)-4-hydroxypyrrolidine-2-carboxylic acid (2.50 g, 19.07 mmol, 1 eq) was first dissolved in THF (9 ml) and H_2O (9 ml) before $NaHCO_3$ (3.20 g, 38.13 mmol, 2 eq) was added. After being cooled to 0°C for 0.5 h, benzyl chloroformate (3.90 g, 22.88 mmol, 1.2 eq) was added dropwise over the course of 0.5 h, after which the reaction was allowed to warm to room temperature and stirred for 24 h. TLC was used to monitor reaction progress (hexane:EtOAc, 1:1, v:v) and after 24 h, the reaction was quenched with H_2O (20 ml) before being washed with cold di-ethyl ether. The aqueous layer was retained and acidified to pH 2 before being extracted into EtOAc. The combined organic layers were washed with brine, dried over anhydrous Mg_2SO_4 before being concentrated under reduced pressure to yield compound **5.0** as a colourless oil **(4.35 g, 16.40 mmol, 86%).** ^{1}H NMR (400 MHz, MeOD) δ 7.39 – 7.25 (m, 5H), 5.16 – 5.03 (m, 2H), 4.47 – 4.36 (m, *J* = 16.0, 8.0 Hz, 2H), 3.65 – 3.49 (m, 2H), 2.38 – 2.23 (m, *J* = 12.9, 9.7, 8.1, 2.9, 1.5 Hz, 1H), 2.16 – 2.01 (m, 1H). ^{13}C NMR (101 MHz, MeOD) δ 176.26 (s), 175.97 (s), 156.84 (s), 156.52 (s), 137.87 (s), 137.73 (s), 129.47 (s), 129.38 (s), 129.07 (s), 128.87 (s), 128.84 (s), 128.55 (s), 70.65 (s), 69.96 (s), 68.33 (s), 68.26 (s), 59.29 (s), 59.02 (s), 56.02 (s), 55.65 (s), 40.16 (s), 39.31 (s). LCMS (ESI-MS) *m/z*: $[M + Na]^+$ calcd for $C_{13}H_{15}NO_5$ = 288.08, found = 288.00.

Synthesis of dibenzyl (2S,4R)-4-hydroxypyrrolidine-1,2-dicarboxylate (5.1):

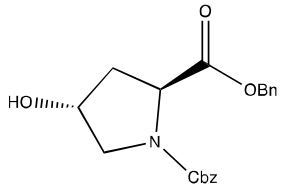

5.1

Compound **5.0** (4.35 g, 16.40 mmol, 1 eq) was first dissolved in anhydrous DMF (13 ml) and the reaction vessel purged with nitrogen gas. To this solution was added NaI (0.25 g, 1.64 mmol, 0.1 eq) and K_2CO_3 (5.00 g, 36.07 mmol, 2.2 eq) were added with stirring before benzyl bromide (4.84 ml, 49.19 mmol, 3 eq) was added dropwise over the period of 1 h, leading to the formation of a white suspension. After 24 h of room temperature stirring, the reaction was diluted with EtOAc (30 ml) and washed with H_2O (20 ml) 8 times in order to remove DMF from the solution. Following this, the collected EtOAc layer was washed with brine to remove any residual salts and then with hexane to remove any un-reacted benzyl bromide. After washing, some benzyl bromide remained so column chromatography on silica (gradient

elution, 0 – 40% EtOAc in hexane) was used to isolate compound **5.1 (5.76 g, 13.93 mmol, 85%)** as a colourless oil. ^{1}H NMR (400 MHz, $CDCl_3$) δ 7.42 – 7.18 (m, 10H), 5.20 (q, *J* = 26.0, 13.2 Hz, 1H), 5.05 – 5.00 (m, *J* = 10.8, 5.7 Hz, 2H), 4.57 (dt, *J* = 15.6, 7.9 Hz, 1H), 4.47 – 4.38 (m, *J* = 7.3, 3.0 Hz, 1H), 3.71 – 3.52 (m, 2H), 3.10 (s, 1H), 2.38 – 2.21 (m, 1H), 2.11 – 2.00 (m, 1H). ^{13}C NMR (101 MHz, $CDCl_3$) δ 172.46 (s), 172.35 (s), 155.02 (s), 154.55 (s), 136.19 (s), 136. 06 (s), 135.36 (s), 135.24 (s), 128.57 – 128.06 (m), 128.06 – 127.78 (m), 127.69 (s), 127.61 (s), 69.72 (s), 68.99 (s), 67.16 (s), 67.09 (s), 66.75 (s), 66.67 (s), 60.36 (s), 57.92 (s), 57.79 (s), 55.07 (s), 54.47 (s), 38.95 (s), 38.15 (s), 20.90 (s), 14.03 (s). LCMS (ESI-MS) *m/z*: $[M + H]^+$ calcd for $C_{20}H_{21}NO_5$ = 355.14, found = 355.40.

Synthesis of dibenzyl (2S,4R)-4-(2-(tert-butoxy)-2-oxoethoxy)pyrrolidine-1,2-dicarboxylate (5.2):

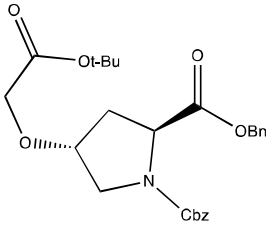

5.2

In a flame-dried r.b flask under an inert atmosphere was first added NaH (60% in mineral oil (0.67 g, 27.87 mmol, 2 eq)), TBAI (0.52 g, 1.39 mmol, 0.1 eq), t-butyl bromo-acetate (4.76 g, 24.39 mmol, 1.75 eq) and anhydrous THF (50 ml). Compound **5.1** (6.54 g, 13.93 mmol, 1 eq) was next dissolved in anhydrous THF (50 ml) with this solution the being added dropwise to the basic solution over a period of 1.5 h. After monitoring the reaction with TLC (3:7, EtOAc:hexane, v:v), all starting material had been consumed after 24 h and so the reaction was quenched with cold H_2O, acidified to pH 3 before being extracted with DCM. The crude mixture obtained was purified with the use of column chromatography on silica (gradient elution, 0 – 30% EtOAc in hexane) to yield compound **5.2 (4.45 g, 9.48 mmol, 68%)** as a yellowish oil. ^{1}H NMR (400 MHz, $CDCl_3$) δ 7.43 – 7.18 (m, 10H), 5.29 – 5.15 (m, 2H), 5.07 (s, 1H), 5.01 (s, 1H), 4.62 – 4.48 (m, 1H), 4.27 – 4.19 (m, 1H), 3.96 (q, *J* = 16.7 Hz, 2H), 3.84 – 3.61 (m, 2H), 2.56 – 2.37 (m, 1H), 2.19 – 2.07 (m, 1H), 1.48 (d, 9H). ^{13}C NMR (101 MHz, $CDCl_3$) δ 172.33 (s), 172.10 (s), 169.02 (s), 154.70 (s), 154.18 (s), 136.30 (s), 136. 25 (s), 135.42 (s), 135.32(s), 128.57 – 127.55 (m), 81.84 (s), 77.84 (s), 67.28 – 66.49 (m), 57.94 (s), 57.70 (s), 51.72 (s), 51.64 (s), 36.61 (s), 35.32 (s), 27.85 (s). LCMS (ESI-MS) *m/z*: $[M + Na]^+$ calcd for $C_{26}H_{31}NO_7$ = 492.20, found = 492.10.

Synthesis of (2S,4R)-4-(2-(tert-butoxy)-2-oxoethoxy)pyrrolidine-2-carboxylic acid (5.3):

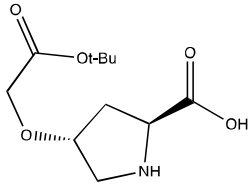

5.3

To a 3-necked r.b flask attached to a Schlenk line, was added 5% palladium on carbon (0.67 g, 15 weight%) before the vessel was evacuated and re-filled with nitrogen three times. EtOAc (enough to cover the solid) was then dripped into the vessel slowly and the evacuation/re-filling procedure repeated 3 times again. Compound **5.2** (4.45 g, 9.48 mmol, 1 eq) dissolved in MeOH (50 ml) was then added slowly to the palladium-charged r.b flask and once complete, the evacuation/re-filling procedure was repeated 3 times. After evacuating the vessel, a H_2 filled balloon was inserted so that it's needle was suspended above the reaction mixture for 3 seconds. This was repeated twice before the third occasion whereby the H_2 balloon was submerged beneath the surface of the mixture and the reaction was left to stir vigorously for 12 h with the H_2 balloon replaced when necessary. After 12 h, the suspension was diluted with MeOH before being filtered with a 0.45 μm filter to remove residual Pd/C. After removing the MeOH under reduced pressure, compound **5.3** was isolated as a white solid **(2.11 g, 8.62 mmol, 91%).** ^{1}H NMR (400 MHz, $CDCl_3$) δ 4.35 – 4.21 (m, 1H), 4.17 – 4.09 (m, 1H), 4.04 (d, 2H), 3.46 – 3.21 (m, 2H), 2.57 – 2.45 (m, 1H), 2.09 – 1.94 (m, 1H), 1.43 (d, *J* = 4.1 Hz, 9H). ^{13}C NMR (101 MHz, $CDCl_3$) δ 174.09 (s), 171.73 (s), 83.41 (s), 83.35 (s), 80.60 (s), 79.43 (s), 68.21 (s), 67.89 (s), 67.35 (s), 61.65 (s), 58.80 (s), 56.94 (s), 52.33 (s), 37.38 (s), 37.32 (s), 36.66 (s), 28.60 (s), 19.22 (s), 18.09 (s). LCMS (ESI-MS) *m/z*: $[M + Na]^+$ calcd for $C_{11}H_{19}NO_5$ = 268.12, found = 268.10.

Synthesis of (2S,4R)-1-(((9H-fluoren-9-yl)methoxy)carbonyl)-4-(2-(tert-butoxy)-2-oxoethoxy)pyrrolidine-2-carboxylic acid (5.4):

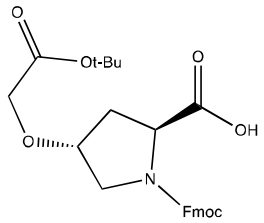

5.4

Compound **5.3** (2.11 g, 8.62 mmol, 1 eq) was first dissolved in THF (9 ml) and H_2O (9 ml) before $NaHCO_3$ (1.45 g, 17.24 mmol, 2 eq) was added and the solution cooled to 0°C in an ice bath with stirring. To this solution was added Fmoc-Cl (3.35 g, 12.93 mmol, 1.5 eq), with the solution maintained at 0°C for 0.5 h before being raised to room temperature and stirred for 24 h. TLC was used to monitor the reaction (3:7, EtOAc:hexane, v:v) and once all starting material had been consumed, the white suspension concentrated under reduced pressure to remove the THF before being acidified to pH 3 using 1 M HCl and extracted into DCM. The retained organic layers were washed with brine, dried over anhydrous Mg_2SO_4 before being concentrated under reduced pressure. Due to the presence of residual Fmoc-cl, the crude oil was subjected to column chromatography on silica (gradient elution, 0 – 40% EtOAc in hexane) to purify the pure compound **5.4** as a colourless oil **(2.82 g, 6.04 mmol, 70%).** ^{1}H NMR (400 MHz, $CDCl_3$) δ 7.65 (dd, *J* = 25.8, 7.5 Hz, 2H), 7.53 – 7.43 (m, 2H), 7.36 – 7.19 (m, 4H), 6.49 (s, 1H), 4.49 – 4.02 (m, 5H), 3.94 – 3.79 (m, 2H), 3.74 – 3.50 (m, 2H), 2.50 – 2.30 (m, 1H), 2.24 – 2.03 (m, 1H), 1.40 (d, *J* = 8.8 Hz, 9H). ^{13}C NMR (101 MHz, $CDCl_3$) δ 177.21 (s), 175.54 (s), 169.34 (s),

155.95 (s), 154.69 (s), 144.07 (s), 143.84 (s), 143.75 (s), 141.40 (s), 141.34 (s), 141.28 (s), 127.86 (s), 127.74 (s), 127.24 (s), 127.20 (s), 125.16 (s), 125.06 (s), 120.11 (s), 120. 02 (s), 82.30 (s), 82.26 (s), 77.85 (s), 68.24 – 67.84 (m), 67.05 (s), 66.99 (s), 58.14 (s), 57.48 (s), 51.91 (s), 51.82 (s), 47.21 (s), 47.15 (s), 36.99 (s), 34.98 (s), 28.25 (s), 28.15 (s), 25.67 (s). LCMS (ESI-MS) *m/z*: $[M + Na]^+$ calcd for $C_{26}H_{29}NO_7$ = 490.18, found = 490.10.

Synthesis of 1-(tert-butyl) 2-methyl (2S,4R)-4-phenoxypyrrolidine-1,2-dicarboxylate (6.0):

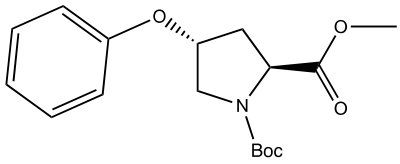

6.0

To a solution of 1-(*tert*-butyl) 2-methyl (2*S*,4*R*)-4-hydroxypyrrolidine-1,2-dicarboxylate (0.94 g, 3.81 mmol, 1 eq) in anhydrous THF (7 ml) and under a nitrogen atmosphere, was added phenol (0.90 g, 9.53 mmol, 2.5 eq), PPh_3 (2.50 g, 9.53 mmol, 2.5 eq) and DEAD (1.50 ml, 9.53 mmol, 2.5 eg). After addition of the DEAD, the solution thickened significantly and was left to stir at room temperature for 24 h. The reaction was monitored using TLC (8:2, hexane:EtOAc, v:v) and once all of the starting material had been consumed, the THF was removed under reduced pressure before being dissolved in EtOAc and washed with brine. The crude mixture left was next purified using column chromatography on silica (gradient elution, 0-30% EtOAc in hexane) to yield the final product **6.0** (**980 mg, 3.05 mmol, 80%**). ^{1}H NMR (400 MHz, $CDCl_3$) δ 7.35 – 7.21 (m, 2H), 6.95 (q, *J* = 6.9 Hz, 1H), 6.83 (d, *J* = 8.0 Hz, 2H), 4.88 (s, 1H), 4.45 (dt, *J* = 30.2, 7.8 Hz, 1H), 3.87 – 3.61 (m, 5H), 2.63 – 2.43 (m, *J* = 22.5, 11.4 Hz, 1H), 2.29 – 2.12 (m, 1H), 1.44 (d, *J* = 15.3, 8.4 Hz, 9H). ^{13}C NMR (101 MHz, $CDCl_3$) δ 173.29 (s), 173.13 (s), 156.84 (s), 156.81 (s), 154.31 (s), 153.61 (s), 129.45 (s), 121.40 (s), 115.58 (s), 115.52 (s), 80.29 (s), 75.27 (s), 74.53 (s), 57.87 (s), 57.67 (s), 52.55 – 51.65 (m), 36.34 (s), 35.56 (s), 28.29 (s), 28.19 (s), 14.11 (s) 14. 05 (s). FT-IR = V_{max}/cm^{-1} 1732, 1688 (C=O), 1170 (C-O). LCMS (ESI-MS) *m/z*: $[M + Na]^+$ calcd for $C_{17}H_{23}NO_5$ = 344.15, found = 344.10.

Synthesis of (2S,4R)-1-(tert-butoxycarbonyl)-4-phenoxypyrrolidine-2-carboxylic acid (6.1):

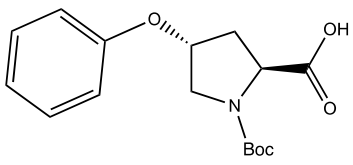

6.1

Compound **6.0** (980 mg, 3.05 mmol, 1 eq) was dissolved in THF:MeOH, 1:1 (8 ml) before LiOH (256 mg, 6.10 mmol, 2 eq) in H_2O (2 ml) was added to the solution dropwise. This solution was then left to

stir for 4 h at room temperature with TLC used to monitor the reaction's progress (7:3, hexane:EtOAc, v:v). After 4 h, the THF and MeOH were removed under reduced pressure before acidifying the resulting solution to pH 3 and extracting with DCM to isolate the final product **6.1** (**853 mg, 2.78 mmol, 91%**). ^{1}H NMR (400 MHz, $CDCl_3$) δ 10.48 (s, 1H), 7.34 – 7.23 (m, 2H), 6.97 (q, *J* = 7.7 Hz, 1H), 6.90 – 6.81 (m, 2H), 4.90 (s, 1H), 4.50 (dt, 1H), 3.86 – 3.66 (m, 2H), 2.64 – 2.46 (m, 1H), 2.44 – 2.22 (m, 1H), 1.47 (d, 9H). ^{13}C NMR (101 MHz, $CDCl_3$) δ 177.41 (s), 176.11 (s), 171.52 (s), 156.81 (s), 155.26 (s), 153.97 (s), 129.63 (s), 129.58 (s), 129.38 (s), 124.55 (s), 124.41 (s), 121.55 (s), 121.45 (s), 119.74 (s), 115.61 (s), 115.54 (s), 115.47 (s), 81.35 – 80.77 (m, *J* = 21.7, 11.9 Hz), 75.08 (s), 74.55 (s), 60.51 (s), 57.87 (s), 57.78 (s), 52.10 (s), 51.99 (s), 36.42 (s), 35.18 (s), 28.26 (d), 20.95 (s), 14.11 (s). V_{max}/cm^{-1} 1683 (C=O), 1224, 1168 (C-O).

Synthesis of (2S,4R)-1-(((9H-fluoren-9-yl)methoxy)carbonyl)-4-phenoxypyrrolidine-2-carboxylic acid (6.2):

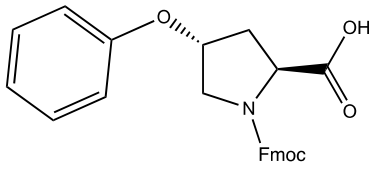

6.2

Compound **6.1** (853 mg, 2.78 mmol, 1 eq) was first dissolved in TFA (4.14 ml, 55.6 mmol, 20 eq) and DCM (4 ml) before being stirred for 3 h to remove the Boc protecting group. After 3 h had passed, the DCM and TFA were removed under reduced pressure, yielding an off-white oil. This oil was then dissolved in THF (6 ml) before $NaHCO_3$ (700 mg, 8.34 mmol, 3 eq) in H_2O (6 ml) was added, before chilling the solution down to 0°C. Once at 0°C, Fmoc-Cl (1.08 g, 4.17 mmol, 1.5 eq) was added, the solution left in the ice bath for 30 mins before allowing the flask to warm to room temperature and stir for 24 h. After monitoring reaction progress with TLC (6:4, hexane:EtOAc, v:v) all starting material had been consumed after 24 h so the THF was removed under reduced pressure. Acid-base extraction with diethyl-ether was known to cause problems in isolation of the desired product for this reaction so the crude viscous oil was straight away purified using column chromatography on silica (0-40% EtOAc in hexane) to yield the final compound **6.2** (**489 mg, 1.89 mmol, 68%**) as a colourless oil. ^{1}H NMR (400 MHz, $CDCl_3$) δ 8.36 (s, 1H), 7.69 – 7.56 (m, 2H), 7.54 – 7.34 (m, *J* = 24.1, 16.8, 8.7 Hz, 2H), 7.32 – 7.05 (m, 6H), 6.90 (dt, *J* = 22.1, 7.4 Hz, 1H), 6.82 – 6.68 (m, *J* = 14.6, 8.0 Hz, 2H), 4.80 (d, *J* = 29.0 Hz, 1H), 4.47 (dt, *J* = 42.9, 7.9 Hz, 1H), 4.39 – 4.21 (m, 2H), 4.10 (dt, *J* = 13.2, 6.9 Hz, 1H), 3.86 – 3.63 (m, 2H), 2.62 – 2.41 (m, 1H), 2.34 – 2.10 (m, 1H). ^{13}C NMR (101 MHz, $CDCl_3$) δ 177.36 (s), 176.05 (s), 156.81 (s), 156.75 (s), 155.75 (s), 154.69 (s), 144.06 (s), 143.76 (s), 143.71 (s), 141.38 (s), 141.35 (s), 129.88 (s), 129.82 (s), 127.85 (s), 127.79 (s), 127.19 (s), 125.12 (s), 125.04 (s), 121.80 (s), 121.76 (s), 120.08 (s), 120.03 (s), 115.70 (s), 115.67 (s), 75.09 (s), 74.49 (s), 68.15 (s), 68.01 (s), 58.23 (s), 57.61 (s), 52.69 (s), 52.16 (s), 47.24 (s), 47.14 (s), 36.80 (s), 35.36 (s). FT-IR = V_{max}/cm^{-1} 1703 (C=O), 1224, 1165 (C-O). LCMS (ESI-MS) *m/z*: $[M + Na]^+$ calcd for $C_{26}H_{23}NO_5$ = 452.46, found = 452.10.

Synthesis of 1-(tert-butyl) 2-methyl (2S,4R)-4-(4-(benzyloxy)phenoxy)pyrrolidine-1,2-dicarboxylate (7.0):

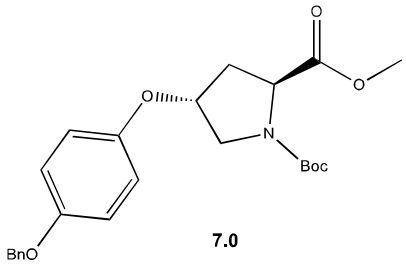

7.0

A solution of 1-(*tert*-butyl) 2-methyl (2*S*,4*S*)-4-hydroxypyrrolidine-1,2-dicarboxylate (1.00 g, 4.08 mmol, 1 eq) in THF (15 ml) was placed under nitrogen before 4-(benzyloxy)phenol (0.90 g, 4.49 mmol, 1.1 eq), and triphenylphosphine (1.18 g, 4.49 mmol, 1.1 eq) were added. After cooling the solution to 0°C, 1,1'-(Azidocarbonyl)dipiperidine (1.54 g, 6.12 mmol, 1.5 eq) in THF (5 ml) was added dropwise, with a yellow suspension forming 5 minutes after addition. The solution was then allowed to warm to room temperature and stirred for 24 h. After 24 h, TLC analysis showed complete conversion of starting material (25:75, EtOAc:hexane, v:v) and so column chromatography on silica (gradient elution, 0-30% EtOAc in pet ether) was carried out, isolating the pure compound **7.0** as a white solid **(1.34 g, 3.14 mmol, 77 %)**. ^{1}H NMR (400 MHz, $CDCl_3$) δ 7.45 – 7.29 (m, 5H), 6.94 – 6.83 (m, *J* = 6.1, 3.0 Hz, 2H), 6.80 – 6.68 (m, 2H), 5.01 (s, 2H), 4.87 – 4.74 (m, *J* = 6.0, 3.1 Hz, 1H), 4.58 – 4.36 (m, 1H), 3.80 – 3.60 (m, 5H), 2.50 – 2.41 (m, 1H), 2.41 – 2.32 (m, *J* = 13.8, 9.1, 4.8 Hz, 1H), 1.45 (d, *J* = 17.7 Hz, 9H). ^{13}C NMR (101 MHz, $CDCl_3$) δ 173.38 (s), 173.25 (s), 154.36 (s), 153.63 (s), 151.03 (s), 137.09 (s), 128.52 (s), 127.88 (s), 127.41 (s), 117.05 (s), 117.01 (s), 115.93 (s), 80.32 (s), 75.55 (s), 70.58 (s), 57.98 (s), 57.57 (s), 52.25 (s), 52.04 (d), 51.82 (s), 36.54 (s), 35.58 (s), 28.31 (s), 28.23 (s). FT-IR = V_{max}/cm^{-1} 1753, 1697 (C=O), 1207, 1161 (C-O). LCMS (APCI-MS) *m/z*: $[M + H]^+$ calcd for $C_{24}H_{29}NO_6$ = 428.49, found = 428.10.

Synthesis of (2S,4R)-4-(4-(benzyloxy)phenoxy)-1-(tert-butoxycarbonyl)pyrrolidine-2-carboxylic acid (7.1):

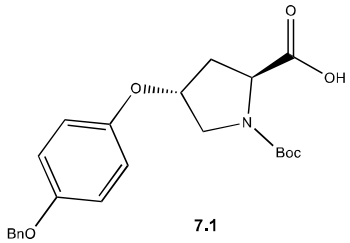

7.1

Compound **7.0** (1.34 g, 3.14 mmol, 1 eq) was first dissolved in THF (5 ml) and MeOH (5 ml) with stirring before LiOH (0.23 g, 5.50 mmol, 1.75 eq) in water (4 ml) was added to the solution and left to stir for 2 h. TLC was used to monitor the reaction (1:1, hexane:EtOAc, v:v) and once complete, THF and MeOH were removed under reduced pressure. The crude product **7.1** was isolated as a white solid **(1.20 g, 2.89 mmol, 92 %)**. ^{1}H NMR (400 MHz, $CDCl_3$) δ 7.44 – 7.26 (m, 5H), 6.93 – 6.85 (m, *J* = 13.6, 10.0 Hz, 2H), 6.83 – 6.75 (m, 2H), 5.00 (s, 2H), 4.78 (d, *J* = 2.9 Hz, 2H), 4.49 (dt, *J* = 45.2, 7.8 Hz, 1H), 3.84 – 3.51 (m, 2H), 2.65 – 2.17 (m, *J* = 21.2, 16.5, 10.4 Hz, 2H), 1.44 (d, *J* = 16.2 Hz, 9H). LCMS (ESI-MS) *m/z*: $[M + Na]^+$ calcd for $C_{23}H_{27}NO_6$ = 437.46, found = 437.10.

Synthesis of (2S,4R)-1-(((9H-fluoren-9-yl)methoxy)carbonyl)-4-(4-(benzyloxy)phenoxy)pyrrolidine-2-carboxylic acid (7.2):

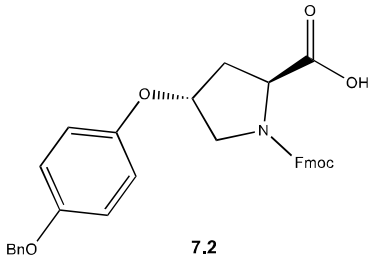

7.2

The crude compound **7.1** (1.20 g, 2.89 mmol, 1 eq) was dissolved in TFA (4.31 ml, 57.82 mmol, 20 eq) and DCM (4.31 ml) before being left to stir at 25^{0}C for 1.5 h. After 1.5 h, DCM and TFA were removed under reduced pressure and the resultant oil was dissolved in THF (7 ml) before saturated sodium bicarbonate (7 ml) was slowly added to the solution at 0°C. Following this, Fmoc-Cl (1.12 g, 4.34 mmol, 1.5 eq) was added and the solution left to stir for 30 min at 0°C before being warmed to room temperature and left to stir for 24 h. TLC analysis was used to monitor progress of the reaction (1:1, hexane:EtOAc, v:v) and when complete, the reaction was quenched with cold water (20 ml) and washed with cold di-ethyl ether (10 ml). The collected aqueous layers were then acidified with 3 M HCl to pH 3 before being quickly extracted into di-ethyl ether. The di-ethyl ether wash was also retained for fear of product presence in the wash. Both of the crude compounds obtained from the two separate ether fractions were then subjected to column chromatography on silica (gradient elution, 0 – 60% EtOAc in pet ether) where the pure product **7.2** was isolated (**1.16 g, 2.17 mmol, 75%**). ^{1}H NMR (400 MHz, $CDCl_3$) δ 7.72 (d, *J* = 7.6 Hz, 2H), 7.56 (d, *J* = 7.3 Hz, 2H), 7.45 – 7.27 (m, 9H), 6.95 – 6.67 (m, 4H), 4.98 (d, 2H), 4.84 (s, 1H), 4.59 (s, 2H), 4.41 (s, 1H), 4.27 (s, 1H), 3.84 – 3.64 (m, 2H), 2.72 (d, *J* = 14.4 Hz, 1H), 2.37 (s, 1H). ^{13}C NMR (101 MHz, $CDCl_3$) δ 153.83 (s), 150.48 (s), 143.73 (s), 141.31 (s), 137.10 (s), 128.55 (s), 127.89 (s), 127.77 (s), 127.47 (s), 127.11 (s), 124.93 (s), 119.99 (s), 117.37 (s), 115.92 (s), 70.54 (s), 52.11 (s), 47.16 (s). FT-IR = V_{max}/cm^{-1} 1707 (C=O), 1203 (C-O). LCMS (ESI-MS) *m/z*: $[M + Na]^+$ calcd for $C_{33}H_{29}NO_6$ = 558.19, found = 558.10.

Generic experimental procedure for mimetic peptide RCM reactions:

To a flame dried 10 ml r.b. flask under a nitrogen atmosphere, the respective peptide (1.0 eq) was first dissolved in anhydrous DCM to a concentration of 33 mM. After purging and re-filling the reaction vessel with nitrogen three times, the Hoveyda-Grubbs 2nd generation catalyst (0.15 eq) was next dissolved in the minimum quantity of anhydrous DCM and added dropwise to the reaction vessel with stirring. After addition of the catalyst, the reaction vessel was purged and re-filled with nitrogen once more before allowing the reaction to stir for 24 h. Reaction progression was monitored using analytical HPLC.

Generic experimental procedure for mimetic peptide hydrogenation reactions:

The same experimental procedure was used for hydrogenation of the mimetic peptides as was employed for the three basis peptides. This method can be found earlier in section **4.0**.

5.0 References

(1) (a) V. Kubyshkin, S. L. Grage, J. Bürck, A. S. Ulrich and N. Budisa, *J. Phys. Chem. Lett.* 2018, **9**, 2170-2174.

(b) I. Z. Steinberg, W. F. Harrington, A. Berger, M. Sela and E. Katchalski, *J. Am. Chem. Soc.* 1960, **82**, 5263-5379.

(c) K. H. Forsythe and A. J. Hopfinger, *"The influence of solvent on the secondary structures of poly(L-alanine) and poly(L-proline)". Macromolecules.* 1973, **6**, 423-437.

(2) A. A. Adzhubei, M. J. E. Sternberg and A. A. Makarov, *J. Mol. Biol.* 2013, **425**, 2100-2132.

(3) A. A. Makarov, N. G. Esipova, Y. A. Pankov, V. M. Lobachev and B. A. Grishkovsky, *Biochem. Biophys. Res. Commun.* 1975, **67**, 1378–1383.

(4) A. A. Adzhubei, F. Eisenmenger, V. G. Tumanyan, M. Zinke, S. Brodzinski and N. G. Esipova, *Biochem. Biophys. Res. Commun.* 1987, **146**, 934–938.

(5) A. A Makarov, N. G. Esipova, V. M. Lobachov, B. A. Grishkovsky and Y. A. Pankov, *"Secondary structure of polypeptide hormones of the anterior lobe of the pituitary gland". Biopolymers.* 1984, **23**, 5–22.

(6) A. A. Makarov, V. M. Lobachov, I. A. Adzhubei and N. G. Esipova, "*Natural polypeptides in left-handed helical conformation. A circular dichroism study of the linker histones' C-terminal fragments and beta-endorphin". FEBS Lett.* 1992, **306**, 63–65.

(7) R. W. Newberry and R. T. Raines, *"The n→π* Interaction". Acc. Chem. Res.* 2017, **50**, 1838−1846.

(8) M. P. Hinderaker and R. T. Raines, *"An Electronic Effect on Protein Structure". Protein Sci.* 2003, **12**, 1188−1194.

(9) R. Wieczorek and J. J. Dannenberg, *J. Am. Chem. Soc.* 2003, **125**, 8124-8129.

(10) L. Shi, A. E. Holliday, N. Khanal, D. H. Russell and D. E. Clemmer, *J. Am. Chem. Soc.* 2015, **137**, 8680-8683.

(11) (a) L. Shi, A. E. Holliday, H. Shi, F. Zhu, M. A. Ewing, D. H. Russell and D. E. Clemmer, *J. Am. Chem. Soc.* 2014, **136**, 12702-12711.

(b) L. Shi, A. E. Holliday, M. S. Glover, M. A. Ewing, D. H. Russell and D. E. Clemmer, *J. Am. Chem. Soc. Mass Spectrom.* 2015.

(12) R. K. Dukorm and T. A. keiderling, *"Reassessment of the random coil conformation: Vibrational CD study of proline oligopeptides and related polypeptides," Biopolymers,* 1991, **31**, no. 14, 1747-1761.

(13) J. D. Hostert, C. N. Loney, N. Pramounmat, K. Yan, Z. Su and J. N. Renner, *Langmuir,* 2021, **37**, 6115-6122.

(14) (a) C. L. Tsai, S. Y. Wu, H. K. Hsu, S. B. Huang, C. H. Lin, Y. T. Chan and S. K. Wang, *Nanoscale,* 2021, **13**, 4592-4601.

(b) T. Schnitzer, E. Paenurk, N. Trapp, R. Gershoni-Poranne and H. Wennemers, *J. Am. Chem. Soc.* 2021, **143**, 644-648.

(15) T. M. Klingler and D. L. Brutlag, *"Discovering structural correlations in alpha-helices". Protein Sci.* 1994, **3**, 1847−1857.

(16) P. Balaram, *"Non-standard amino acids in peptide design and protein engineering". Curr. Opin. Struct. Biol.* 1992, **2**, 845−851.

(17) D. Y. Jackson, D. S. King, J. Chmielewski, S. Singh and P. G. Schultz, *J. Am. Chem. Soc.* 1991, **113**, 9391−9392.

(18) C. Bracken, J. Gulyas, J. W. Taylor and J. Baum, *J. Am. Chem. Soc*. 1994, **116**, 6431−6432.

(19) S. T. Chen, H. J. Chen, H. M. Yu and K. T. Wang, *J. Chem. Res., Synop.* 1993, 228−229.

(20) H. E. Blackwell and R. H. Grubbs, *Angew. Chem., Int. Ed*. 1994, **37**, 3281−3284.

(21) K. Sakagami, T. Masuda, K. Kawano and S. Futaki, *"Importance of Net Hydrophobicity in the Cellular Uptake of All-Hydrocarbon Stapled Peptides", Molecular Pharmaceutics.* 2018, **15, (3),** 1332-1334.

(22) (a) C. E. Schafmeister, J. Po and G. L. Verdine, *J. Am. Chem. Soc.* 2000, **122**, 5891−5892.

(b) D. Burtscher, K. Grela, *Angew. Chem. Int. Ed.* 2008, **48, (3),** 442-454.

(23) L. D. Walensky and G. H. Bird, *J. Med. Chem.* 2014, **57**, 6275-6288.

(24) X. Li, S. Chen, W. D. Zhang and H. G. Hu, *Chem. Rev.* 2020, **120**, 10079-10144.

(25) C. E. Schafmeister, J. Po and G. L. Verdine, *J. Am. Chem. Soc.* 2000, **122**, 5891-5892.

(26) M. Kümin, L. S. Sonntag and H. Wennemers, *J. Am. Chem. Soc.* 2007, **129,** (**3**), 466-467.

(27) E. Beausoleil and W. Lubell, *Biopolymers,* 2000, **53**, (**3**), 249-256.

(28) W. H. Tseng, M. C. Li, J. C. Horng and S. K. Wang, *ChemBioChem,* 2019, **20**, 153-158.

(29) S. Kakinoki, Y. Hirano and M. Oka, *Polymer Bulletin,* 2005, **53**, 109-115.

(30) R. K. Dukorm and T. A. Keiderling, *Biopolymers.* 1991, **31**, (**14**), 1747-1761.

(31) B. C. Bohrer, S. I. Merenbloom, S. L. Koeniger, A. E. Hilderbrand, and D. E. Clemmer, *"Biomolecule Analysis by Ion Mobility Spectrometry," Annual Review of Analytical Chemistry,* 2008, **1**, 293-327.

(32) V. Mihali, F. Foschi, M. Penso and G. Pozzi, *J. Org. Chem.* 2014*,* **24**, 5351-5355.

(33) D.F. Brightwell, *"The synthesis of an array of stapled polyproline peptides", Masters thesis,* 2019, 15-16.

(34) Young-Woo Kim, Tom N Grossmann, Gregory L Verdine, *Nature Protocols.* 2011, **6, (6),** 761-771.

(35) J.C. Horng and R.T. Raines, "*Stereoelectronic effects on polyproline conformation".* 2006, **15**, 74-83.

(36) B. N. Bullock, A. L. Jochim and P. S. Arora, *J. Am. Chem. Soc.* 2011, **133(36)**, 14220.

(37) D. P. Ryan and J. M. Matthews, *Curr. Opin. Struct. Biol*. 2005, **15**, 441.

(38) M. R. Arkin and J. A. Wells, *Nat. Rev. Drug Discovery*. 2004, **3**, 301.

(39) P. J. Hajduk and J. Greer, *J. Nat. Rev. Drug Discovery.* 2007, **6**, 211.

(40) L. Lo Conte, C. Chothia and J. J. Janin, *Mol. Biol.* 1999, **285**, 2177.

(41) M. Guharoy and P. Chakrabarti, *Bioinformatics.* 2007,**23**,1909.

(42) S. Jones and J. M. Thornton, *Prog. Biophys. Mol. Biol.* 1995, **63**, 31.

(43) L. K. Henchey, S. Kushal, R. Dubey, R. N. Chapman, B. Z. Olenyuk and P. S. Arora, *J. Am. Chem. Soc.* 2010, **132**, 941.

(44) A. Patgiri, K. K. Yadav, P. S. Arora and D. Bar-Sagi, *Nat. Chem. Biol.* 2011, **7**, 585.

(45) P. S. Kutchukian, J. S. Yang, G. L. Verdine and E. I. Shakhnovich, *J. Am. Chem. Soc.* 2009, **131, (13),** 4622-4627.

(46) F. Bernal, A. F. Tyler, S. J. Korsmeyer, L. D. Walensky and G. L. Verdine, *J. Am. Chem. Soc.* 2007, **129**, 2456-2457.

(47) Kastan, M. B.; Onyekwere, O.; Sidransky, D.; Vogelstein, B.; Craig, R. W. Cancer Res. 1991, 51, 6304-6311.

(48) (a) X. Wu, J. H. Bayle, D. Olson and A. J. Levine, *Genes Dev.* 1993, **7**, 1126- 1132.

(b) E. Yonish-Rouach, D. Resnftzky, J. Lotem, L. Sachs, A. Kimchi and M. Oren, *Nature.* 1991, **352**, 345-347.

(c) J. Momand, G. P. Zambetti, D. C. Olson, D. George and A. J. Levine, *Cell.* 1992, **69**, 1237.

(49) P. Chéne, *Nat. Rev. Cancer.* 2003, **3**, 102-109.

(50) P. H. Kussie, S. Gorina, V. Marechal, B. Elenbaas, J. Moreau, A. J. Levine and N. P. Pavletich, *Science.* 1996, **274**, 948-953.

(51) (a) K. Sakurai, H. S. Chung and D. J. Kahne, *Am. Chem. Soc.* 2004, **126**, 16288-16289.

(b) L. T. Vassilev, B. T. Vu, B. Graves, D. Carvajal, F. Podlaski, Z. Filipovic, N. Kong, U. Kammlott, C. Lukacs, C. Klein, N. Fotouhi and E. A. Liu, *Science* 2004, **303**, 844-848.

(52) S. Baek, P. S. Kutchukian, G. L. Verdine, R. Huber, T. A. Holak, K. W. Lee and G. M. Popowicz, *J. Am. Chem. Soc.* 2012, **134**, 103-106.

(53)R. E. Gough, M. C. Jones, T. Zacharchenko, S. Le, M. Yu, G. Jacquemet, S. P. Muench, J. Yan, J. D. Humphries, C. Jorgensen, M. J. Humphries and B. T. Goult, *J. Biol. Chem.* 2021, **297(1)**, 100837.

(54) P. S. Humphries, Q. Q. T. Do and D. M. Wilhite, *Beilstein Journal of Organic Chemistry,* 2006, **2:**21, 2.

6.0 Appendices

Contents:

Appendix A – NMR Spectra

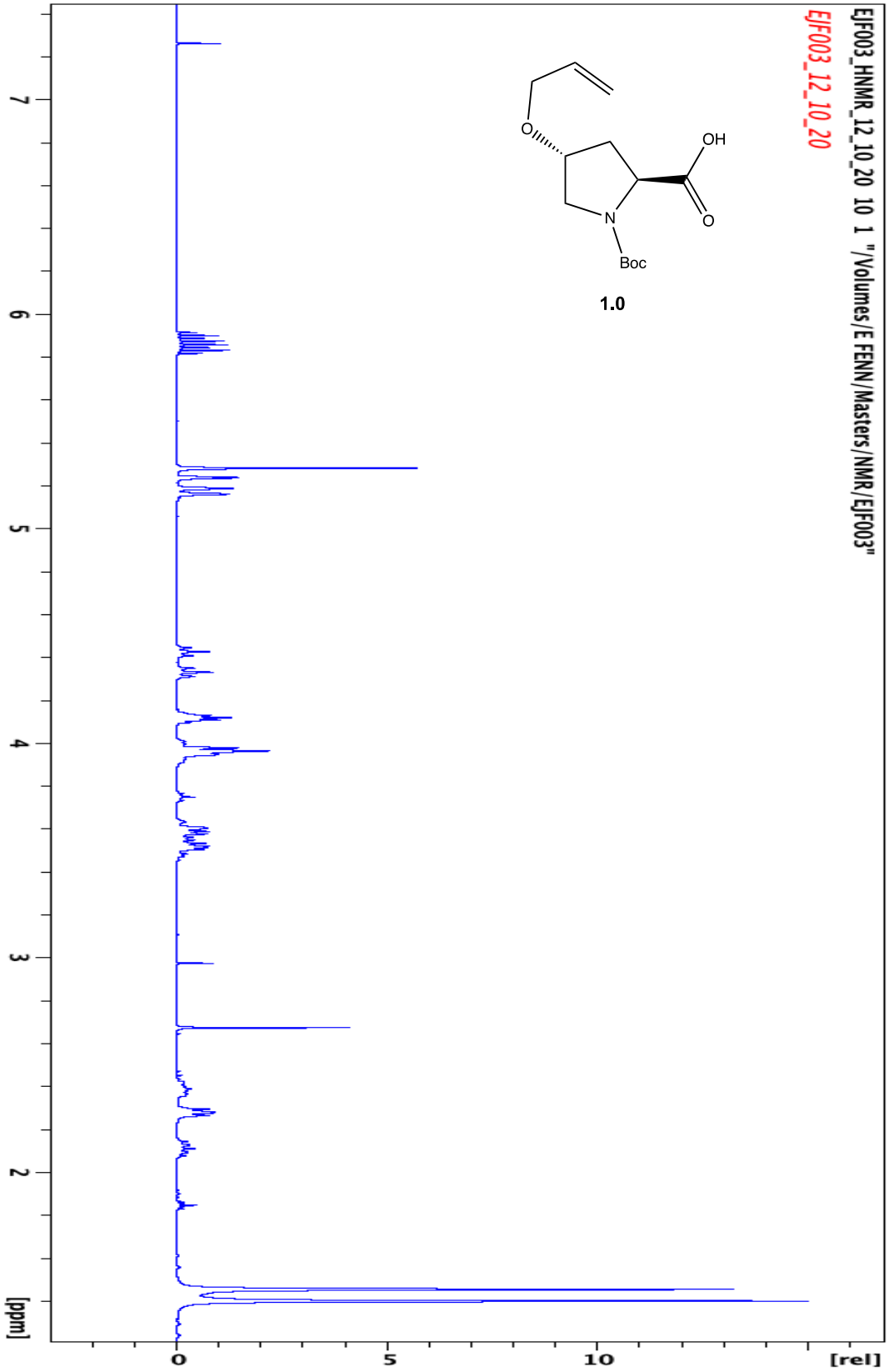

1.0 – ^{1}H NMR (25^{0} C, $CDCl_3$)

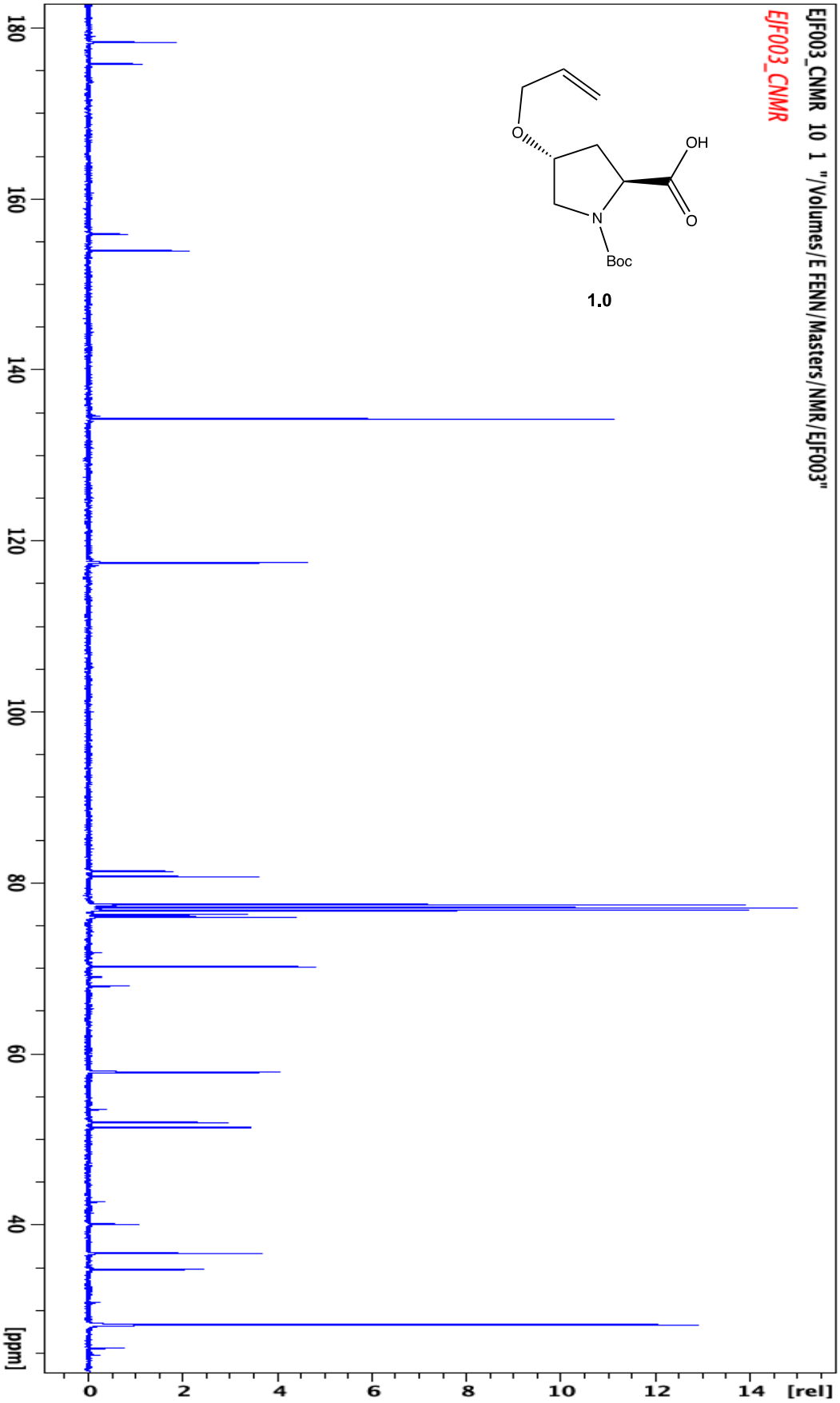

1.0 – ^{13}C NMR (25^0 C, $CDCl_3$)

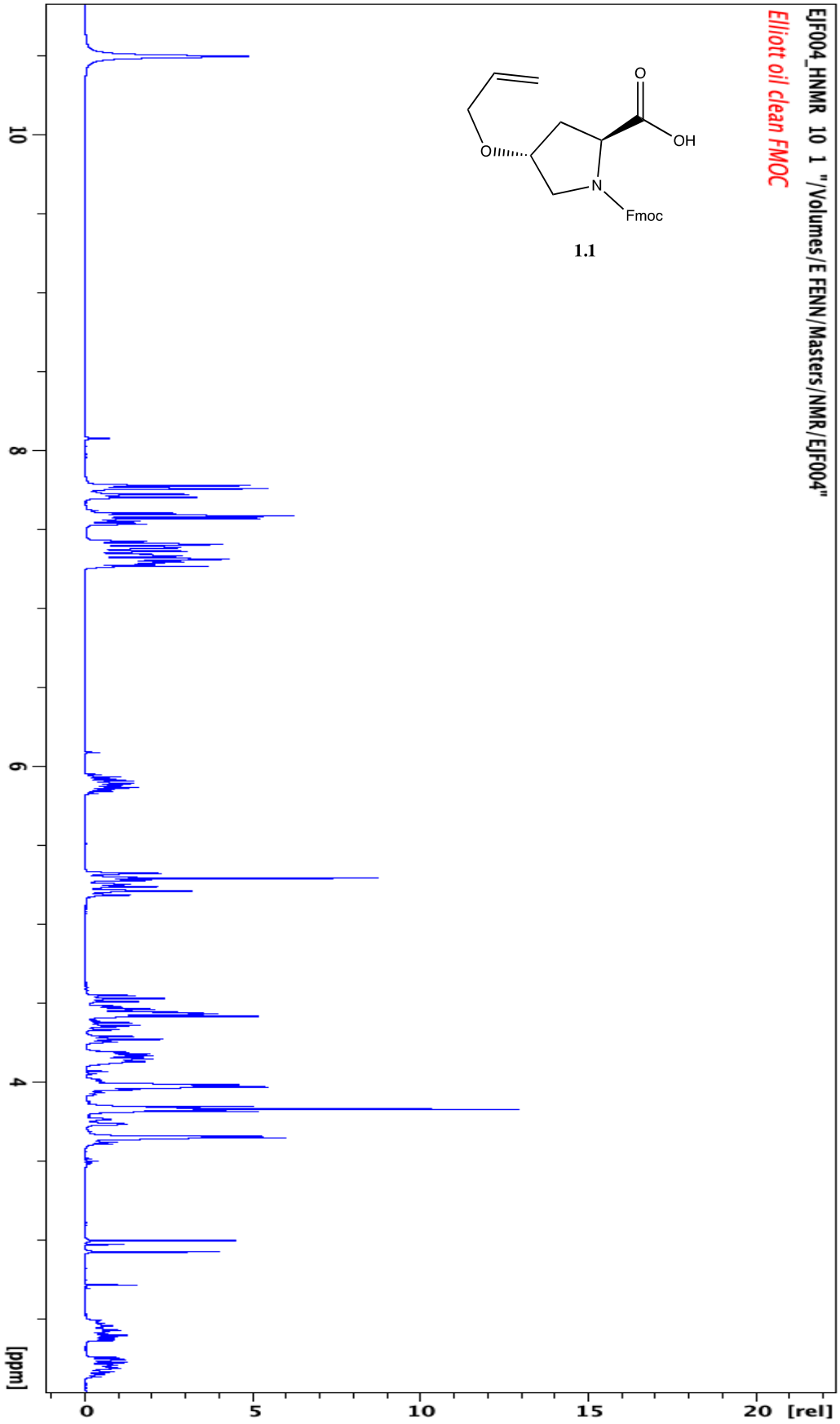

1.1 – ^{1}H NMR (25^{0} C, $CDCl_3$)

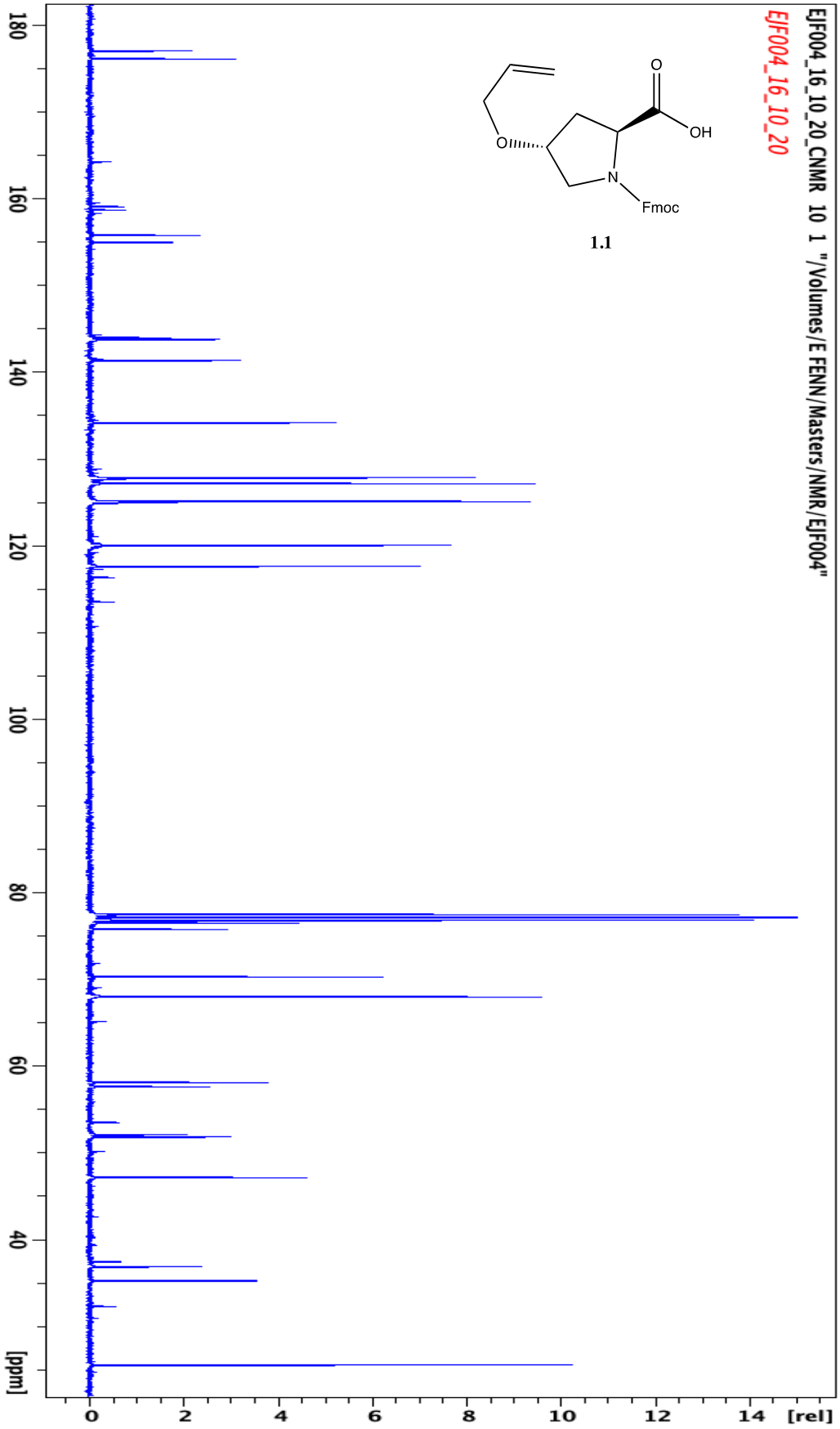

1.1 – ^{13}C NMR (25^0 C, $CDCl_3$)

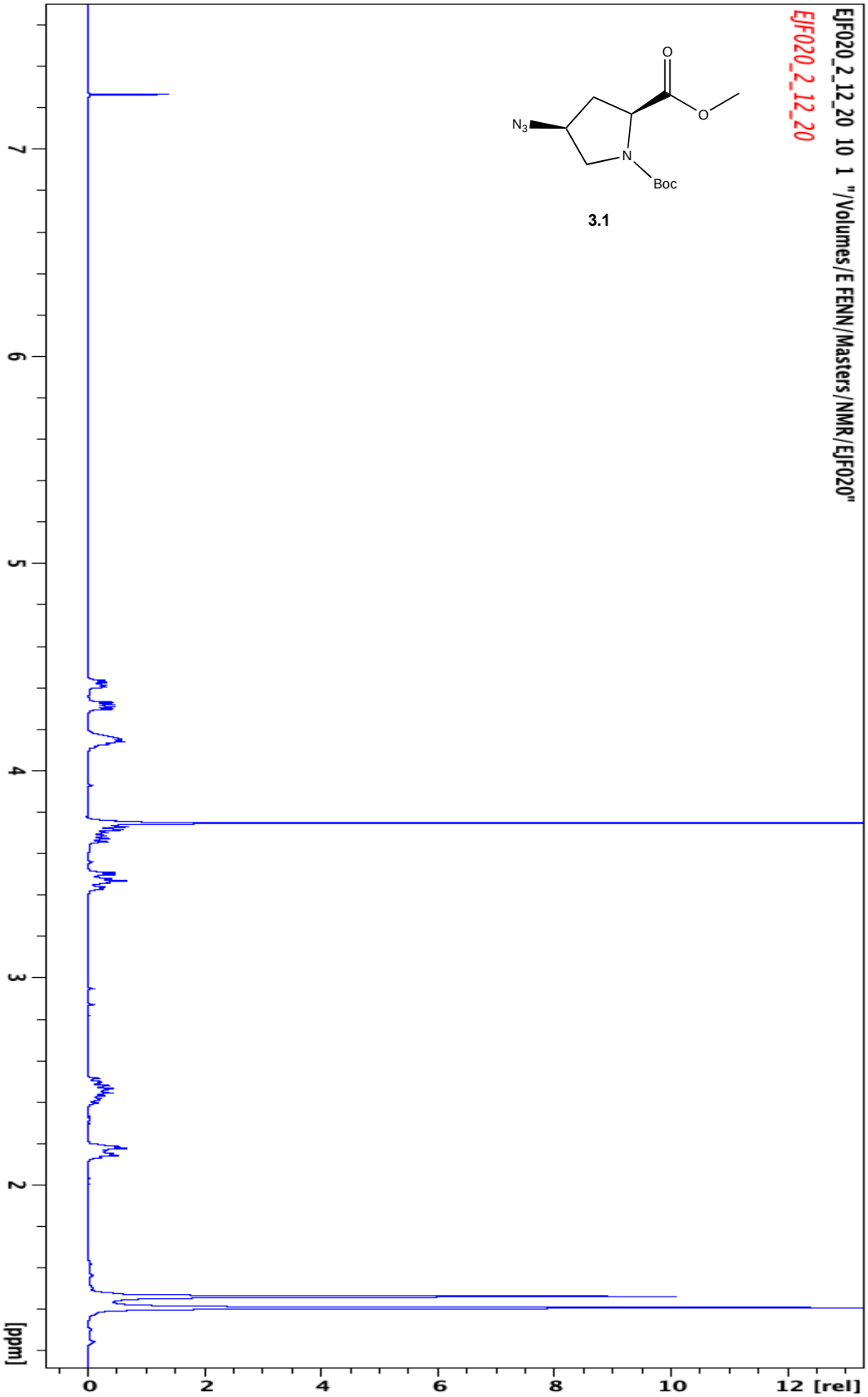

3.1 – ^{1}H NMR (25^{0} C, $CDCl_3$)

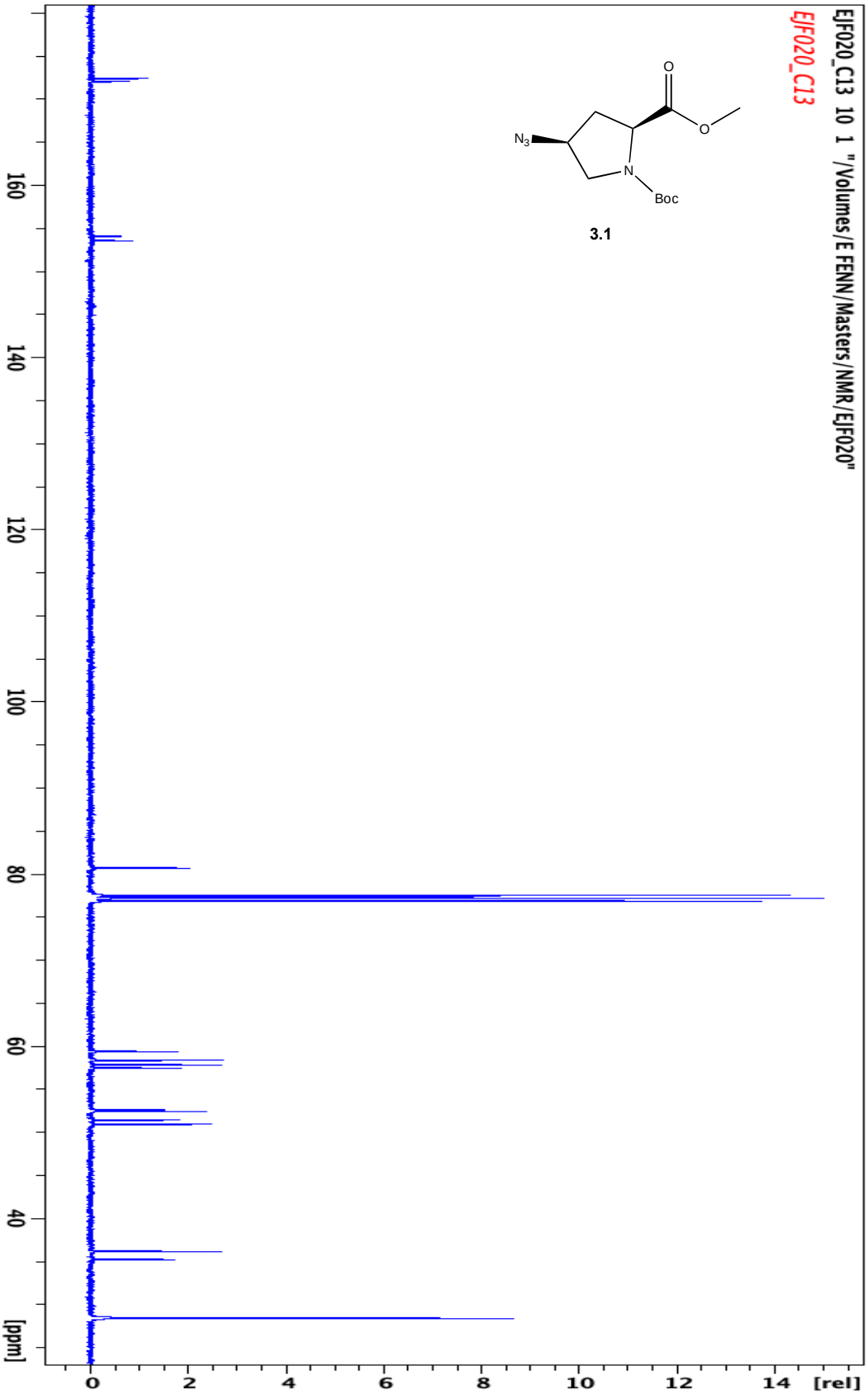

3.1 – ^{13}C NMR (25^0 C, $CDCl_3$)

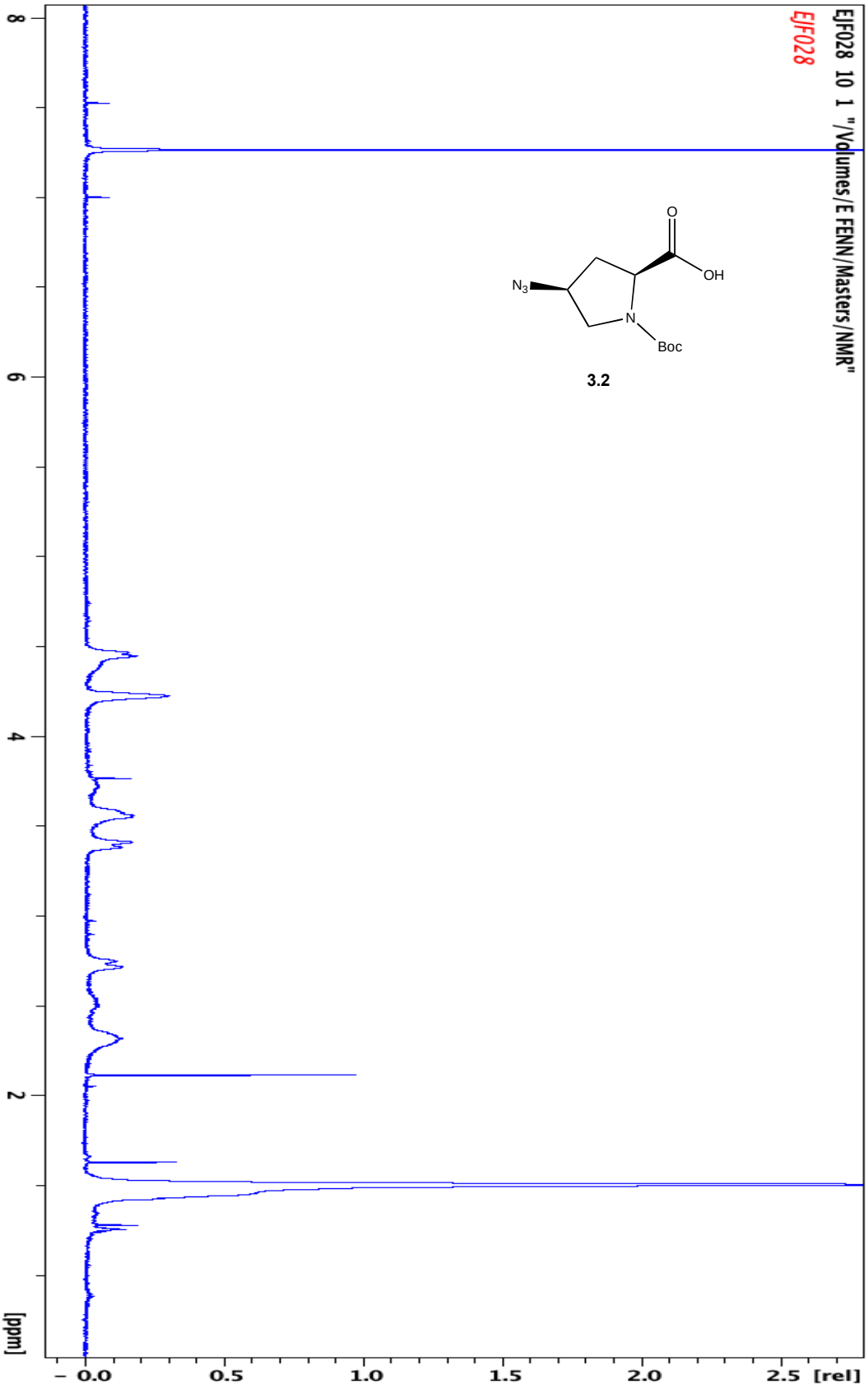

3.2 – ^{1}H NMR (25^{0} C, $CDCl_3$)

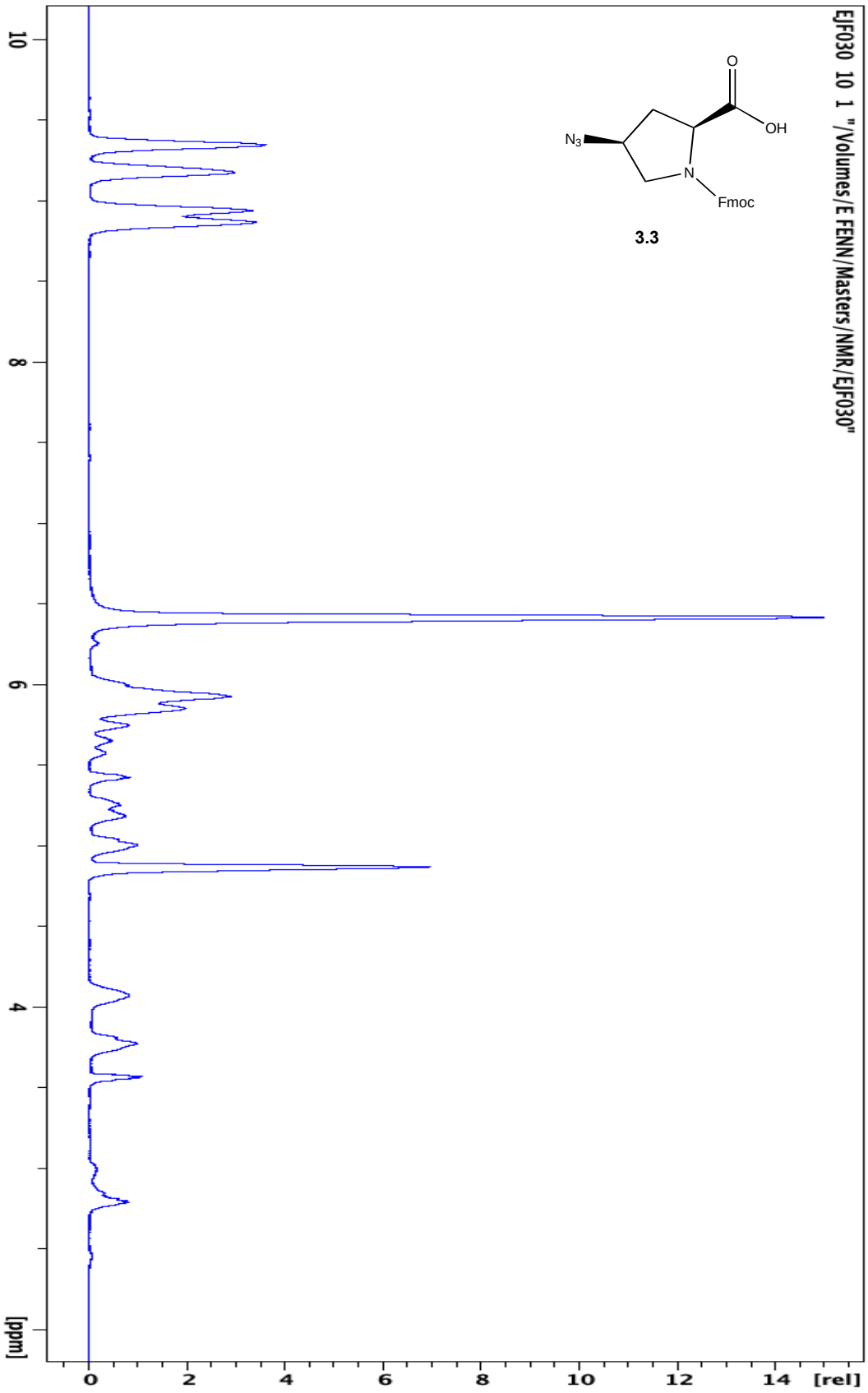

3.3 – ^{1}H NMR (25^{0} C, MeOD)

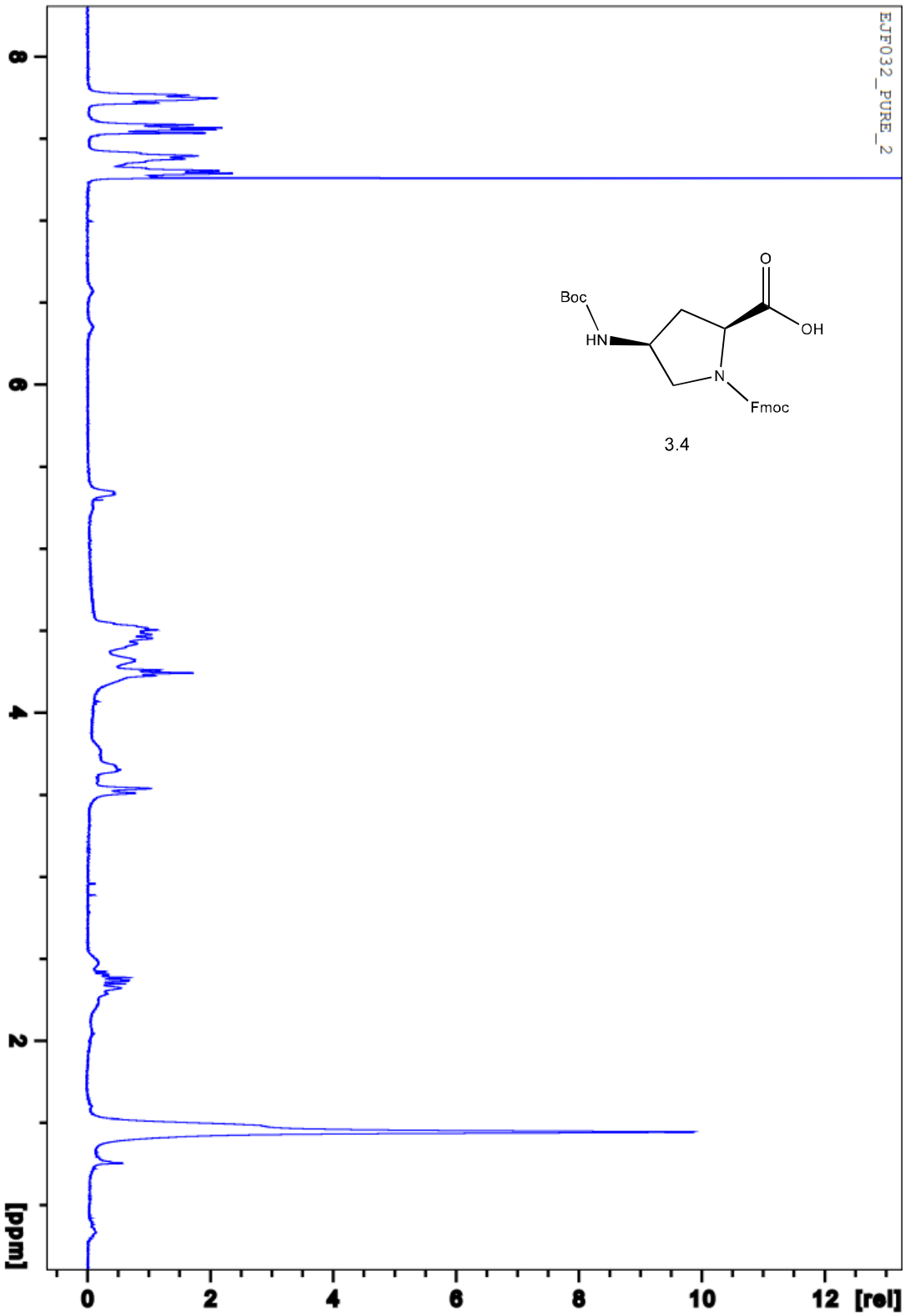

3.4 – ^{1}H NMR (25^{0} C, $CDCl_3$)

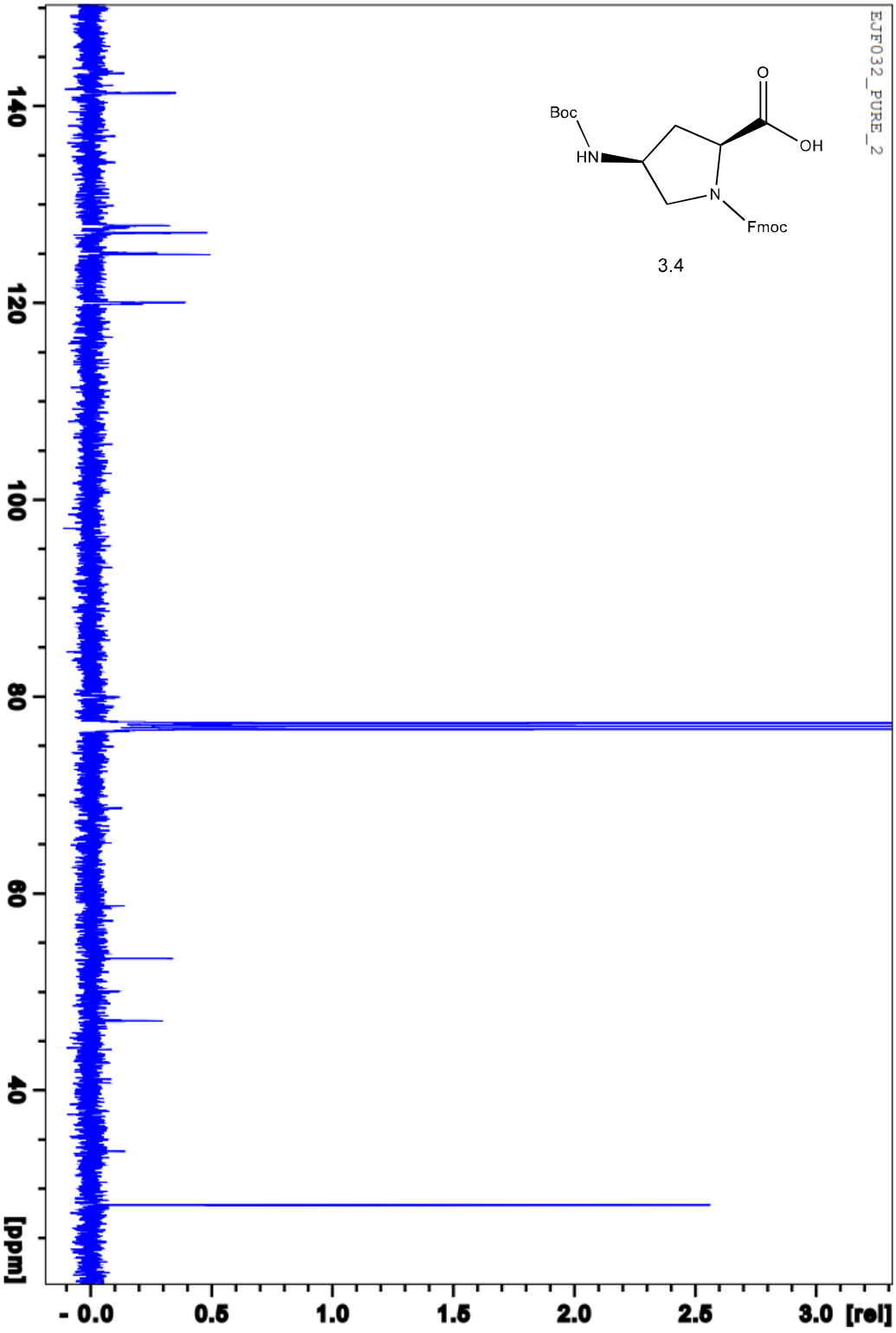

3.4 – ^{13}C NMR (25^0 C, $CDCl_3$)

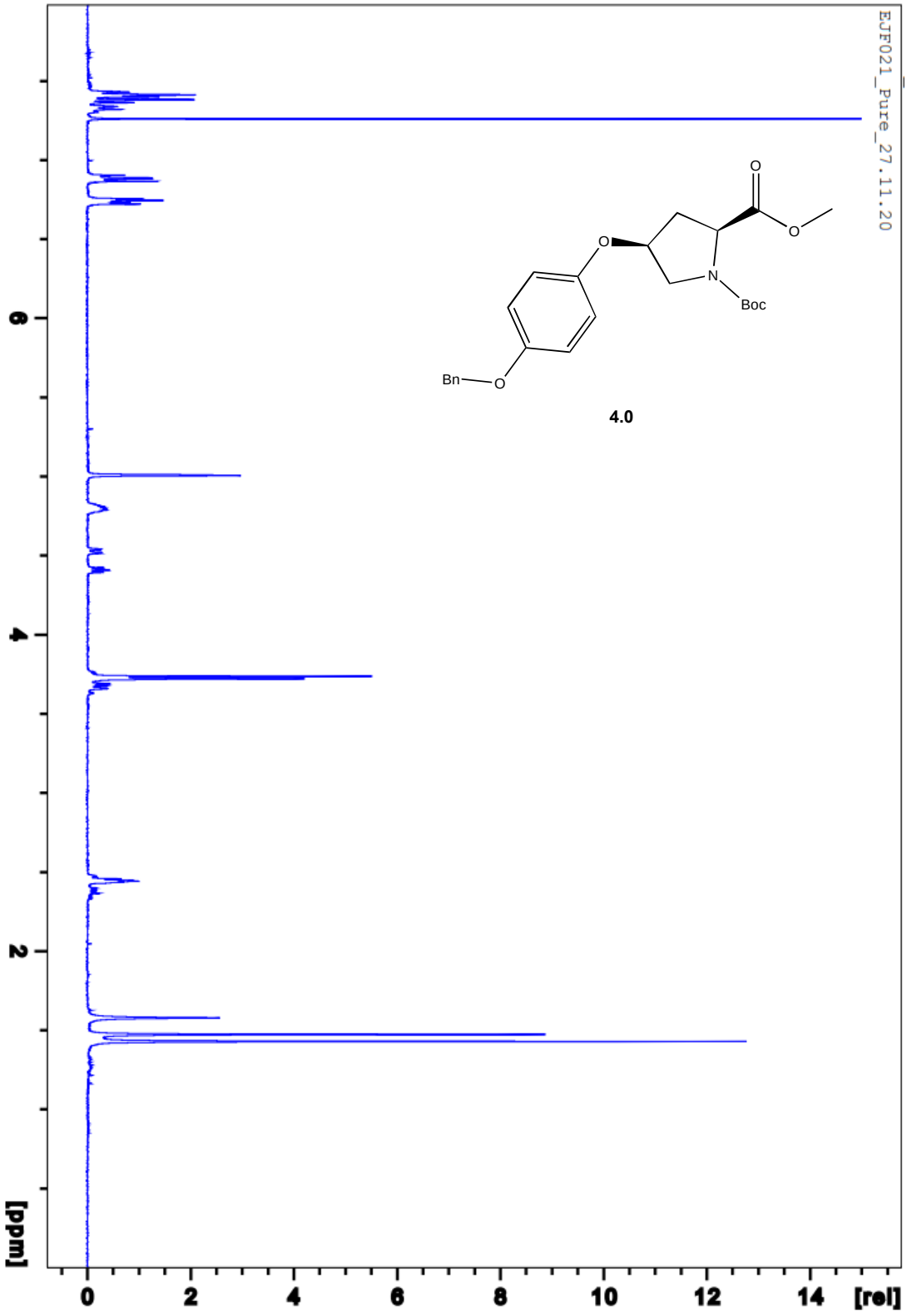

4.0 – ^{1}H NMR (25^{0} C, $CDCl_3$)

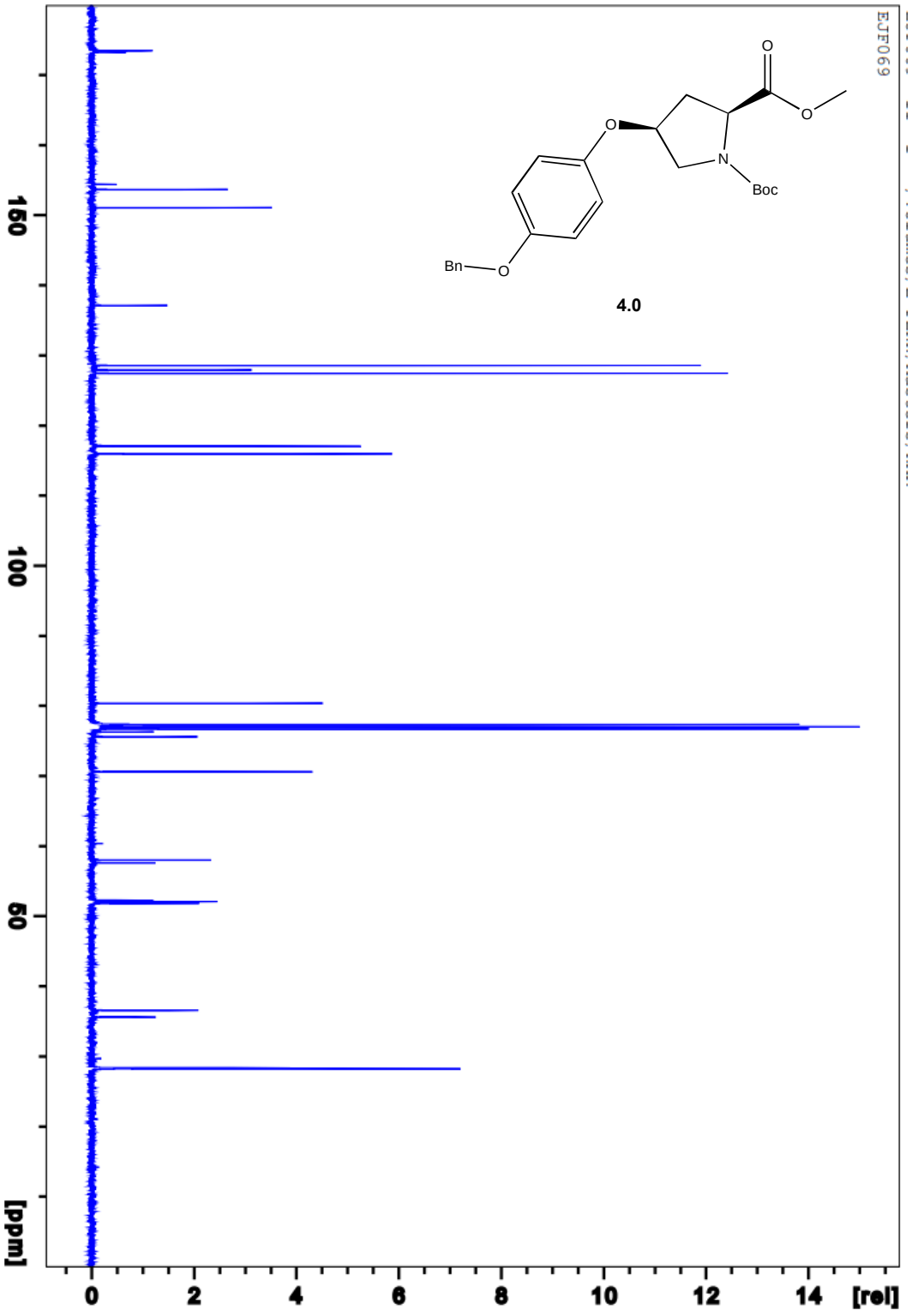

4.0 – ^{13}C NMR (25^0 C, $CDCl_3$)

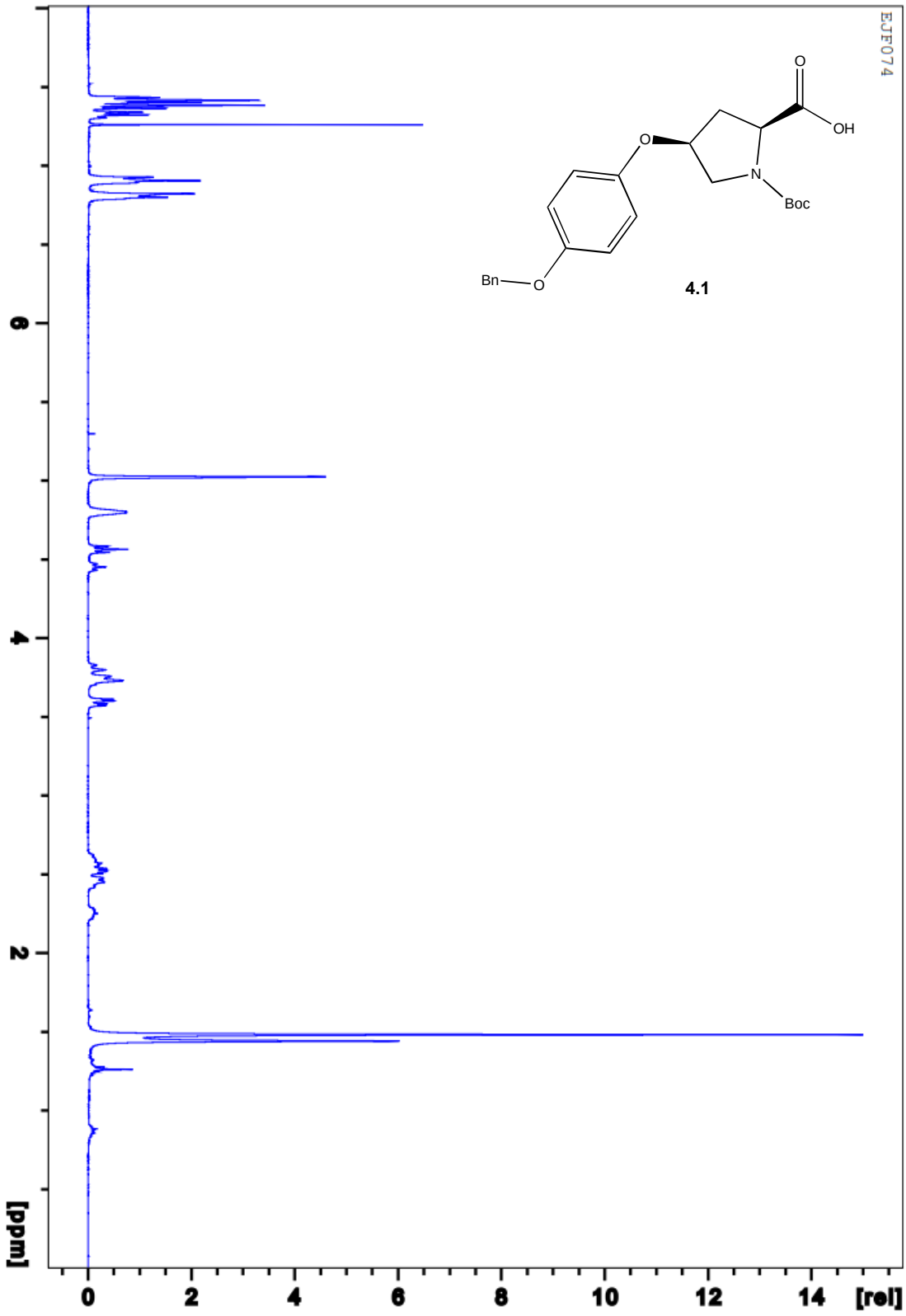

4.1 – ^{1}H NMR (25^{0} C, $CDCl_3$)

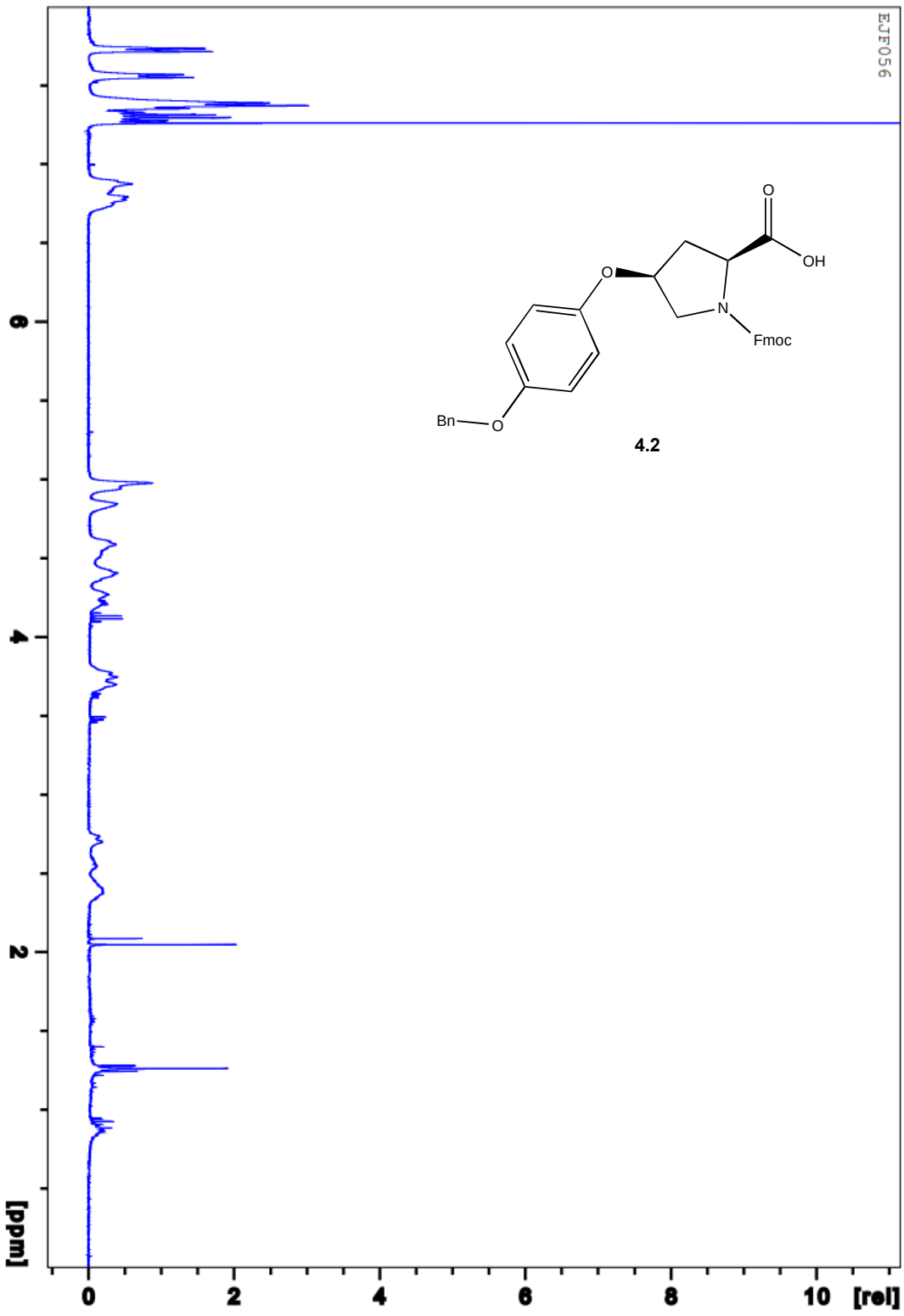

4.2 – ^{1}H NMR (25^{0} C, $CDCl_3$)

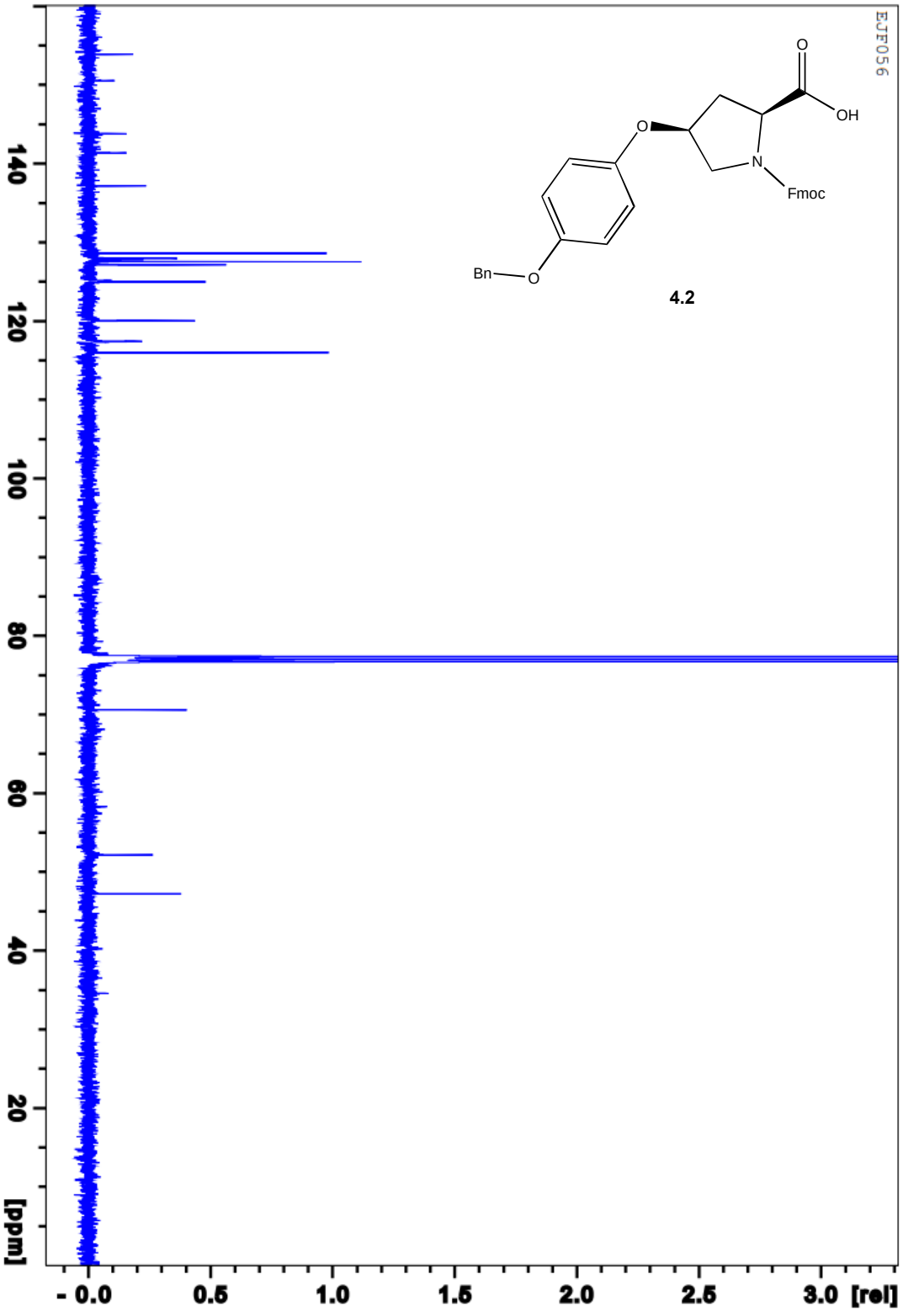

4.2 – ^{13}C NMR (25^0 C, $CDCl_3$)

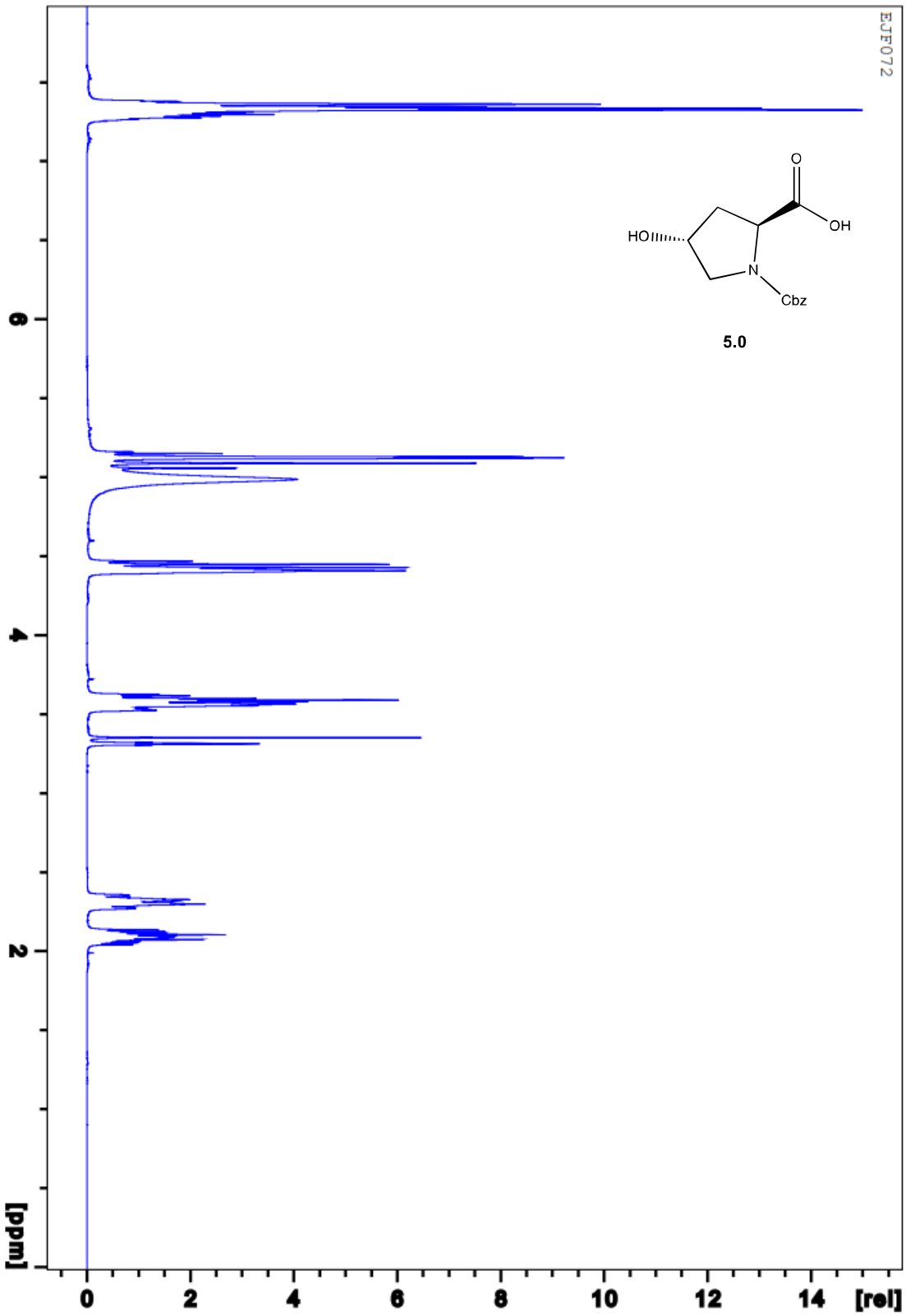

5.0 – ^{1}H NMR (25^{0} C, Methanol-d$_4$)

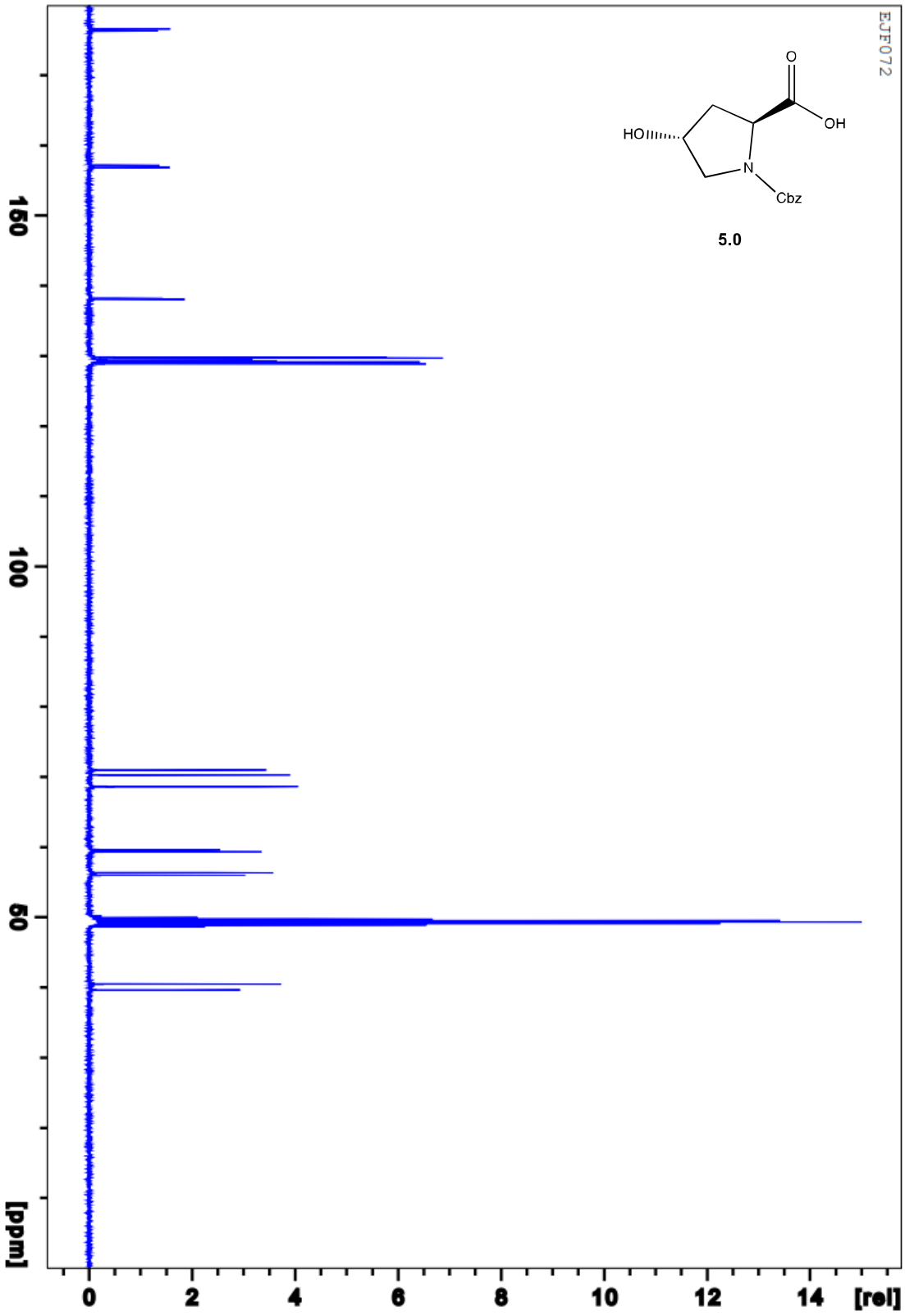

5.0 – ^{13}C NMR (25^0 C, Methanol-d_4)

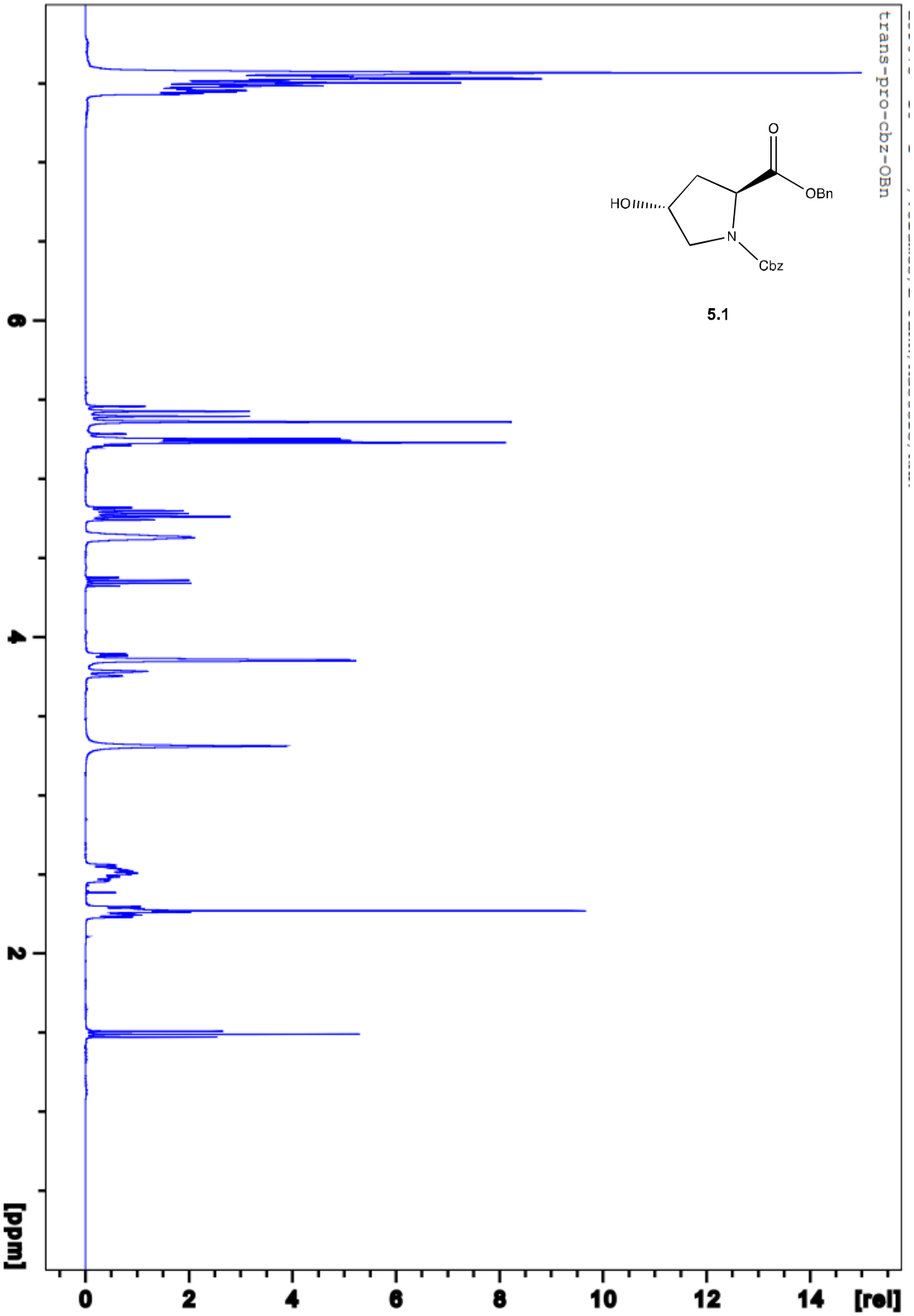

5.1 – ^{1}H NMR (25^{0} C, Methanol-d$_4$)

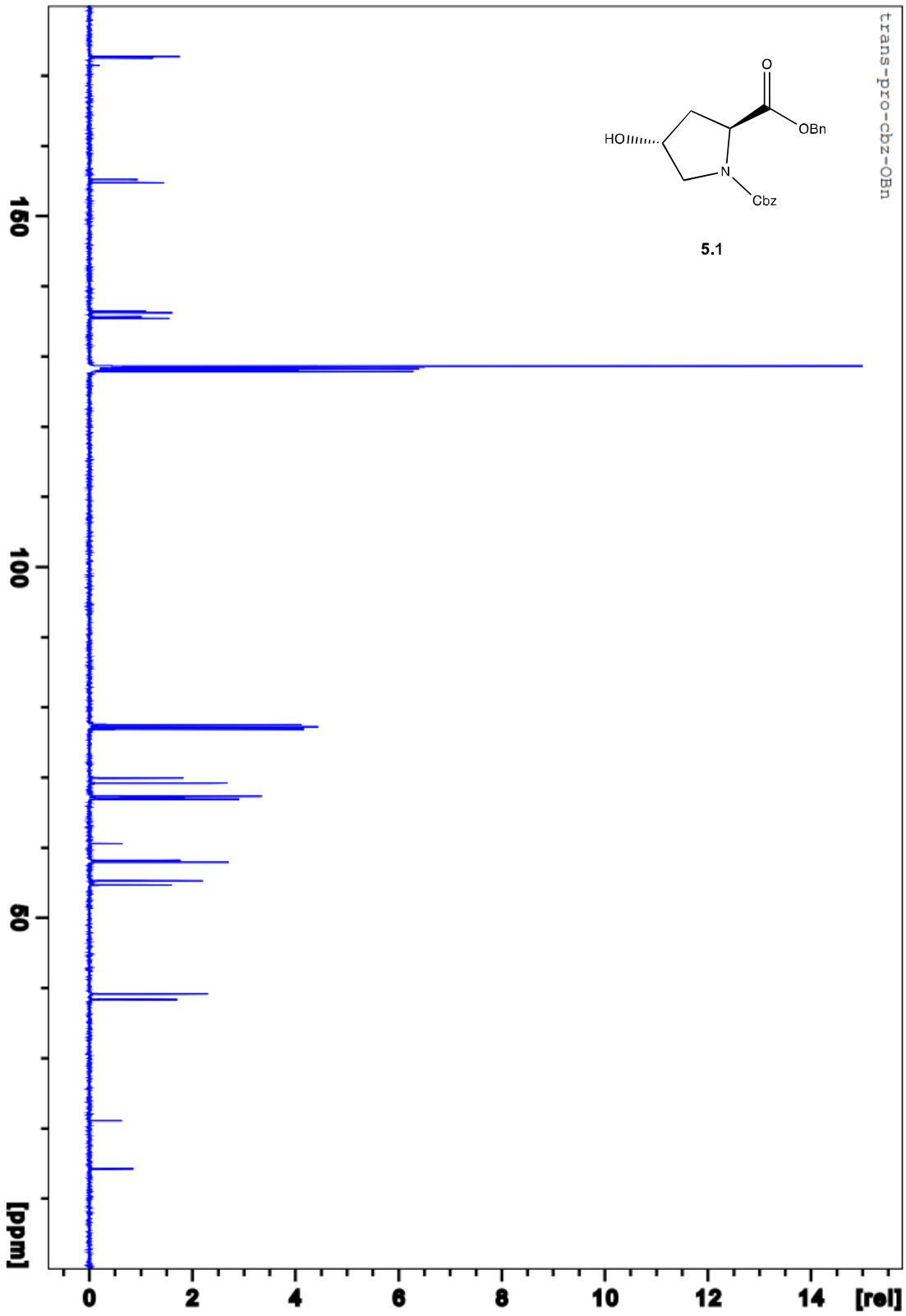

5.1 – ^{13}C NMR (25^{0} C, Methanol-d_4)

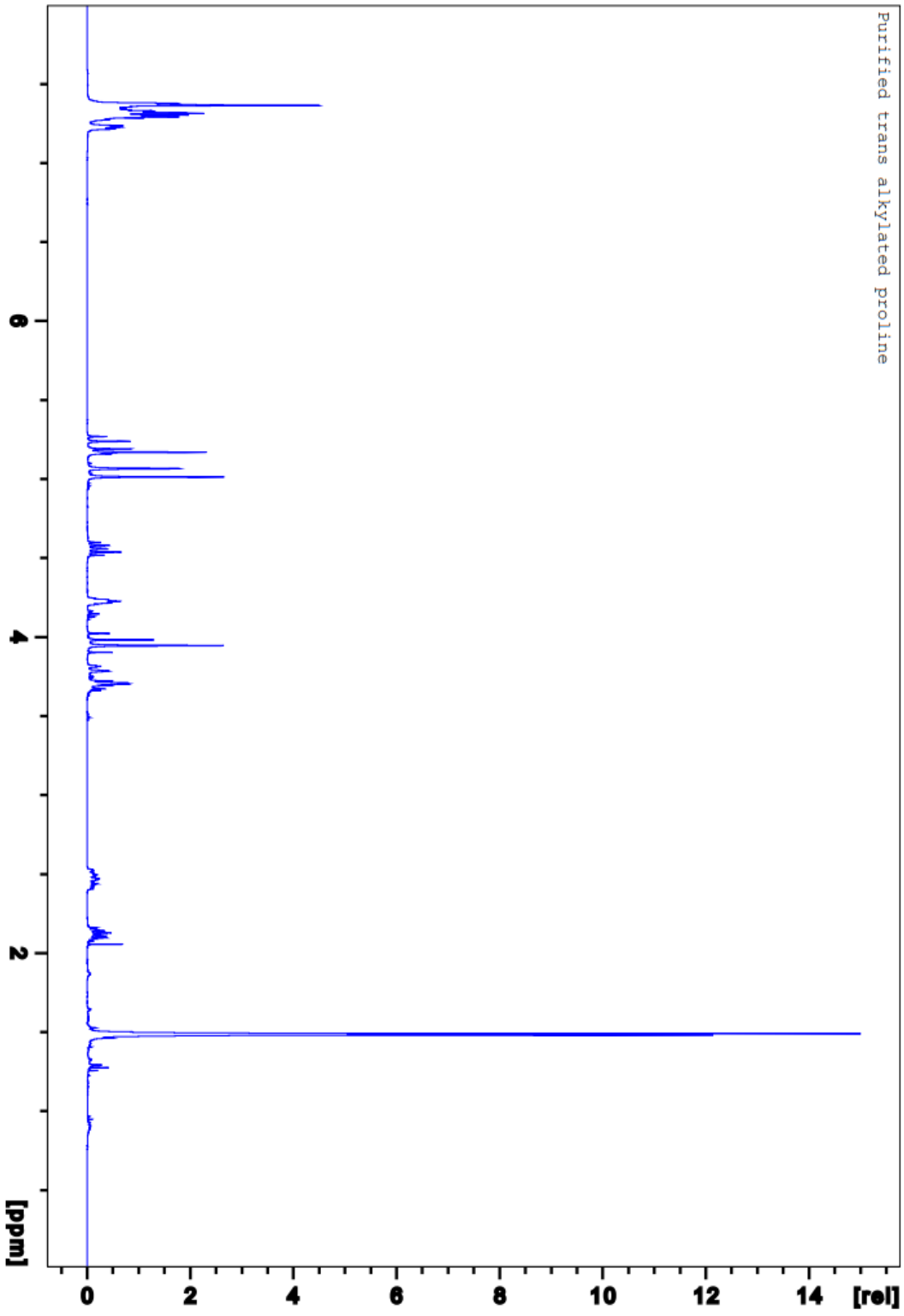

5.2 – ^{1}H NMR (25^{0} C, $CDCl_3$)

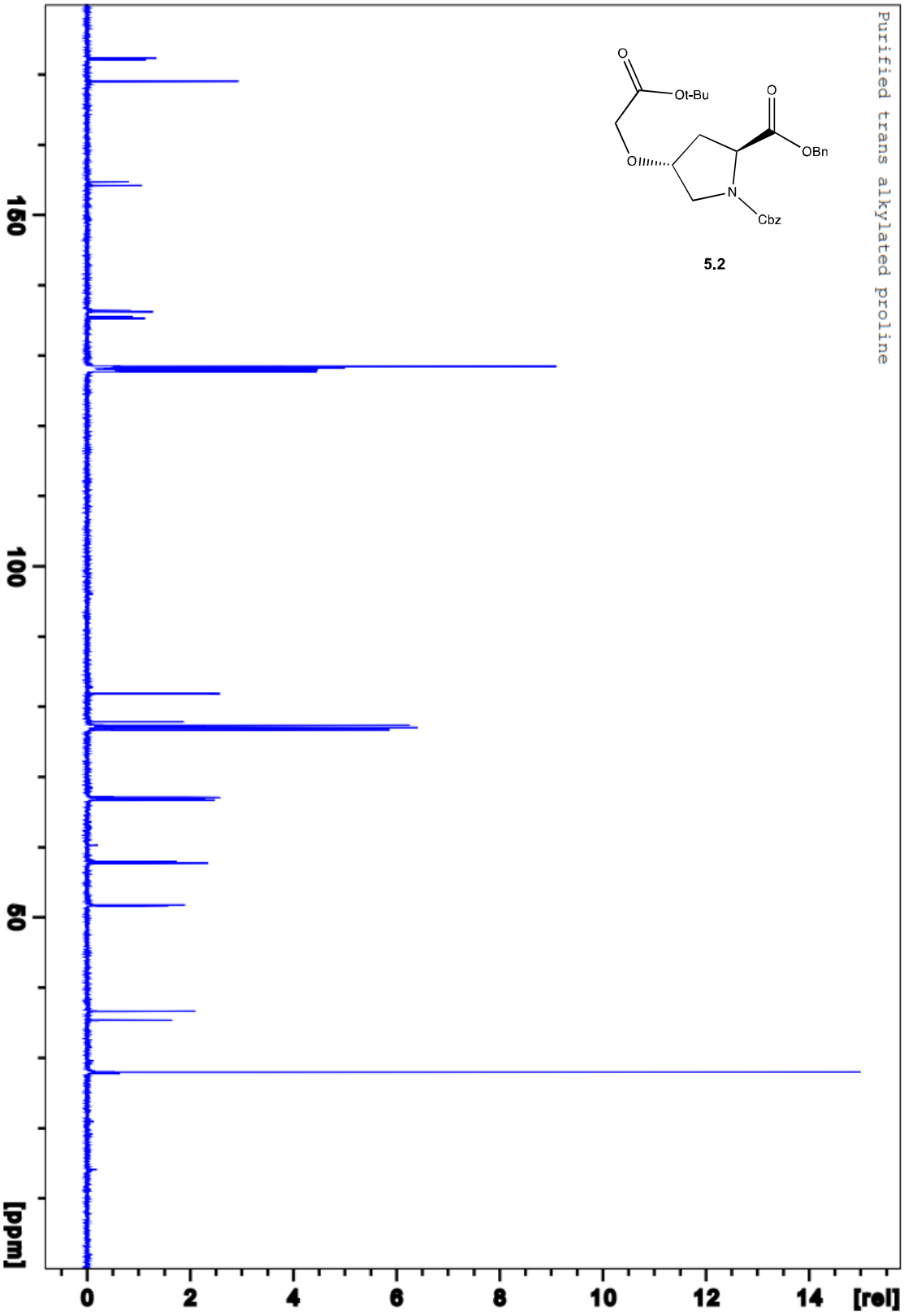

5.2 – ^{13}C NMR (25^0 C, $CDCl_3$)

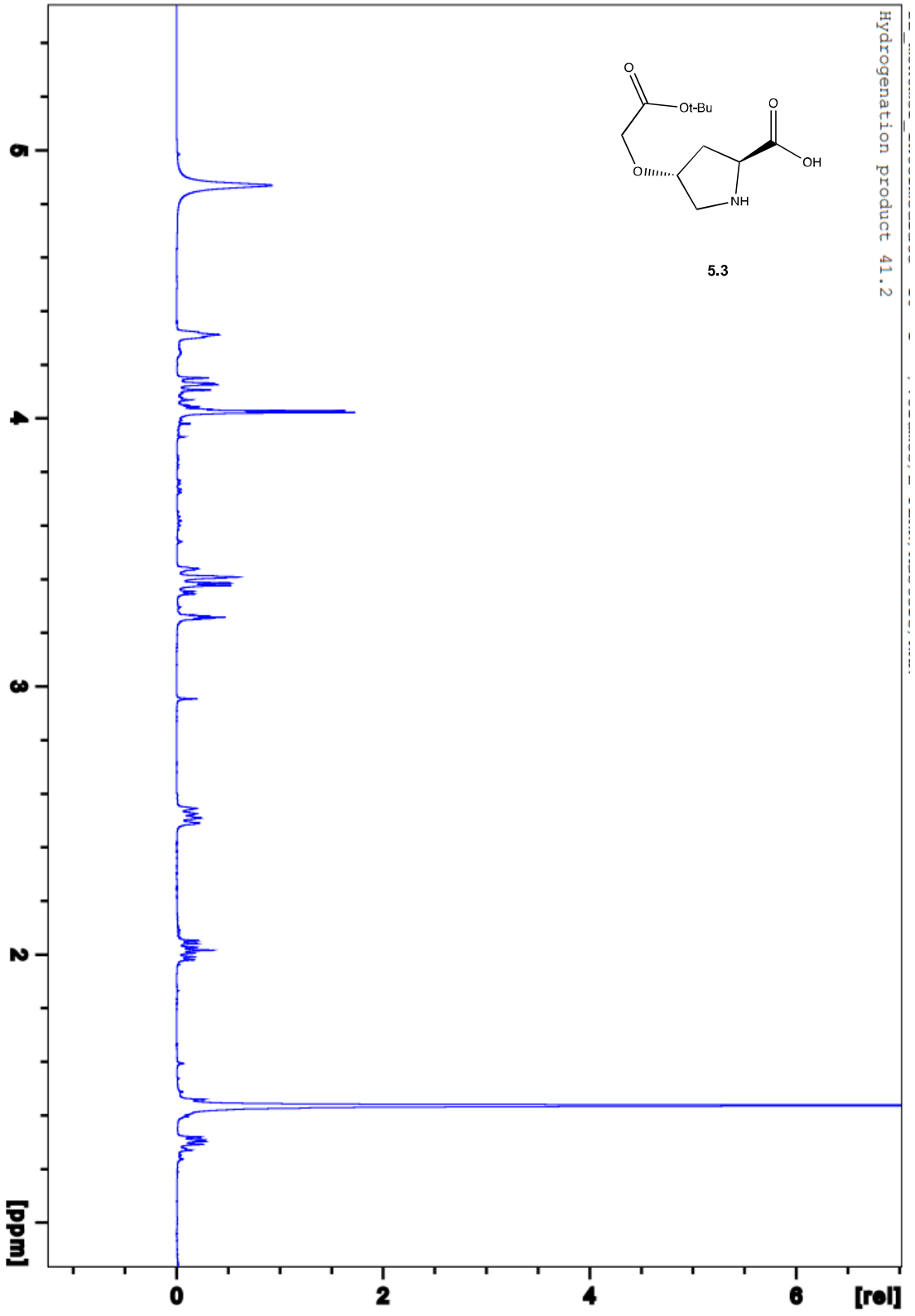

5.3 – ^{1}H NMR (25^{0} C, Methanol-d$_4$)

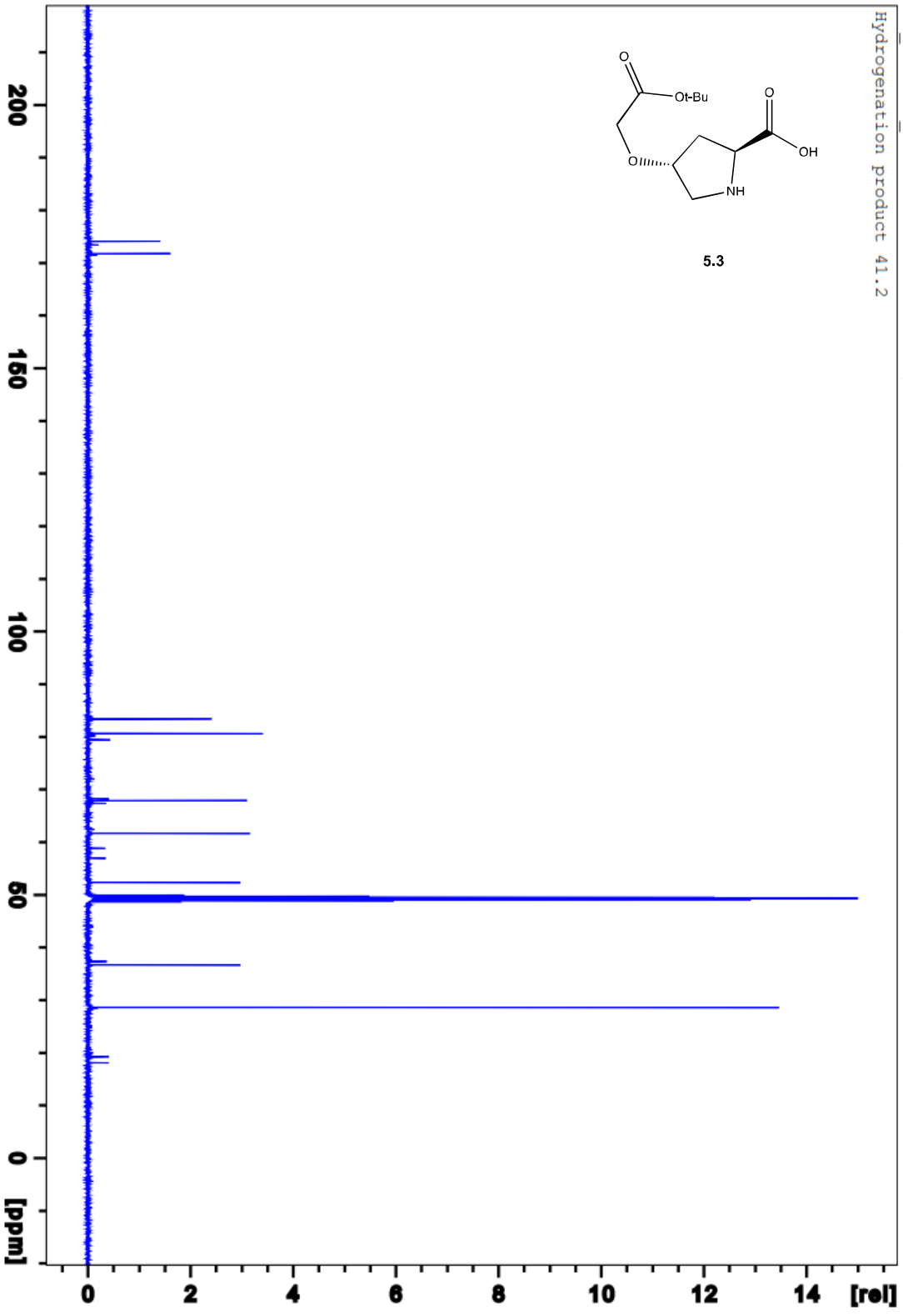

5.3 – ^{13}C NMR (25^{0} C, Methanol-d_4)

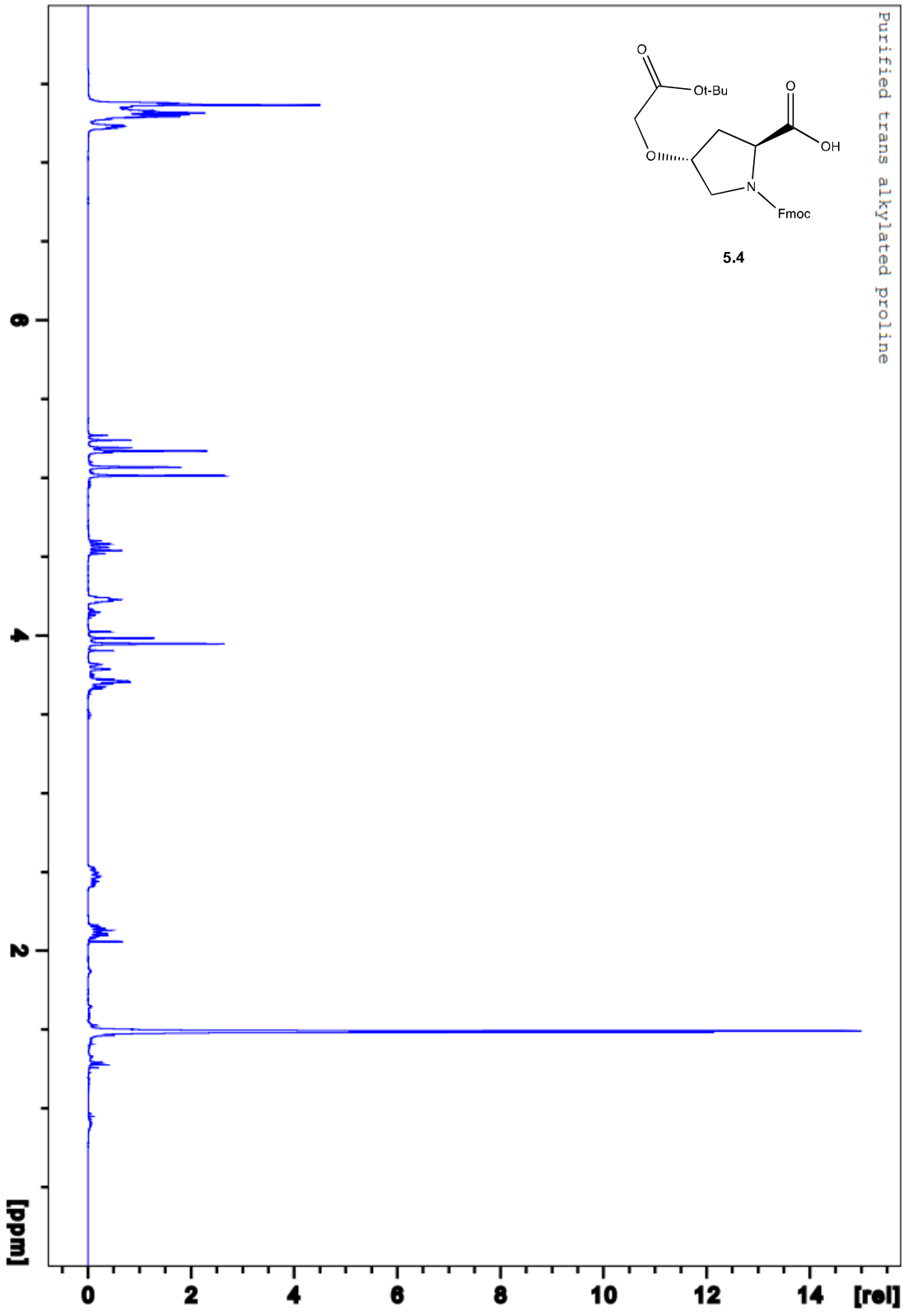

5.4 – ^{1}H NMR (25^{0} C, $CDCl_3$)

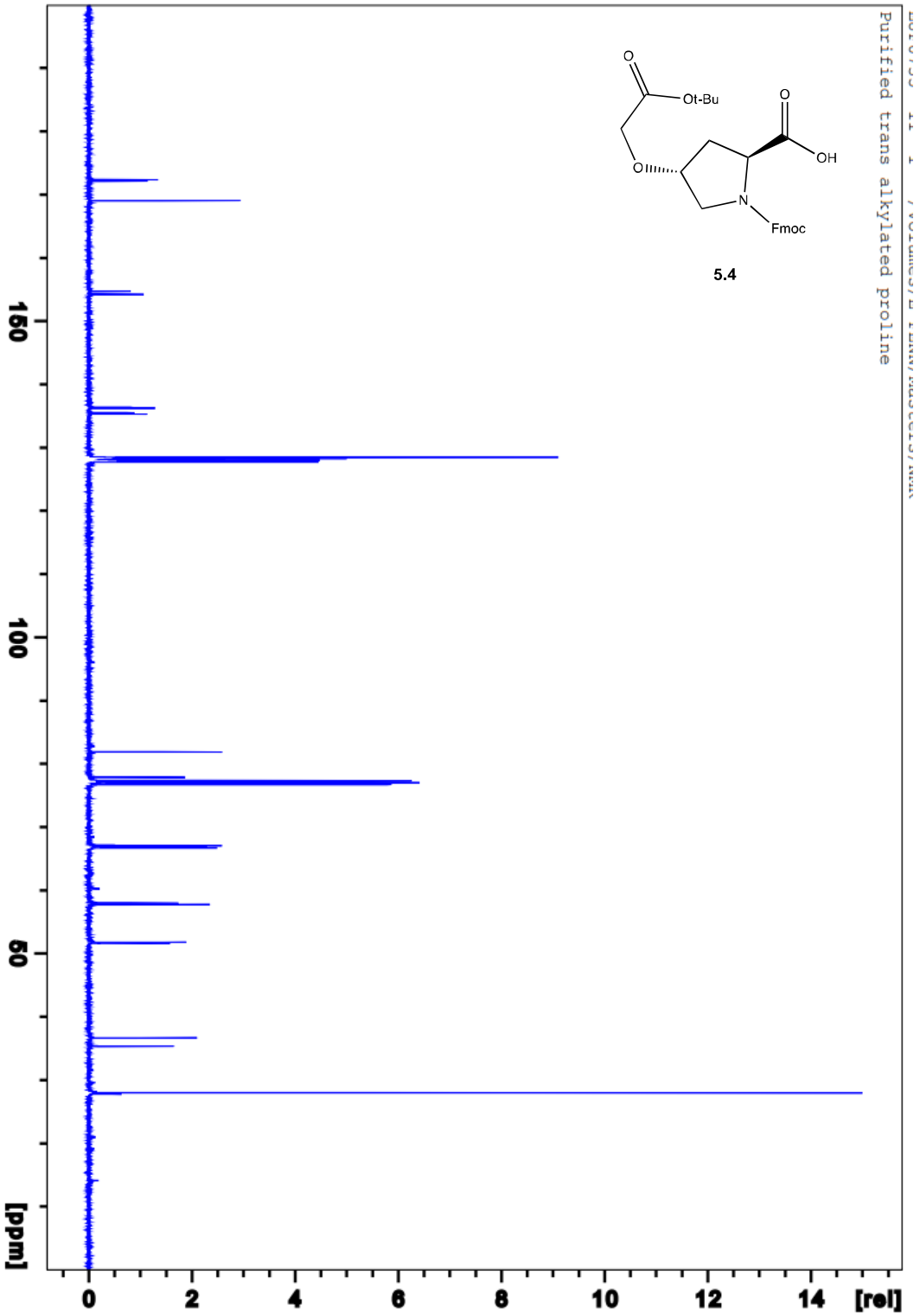

5.4 – ^{13}C NMR (25^0 C, $CDCl_3$)

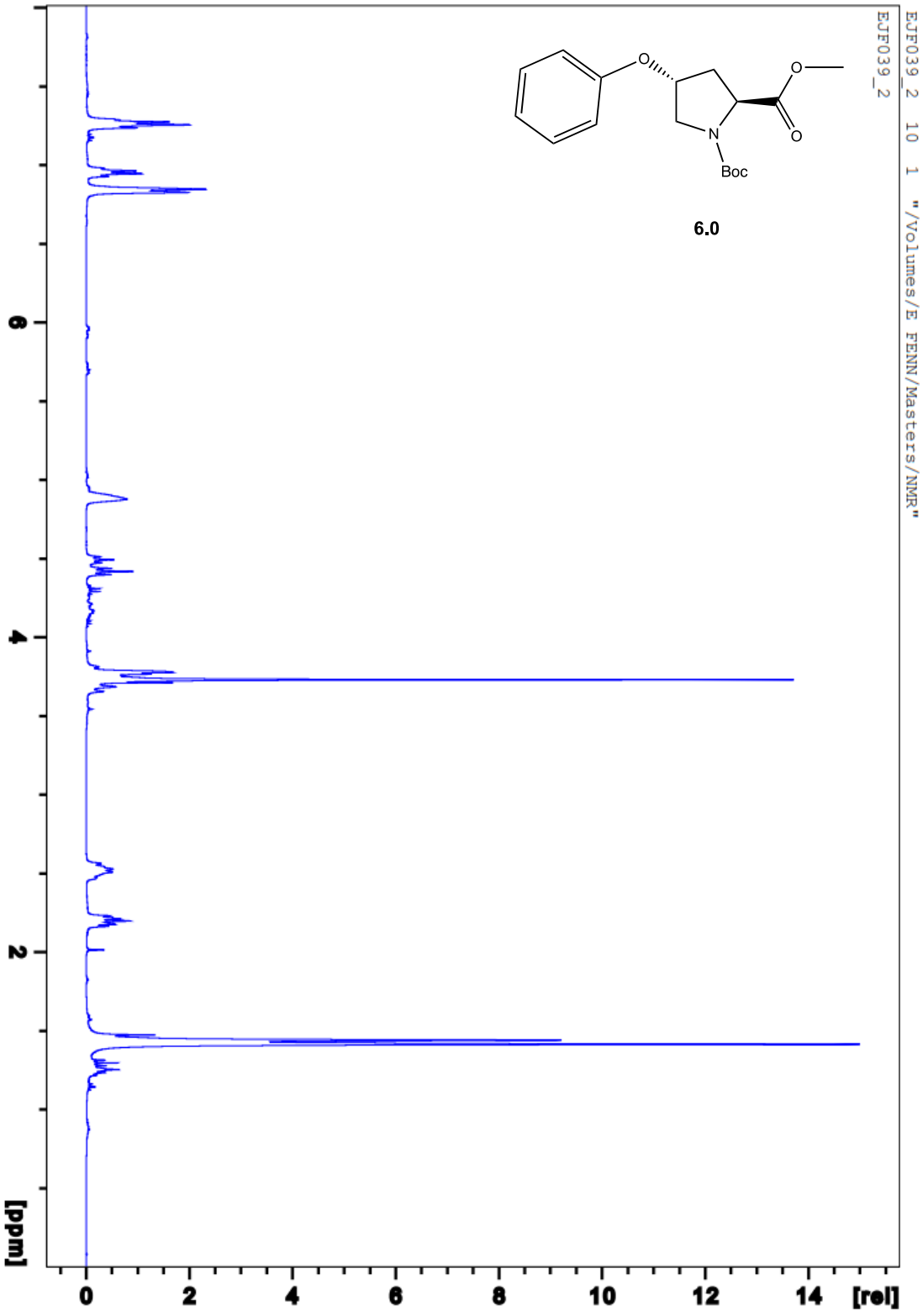

6.0 – ^{1}H NMR (25^{0} C, $CDCl_3$)

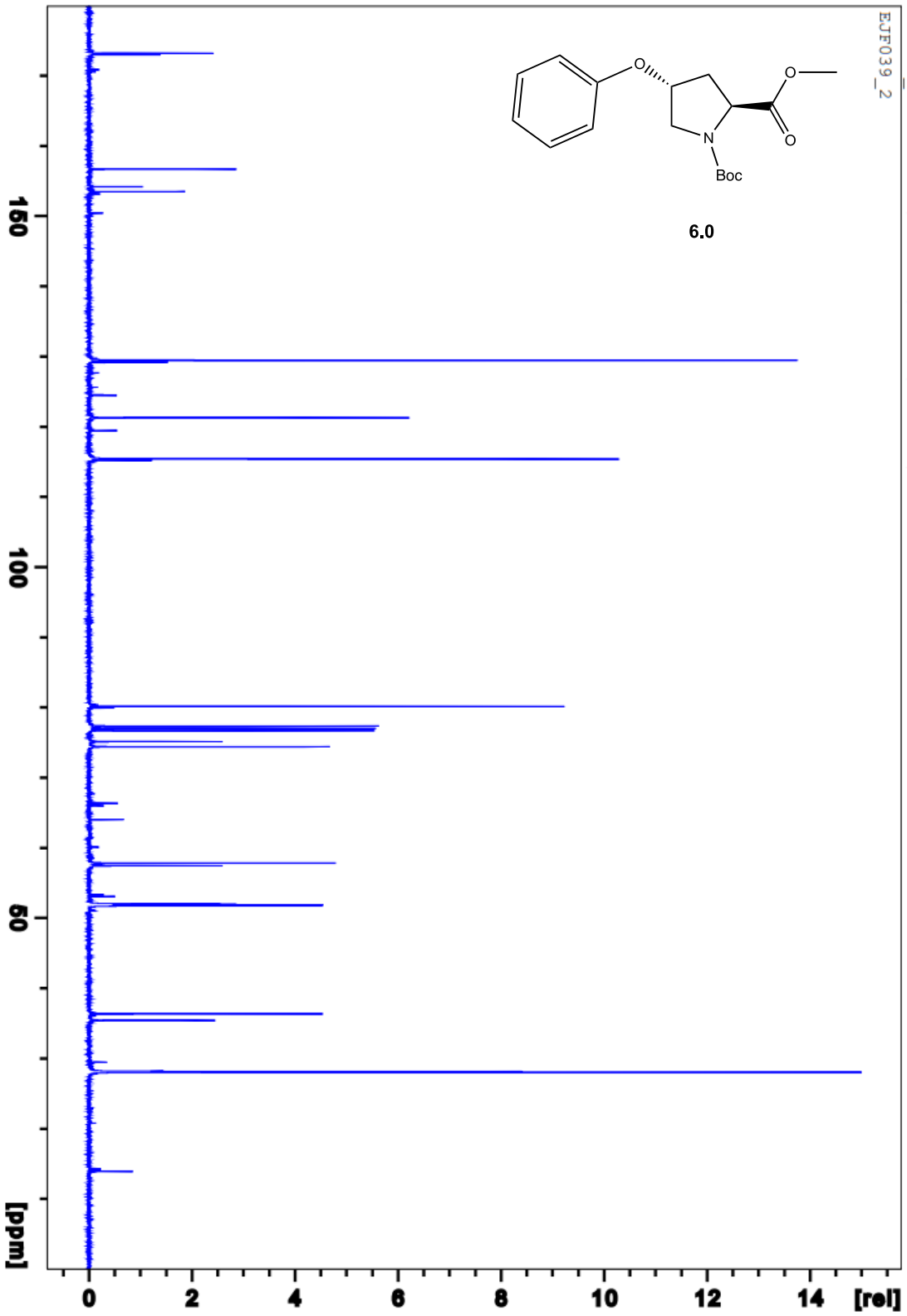

6.0 – ^{13}C NMR (25^0 C, $CDCl_3$)

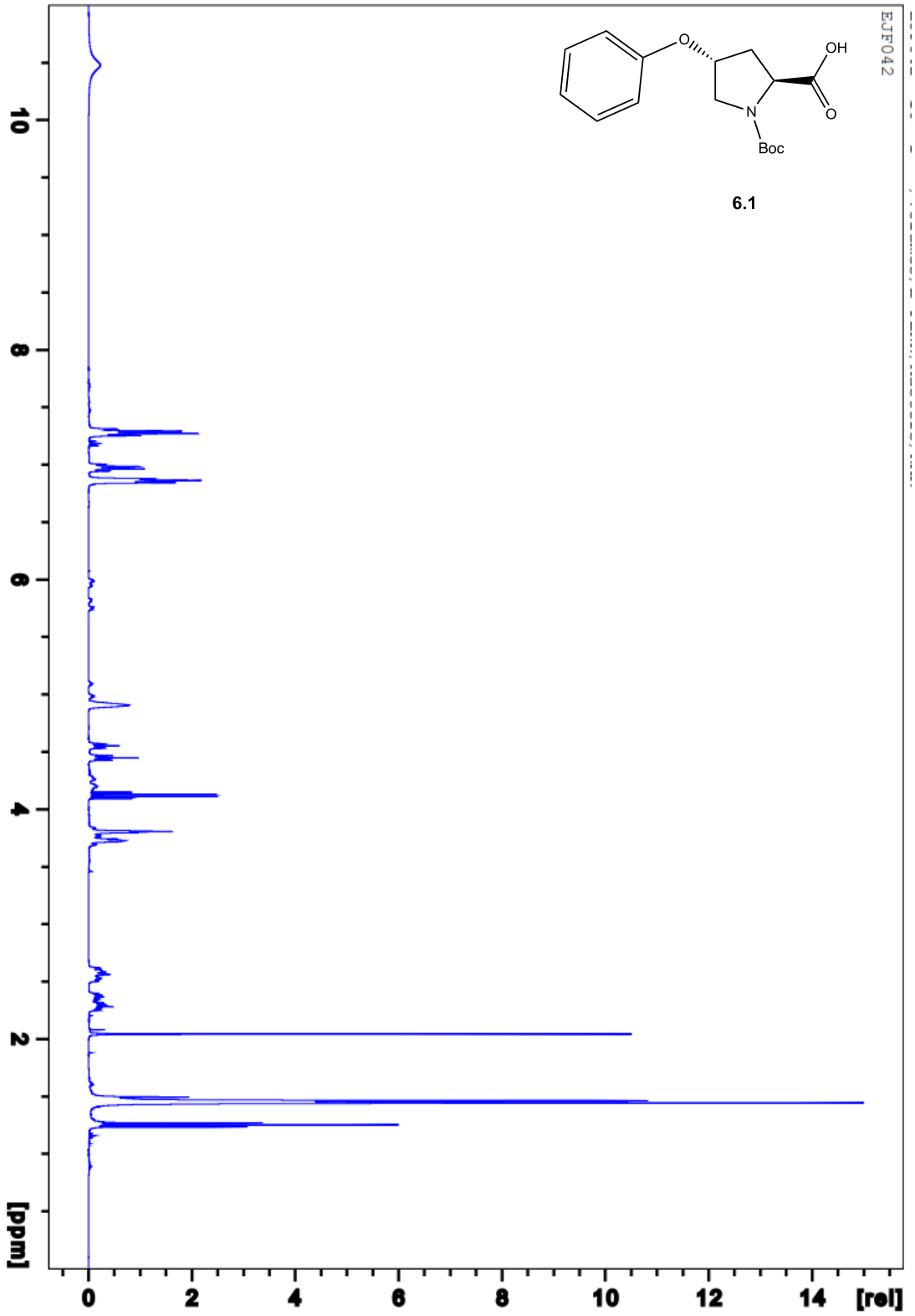

6.1 – ^{1}H NMR (25^{0} C, $CDCl_3$)

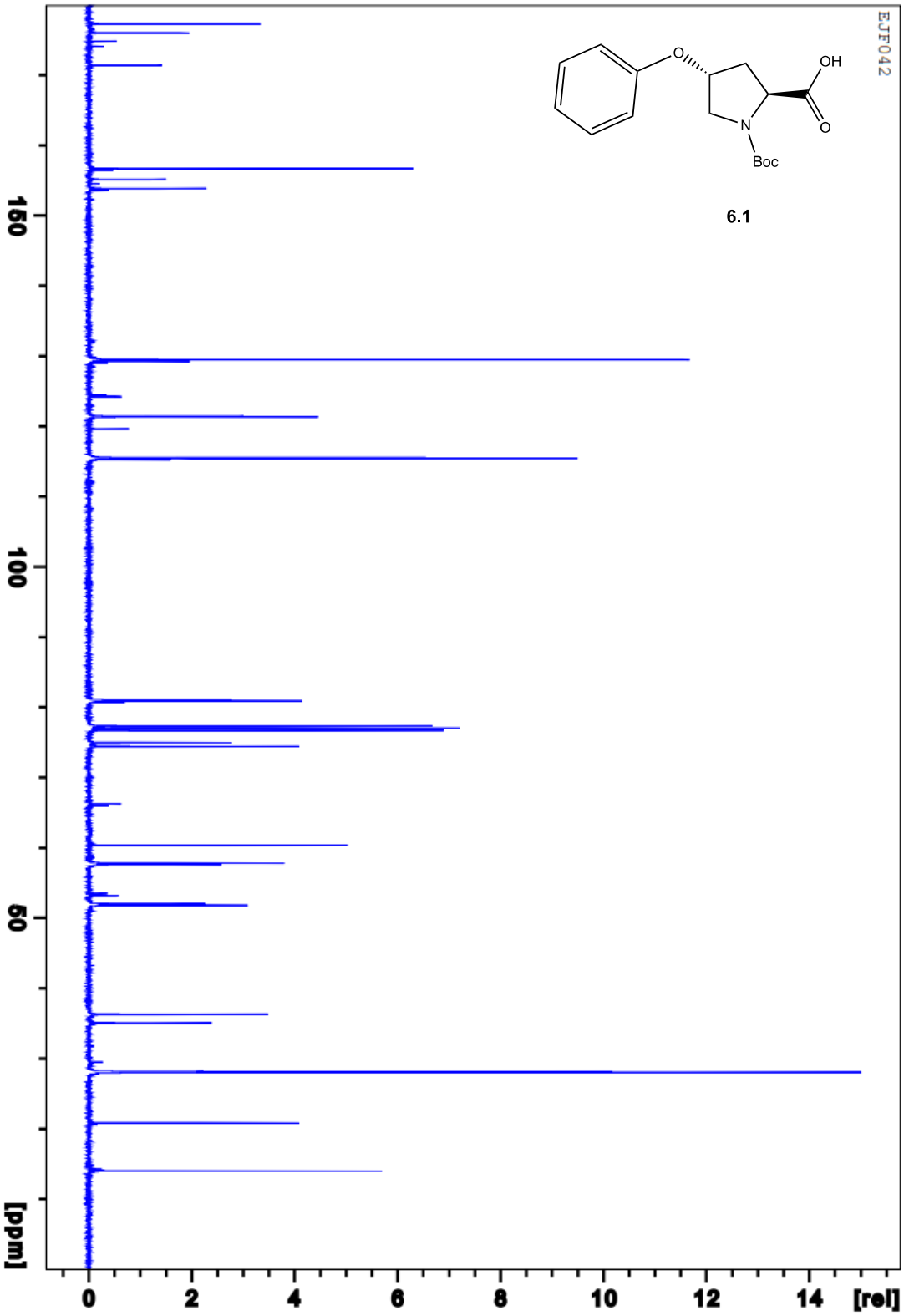

6.1 – ^{13}C NMR (25^0 C, $CDCl_3$)

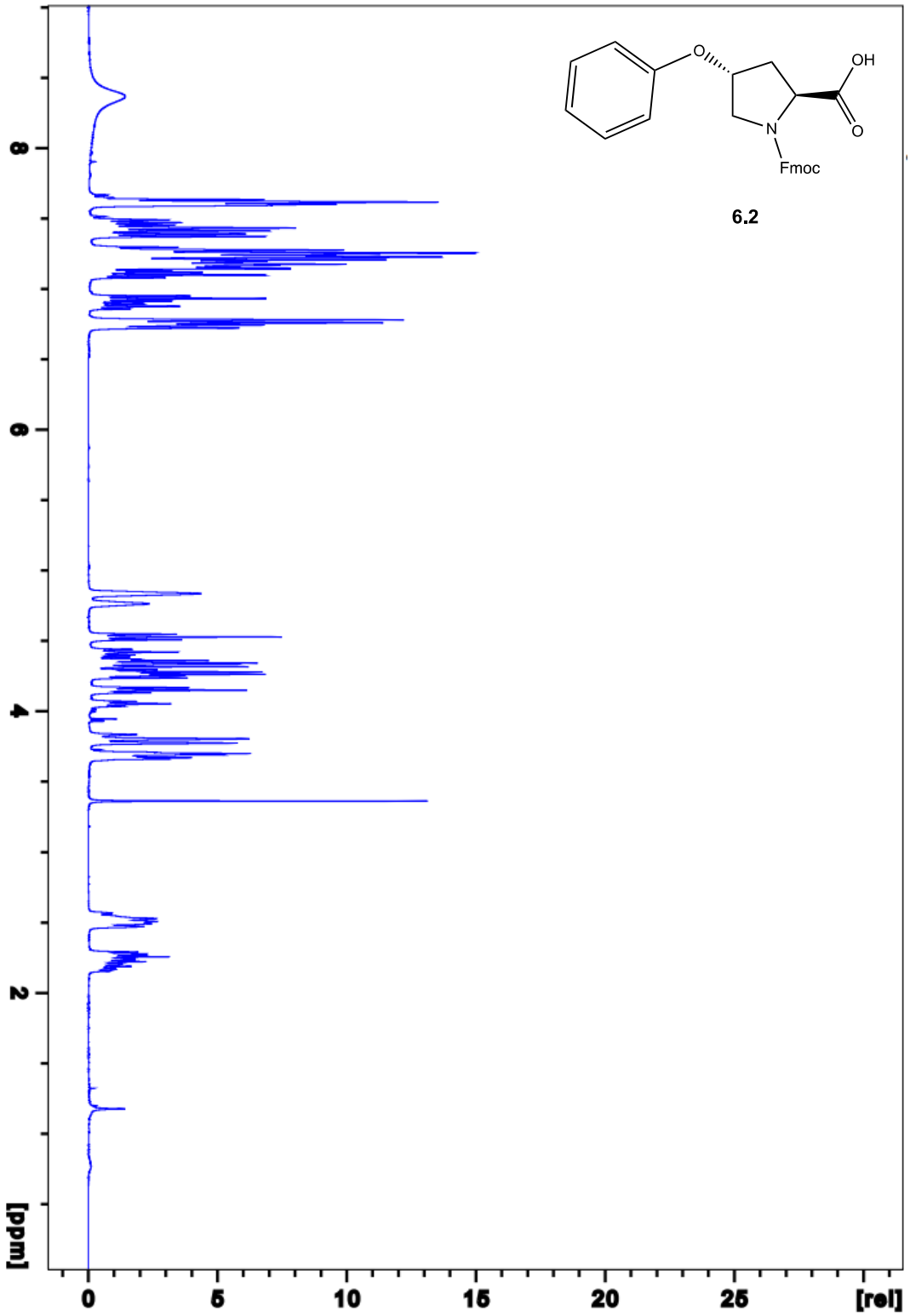

6.2 – ^{1}H NMR (25^{0} C, $CDCl_3$)

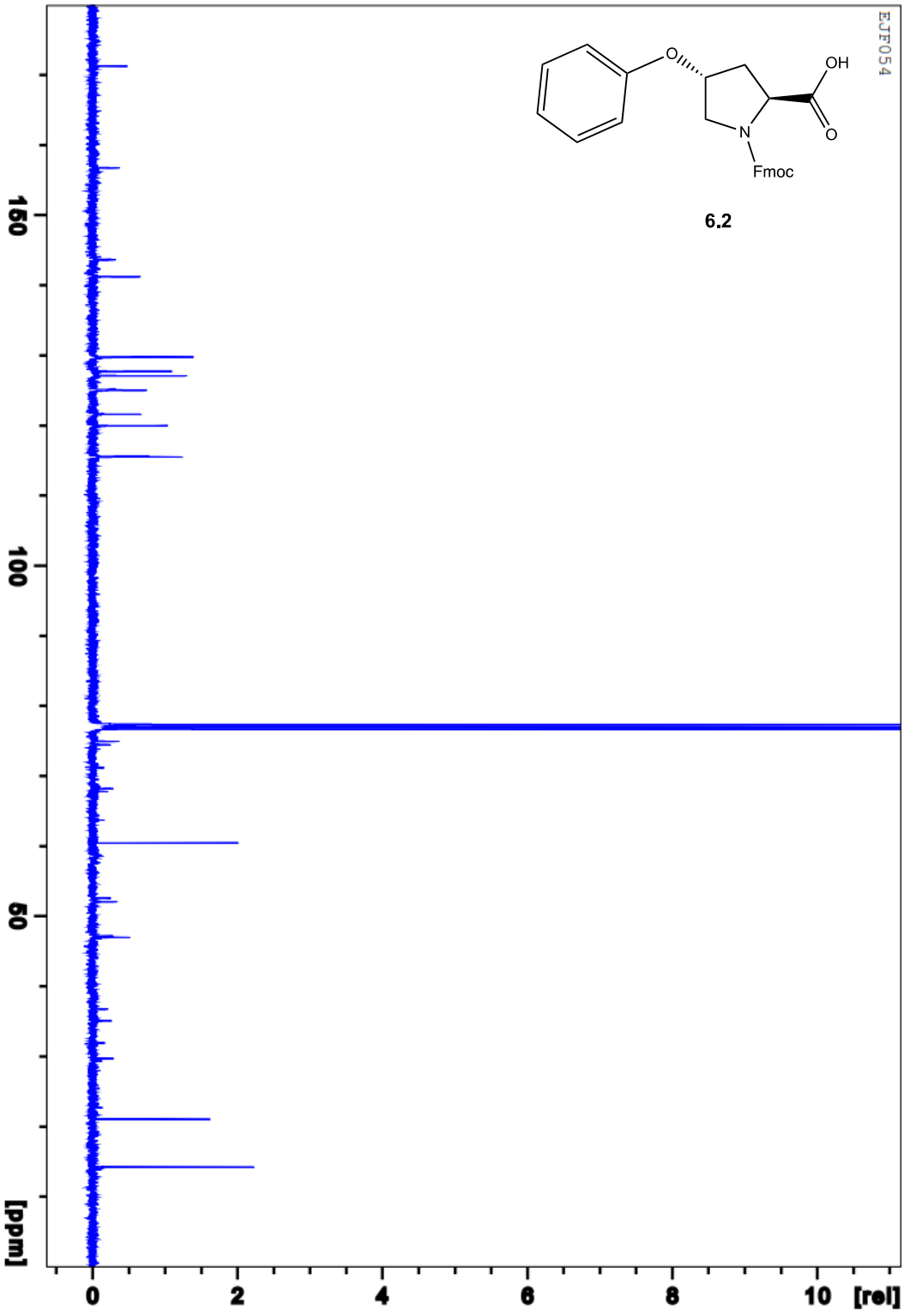

6.2 – ^{13}C NMR (25^0 C, $CDCl_3$)

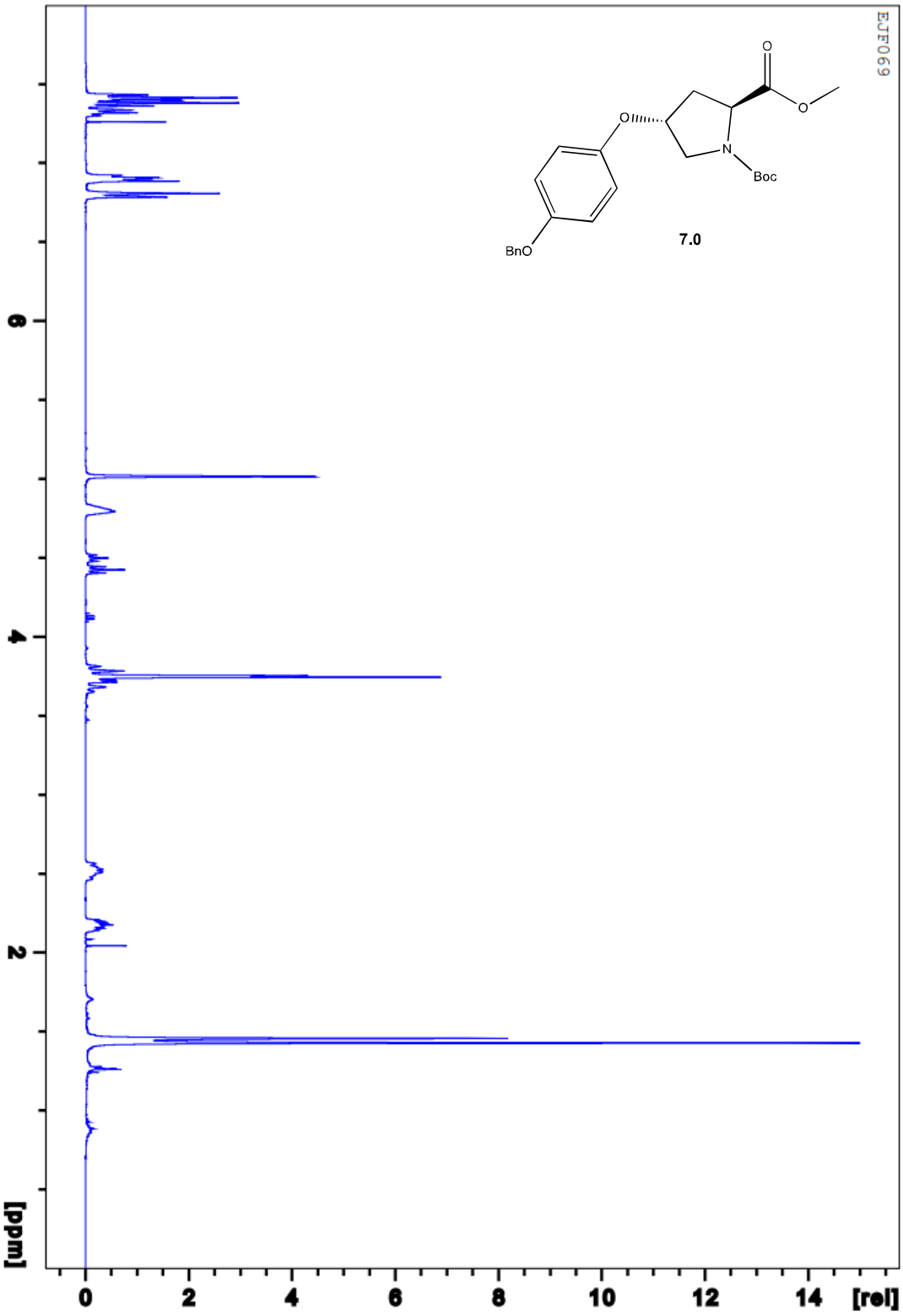

7.0 – ^{1}H NMR (25^{0} C, $CDCl_3$)

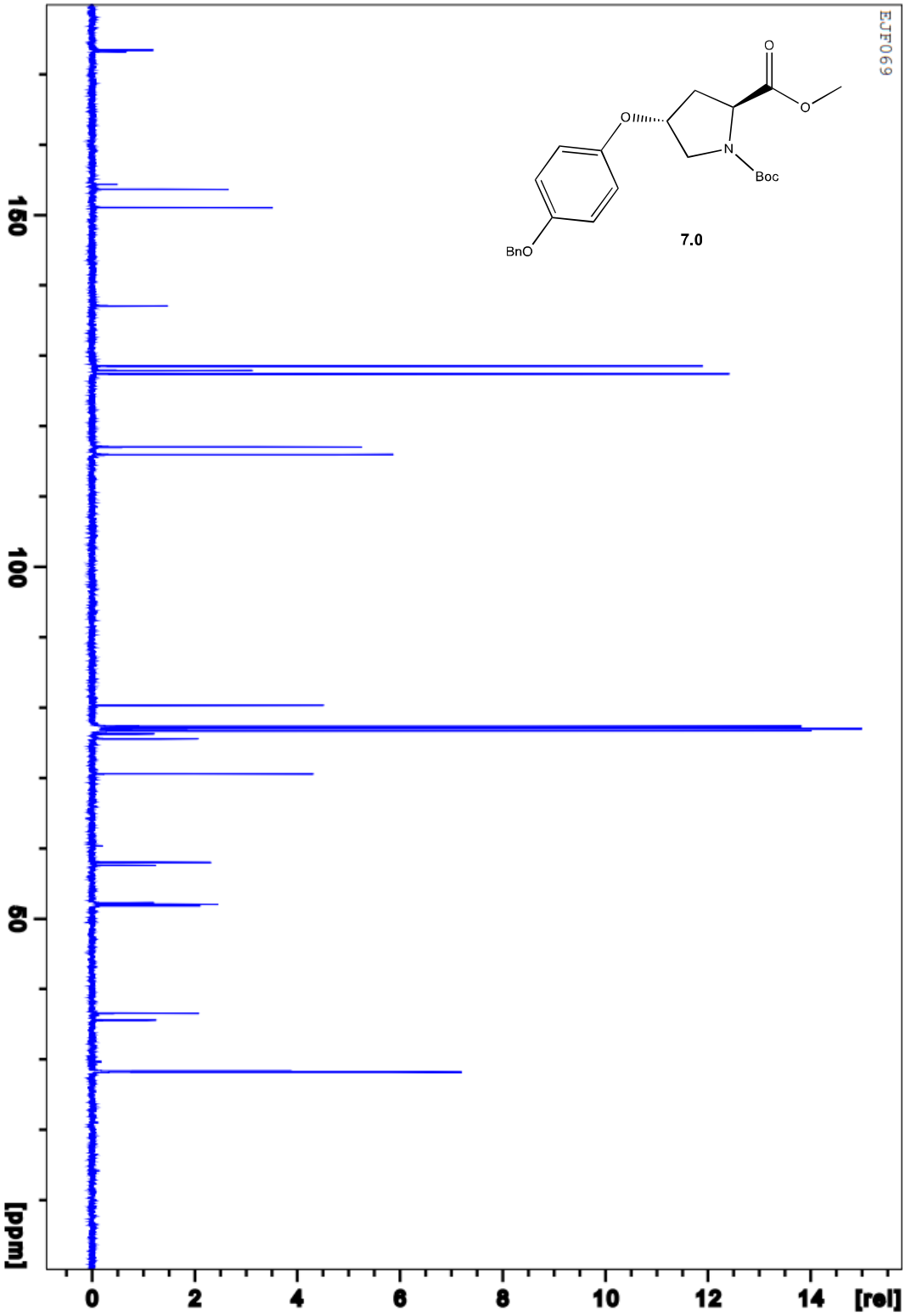

7.0 – ^{13}C NMR (25^0 C, $CDCl_3$)

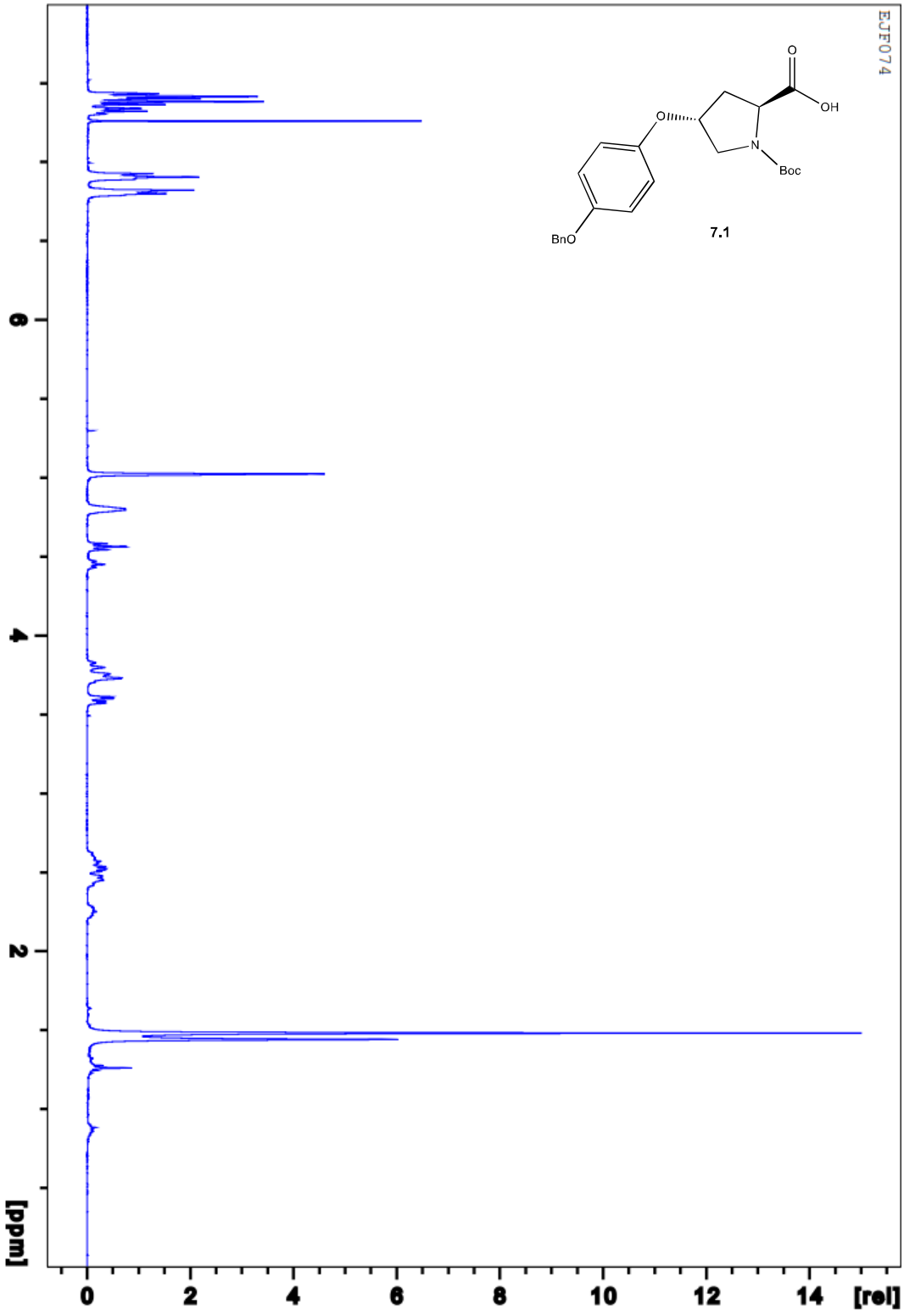

7.1 – ^{1}H NMR (25^{0} C, $CDCl_3$)

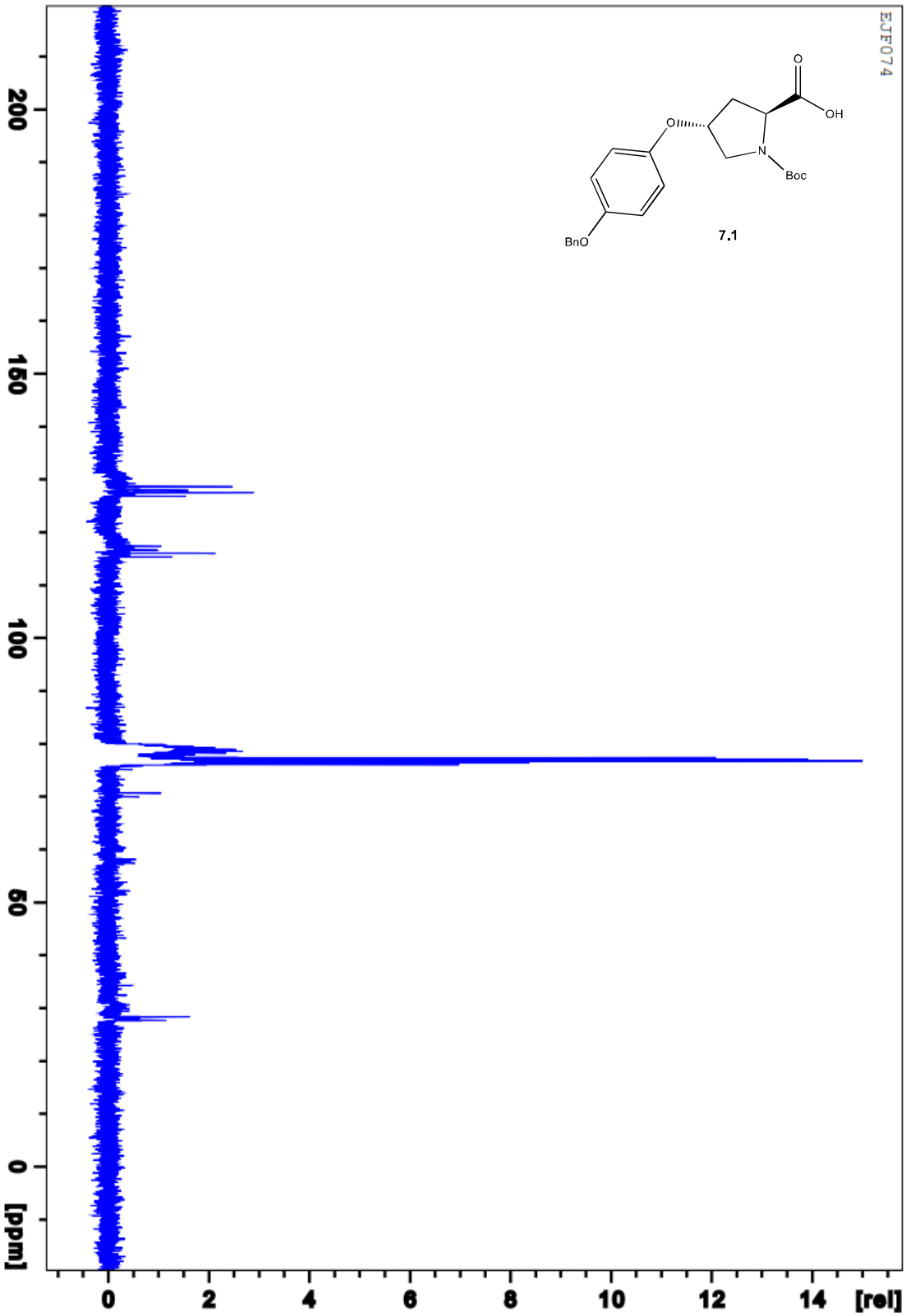

7.1 – ^{13}C NMR (25^0 C, $CDCl_3$)

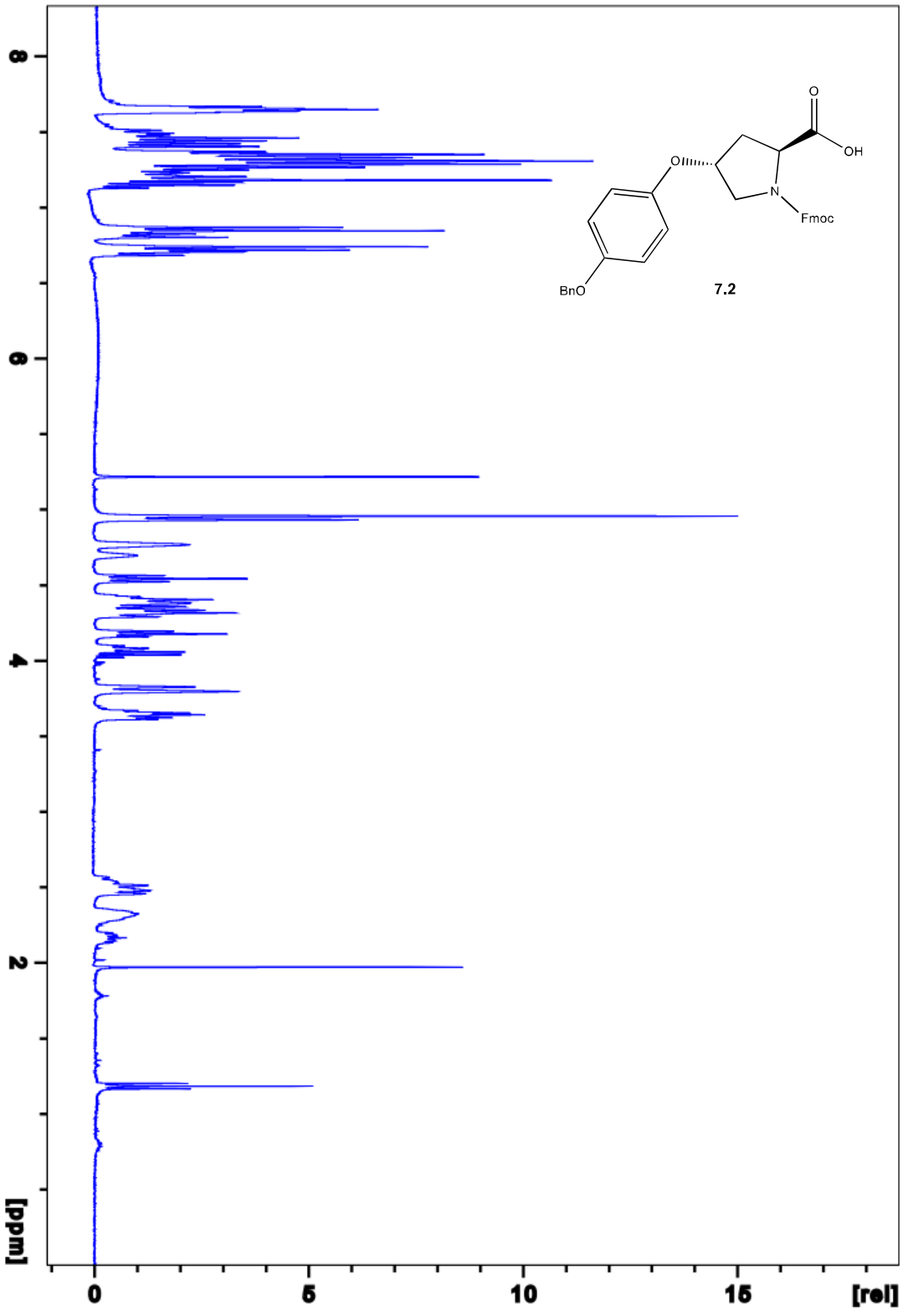

7.2 – ^{1}H NMR (25^{0} C, $CDCl_3$)

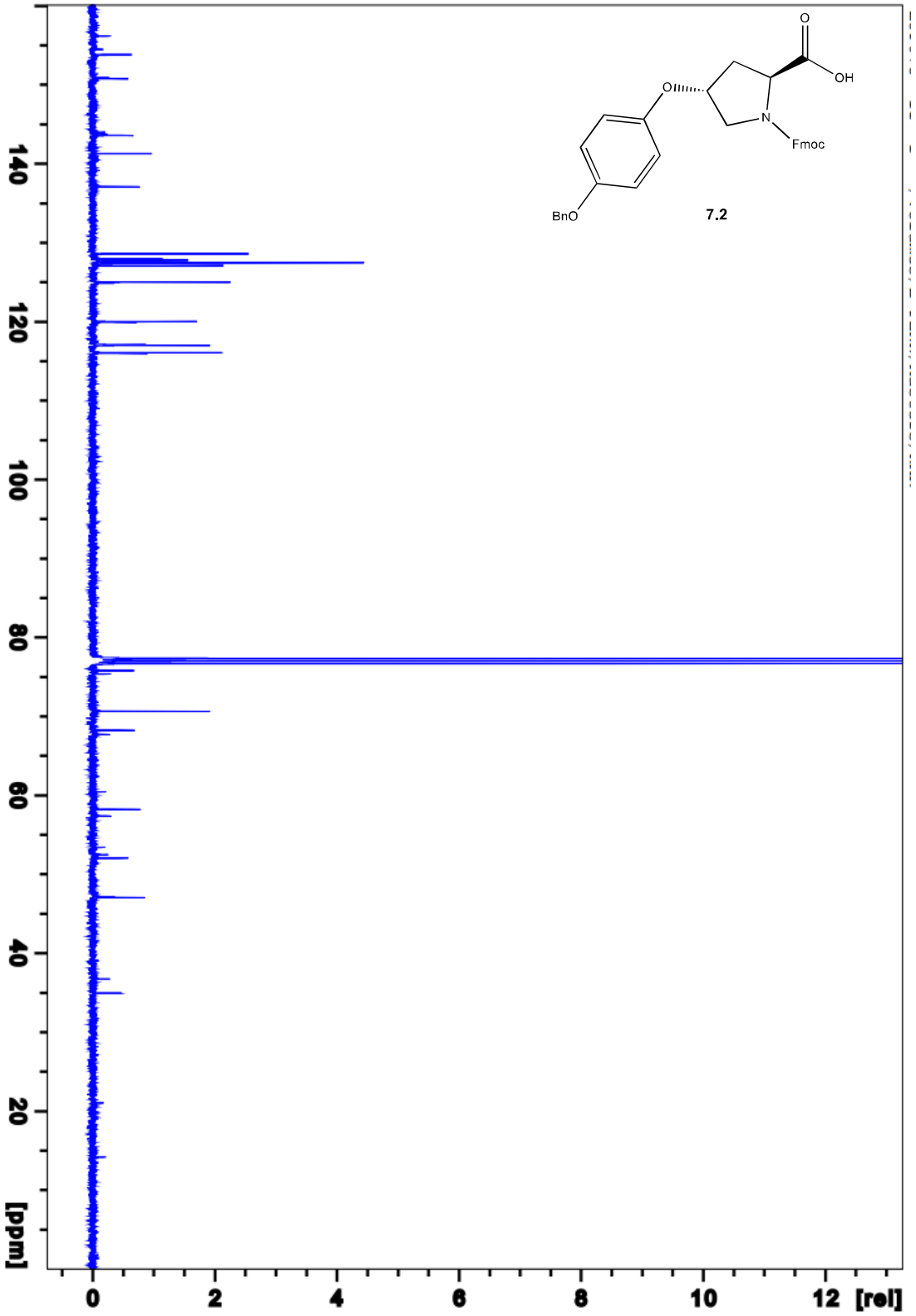

7.2 – ^{13}C NMR (25^0 C, $CDCl_3$)

Appendix B – LCMS spectra

LCMS spectra of the three open-chain basis peptides:

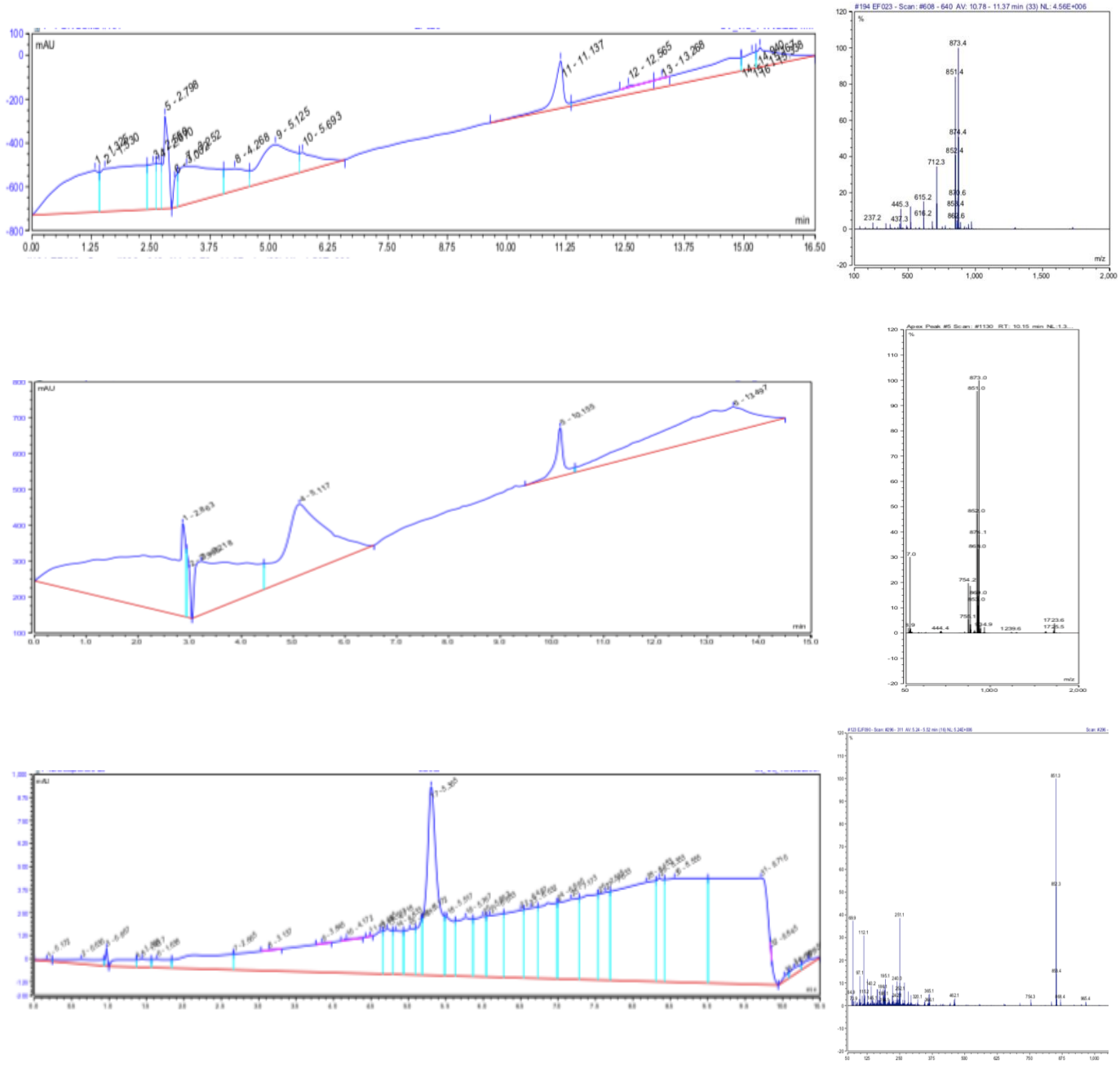

Reversed-phase LCMS spectra showing the 225 nm chromatogram and relevant peak TIC traces for the three open chain basis peptides with staple attached to the N-terminus (top), middle (middle) and C-terminus (bottom).

LCMS spectra of the three stapled, reduced basis peptides:

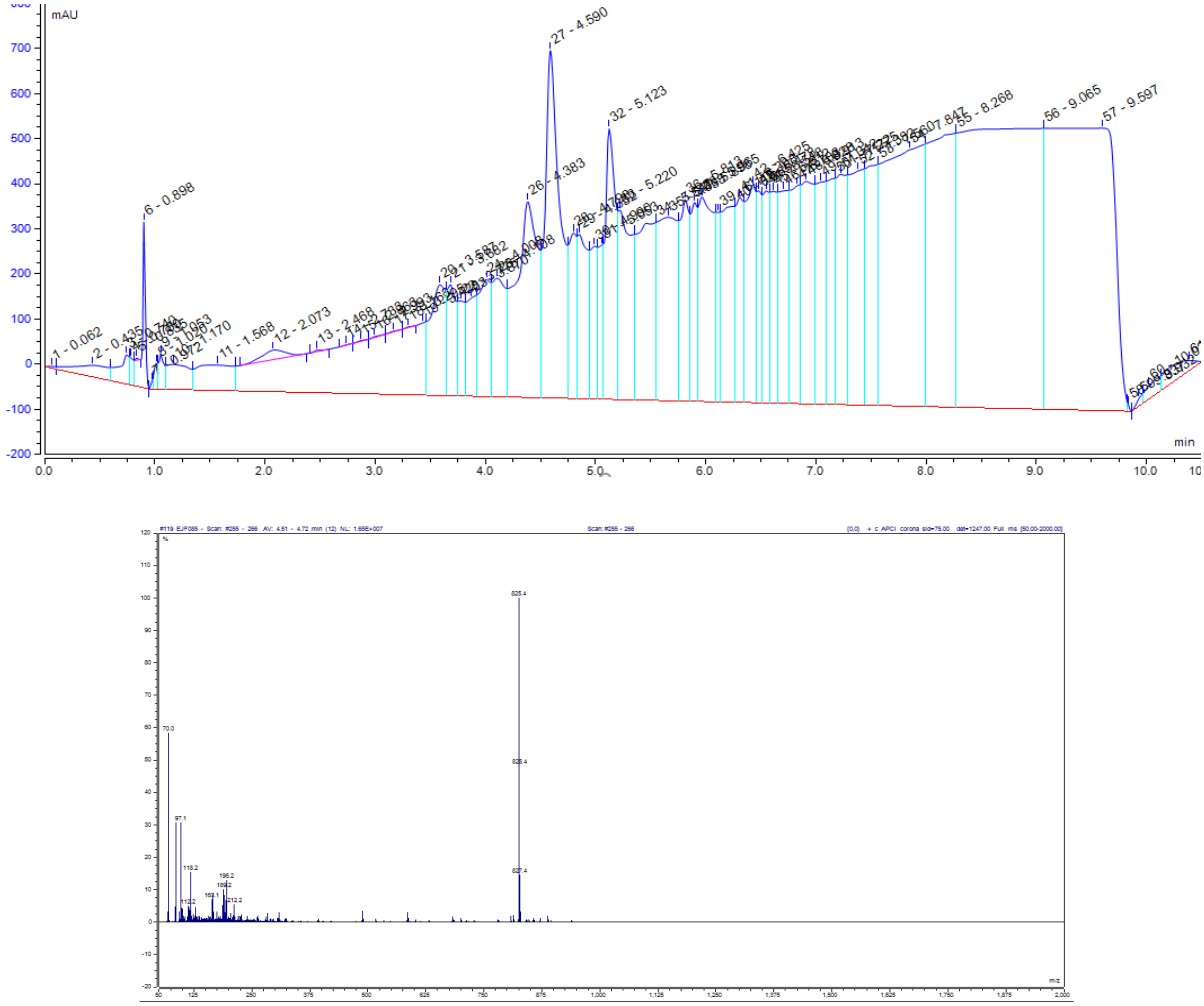

Reversed-phase LCMS spectra showing the 225 nm chromatogram (top) and TIC trace (bottom) for the ring-closed, reduced basis peptide with hydrocarbon staple attached to the N-terminus.

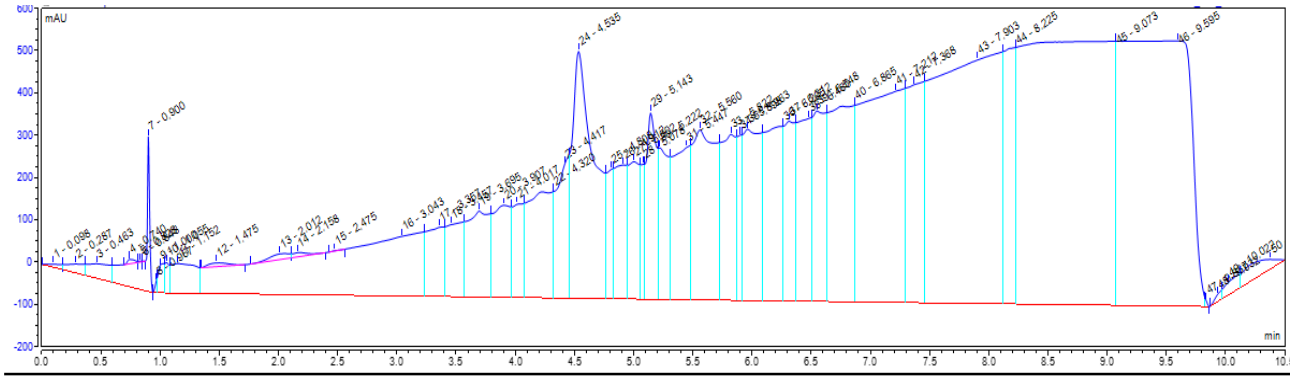

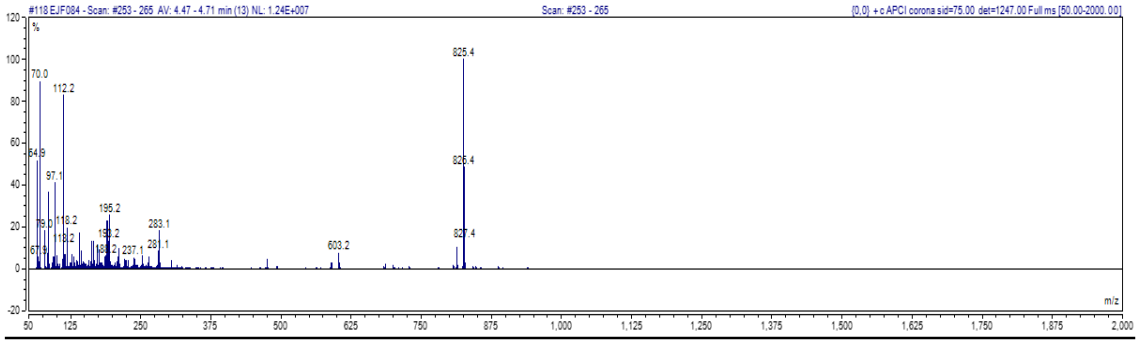

Reversed-phase LCMS spectra showing the 225 nm chromatogram (top) and TIC trace (bottom) for the ring-closed, reduced basis peptide with hydrocarbon staple attached in the middle position.

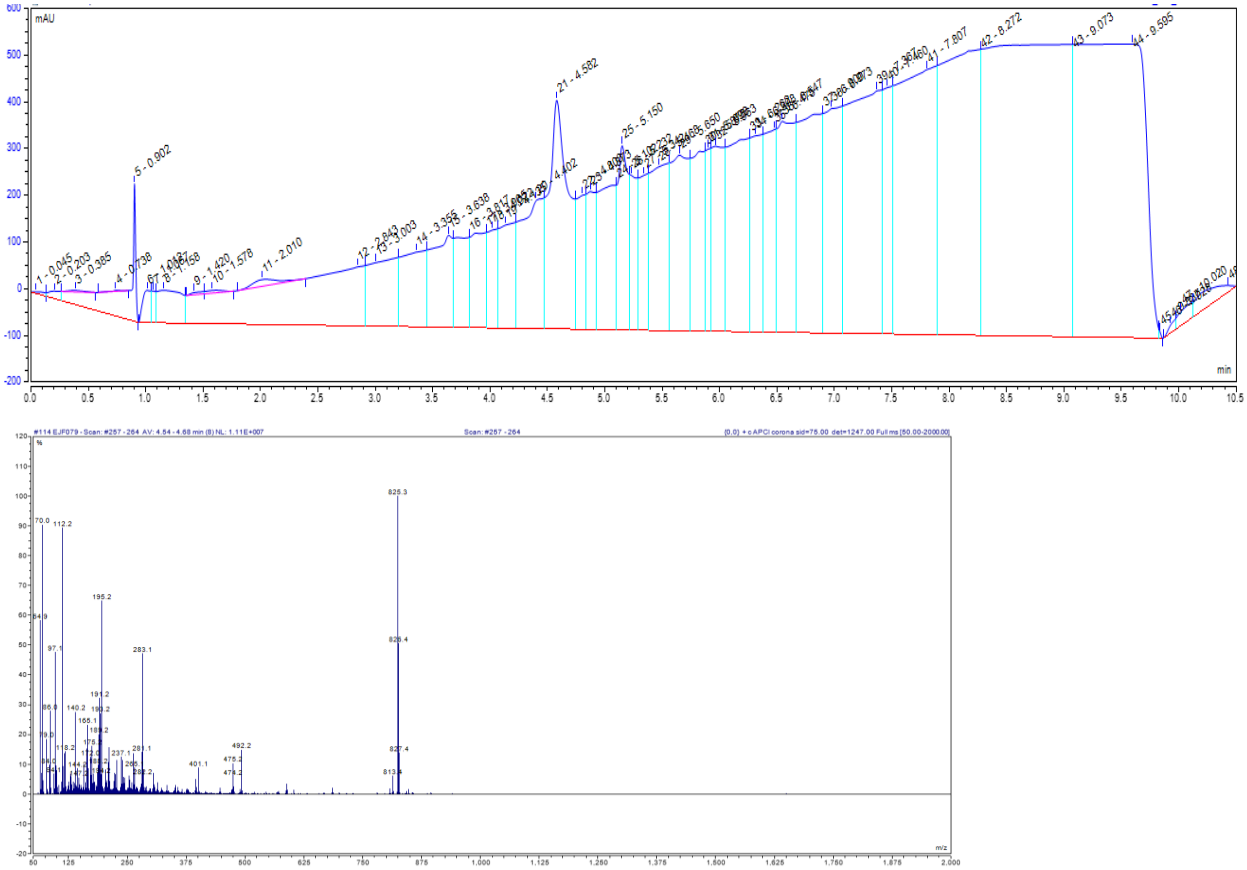

Reversed-phase LCMS spectra showing the 225 nm chromatogram (top) and TIC trace (bottom) for the ring-closed, reduced basis peptide with hydrocarbon staple attached at the C-terminus.

LCMS spectrum of the Fmoc-capped, N-terminus stapled peptide:

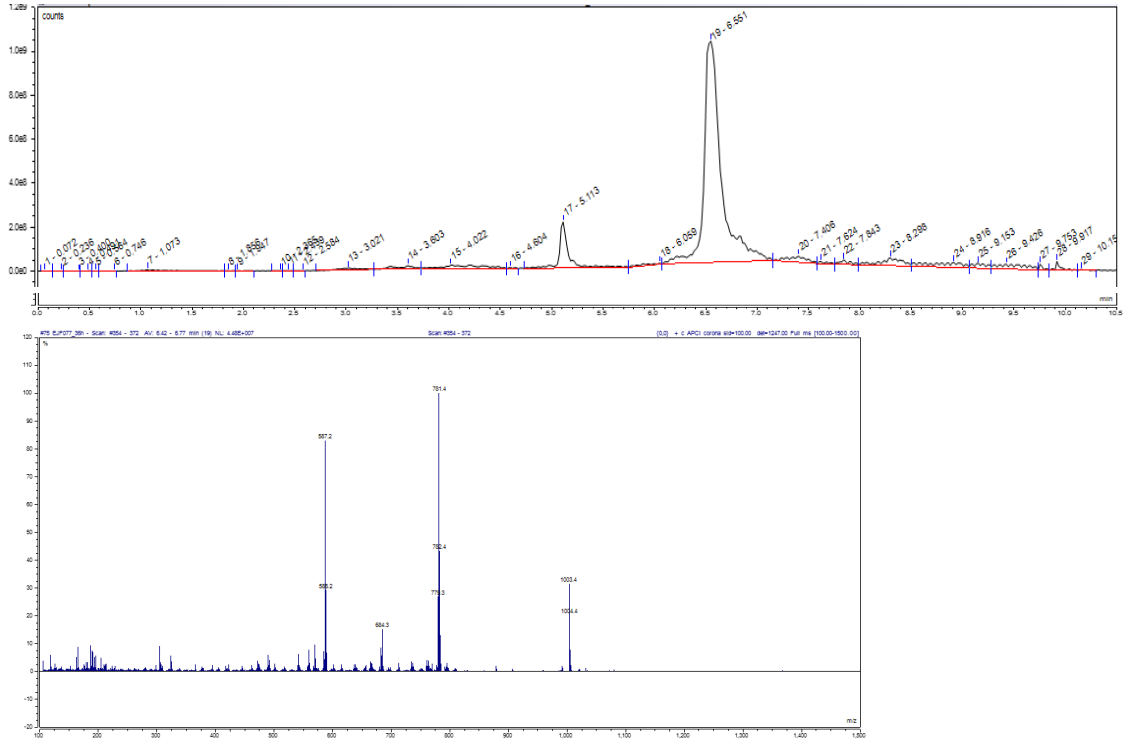

Reversed-phase LCMS spectra showing the 225 nm chromatogram (top) and TIC trace (bottom) for the Fmoc-capped, ring-closed and reduced peptide with hydrocarbon staple attached to the N-terminus.

LCMS spectrum for the open chain i, i + 4 residue functionalised basis peptide:

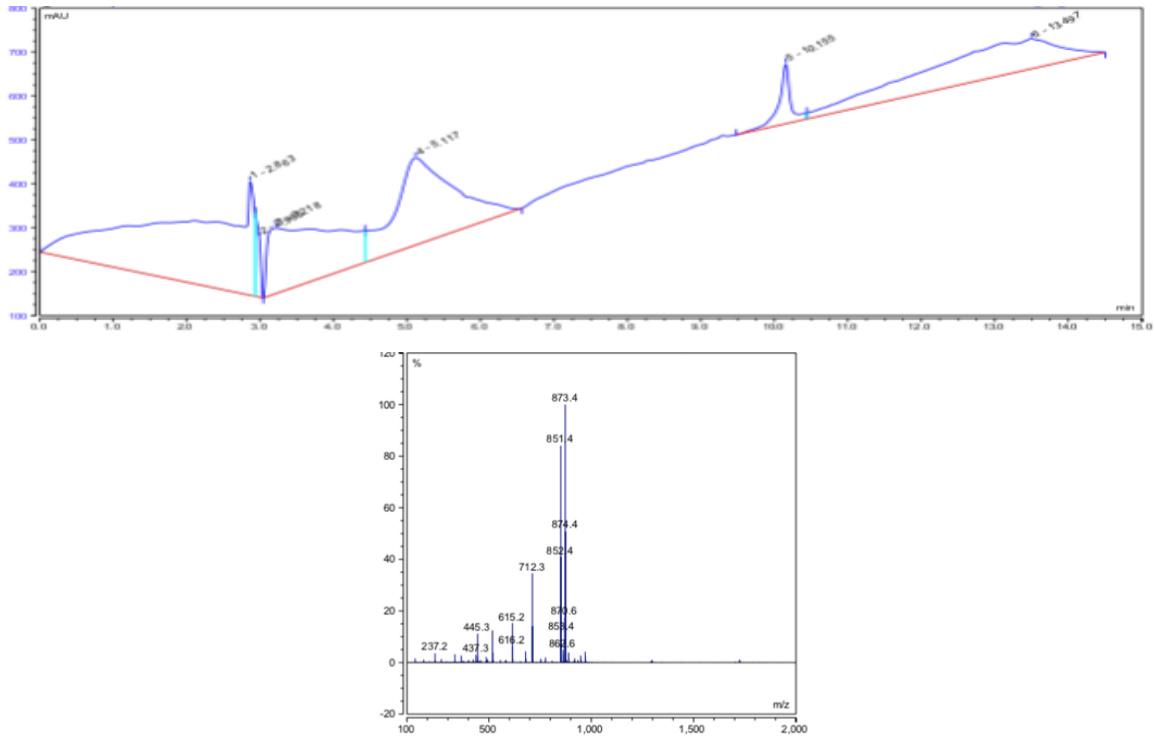

Reversed-phase LCMS spectra showing the 225 nm chromatogram (top) and TIC trace (bottom) for the open chain i, i + 4 residue functionalised basis peptide.

LCMS spectra for mimetic peptide A:

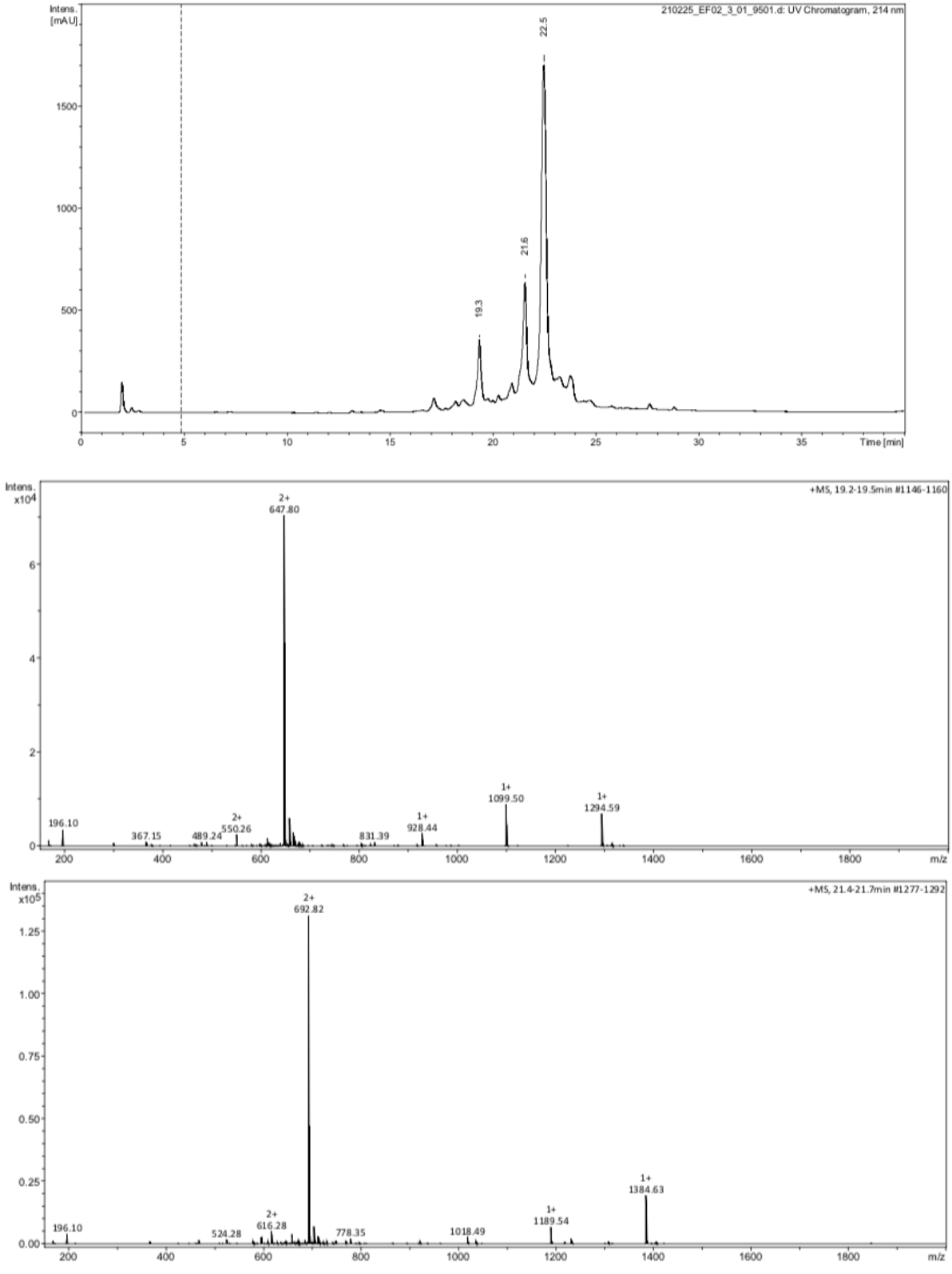

Reversed-phase LCMS spectra showing the 214 nm chromatogram (top) and TIC traces (middle + bottom) for the relevant peaks of the open-chain mimetic peptide A(i), first cleavage sample.

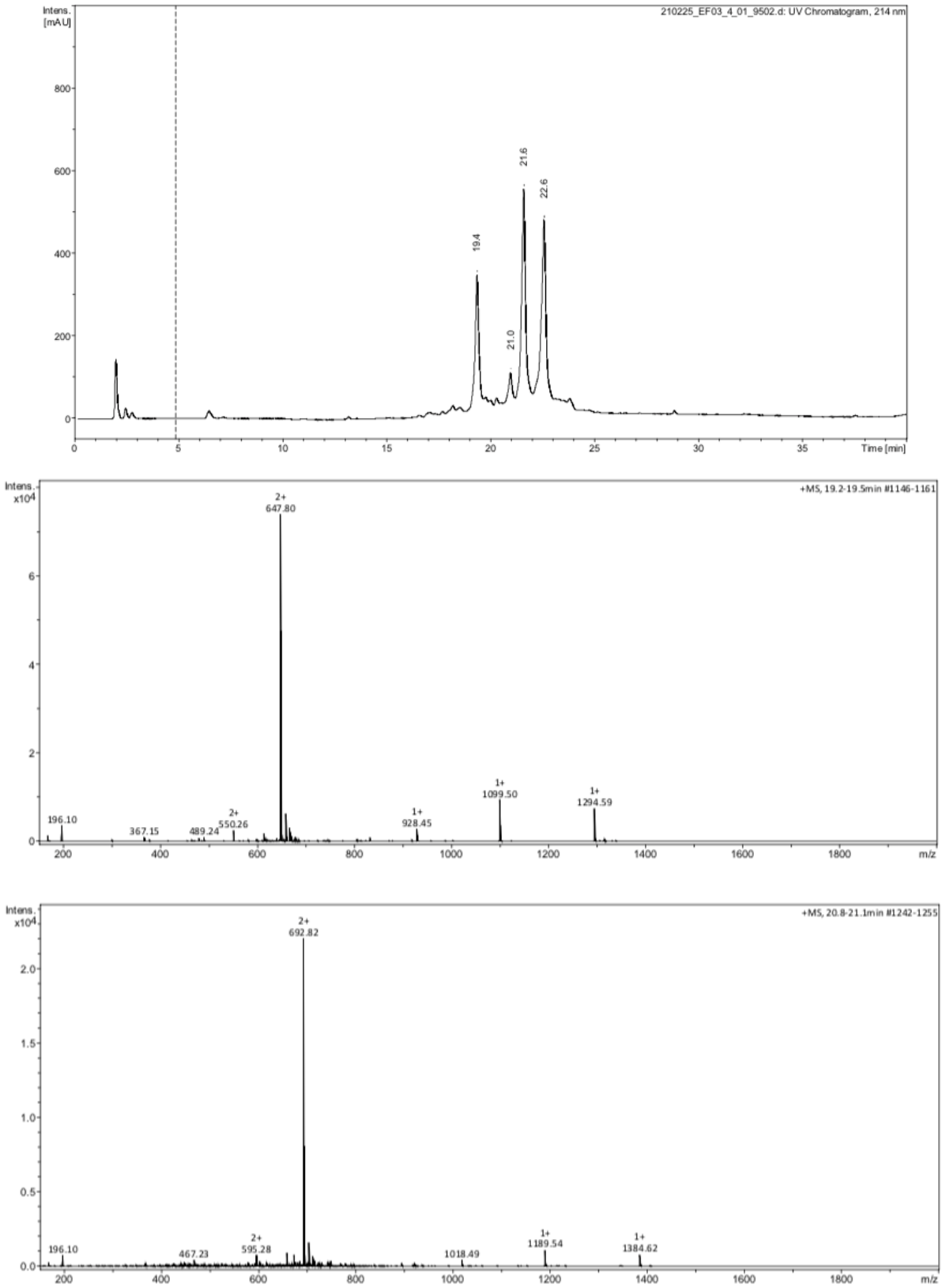

Reversed-phase LCMS spectra showing the 214 nm chromatogram (top) and TIC traces (middle + bottom) for the relevant peaks of the open-chain mimetic peptide A(i), second cleavage sample.

LCMS spectra for mimetic peptide B:

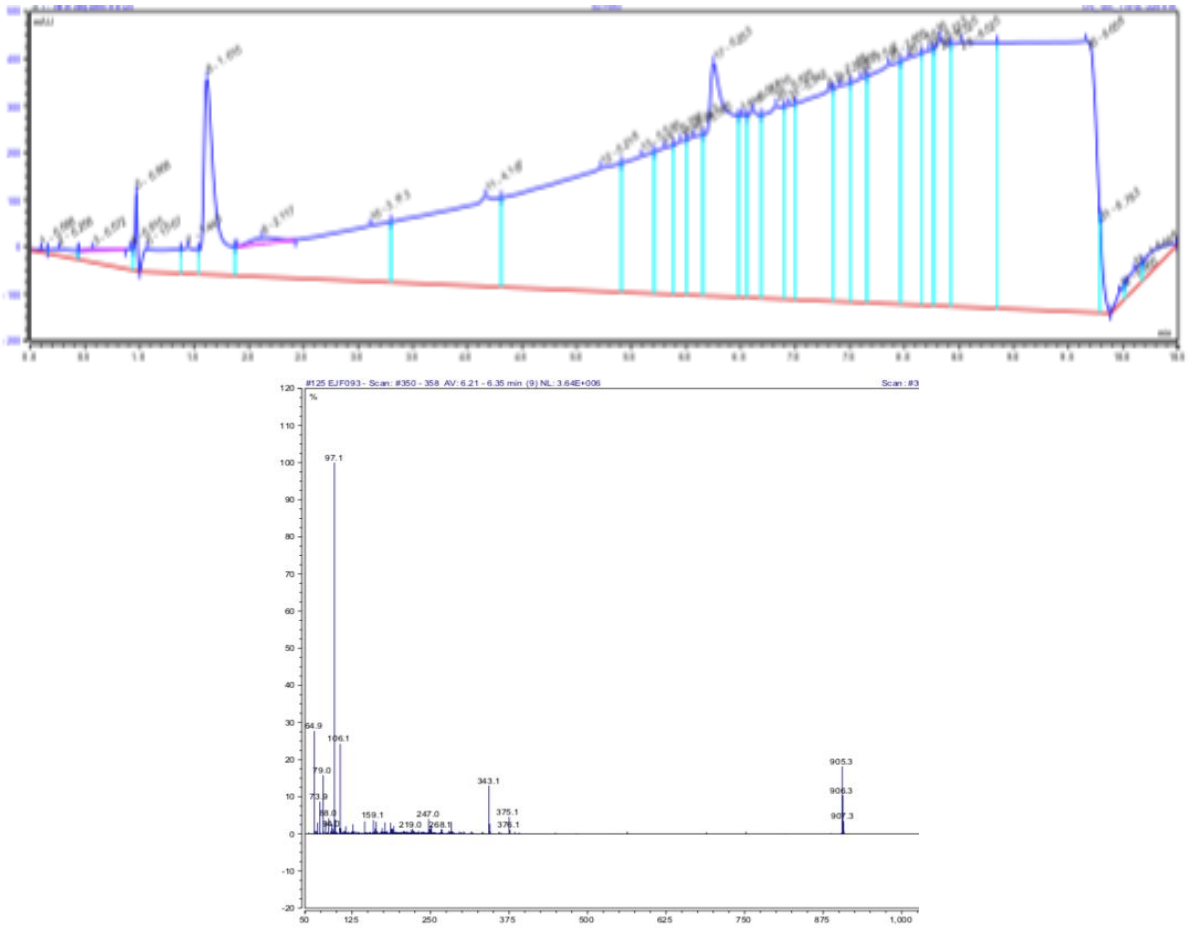

Reversed-phase LCMS spectra showing the 254 nm chromatogram (top) and TIC trace (bottom) for the relevant peaks of the open-chain mimetic peptide B(i) (N-terminal free amine TFA salt).

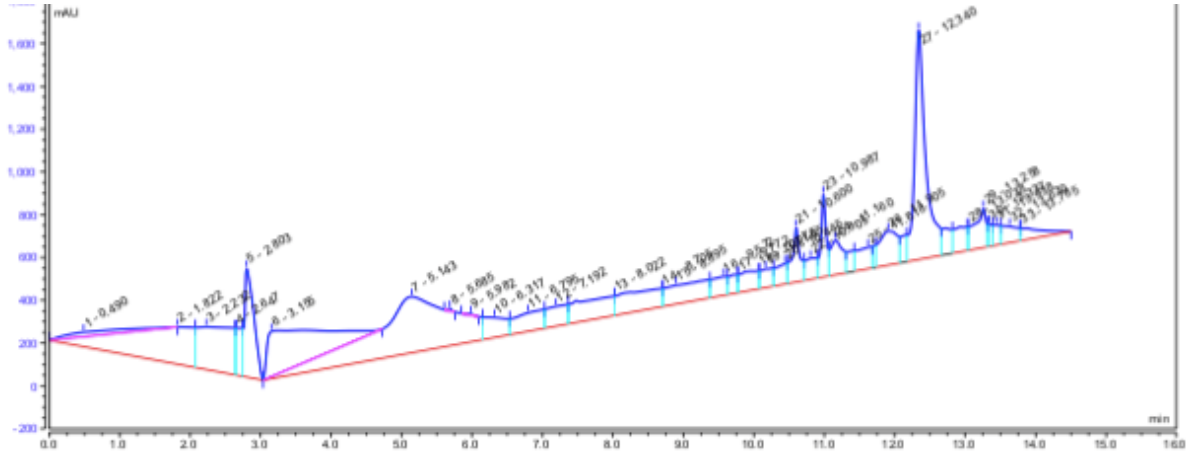

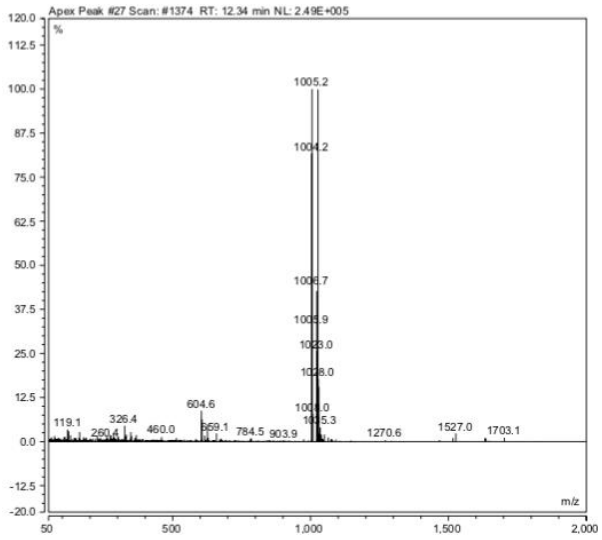

Reversed-phase LCMS spectra showing the 254 nm chromatogram (top) and TIC trace (bottom) for the relevant peaks of the open-chain mimetic peptide B(i) with N-terminus succinimide cap.

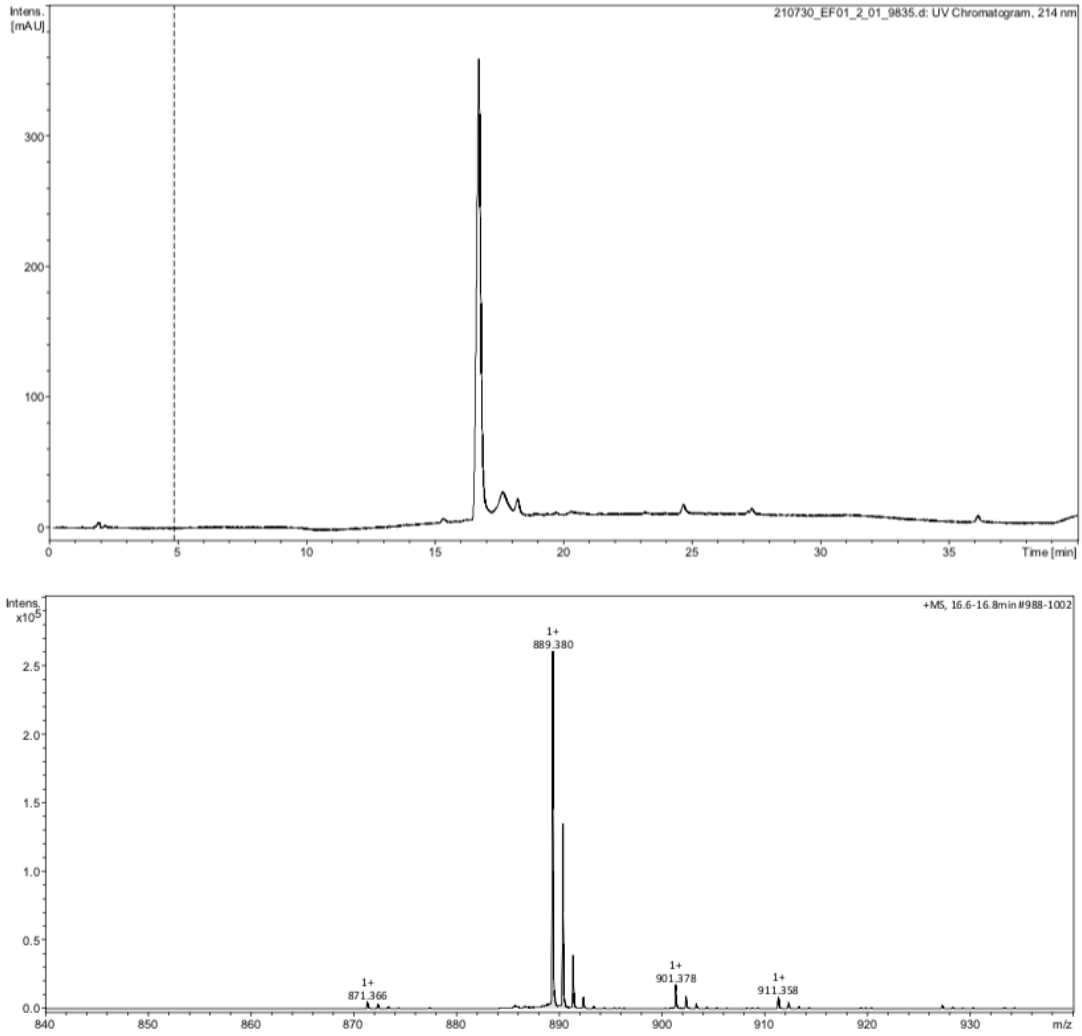

Reversed-phase HRMS spectra showing the 214 nm chromatogram (top) and TIC trace (bottom) for the ring-closed, reduced mimetic peptide B(ii).

LCMS spectra for mimetic peptide C:

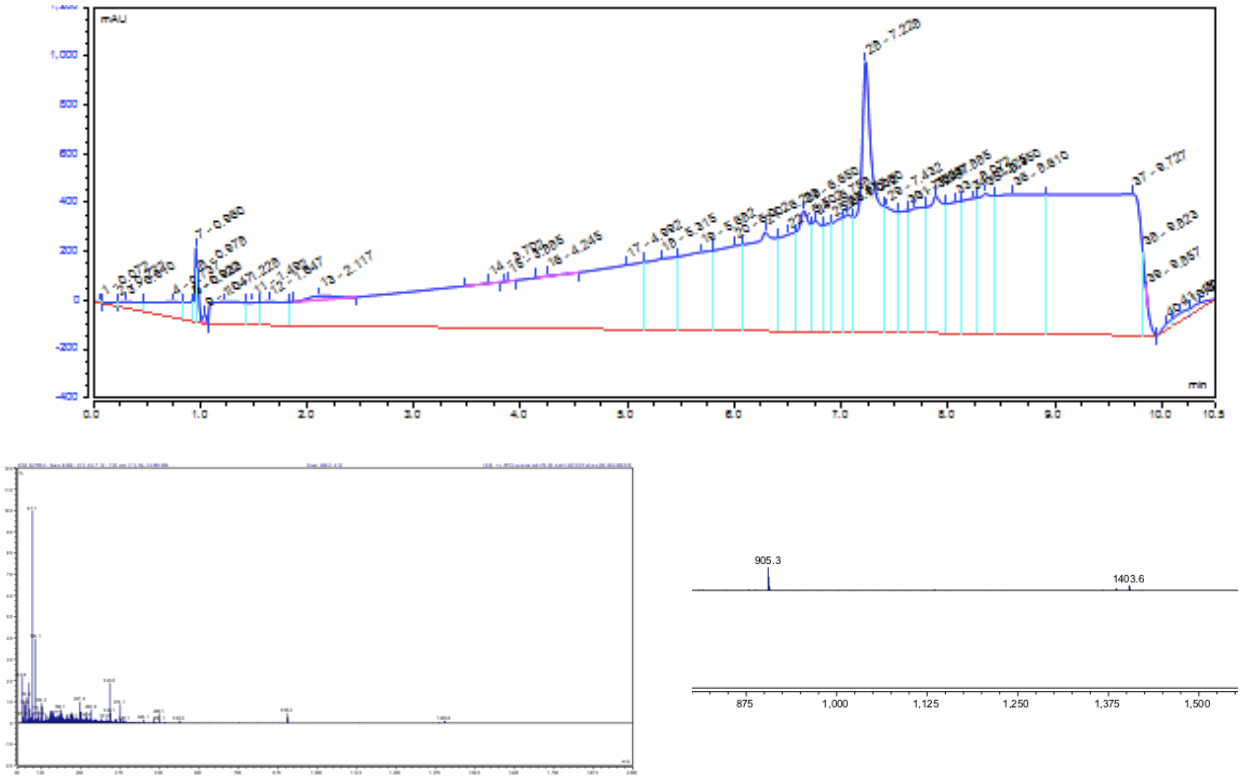

Reversed-phase LCMS spectra showing the 254 nm chromatogram (top) and TIC trace (bottom) for the relevant peaks of the open-chain mimetic peptide C(i).

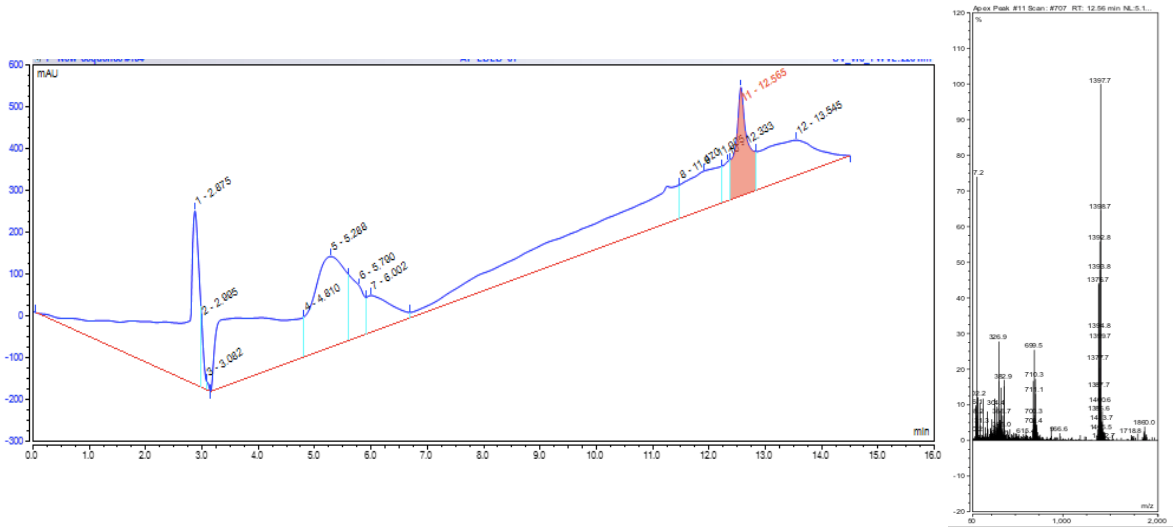

Reversed-phase LCMS spectra showing the 254 nm chromatogram (left) and TIC trace (right) for the relevant peaks of the ring-closed derivative of mimetic peptide C(i) prior to hydrogenation.

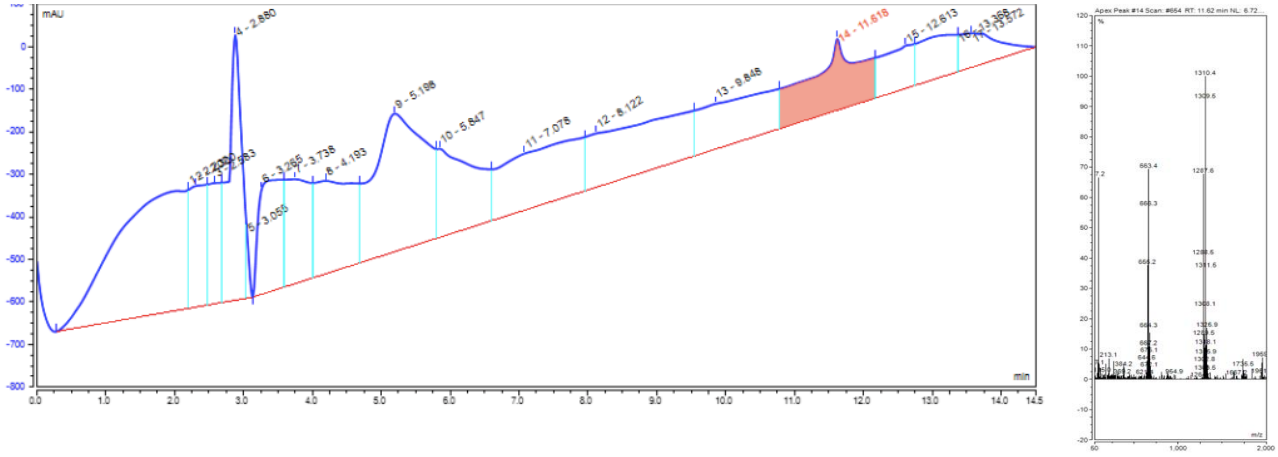

Reversed-phase LCMS spectra showing the 254 nm chromatogram (left) and TIC trace (right) for the relevant peaks of the isolated mimetic peptide C(ii).

Appendix C – CD spectra

CD spectra of the isolated stapled and reduced basis peptides:

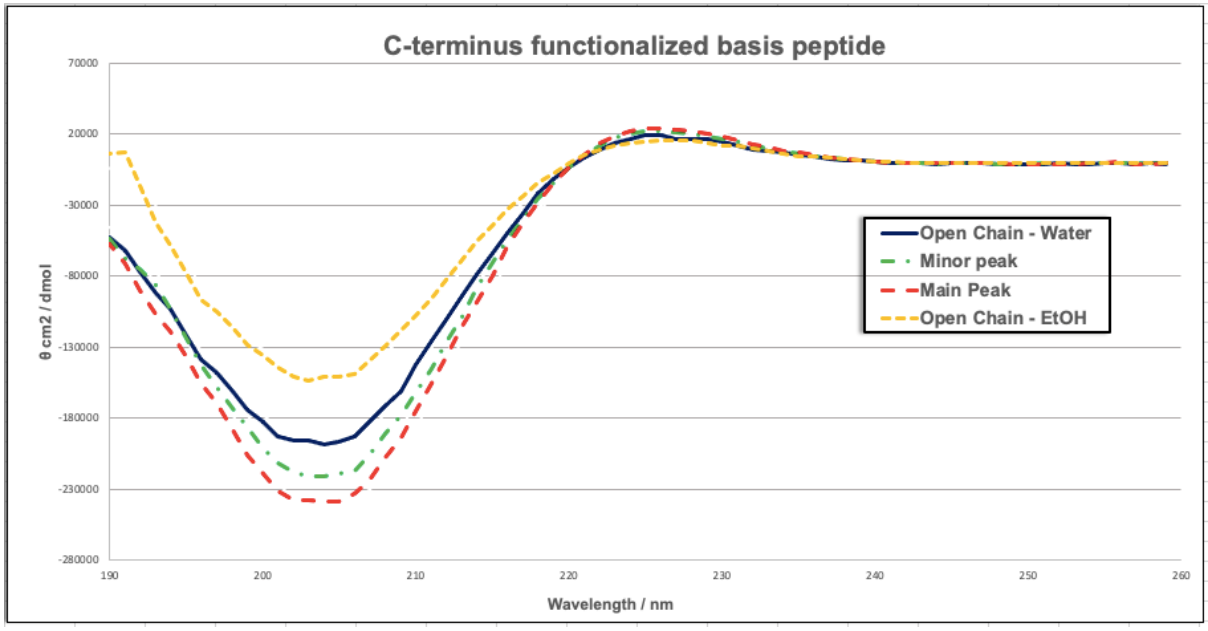

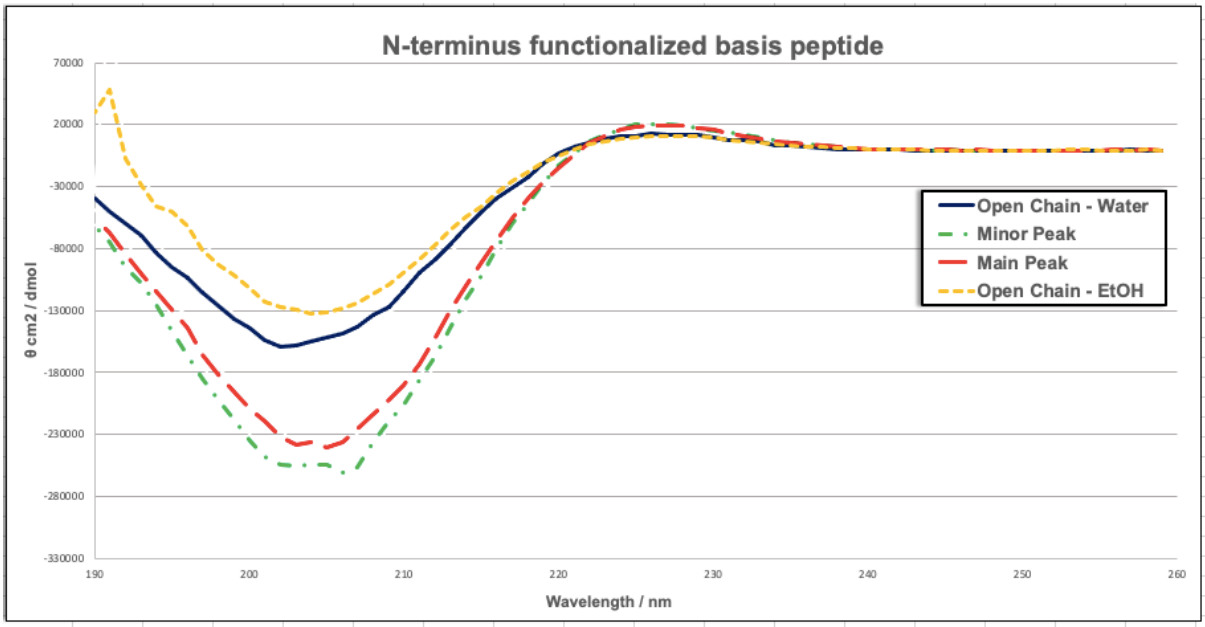

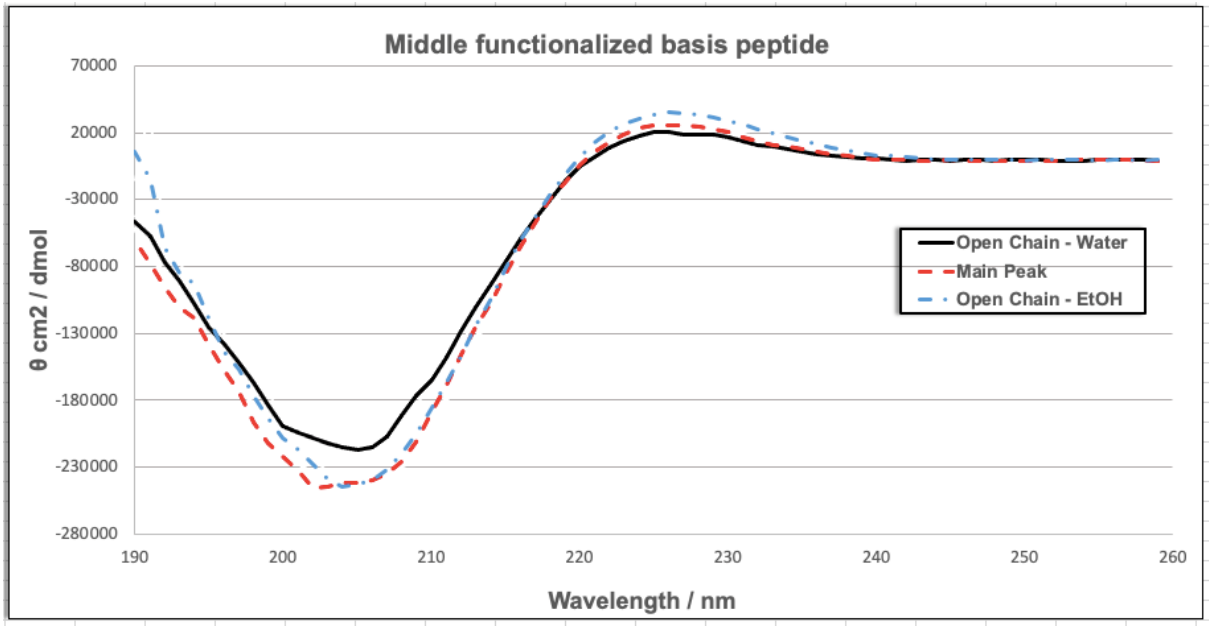

CD spectra of the basis peptide isolated peak(s) overlaid on their respective open-chain derivatives. C-terminus functionalised (top), middle-functionalised (middle) and N-terminus functionalised (bottom).

Appendix D – FT-IR spectra

FT-IR spectra of the isolated stapled and reduced basis peptides:

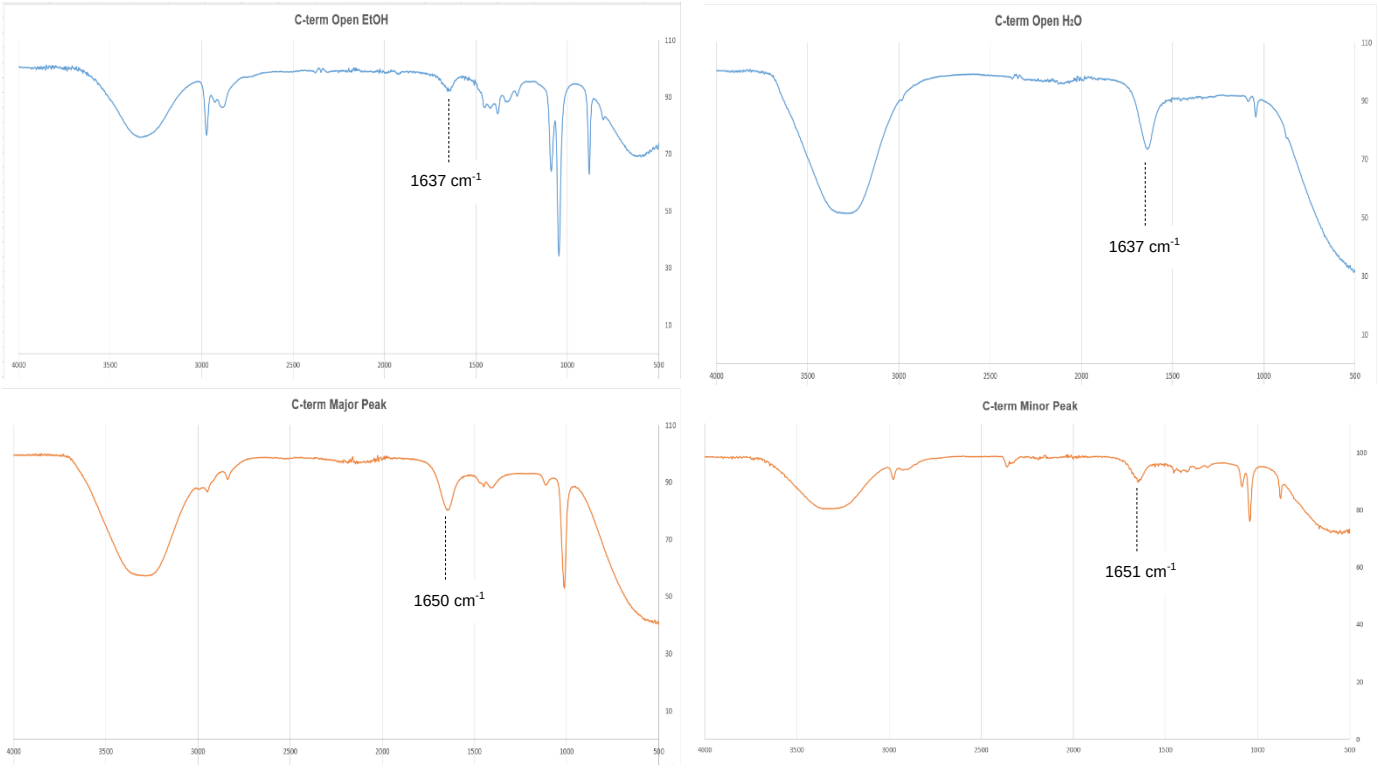

FT-IR spectra of the major and minor peaks isolated for the C-terminus functionalised basis peptide (bottom). The open chain derivative is also shown in EtOH and H_2O for comparison (top).

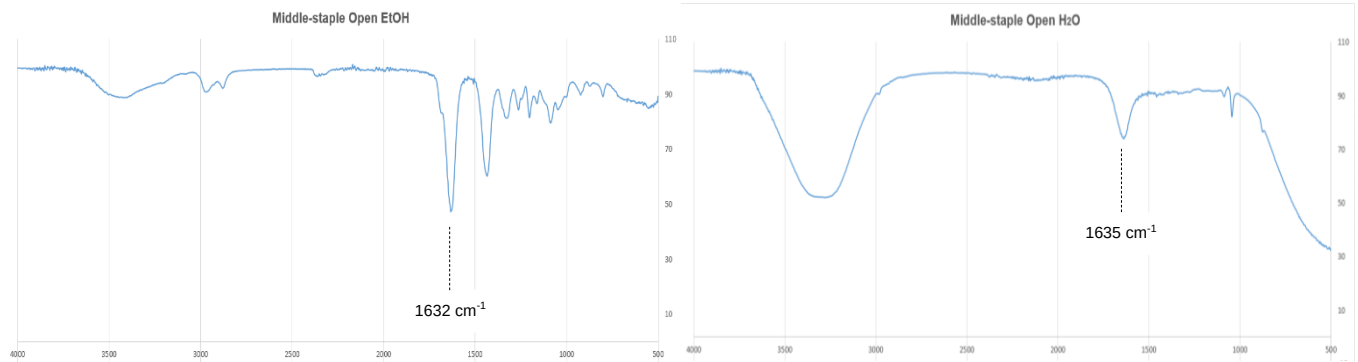

FT-IR spectra of the major peak isolated for the middle-functionalised basis peptide (bottom). The open chain derivative is also shown in EtOH and H_2O for comparison (top).

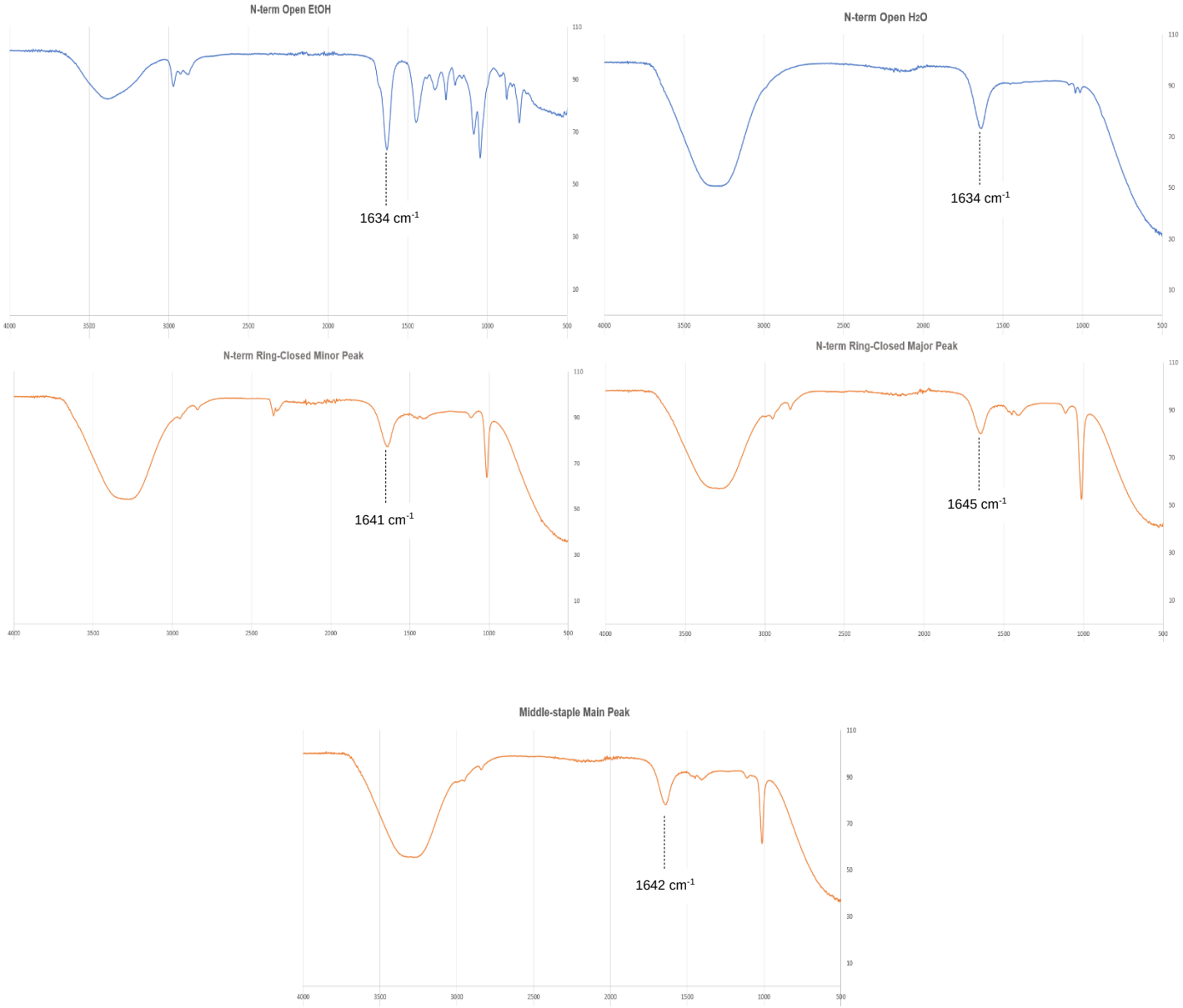

FT-IR spectra of the major and minor peaks isolated for the N-terminus functionalised basis peptide (bottom). The open chain derivative is also shown in EtOH and H_2O for comparison (top).